96 Topics in Current Chemistry

Fortschritte der Chemischen Forschung

Inorganic Chemistry

With Contributions by
E. Colomer, R. J. P. Corriu, I. Hargittai,
R. F. Porter, K. Schwochau, L. J. Turbini

With 52 Figures and 24 Tables

This series presents critical reviews of the present position and future trends in modern chemical research. It is addressed to all research and industrial chemists who wish to keep abreast of advances in their subject.

As a rule, contributions are specially commissioned. The editors and publishers will, however, always be pleased to receive suggestions and supplementary information. Papers are accepted for "Topics in Current Chemistry" in English.

Table of Contents

Photochemistry of Boron Compounds

Richard F. Porter and Laura J. Turbini

Department of Chemistry, Baker Laboratory, Cornell University, Ithaca, New York 14853, USA
Western Electric Engineering Research Center, Princeton, New Jersey 08540, USA

Table of Contents

I. Introduction

Scientific interest in the chemistry of boron has expanded noteably in the past 20 years. There has, however, been relatively little emphasis on the photochemistry of boron compounds. Since the volume of published work on boron photochemistry is not excessive, it is possible in this review to include the major fraction of the photochemical literature dating back to the initial work of Stock[99]. This article deals primarily with the inorganic photochemistry of boron compounds. Many simple boron compounds with B-H, B-O, B-N or B-halogen bonds do not absorb radiation in the visible or near UV regions of the optical spectrum. For this reason photochemical experiments with these compounds frequently require the use of sources of short wavelength radiation below 200 nm, a spectral region requiring vacuum optical techniques. This limitation and the need for special handling of boron compounds that may be thermally unstable or highly reactive have probably contributed to the lack of systematic efforts to investigate the photochemistry of these systems. Nevertheless, it is anticipated that the interest in structures of poly-hedral boron compounds[68] will be an impetus to further exploration of their photo-chemical behavior.

With the development of CO_2 lasers, work on the infrared photochemistry of boron compounds is now appearing in the literature. Future work on these compounds with UV laser sources is also expected. In this review the effect of radiation on boron compounds in the photon energy range 0.1 eV (CO_2 laser) to 10.2 eV (H-α line) is examined. The range of tropics extends from the use of photochemical techniques for synthesis of new compounds to the production and isolation of reactive photochemical intermediates. The photochemistry of borazine is most extensively discussed.

Some speculation is inevitable in proposing any photochemical mechanism and some liberty has been taken in this regard in the present discussion. Areas of boron photochemistry are indicated where proposed mechanisms are controversial and where further experimental work is necessary. For example, very little is known about triplet states of boron molecules. Some of these questions may be answered in the future by non-photochemical techniques[30].

II. Boron Hydrides

Interest in the photochemistry of boron compounds dates back as far as 1913 when Alfred Stock[99] investigated the effects of light from a mercury vapor lamp on diborane(6) and on tetraborane(10). In the case of diborane(6) he commented: "UV light will also decompose B_2H_6. The volume of a sample in a quartz tube increased by 1/6 after 24 hours exposure to a mercury-arc lamp, and a pale yellow crystalline substance appeared." Stock also observed that B_4H_{10} decomposition to B_2H_6 is not noticeably influenced by sunlight.

Further observations on the effect of light on diborane(6) did not appear until the 1950's. At that time, Hirata and Gunning[52] studied the mercury-sensitized de-

composition, leading to H_2 and B_4H_{10} as the main products. The proposed mechanism involves the mercury-sensitized cleavage of a boron-hydrogen bond followed by recombination of the radicals as follows:

$$B_2H_6 + Hg\,6\,(^3P_1) \longrightarrow B_2H_5 + H + Hg\,6\,(^1S_o) \tag{1}$$

$$2\,B_2H_5 \longrightarrow B_4H_{10} \tag{2}$$
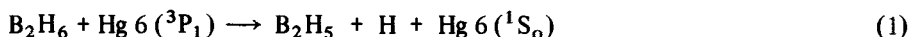
It should be noted that as of now there is no direct physical evidence (e. g., ESR spectrum) for the existence of the B_2H_5 radical and *much* of the mechanistic discussion of the photochemistry of diborane(6) is speculative. If Eqs. (1) and (2) represent the correct mechanisms the rate of the quantum yields for H_2 to B_4H_{10} production would be unity. Although this ratio tends towards unity at lower pressures, this simple mechanism did not explain the ratio of two approached at higher pressures. In order to explain this, an additional primary process was proposed, i. e., a disproportionation of two B_2H_5 radicals:

$$2B_2H_5 \longrightarrow B_2H_4 + B_2H_6 \tag{3}$$
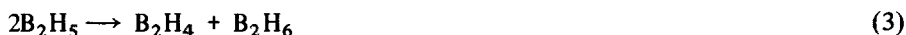
The reactive B_2H_4 is presumed to decay rapidly to pentaboranes and solid product.

Direct photolysis of B_2H_6 using 184.9 nm radiation was reported by Kreye and Marcus[62] in 1962. A UV absorption spectrum of B_2H_6 is shown in Fig. 1. The spectrum has been interpreted as a σ to π^* transition which is weakly allowed. Thus, the 184.9 nm mercury line is a useful radiation to study the photochemical reactions of this compound. The study of Kreye and Marcus limited itself to low percent conversions, but included variations in light intensity, and diborane(6) pressures. The major products in the photolysis were identified as B_4H_{10}, B_5H_{11}, a polymeric solid, and H_2. The formation of B_4H_{10} and polymer were linked to the proposed primary radical, B_2H_5, in the mechanism:

$$B_2H_6 \xrightarrow{\;h\nu\;} B_2H_5 + H \tag{4}$$

$$B_2H_5 + H \longrightarrow (-B_2H_2-) + 2H_2 \tag{5}$$
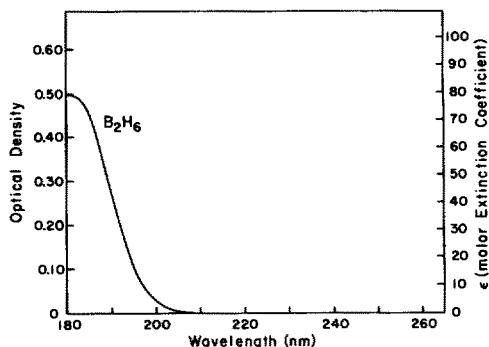
Fig. 1. Ultraviolet absorption spectrum of diborane (6)

3

$$2B_2H_5 \longrightarrow B_4H_{10} \tag{6}$$

$$2H + M \longrightarrow H_2 \tag{7}$$
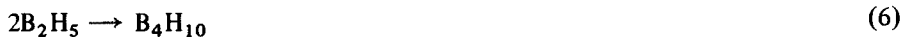
The formation of B_5H_{11} is linked to a second intermediate BH_3:

$$B_2H_6 \xrightarrow{\ h\nu\ } 2BH_3 \tag{8}$$

$$BH_3 + B_2H_6 \longrightarrow B_3H_7 + H_2 \tag{9}$$

$$B_3H_7 + B_2H_6 \longrightarrow B_5H_{11} + H_2 \tag{10}$$
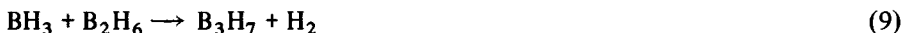
The overall mechanism for the reaction is consistent with the quantum yields observed for photolysis at various pressures of B_2H_6. Attempts to produce BH_3 by photolysis of diborane(6) in matrix studies have consistently failed. At the present time there is no physical evidence to support this step in the mechanism.

Grimm and Porter[41] investigated the photochemical reaction of diborane(6) with oxygen by direct coupling of their photochemical vessel with a mass spectrometer (Fig. 2). Using 184.9 nm radiation, they varied the oxygen/diborane(6) mixtures in molar proportions from 1:1 to 2:1 at total pressures ranging from 12 to 40 torr. The course of the reaction is illustrated in Fig. 3 which shows an initial rise in the formation of $H_2B_2O_3$ (I) and a time-delayed rise in the formation of $H_3B_3O_3$ (II). When the reaction was run with unscrambled mixtures of $^{16}O_2 - {}^{18}O_2$, it was found that the $H_2B_2O_3$ consisted of a non-statistical distribution of isotopic species. This suggested that an O_2 molecule participated directly in the formation of $H_2B_2O_3$. The overall stoichiometry was observed as follows:

$$B_2H_6 + 2O_2 \xrightarrow{\ h\nu\ } H_2B_2O_3 + H_2O + H_2 \tag{11}$$
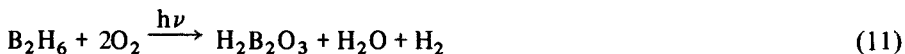
The results suggest the possible addition reaction of O_2 to a diborane-type intermediate in the primary step. Despite the fact that B_2H_6 is the simplest boron-hydride, there are a number of unanswered questions regarding the photochemical behavior of this molecule.
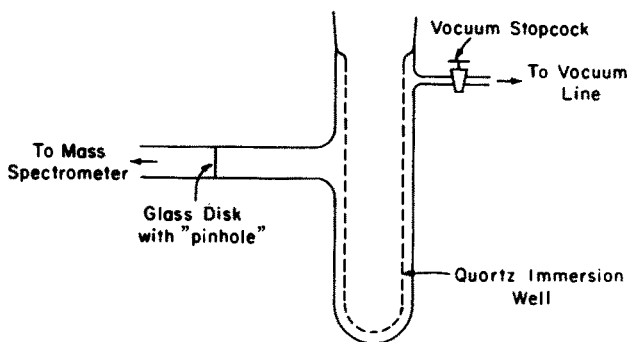
Fig. 2. System for sampling photolysis products in a mass spectrometer
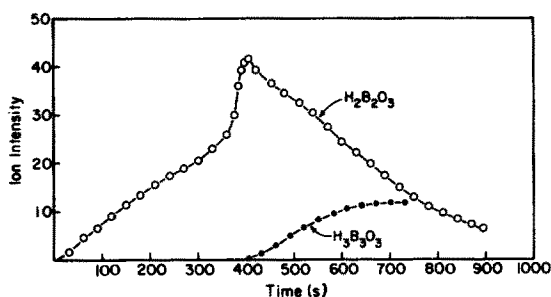
In 1956, Burwasser and Pease[18a] presented preliminary work on penta-borane(9) photolysis, in which they suggested that the major radical formed is B_5H_8. The products identified in their photolysis are H_2, B_2H_6, and a colorless crystalline material, postulated to be $B_{10}H_{14}$. Photolysis of B_5H_9 in the presence of deuterium, produced H_2, HD, and D_2 in the product. This led to the following proposed primary mechanism:

$$B_5H_9 + h\nu \longrightarrow H + B_5H_8 \tag{12}$$

$$H + D_2 \longrightarrow HD + D \tag{13}$$

$$H \text{ or } D + B_5H_9 \longrightarrow B_5H_8 + H_2 \text{ (or HD).} \tag{14}$$

No explanation is presented for the B_2H_6 or $B_{10}H_{14}$ products. More recently, Plotkin and Sneddon[81] showed the results of Hg-sensitized photolysis of penta-borane(9) leading to a $(B_5H_8)_2$ dimer, H_2, $B_{10}H_{14}$, and a viscous oil. They suggested that the $(B_5H_8)_2$ is formed to the recombination of B_5H_8 radicals. They identify the compound as $2,2'\text{-}(B_5H_8)_2$ (Fig. 4). This system was studied in detail by Kline and Porter[61] in an attempt to obtain evidence for the B_5H_8 radical. These investigators were unable to obtain the $(B_5H_8)_2$ dimer in the photolysis of B_5H_9 with di-t-butylperoxide which is known to act as a H-abstraction reagent. When mixtures of nonscrambled B_5H_9 and B_5D_9 were investigated, the hydrogen produced for short photolysis periods consisted of H_2 and D_2 with very small quantities of HD, much below an equilibrium proportion. These results are inconsistent with the mechanism described in Eqs. (12), (13), and (14) which is expected to lead to a statistical distribution of hydrogen isotopes. Kline and Porter[61] also investigated the photolysis of $1\text{-}DB_5H_8$ and $\mu\text{-}D_4B_5H_5$. They concluded from the isotopic hydrogen analysis, that the elimination of a hydrogen molecule from any pair of H sites in pentaborane is a random but not strictly statistical process. From these results, a
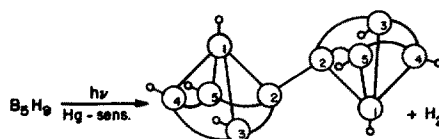
Fig. 4. Pyrolysis product of B_5H_9

(I)   (II)
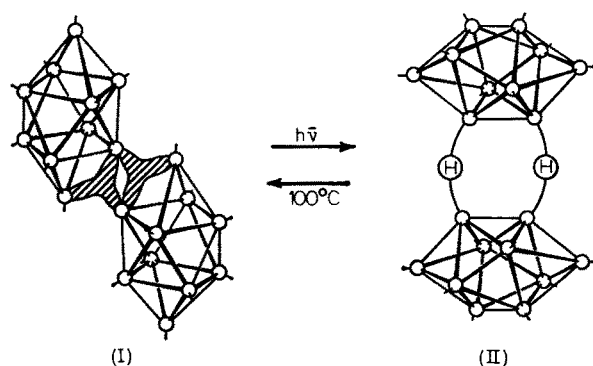
Structures of $B_{20}H_{18}^{-2}$ (I) and photo-$B_{20}H_{18}^{-2}$ (II)

Fig. 5. Photoisomers of $B_{20}H_{18}^{2-}$

mechanism is postulated which involves the formation of B_5H_7 as a primary inter-mediate leading to the formation of $B_{10}H_{14}$ and $B_{10}H_{16}$. Similar studies with 1-methyl- and 2-methylpentaborane(9) gave methylated derivatives of $B_{10}H_{14}$ and $B_{10}H_{16}$. Photochemical isomerization of these methylboranes was not observed. An interesting photo-isomerization was reported by Hawthorne and Pilling[50] in 1966. They irradiated $B_{20}H_{18}^{2-}$ (I) in acetonitrile solution to obtain the photoisomer $B_{20}H_{18}^{2-}$ (II), which can be converted back to (I) by heating at 100 °C for 36 hours (Fig. 5).

Trofimenko and Cripps[98] report that $B_{10}X_{10}^{2-}$ and $B_{12}X_{12}^{2-}$ (X = halogen) undergo photoinduced nucleophilic substitution reactions which are useful in preparing some previously inaccessible polyhedral boranes.

III. Boron-Carbon Compounds

A. Trialkylboranes

The literature contains several articles on the photochemical reactions of trialkyl-boranes with organic moieties. In some cases it appears that the organic reagent is absorbing the light rather than the borane. Examples of this are the reaction of trial-kylboranes with (a) β-substituted α,β-unsaturated carbonyl compounds[15], (b) with cyclohexene[75], (c) with cycloocta-27,7-dienone[75], (d) with acridine[75], (e) with ethyl acetoacetate[109], (f) with acetylacetone[109], and (g) with ethyl 2,2-dimethyl-acetoacetate[109]. Iodine has been photolyzed in the presence of triethylborane[1]. Finally, thioborinates have been produced in the photolysis of 4,4'-bisdimethyl-aminobenzothiophenone with trialkylboranes[55], and of phenyl disulfide or methyl disulfide with tri-n-butylborane[16]. In all of these examples, the borane is not the primary photochemical reagent.

There are examples where the trialkylborane is the photochemical excited species. Lissi and Larrondo[69] studied the Hg-photosensitized decomposition of

triethylborane. Although they did not analyze the boron-containing products, they proposed two main processes, and possibly a third, which involved the triethylborane in the primary step:

$$Hg^* + (C_2H_5)_3B \longrightarrow Hg + H_2 + products \tag{15}$$

$$Hg^* + (C_2H_5)_3B \longrightarrow Hg + C_2H_5 + (C_2H_5)_2B \tag{16}$$

and probably

$$Hg^* + (C_2H_5)_3B \longrightarrow Hg + C_2H_4 + (C_2H_5)_2BH \tag{17}$$
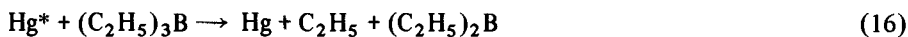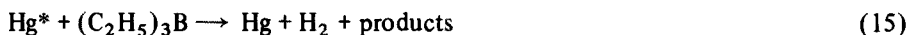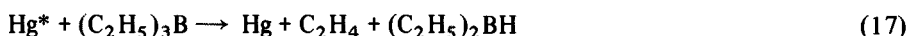
The quantum yields determined are 0.3, $\geqslant 0.3$, and $\leqslant 0.07$, respectively.

B. Carboranes

Only a few photochemical reactions of carboranes have been reported in the literature. Plotkin and Sneddon[87] synthesized a carborane dimer by the Hg-sensitized photolysis of $C_2B_5H_7$ (Fig. 6).

$$C_2B_5H_7 \xrightarrow[Hg]{h\nu} 3,3'\text{-}(2,4\text{-}C_2B_5H_6)_2 + H_2 \tag{18}$$

Spielman and Scott[98] obtained improved yields in the synthesis of $C_2B_3H_5$, $1,6\text{-}C_2B_4H_6$ and $1,2\text{-}C_2B_4H_6$ from the photolysis of $2,3\text{-}C_2B_4H_8$. Finally, photochemical chlorination of carboranes has been reported[101].

C. Organoboron Compunds

There is pertinent literature on the photochemistry of complex organic molecules containing a structurally significant boron atom. The Eastman Kodak group[31, 42,

PROPOSED STRUCTURE FOR $3,3'\text{-}(2,4\text{-}C_2B_5H_6')_2$
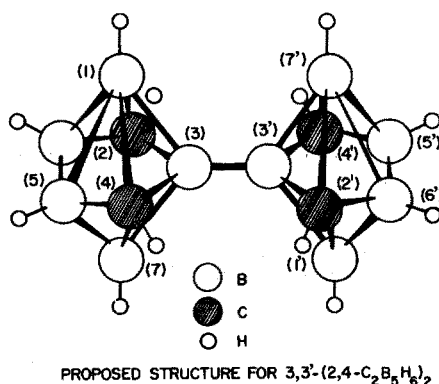
Fig. 6. Photolysis product of $C_2B_5H_7$

7

[43, 44, 113, 114, 115, 116, 117] has been especially active in this area. In general these molecular systems with organic chromophores are photochemically active in the near ultraviolet. Doty and coworkers[31a] report absorption maxima and fluorescence quantum yields for a series of p-substituted phenyldimesitylboranes. Quantum yields and Stoke's shifts are strongly dependent on the dipolar character of the solvent used. From the solvent effect it is inferred that the excited state of the borane is highly polar relative to the ground state.

Photolysis of sodium tetraphenylborate in aqueous solution with 253.7 nm radiation yields products of biphenyl and 1-phenylcyclohexa-1,4-diene as well as other dienes[113]. The yield of biphenyl was decreased when the reaction was run under nitrogen to exclude atmospheric oxygen. These hydrocarbon products were not observed when triphenylborane was irradiated at 253.7 nm under nitrogen in cyclohexane solution[114]. However, when this reaction was run under the same conditions in alcohol solutions, products similar to those observed in borate salt photolyses were obtained[116]. The solvent effect is probably a consequence of the varying capacity of basic solvents to transfer electron pairs to the borane resulting in complexes which exhibit photochemical behavior of tetra coordinate (ate-type) systems. The mechanism of the photochemical reaction of tetraphenylborate anion with singlet oxygen is believed to involve an electron transfer process from the anion to form O_2^-, not direct attack of $^1O_2$ on the borate[31]. Grisdale and coworkers have observed some interesting photochemical rearrangements of hindered tetraaryl-borates[44]. In the presence of oxygen photolysis of dimesityldiphenylborate anion yields products of 2,4,6-trimethylbiphenyl and (2,4,6-trimethyl-3-biphenylyl)-mestiylphenylborane. Eisch and coworkers[32] have also contributed to our understanding of the photochemical mechanisms in borate systems. Irradiation of sodium tetraphenylborate at 254 nm in anhydrous THF or 1,2-dimethoxyethane leads to products of diphenyl and toluene. Two pathways were proposed to account for these products. From the chemical behavior of this system with organic reagents in aprotic solvents a photochemical mechanism was proposed that involves the formation of an intermediate diphenylborate anion (a carbene analogue).

Irradiation of tribenzylborane in alcoholic solvents gives good yields of toluene. The mechanism of the reaction involves heterolytic cleavage of the benzylcarbon-boron bond[24].

IV. Boron-Nitrogen Compounds

A. Borazine

1. Spectroscopic Studies

Borazine, (-BH-NH-)$_3$, an inorganic isoelectronic analog of benzene, is the single boron compound that has been most completely investigated by photochemical techniques. An early theoretical study of the structure of borazine was made by Hoffmann[53]. A UV absorption spectrum of borazine is shown in Fig. 7. Unlike the
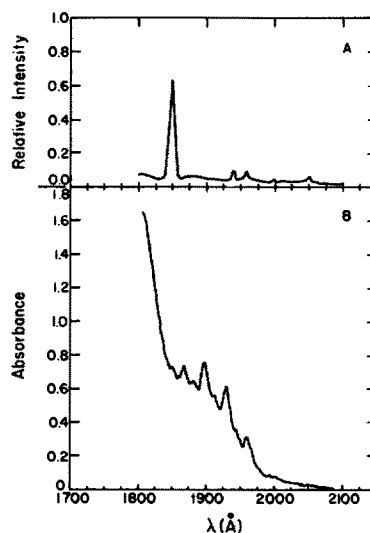
Fig. 7. Ultraviolet absorption spectrum of borazine (B). Curve A is a line spectrum from a medium pressure Hg lamp showing the location of the strong 184.9 nm line in relation to the borazine absorption spectrum

spectrum of diborane(6), the spectrum of borazine exhibits structural features. Before proceeding to the specifics of the photochemical reactions, spectral considerations based on current available physical evidence will be discussed.

The photoelectron spectrum of a molecule gives vertical ionization potentials for photoionization from molecular orbitals of various energies (Table 1). In this manner, it has been used as a convenient method for determining the position and ordering of the orbitals of a given molecule. A majority of the theoretical calculations reported on borazine — which include all valence electrons in the calculations — have suggested that the HOMO is the e'(σ). Those which consider only π electrons and some which consider both σ and π electrons have suggested that the HOMO is

Table 1. Experimental and theoretical vertical ionization potentials for borazine (eV)

	1e''(π)	4e'(σ)	a_2''(π)	3e'(σ)	$1a_2$'(σ)	$3a_1$'(σ)
Experimental						
Boch[13]	10.09	11.42	12.83	14.75	14.75	13.72
Brundle[17]	10.14	11.42				
Frost[36]	11.42	10.09	17.10	13.98	14.70	12.82
Lloyd[70]	10.14	11.42	12.06	14.76	12.83	13.84
	10.50 sh	11.73				
Theoretical						
Armstrong[4]	12.70	13.59				
Chalvet[19]	12.3					
Davies[26]	11.0	10.2	18.3	14.9	16.7	14.6
Frost[36]	10.4	9.8	17.7	14.8	16.6	14.0
Kuznesof[64]		13.72				
Peyerimhoff[85]	11.69	13.10	14.64	19.14	16.78	15.77

9

$e''(\pi)$. In 1970, two research groups independently reported the experimental photoelectron spectrum of borazine. Although both published spectra were superimposable through 16 eV, the interpretations of the data were decidedly different. Frost and co-workers[36], who based their analysis on theoretical calculations, reported that the $e'(\sigma)$ level is the HOMO. Lloyd and co-workers[70], on the other hand, used arguments based on peak contours and vibrational fine structure to interpret the spectrum in terms of an $e''(\pi)$ HOMO. In 1971, Bock and Fuss[13] published convincing arguments that the $e''(\pi)$ orbital is the HOMO. They began with the assigned orbital levels of benzene from its photoelectron spectrum. Introducing a perturbation of D_{3h} symmetry into these levels causes a mixing of molecular orbitals of like symmetry. The smaller the initial energy difference is between the two symmetry-matched orbitals, the larger the interaction. By examining benzene and borazine spectra together, Bock and Fuss were able to correlate all the borazine and benzene bands on the basis of this mixing, assigning the first borazine band at 10.09 eV to the $e''(\pi)$ orbital. Further proof of the π-assignment comes from examining halogen derivatives of borazine where lowering of the highest occupied σ level and raising of the π level is predicted theoretically. In line with this prediction, they report a 10.66 eV ionization potential for B-trifluoroborazine, $(-BF-NH-)_3$, and 10.55 eV ionization potential for B-trichloroborazine, $(-BCl-NH-)_3$.

On the basis of the ordering of the molecular orbitals, one can determine the symmetry of the low lying electronically-excited states to be $^1A_1$, $^3A_1$, $^1A_2$, $^3A_2$, $^1E'$ and $^3E'$. Transitions from the ground $^1A_1'$ state to the $^1E'$ state is dipole allowed, but transitions to all the triplet states are spin-forbidden. The $^1A_1' \leftarrow {}^1A_1$, and the $^1A_1 \leftarrow {}^1A_2'$ transitions are electric dipole-forbidden but become allowed by vibronic coupling to the $^1E'$ level. A vibration of e' or a_2'' symmetry makes the former absorption allowed, while the latter is allowed only by a vibration of e' symmetry.

Platt and coworkers[86] first recorded the UV spectrum of borazine from 225.0 to 170.0 nm in 1947. Later, an attempt was made to locate bands above 200 nm, but none were observed. Improved instrumentation led to a series of papers on the absorption spectrum of borazine in the vacuum ultraviolet. Kaldor[59] assigns the most intense absorption whose maximum occurs at 165.0 nm to the allowed $^1E' \leftarrow {}^1A_1'$ transition. He analyzes the vibrational structure of the remaining absorptions and divides them into 4 progressions: (1) 199.5, 196.1, 192.9, 187.9 and 186.7 nm; (2) 194.4, 191.3, 183.1, and 185.0 nm; (3) 186.0, 182.9 and 179.9 nm; and (4) 187.7, 184.5, and 181.4 nm. Interpreting the 199.5 nm band of the first progression as a hot band, he assigns the spacing e' symmetry. For progressions (3) and (4) the exciting vibration is not observed but the 0-0 transition for this state is estimated to be at 188.9 nm. Since Kaldor can find no active vibration of a_2'' symmetry, he cannot distinguish the $^1A_1'$ and $^1A_2'$ states on the basis of the experimental data. However, he has assigned these states according to the sequence observed for the analogous benzene states, which is also the ordering predicted by theoretical calculations.

Yanase and coworkers[118] examined the UV spectrum of borazine from 210.0 to 185.0 nm, reporting the same vibrational progressions as Kaldor. Yanase interprets the data in terms of a 0-0 transition at 198.4 nm allowed by vibrations of e' symmetry ($\nu_{17} = 525$ cm^{-1} and $\nu_{13} = 1649$ cm^{-1}). Although the latter exciting vibra-

tion is not observed experimentally, he suggests that this is due to the weakness of the singal. Despite the fact that Yanase assigns the 1984nm transition to the $^1A_2{}'$ state without consideration of whether it could also be the $^1A_1{}'$ state, his calculations of the predicted intensity of the band as a $^1A_2{}' \leftarrow {}^1A_1{}'$ transition give good agreement with the observed intensity. This location of the $^1A_2{}'$ state is in general agreement with that assigned by Kaldor.

A third analysis of the UV absorption spectrum of borazine reported by Bernstein and Reilly[12] is not in agreement with Kaldor's assignments. Bernstein interprets the first vibrational progression in the same manner as Kaldor. However, for the second progression he reports a band at 2011 nm (not observed by Kaldor) which he interprets as a ν_1 hot band of $a_2{}''$ symmetry. He identifies the 197.5 nm origin of this band as the location of the $^1A_1'$ state.

Table 2 summarizes the theoretical predictions and experimental data on the excited states of borazine. It can be noted that the three excited singlet states of borazine are closely spaced and overlap. Consider, for example, the absorption of 184.9 nm radiation by borazine. It is not clear whether the $^1A_1'$, $^1A_2'$ or $^1E'$ state is reached preferentially. There is a vibrational band at 185.0 nm assigned to the $^1A_2{}'$ state, and another one nearby at 184.5 nm assigned to the $^1A_1{}'$ state. The $^1E'$ absorption whose maximum is at 165.5 nm can be thought to begin somewhere in this region as well. Thus, one expects that the potential surface describing this region will allow for facile interconversion. This may be one of the reasons for the repeated failures to observe fluoroescence from borazine. The location of the triplet states of borazine has been studied theoretically. However, the only piece of experimental evidence for the location of a triplet state of this molecule comes from the work of

Table 2. Experimental and theoretical transition energies to the low lying excited state of borazine (eV)

	$^1A_2{}'$	$^1A_1{}'$	$^1E'$	$^3A_1{}'$	$^3A_2{}'$	$^3E'$
Experimental						
Platt[86, 58]	6.2	6.7	7.2			
Kaldor[59]	6.28	6.56	7.55			
Yanase[118]	6.25					
Kroner[63]	6.41–6.52	7.13	7.65			
Bernstein[12]	(7.0)	6.5	7.5			
Theoretical						
Chalvet[19] I	6.51	5.74	7.14	5.74	5.82	5.78
Davies[25]	5.7	6.1	8.8			
Kuznesof[64]	8.48	9.65	9.86	8.48	7.96	8.27
Perkins[84]	6.58	7.26	7.51	6.58	6.88	6.58
Peyerimhoff[85] I	6.97	8.75	9.57	6.46	8.52	7.30
II	7.88	9.01	9.59	7.93	8.05	8.33
Roothaan[93]	6.5	7.2	7.7	5.9	6.9	6.4
Young[119] I	6.51	7.80	7.30	6.03	6.51	6.05
II	6.52	7.84	7.18	5.57	6.53	5.92
Kroner[63]	6.45	7.22	7.61			

Young and coworkers[119] who showed a direct relationship between borazine pressure and the quenching of the triplet state of benzene excited at 258.0 nm. These investigators concluded that the triplet state of borazine lies at an energy not higher than 4.9 eV., which is at least 1 eV lower than the calculated values. It was further concluded that the lifetime of the borazine triplet is much shorter than the benzene triplet because of the failure of borazine to transfer its triplet energy to biacetyl. Experiments involving borazine with photoexcited biacetyl show borazine to have the effect of a vibrational quencher. Neither the singlet nor triplet emissions of biacetyl have been quenched by this molecule.

In contrast to borazine, the three corresponding excited singlet states of benzene have a much wider spread of absorbing wavelengths and exhibit easily distinguished vibrational fine structure. Many photolysis experiments have been performed using laser lines tuned to selective excite a particular vibrational level of a particular excited state of benzene. Such experiments are more difficult with borazine. The triplet states of benzene have been located experimentally and quantum yields for fluorescence and phosphorescence at various wavelengths and pressure conditions have been determined.

2. Photochemical Studies

A detailed study of the photochemistry of borazine with 184.9 nm radiation was reported by Neiss and Porter[80] in 1972. Products formed at low pressures (0.1 to 15 Torr) include H_2, borazanaphthalene, diborazinyl, and a polymer. When B-trideuterioborazine was used in the photolysis, HD was produced as the major noncondensible gas. Equimolar mixtures of borazine and borazine-d_6, irradiated for short periods produced predominantly H_2 and D_2, while those samples photolyzed for longer periods produced appreciable amounts of HD. An H-D exchange reaction at boron sites was noted. The ratio $B_3N_3D_5H/B_3N_3D_6$ was determined and used as a measure of this exchange. At low pressures, this ratio varied linearly with the total pressure, reaching a limiting value of 3 at long photolysis times. Quantum yield data from the photolysis of borazine indicates that the production of H_2 depends directly upon the amount of light absorbed by borazine and inversely upon the total pressure of the system. The limiting value of Φ_{H_2}, obtained by extrapolation to zero pressure, is 0.21. This value drops to $\Phi_{H_2} = 0.11$ at 13.5 torr (Fig. 8). The formation of a polymer was noted and found to depend linearly upon $I_a t/A$ (where $I_a t$ is the integrated intensity of light absorbed and A is the absorbance of the polymer). The addition of a low molecular weight inert gas such as H_2 or Ar decreased the production of polymer. No data were reported relative to the quantum yield for the production of H_2 when these inert gases were used. Cyclohexane vapor which is transparent to 184.9 nm light was also added in some experiments since it can provide many vibrational degrees of freedom for collisional deactivation without reacting chemically. The effect of cyclohexane addition was to decrease Φ_{H_2} and the amount of polymer produced.

Borazine + D_2. Nadler and Porter[79] reported on the photochemical exchange reaction of borazine with D_2 at 184.9 nm. Products observed include B-mono-, B-di,

Fig. 8. Data showing (*a*) the pressure dependence of the quantum yield of H_2 produced in the 184.9 nm pyrolysis of borazine and (*b*) the build-up of solid polymer during the pyrolysis reaction
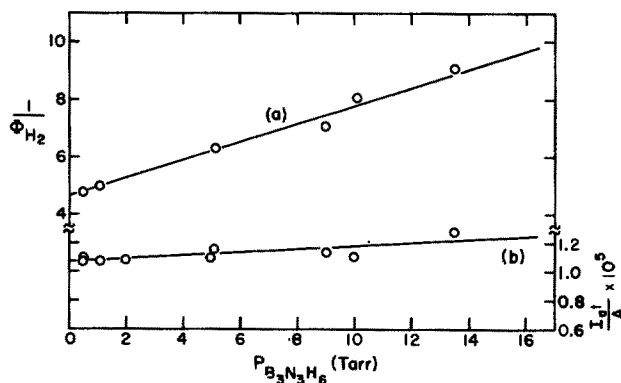
and B-trideuterioborazine as well as HD and H_2. The photolysis vessel was joined through a small pin-hole to a mass spectrometer (Fig. 2). The relative ion intensities of D_2^+ and HD^+ were monitored periodically during the photolysis, while the H_2^+ intensity was determined only at the termination. A plot (Fig. 9) of the result for initial pressures of 7.7 torr borazine and 31.3 torr D_2 shows (1) a decrease in the intensity of D_2^+ and (2) an increase in the intensity of HD^+ with the length of time of photolysis. When the photolysis reaction was limited to less than 2% exchange per boron atom, $B_3N_3H_5D$ and HD were found in equimolar quantities. Quantum yield studies were undertaken to determine the efficiency of the exchange reaction. A plot of these results is given in Fig. 10. For a fixed pressure of borazine (1 Torr) the quantum yield for exchange at 184.9 nm was found to increase with D_2 pressures,
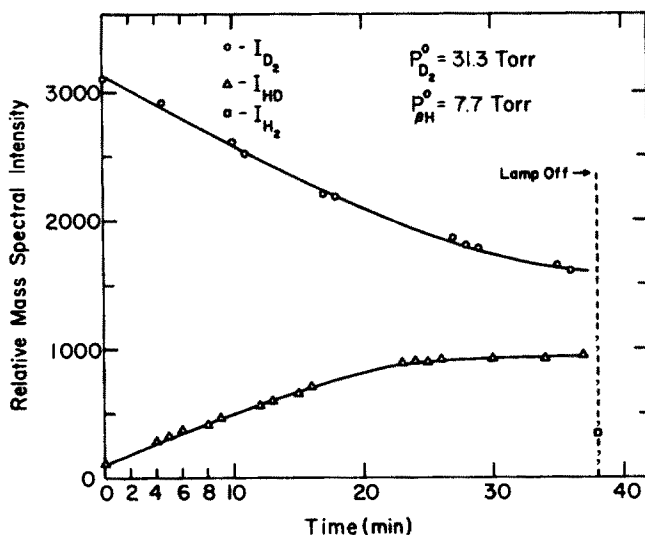

Fig. 9. Data from a mass spectrometric study of the photochemical exchange reaction of $(-BHNH-)_3$ with D_2. Initial conditions are indicated
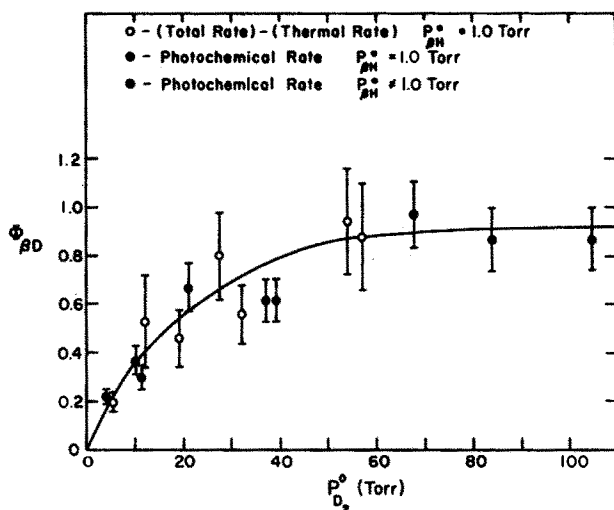
13

Fig. 10. Quantum yield dependence of the borazine-D_2 exchange reaction on the initial pressure of D_2. (The initial pressure borazine was 1.0 torr.)

approaching a limiting value of 0.93 ± 0.14 at D_2 pressures greater than 50 Torr. For a constant D_2 pressure, varying the pressure of borazine did not effect the quantum yield. However, addition of He or N_2 increased the quantum yield, while the addition of H_2 decreased the quantum yield.

The influence of mercury sensitization on the exchange rate was checked by Nadler and Turbini[103] using a Vycor filter to eliminate light absorbed by borazine. In both cases the effect of mercury-sensitized photolysis was small compared to the effect of direct photolysis.

Synthesis of B-monosubstituted Borazine Derivatives. The photolytic reaction of borazine with a second reagent is a convenient method for synthesizing a number of B-monosubstituted borazine derivatives. B-monoaminoborazine, produced in the gas phase photolysis of borazine ammonia mixtures with 184.9 nm radiation, was first synthesized by Lee and Porter[66] in 1967. This is the only method currently known for generating this compound. A detailed study of the photochemical reaction, under varying conditions of borazine and ammonia pressures, was reported by Neiss and Porter[81] in 1972. The quantum yield for the production of H_2 according to the overall Eq. (19) varies from 0.27 and 1.17 when the initial NH_3 pressures are varied from 0.1 to 7.0 Torr and the borazine pressure is maintained at 5.0 Torr (Fig. 11).

$$H_3B_3N_3H_3 + NH_3 \longrightarrow H_2NH_2B_3N_3H_3 + H_2 \tag{19}$$
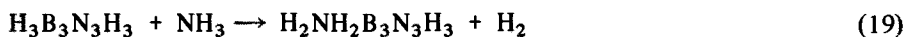
The reaction was not quenched significantly when cyclohexane was added to the photochemical mixture. A number of D and ^{15}N labeled derivatives of B-mono-aminoborazine have been reported by Yeung and Porter[88].

Several B-haloborazines have been prepared by photochemical reactions. B-monochloroborazine was prepared photochemically by Oertel and Porter[82] using a number of chlorinating reagents (HCl, CH_3Cl, $CHCl_3$, HSO_3Cl). Other synthetic methods reported for this compound and for B-monobromoborazine involve the for-
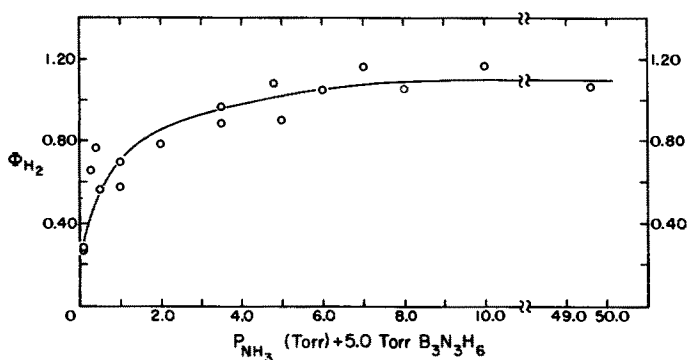
Fig. 11. Quantum yield dependence of the photochemical production of H_2 in NH_3/borazine mixtures. (The initial pressure of borazine was 5.0 torr in each experiment.) Radiation: 184.9 nm

mation of the B-dihaloborazine in addition to the B-monohaloborazine and are limited to poor yields and difficulty of separation, although Beachley has recently reported an efficient synthesis of B-monochloroborazine. No product was isolated from the photolysis of CH_3I with borazine, nor has B-iodoborazine been synthesized by any other method.

The photochemical synthesis of B-monobromoborazine by the reaction of methylbromide with borazine was initially reported by Oertel[83]. Neiss and Porter[81] extended the study of this reaction to include a determination of quantum yields. Non-condensible gaseous products from the photolysis of $B_3N_3H_6$ with CH_3Br and CH_4 and H_2. When $B_3N_3D_6$ was used as the borazine species, CH_3D and D_2 were formed, while the use of $D_3B_3N_3H_3$ gave an unexpectedly high ratio of CH_4 to CH_3D in addition to HD as the predominant hydrogenic species. B-mono-bromoborazine and borazanaphthalene (or their deuterium labelled analogs) were the condensible products formed in all cases. When large excesses of CH_3Br are present in the reaction flask, C_2H_6, B-dibromoborazine and CH_2Br_2 were observed among the photolysis products in addition to those mentioned above. Quantum yield data on the CH_3Br/borazine reaction were plotted in terms of the H_2 and CH_4 formed relative to the variations in, (a) the partial pressure of CH_3Br at a fixed borazine pressure (1 Torr); and (b) the partial pressure of borazine at a fixed CH_3Br pressure (10 Torr) (Fig. 12). At constant borazine pressure, Φ_{H_2} is fairly constant at 0.3, while Φ_{CH_4} increases with an increase in the partial pressure of CH_3Br, reaching a maximum at 25 Torr CH_3Br with $\Phi_{CH_4} = 0.74$. Further increases in CH_3Br pressures above this result in a slight decrease in the methane quantum yield which levels off around 0.6 at 200 Torr CH_3Br. In the absence of borazine, Φ_{CH_4} from CH_3Br photolysis was about 0.14. Large excesses of Xe and CO_2 had little effect on the methane quantum yield, showing only a slight decrease at low CH_3Br pressures. On the other hand, a tenfold excess of cyclohexane lowered the methane quantum yield 25% from the value obtained in its absence. I_2 was used as a radical scavenger in one experiment at high CH_3Br pressures and was found to decrease the methane quantum yield to 14% of its value in the absence of I_2. Although no quantum yield data for CH_3Cl borazine photolysis has been reported, some unpublished results
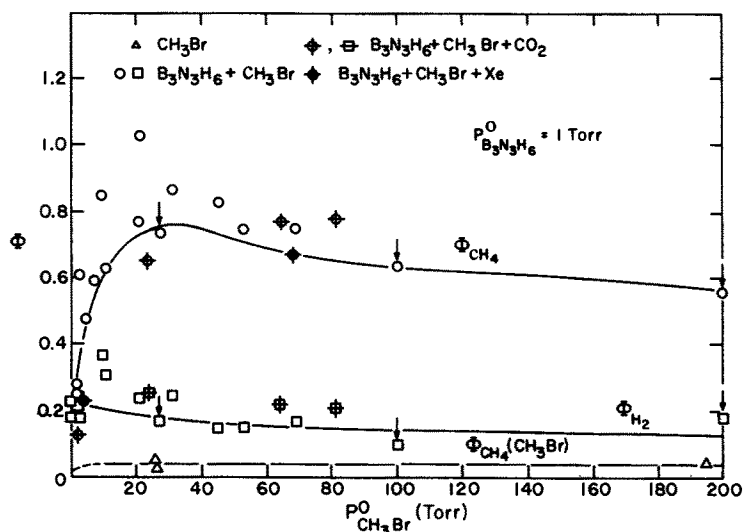
15

Fig. 12. Quantum yield data for CH_4 and H_2 production from the borazine-CH_3Br reaction. In designated runs added gases were CO_2 and Xe. Points with vertical arrows represent true 184.9 nm yields, corrected for the CH_3Br absorption at 253.7 nm

from the photolysis of bromochloromethane with borazine suggest the greater efficiency of B-mono-bromoborazine over B-monochloroborazine formation.

Several B-alkoxyborazines have been produced photochemically. Nadler and Porter[78] reported the synthesis of B-monomethoxyborazine and B-monoethoxyborazine in the 1849 nm photolysis of borazine with methanol and ethanol, respectively. To minimize the thermal reaction of borazine with alcohols, the photolysis was begun as soon as the gaseous reagents were mixed. In the CH_3OH borazine reaction, a gas phase IR cell connected to the photolysis vessel was used to monitor the disappearance of methanol. Termination of the photolysis was dependent upon the complete reaction of the alcohol. Among the photolysis products examined were B-monoalkoxyborazine, trimethoxyborane and ammonia. The latter two compounds come from the decomposition of B-trimethoxyborazine. M. Oertel[83] reports the synthesis and characterization of B-monopropoxyborazine by photolysis of borazine with propanol. B-monomethoxyborazine has also been produced photochemically in the reaction of formaldehyde with borazine. Two new alkoxyborazines,B-(2H-hexafluoro-2-propoxy)borazine and B-(perfluoro-t-butoxy)borazine, have also been reported[106]. These derivatives are formed in the photolysis of borazine with hexafluoroacetone (HFA) using the full light of the mercury lamp, with Vycor or Corex filters. Product identification was verified by photolysis of the appropriate alcohol (2H-hexafluoroisopropanol and perfluoro-t-butanol respectively) with borazine using 184.9 nm radiation. When B-trideuterioborazine was used in the photolysis, product (1) was formed as the isotopic B-(2D-hexafluoro-2-propoxy)deuterioborazine. A third product of the HFA/borazine photolysis whose relative proportions was dependent upon the HFA concentration was identified as $B[OCH(CF_3)_2]_3$; hexafluoroethane was also found among the products.

The photochemical reactions of borazine with oxygen and with water were studied in 1967[66]. The oxygen photolysis reaction produced B-monohydroxyborazine when borazine was present in excess and diborazinyl when O_2 was present in excess. Diborazinyl ether is also produced in the 184.9 nm photolysis of borazine with water. This latter reaction is very efficient and diborazinyl ether is often formed in photolysis reactions whenever small amounts of water are present.

Observation of the list of borazine derivatives produced photochemically (Table 3) reveals that all of the reagents yielding photochemical products have an electronegative element (either O,N,F,Cl, or Br) which substitutes at the boron site. No B-C bonds have been formed photochemically, even when, as in the CH_3Br and the HFA reactions, methyl or perfluoromethyl radicals are present. Also, no B-C bonded compounds were formed when borazine was photolyzed with benzene, pyridine, cyclopentadiene, allene, ketene, acetylene, or acetone.

3. Mechanistic Consideration

From numerous observations on the photochemical behavior of borazine in the presence and in the absence of a second reagent, there appears to be two distinct photochemical pathways. The studies of Neiss and Porter[80] on pure borazine indicate a concerted type process in which an excited borazine molecule eliminates a molecule of hydrogen from adjacent boron-nitrogen sites. However, that process only accounts for about 20% of the absorbed radiation. On the other hand, the photo-

Table 3. Compounds synthesized by photochemical reactions of borazine

Reagent	Photochemical product	Mechanism[1]	Ref.
1. None	H_2, borazanaphthalene, diborazinyl, polymer	A	80) 2)
2. D_2	$H_3N_3B_3D_3$	A, B	79) 2)
3. (a) $NH_3(ND_3)$	$H_3N_3B_3H_2NH_2(ND_2)$	A, B	66, 88, 81) 2)
(b) NH_2CH_3	$H_3N_3B_3H_2NHCH_3$	A, B	3)
(c) $NH(CH_3)_2$	$H_3N_3B_3H_2N(CH_3)_2$	A, B	3)
4. H_2O, O_2	$H_3N_3B_3H_2OH$, $(H_3N_3B_3H_2)O$	B	66)
5. (a) CH_3OH	$H_3N_3B_3H_2OCH_3$	A	78)
(b) C_2H_5OH	$H_3N_3B_3H_2OC_2H_5$	A	78)
(c) $n\text{-}C_3H_7OH$	$H_3N_3B_3H_2OC_3H_7$	A	83)
6. (a) CH_3Cl	$H_3N_3B_3H_2Cl$	A	82)
(b) CH_3Br	$H_3N_3B_3H_2Br$	A	81) 2)
7. CF_3COCF_3	$H_3N_3B_3H_2OCH(CF_3)_2$, $H_3N_3B_3H_2OC(CF_3)3$		106)

1) Mechanism A involves excited $H_3N_3B_3H_3$; mechanism B probably involves the radical $H_3N_3B_3H_2$
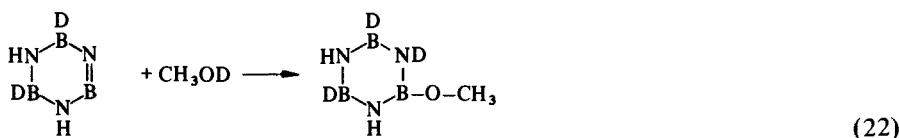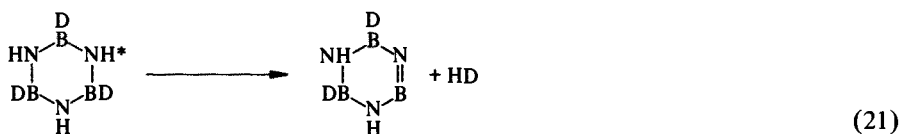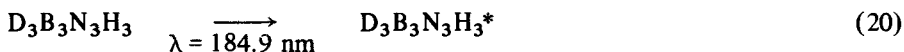2) Quantum yield data available on these reactions
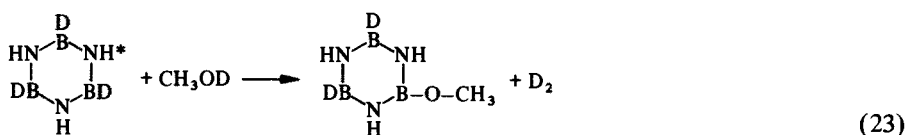3) Procedure given in Ph. D. Thesis of M. Neiss, Cornell University (1971)

chemical yields of borazine for most systems studied, approach unity as the partial pressure of the second reagent is increased. Thus, two types of photochemical processes are proposed. The photochemical mechanism suggested by Neiss and Porter involves excitation of borazine with 184.9 nm radiation, internal conversion to a longer-lived excited state, which is postulated to be a vibrationally excited ground state molecule and collisional quenching of excited borazine or the elimination of H_2 to produce a borazyne intermediate
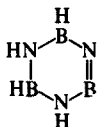

This intermediate then reacts rapidly with another borazine molecule to produce borazanaphthalene and a very reactive species, HBNH, which goes on to form polymer. Evidence for intramolecular elimination of hydrogen is based on (a) the loss of HD in the photolysis of $D_3B_3N_3H_3$; and (b) the loss of H_2 and D_2 for short reaction times in the photolysis of a mixture of $H_3B_3N_3H_3$ and $D_3B_3N_3D_3$. The increase in the relative amount of HD after photolyzing this mixture for longer periods of time results from the exchange reaction occurring at the boron site. As the concentration of $B_3N_3H_5D$ and $B_3N_3D_5H$ build up, the loss of HD from one of these molecules becomes observeable. A free radical mechanism for formation is ruled out by the lack of a statistical distribution of HD as well as by previous studies by Nadler and Porter. Further evidence for the intramolecular formation of a borazyne intermediate is seen in the inverse pressure dependence of the reaction and in the polymer build-up which has been shown to be linearly related to the total integrated intensity of the light absorbed by borazine.

A separate experiment has been reported which lends further support to the existence of a borazyne intermediate. Turbini[102] has photolyzed borazine with CD_3OD (a common benzyne scavenger) and has shown the presence of a deuterium label on the nitrogen in some of the photochemical product, ortho-$(CD_3O)D_2B_3N_3H_2D$. The following reaction sequences were proposed.
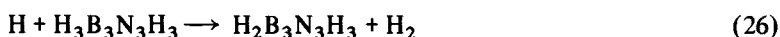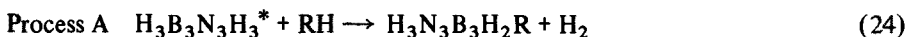
$$D_3B_3N_3H_3 \xrightarrow[\lambda = 184.9 \text{ nm}]{} D_3B_3N_3H_3^* \tag{20}$$

$$\tag{21}$$

$$\tag{22}$$

18

$$\begin{array}{c}\text{(borazine structure with D, HN, NH*, DB, BD, N, H)} + CH_3OD \longrightarrow \text{(borazine structure with D, HN, NH, DB, B-O-CH}_3\text{, N, H)} + D_2\end{array}$$

$$(23)$$

The proportion of products from reactions 22 and 23 were obtained mass spectrometrically. In this experiment the reaction to form borazanaphthalene

$$\text{(borazine structure)} + \text{(borazine structure)} \longrightarrow \text{(borazanaphthalene structure)} + \text{(DBNH)}$$
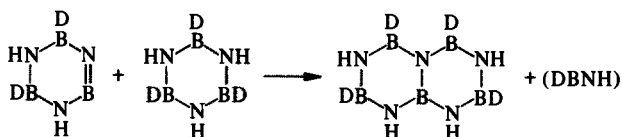
was suppressed indicating that CH_3OD was an effective scavenger for borazyne.

The photolysis reaction of borazine with a second reagent can be classified on the basis of two types of bimolecular processes. In process A, borazine is the photochemical reagent, and the products are formed by bimolecular exchange reactions between an excited borazine molecule and the second reagent. The preparation of a large number of B-substituted borazines is linked to this type of process (Table 3). In process B, the photochemical reagent is a species other than borazine, as for example in the reaction of ammonia with borazine.

Process A $\quad H_3B_3N_3H_3^* + RH \longrightarrow H_3N_3B_3H_2R + H_2$ $\hspace{3cm}$ (24)

Process B $\quad RH \xrightarrow{h\nu} R + H$ $\hspace{4.5cm}$ (25)

$\hspace{2cm} H + H_3B_3N_3H_3 \longrightarrow H_2B_3N_3H_3 + H_2$ $\hspace{2.3cm}$ (26)

$\hspace{2cm} H_2B_3N_3H_3 + R \longrightarrow RH_2B_3N_3H_3$ $\hspace{3.2cm}$ (27)

4. Comparisons of Borazine and Benzene Photochemistry

The photochemistry of borazine delineated in detail in these pages stands in sharp contrast to that of benzene. The present data on borazine photochemistry shows that similarities between the two compounds are minimal. This is due in large part to the polar nature of the BN bond in borazine relative to the non-polar CC bond in benzene. Irradiation of benzene in the gas phase produces valence isomerization to fulvene and 1,3-hexadien-5-ynes[111]. Fluorescence and phosphorescence have been observed from benzene[57]. In contrast, fluorescence or phosphorescence has not been found from borazine, despite numerous attempts to observe it. Product formation results from a borazine intermediate (produced photochemically) which reacts with another borazine molecule to form borazanaphthalene and a polymer. While benzene shows polymer formation, the benzyne intermediate is not known to be formed from photolysis of benzene, but rather from photolysis of substituted derivatives such as 1,2-diiodobenzene[54].

One common feature does exist between the photolysis of borazine and of benzene in the absence of a second reagent; that is the observation of a ring rupture in the matrix isolated species[76]. For benzene, the product is hexatriene diradical, while in the case of borazine, the product has not been identified completely. IR data show it to involve a ring-opening with some loss of hydrogen, leaving B-N triple bonds and a terminal NB moiety[73].

Reagents which are active upon irradiation with benzene are olefins and dienes[18]. None of these react photochemically with borazine. Recently, the photolysis of benzene at $\lambda = 184.9$ nm with D_2 has been shown to produce a small amount of C_6H_5D ($\Phi = 0.01$)[51]. This is contrast to the very efficient deuteration at the boron site of borazine ($\Phi = 0.90$). Hexafluoroacetone as the absorbing species reacts with borazine to produce a B-alkoxyborazine substitution product. Reaction of this reagent with benzene, on the other hand, involves the CF_3 radicals and the products are addition rather than substitution products[20, 21, 55].

B. Alkylborazines

An upsurge of interest in the N-methylborazines in the early 1970's was coupled with a convenient method of synthesis and purification for these compounds[10]. The photoelectron spectrum of N-trimethylborazine has been reported. Table 6 summarizes the theoretical and experimental data comparing the location of the molecular orbitals of N-trimethylborazine with those of borazine. The HOMO is predicted and observed to be an e'' (π) orbital as in borazine[13]. The methyl substitution on nitrogen destabilizes the e'' and the a_2'' π-orbitals, but does not significantly effect the e' (σ) orbital. The result is a lowering of the ionization potential for electrons in the two π-orbitals. This effect, predicted in the theoretical calculations, was also verified experimentally.

The gas phase UV spectrum of N-trimethylborazine has been reported from 250.0 nm to 120.0 nm[63]. Table 4 lists the theoretical and experimental data on the location

Table 4. Electronic transitions to the excited states of N-trimethylborazine (compared with borazine) (eV)

| Borazine	Ref.	$^1A_2'$	$^1A_1'$	$^1E'$	$^3A_2'$	$^3A_1'$	$^3E'$
	59)	6.28	6.56	7.65			
N-Trimethylborazine	Ref.	$^1A_2'$	$^1A_1'$	$^1E'$	$^3A_2$	$^3A_1$	^3E
Experiment	63)	5.63–5.74	6.17	6.66			
		5.5	5.7	6.5			
Theory	64)	7.50	8.37	8.58	7.50	7.20	7.35
	84)	5.11	5.46	5.93	5.11	5.11	5.08
	27) (I)	5.81	6.48	6.66	5.49	5.69	5.81
	(II)	5.75	6.00	6.32	5.53	5.73	5.75
	(III)	·5.75	6.43	6.59	5.40	5.63	5.75

Table 5. The theoretical and experimental vertical ionization potentials of N-trimethylborazine compared with borazine (eV)

Borazine	1e"	4e'	1a$_2$"	3a$_1$"	3e"	1a$_2$'
	10.09	11.40	12.83	13.72	14.75	
N-Trimethylborazine	2e"	2a$_2$"	6e'	2a$_2$'	5e'	4a$_1$'
Experiment[1]	8.99	11.1	11.45	12.38	13.00	14.10
Theory	9.10	11.29	10.61	11.76	13.29	14.28
Experiment[2]	9.28	11.14		11.48		
Theory	9.31	9.88		11.92		

[1] Ref. [63]
[2] Ref. [71]

of the various low lying singlet and triplet states of the molecule while Table 5 is a correlation of photoelectron data. One notes that the spectrum of N-trimethylborazine, while similar in form to that of borazine is red shifted by 30.0 nm. There is no experimental evidence for the location of the triplet state. Desjardins and co-workers[27] have shown that N-trimethylborazine quenches the singlet state of benzene excited at 267.0 nm. This would imply that the singlet state is at most 4.7 eV above the ground state, i. e., 1 eV lower than predicted by calculations. It was tentatively concluded that the singlet state of N-trimethylborazine, and the triplet state of borazine involved in quenching the excited benzene species, are not planar. No fluorescence or phosphorescence has been observed for N-trimethylborazine. It shows the characteristics of a vibrational quencher when tested with photo-excited biacetyl. In order to probe the effect of the methyl substituent on the photochemistry of borazine, Turbini and Porter[105] studied the photochemical reactions of these N-methylborazines. Initially, N-methylborazine was photolyzed in the absence of a second reagent and the resultant products were compared with those from borazine photolysis. H_2 and CH_4 as well as borazanaphthalene, N-methylborazanaphthalene, and N-dimethylborazanaphthalene were formed. All of these products can be related to a borazyne or a N-methylborazyne intermediate reacting with the borazine precursor.

$$\text{N-methylborazine} \xrightarrow{h\nu} \text{borazyne} + CH_4 \tag{28}$$

$$\text{N-methylborazine} \xrightarrow{h\nu} \text{N-methylborazyne} + H_2 \tag{29}$$
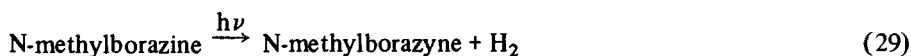
The results of the photolysis of N-methylborazine at pressures of 2 Torr and 5 Torr showed that the production of H_2 was favored over the production of CH_4, implying that N-methylborazyne is the more stable borazyne product. We note that the ratio $H_2:CH_4$ increased when the photolysis pressure of N-methylborazine was increased, while the production of borazanaphthalene decreased considerably. This fact is related to the decrease in the borazyne intermediate produced at higher pressures. A disproportionation was noted in the photolysis of N-methylborazine,

yielding borazine and N-dimethylborazine. This is postulated to occur from the vibrationally excited ground state of N-methylborazine.
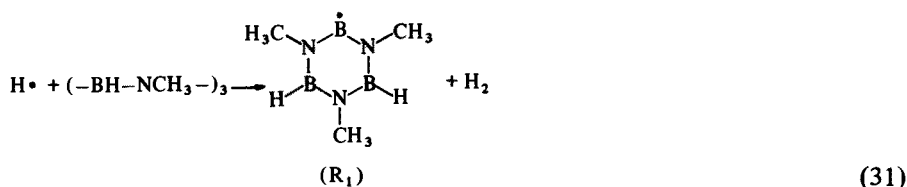
The photolysis of N-methylborazine in the presence of ammonia produced B-amino-N-methylborazine. The major isomer in this reaction, e., the ortho isomer, was identified by labeling the ring nitrogens of N-methylborazine with ^{15}N and observing the ^1H NMR spectrum of the photolysis product[104]. Both N-methylborazine and ammonia absorb 184.9 nm radiation (ϵ_{NH_3} = 1210 l mole cm; $\epsilon_{H_3B_3N_3H_2 (CH_3)}$ = 4100) with ammonia producing NH_2 and H radicals. In those reactions where N-methylborazine absorbed the major fraction of the light, over 90% of the product was the ortho isomer. This suggests that excited $H_3B_3N_3H_2(CH_3)$ leads to ortho substitution. The relative amount of para isomer is probably due to the displacement reaction of NH_2 radicals which occurs in a statistical fashion.

Photolysis of N-methylborazine with CH_3OH (ϵ = 100) yielded 67% ortho substituted product while the reaction with $HN(CH_3)_2$ yielded over 90% para product. These results are explained by sterically hindered attack of the CH_3OH and $HN(CH_3)_2$ at the ortho site. A lower energy barrier is also postulated to explain the statistical distribution of products in the CH_3OH + N-methylborazine reaction.

Theoretical studies on N-methylborazine and N-dimethylborazine predict an electron-density on the boron atoms adjacent to the N-methyl group which is greater than that for the parent borazine molecule. This fact would lead to the expectation that para substitution is favored in the reaction of photoexcited N-methylborazine with ammonia, due to the lower electron density at the para site. However, ^{11}B NMR data and ^1H-^{15}N coupling constant results[104] predict a lower electron density at the ortho site. The photochemical results are in accord with this latter prediction. Beachley[11] produced 70% para B-chloro-N-methylborazine in the substitution reaction of $HgCl_2$ with N-methylborazine in isopentane solution. Because this reaction has been shown to occur by a bimolecular exchange mechanism, these results can be explained by steric factors in the same manner as the $HN(CH_3)_2$ and CH_3OH photochemical results.

When N-dimethylborazine was photolyzed with ammonia, NMR data revealed that 60% of the B-amino-N-dimethylborazine showed substitution between the two N-methyl groups[105]. This is consistent with the proposed mechanism.
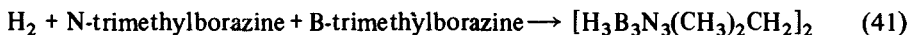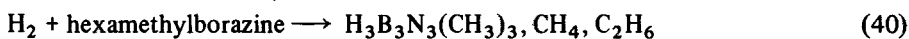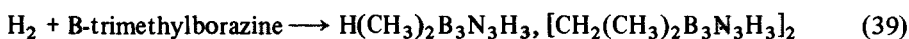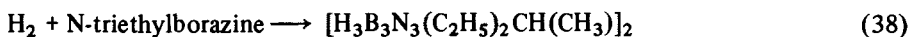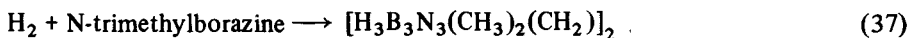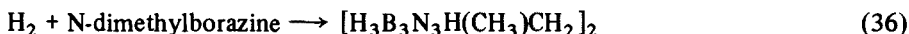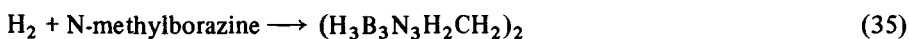
Photolysis of N-trimethylborazine with H_2 yields a crystalline product, identified as 1,2-di(3',5'-dimethylborazinyl)ethane[107]. The following radical mechanism, involving Hg-sensitization is used to explain the photochemistry

$$H_2 \xrightarrow[Hg]{h\nu} 2H \tag{30}$$

$$H\cdot + (-BH-NCH_3-)_3 \longrightarrow (R_1) + H_2 \tag{31}$$

$$H\cdot + (-BH-NCH_3-)_3 \longrightarrow \underset{(R_2)}{\text{[structure]}} + H_2 \tag{32}$$

$$R_1 + (-BH\text{-}NCH_3-)_3 \longrightarrow R_2 + (-BH\text{-}NCH_3-)_3 \tag{33}$$

$$2R_2 \longrightarrow R_2-R_2 \tag{34}$$
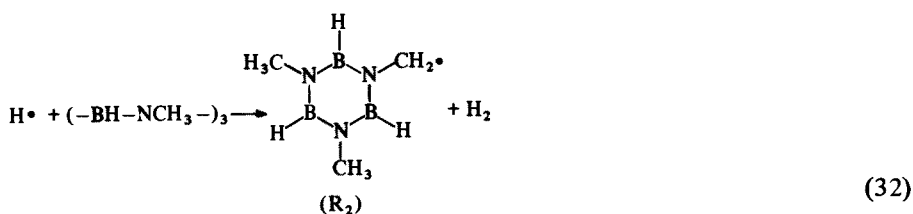
A similar radical mechanism also explains the products of NH_3 + N-trimethyl-borazine photolysis, i. e., 1,3,5-trimethyl-2-aminoborazine, bis(1,3,5-trimethylbora-zinyl)amine, and (1,3,5-trimethylborazinyl-1',3',5'-trimethyl-2'aminoborazinyl)-amine.

Recently, Kline and Porter[60] have investigated the Hg-sensitization at other alkylborazines, including B-trimethylborazine, N-triethylborazine, and hexamethyl-borazine. The results are summarized in the reactions below:

$$H_2 + \text{N-methylborazine} \longrightarrow (H_3B_3N_3H_2CH_2)_2 \tag{35}$$

$$H_2 + \text{N-dimethylborazine} \longrightarrow [H_3B_3N_3H(CH_3)CH_2]_2 \tag{36}$$

$$H_2 + \text{N-trimethylborazine} \longrightarrow [H_3B_3N_3(CH_3)_2(CH_2)]_2 \tag{37}$$

$$H_2 + \text{N-triethylborazine} \longrightarrow [H_3B_3N_3(C_2H_5)_2CH(CH_3)]_2 \tag{38}$$

$$H_2 + \text{B-trimethylborazine} \longrightarrow H(CH_3)_2B_3N_3H_3, [CH_2(CH_3)_2B_3N_3H_3]_2 \tag{39}$$

$$H_2 + \text{hexamethylborazine} \longrightarrow H_3B_3N_3(CH_3)_3, CH_4, C_2H_6 \tag{40}$$

$$H_2 + \text{N-trimethylborazine} + \text{B-trimethylborazine} \longrightarrow [H_3B_3N_3(CH_3)_2CH_2]_2 \tag{41}$$

C. Other Boron Nitrogen Systems

Hancock and coworkers have studied the photochemistry of a series of compounds in which the -B=N- functional group is the essential chromophore[45-49, 108]. The -B=N- linkage in aminoboranes is analogous to the isoelectronic (-C=C-) ethylenic linkage in molecules studied extensively by organic photochemists. Many amino-boranes absorb radiation in the near ultraviolet. Fluorescence spectra have been reported for a number of compounds with the general formula

$$\underset{R_2}{\overset{R_1}{>}}B{=}N\underset{R_4}{\overset{R_3}{<}} \quad \text{(III)}$$
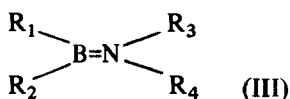
where one of the substituents is an aromatic group[49]. The band assignments for these molecules are comparable to those for the isoelectronic styrene species. The Eastman Kodak group[40] obtained absorption and fluorescence spectra for a series of aminoboranes with R_1 = phenyl, R_2 = R_4 = mesityl and R_3 variable. The dependence of fluorescence wavelength on solvent polarity was interpreted as an indication of the dipolar nature (-B-N-) of the first excited state of the borazene molecule. Photolysis of III involves mechanisms of oxidative photocyclization and methyl rearrangement,

(42)

and

(43)
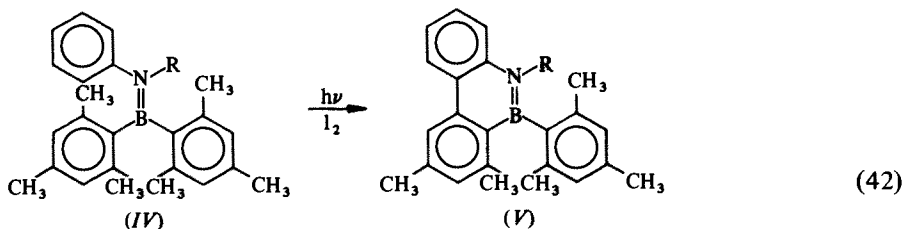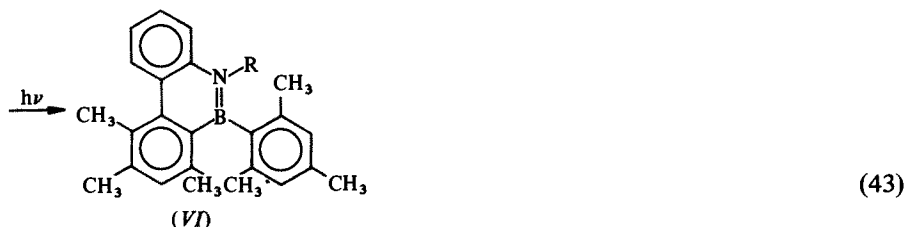
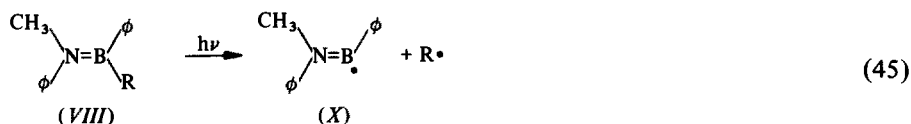Müller and Niedenzu[77] used a photochemical procedure to synthesize VII
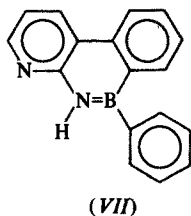
by irradiating a mixture of 2-aminopyridine and diphenylchloroborane in cyclohexane solution in the presence of iodine.
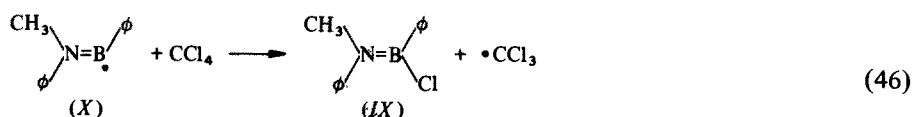
Several types of photochemical mechanisms in borazene systems have been observed. In oxygen free CCl_4 solution VIII is converted to IX[46]

(44)
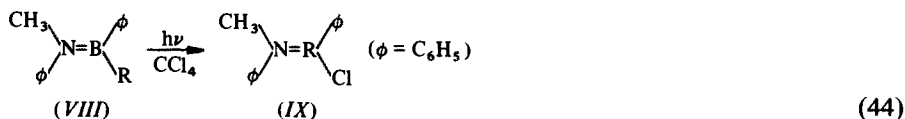
Secondary reaction products include R-R, $R-CCl_3$ and R-Cl. The primary photo-chemical step is believed to involve radical formation at a B site,
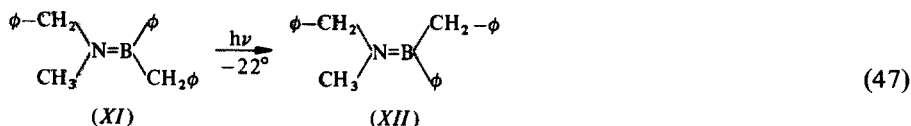
$$
\begin{array}{c}
CH_3 \\
 \diagdown \\
 N=B \\
\phi \diagup \diagdown R \\
(VIII)
\end{array}
\quad \xrightarrow{h\nu} \quad
\begin{array}{c}
CH_3 \\
 \diagdown \\
 N=B \\
\phi \diagup \bullet \\
(X)
\end{array}
\; + \; R\bullet
\tag{45}
$$

and IX is formed in the subsequent process

$$
\begin{array}{c}
CH_3 \\
 \diagdown \\
 N=B \\
\phi \diagup \bullet \\
(X)
\end{array}
+ CCl_4 \longrightarrow
\begin{array}{c}
CH_3 \\
 \diagdown \\
 N=B \\
\phi \diagup \diagdown Cl \\
(IX)
\end{array}
+ \; \bullet CCl_3
\tag{46}
$$

Radical recomination of X and $\cdot CCl_3$ occurs but dimerization of X to form a B-B bonded product is not observed. The quantum efficiency of reaction (44) increases with a substituent effect in the direction $R = \cdot CH_2\phi > iC_3H_7 > C_2H_5$.

Related studies[45a)] indicated that cis-trans isomerization about a B=N bond may be promoted by a photochemical process. At low temperatures the process

$$
\begin{array}{c}
\phi-CH_2 \\
 \diagdown \\
 N=B \\
CH_3 \diagup \diagdown CH_2\phi \\
(XI)
\end{array}
\quad \xrightarrow[-22^\circ]{h\nu} \quad
\begin{array}{c}
\phi-CH_2 \\
 \diagdown CH_2-\phi \\
 N=B \\
CH_3 \diagup \diagdown \phi \\
(XII)
\end{array}
\tag{47}
$$

was observed. This photoinduced rotation, which is not quenched by piperylene, is believed to involve an excited singlet state.

A third photochemical mechanism observed by Hancock and Kramer[47)] involves methyl migration,

$$
\begin{array}{c}
\phi CH_3 \\
 \diagdown \diagup \\
 B=N \\
CH_3-C-H \diagdown CH_3 \\
 | \\
 HC=CH_2 \\
(XIII)
\end{array}
\quad \underset{cyclohexane}{\overset{h\nu}{\rightleftharpoons}} \quad
\begin{array}{c}
\phi CH_3 \\
 \diagdown \diagup \\
 B=N \\
HCH H \diagdown CH_3 \\
 | \\
 HC=C \\
 | \\
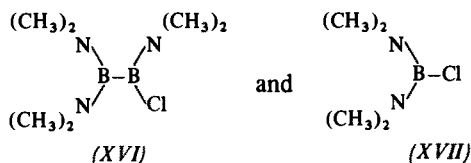 CH_3 \\
(XIV)
\end{array}
\tag{48}
$$
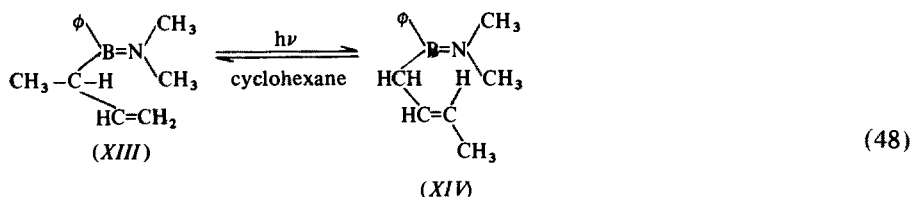
leading to the more thermodynamically stable isomer, XIV. A photochemically stationary state is reached after several hours or irradiation leading to a final composition $(XIV):(XIII) = 1:2$.
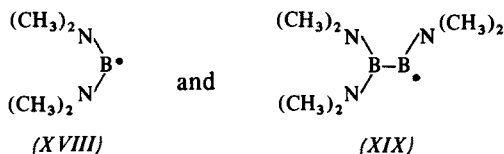
Photolysis studies[48)] of the B-B linked species

$$
\begin{array}{c}
(CH_3)_2N N(CH_3)_2 \\
 \diagdown \diagup \\
 B-B \\
(CH_3)_2N \diagup \diagdown N(CH_3)_2 \\
(XV)
\end{array}
$$
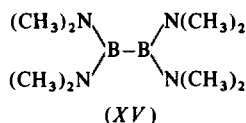
in CCl$_4$ solution leads to

$$(XVI) \qquad \text{and} \qquad (XVII)$$

The chemistry can be interpreted on the basis of competing processes leading to formation of free radial intermediates:

$$(XVIII) \qquad \text{and} \qquad (XIX)$$

V. Boron-Oxygen Compounds

Little experimental data on the photochemistry of compounds with B—O bonds have been reported. Boron-hydride/oxygen mixtures are explosive. These explosions can be initiated by photochemical processes. Grimm and Porter[41] have studied the photochemical decomposition of $H_2B_2O_3$ using a low pressure mercury lamp. The UV spectrum of this compound is illustrated in Fig. 13. The rate of the reaction was increased when mercury was present as a photosensitizer.

$$H-B \underset{O-O}{\overset{O}{\diagup \diagdown}} B-H \xrightarrow{\lambda = 184.9nm} B_2O_3(s) + H_2 \qquad (49)$$
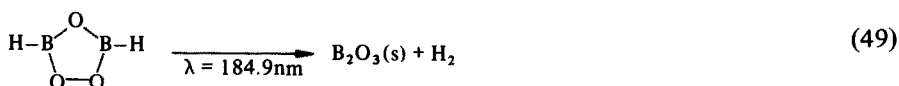
The presence of diborane(6) in the photochemical vessel resulted in the production of boroxine, (-BH-O-)$_3$:

$$H_2B_2O_3 + 0.5B_2H_6 \longrightarrow (-BH-O-)_3 + H_2 \qquad (50)$$
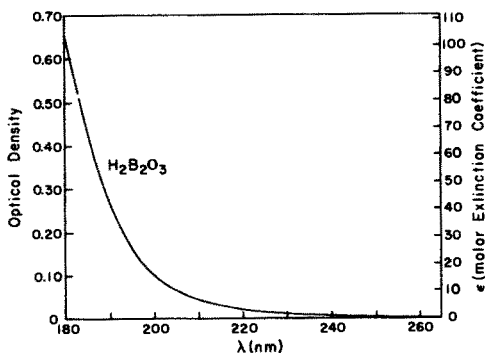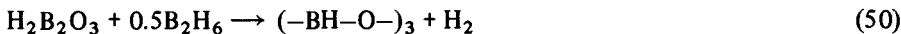
Fig. 13. Ultraviolet absorption spectrum of $H_2B_2O_3$(g)
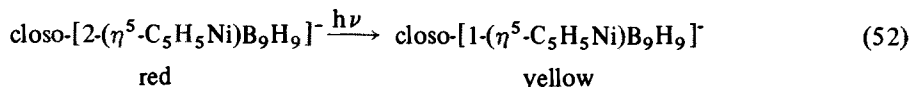
Experiments with (^{18}O)-labelled $H_2B_2O_3$ indicate that the mechanism for this reaction involves fragmentation of the $H_2B_2O_3$ molecule and subsequent reaction of these fragments with the B_2H_6. This observation was also supported by matrix isolation studies discussed subsequently[72].

VI. Boron-Metal Compounds

Some interesting photochemical reactions involving metalloboranes and metallocarboranes have been reported. These include synthesis, isomerization and complexation reactions. Gaines and Hildebrandt[37] have used the following process to synthesize a metalloborane:

$$(\eta^5\text{-}C_5H_5)Fe(CO)_2I \xrightarrow[B_3H_8]{h\nu} (\eta^5\text{-}C_5H_5)Fe(CO)B_3H_8 \qquad (51)$$
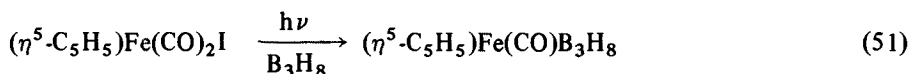
They have also demonstrated a reversible photochemical conversion from a tridentate to a bidentate B_3H_8 (Fig. 14). Fehlner[33] has achieved a photochemical carborane synthesis by irradiating mixtures of $B_4H_8Fe(CO)_3$ and dimethylacetylene. Products of the reactions include $(CH_3)_4C_4B_4H_4$ and $(CH_3)_6C_6B_4H_4$. Leyden and coworkers[67] have observed two examples of metalloborane isomerization reactions initiated by light:

$$\text{closo-}[2\text{-}(\eta^5\text{-}C_5H_5Ni)B_9H_9]^- \xrightarrow{h\nu} \text{closo-}[1\text{-}(\eta^5\text{-}C_5H_5Ni)B_9H_9]^- \qquad (52)$$
$$\qquad\qquad \text{red} \qquad\qquad\qquad\qquad\qquad \text{yellow}$$

$$\text{closo-}[1\text{-}(\eta^5\text{-}C_5H_5Ni)B_9Cl_9]^- \xrightarrow{h\nu} \text{closo-}[2\text{-}(\eta^5\text{-}C_5H_5Ni)B_9Cl_9]^- \qquad (53)$$
$$\qquad\qquad \text{yellow} \qquad\qquad\qquad\qquad\qquad \text{green}$$
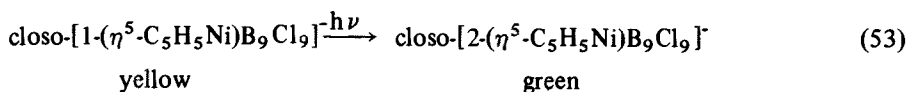
Franz and coworkers[34] reported the photochemical synthesis of a metalloborane from a carborane and $Fe(CO)_5$ (reaction 54).
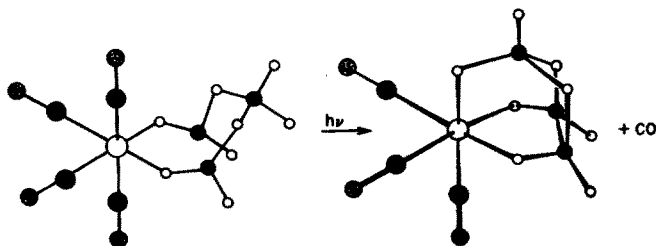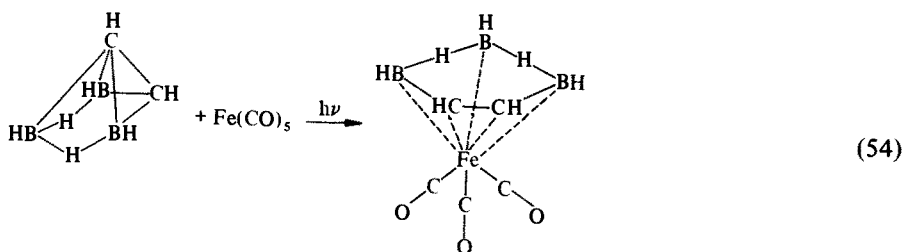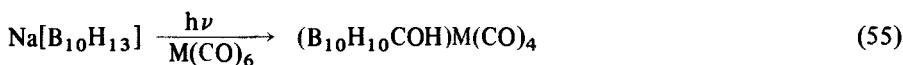

Fig. 14. Photochemical conversion of $Fe(CO)_4B_3H_8$ to $Fe(CO)_3B_3H_8$
Open circles = Fe; Closed circles = C; Lined circles = B; $\circ$ = H; Dotted circles = O

$$(54)$$

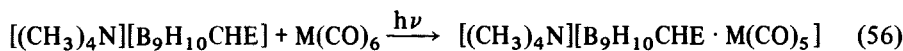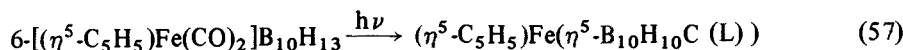while Wegner and coworkers[112] have synthesized a series of metalloboranes through the reaction

$$Na[B_{10}H_{13}] \xrightarrow[M(CO)_6]{h\nu} (B_{10}H_{10}COH)M(CO)_4 \qquad (55)$$

where M = Cr, Mo, W

Finally, two complexation reactions have been reported[97, 94]:

$$[(CH_3)_4N][B_9H_{10}CHE] + M(CO)_6 \xrightarrow{h\nu} [(CH_3)_4N][B_9H_{10}CHE \cdot M(CO)_5] \quad (56)$$

where E = P or As, M = Cr, Mo, W

and

$$6\text{-}[(\eta^5\text{-}C_5H_5)Fe(CO)_2]B_{10}H_{13} \xrightarrow{h\nu} (\eta^5\text{-}C_5H_5)Fe(\eta^5\text{-}B_{10}H_{10}C\ (L)\ ) \qquad (57)$$

whe :e the Lewis base L is THF or diethyl ether.

VII. Other Studies

A. Matrix Isolation Studies

Matrix isolation spectroscopy is a powerful technique for identifying unstable products of photodissociation reactions. The small number of boron compounds investigated by this procedure include trioxaborolane, amine-borane and borazine.

Trioxaborolane, $H_2B_2O_3$

The photodecomposition products of $H_2B_2O_3$ have been observed in argon matrices[72]. The spectra in Fig. 15 were obtained by irradiating a gaseous sample while it was codeposited with argon at 5 K. A xenon resonance lamp was used to provide radiation at 148 nm. The same infrared spectrum can be obtained by irradiating an argon matrix containing $H_2B_2O_3$. A listing of absorption frequencies is given
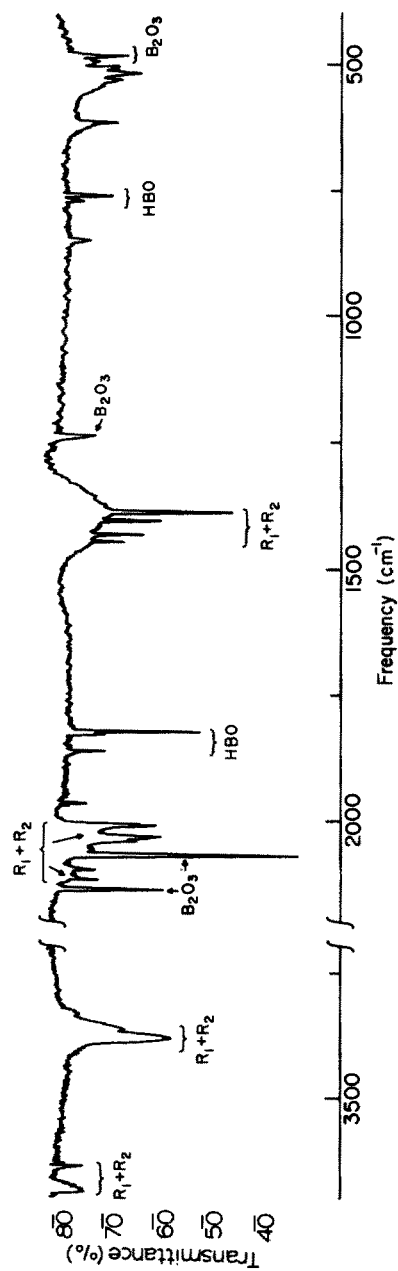
Fig. 15. Infrared spectrum of matrix isolated products from the 148 nm photolysis of $H_2B_2O_3$ in solid argon

Table 6.

Photolysis precursor $H_2{}^nB_2O_3$		Photolysis precursor $D_2{}^nB_2O_3$	
Frequency (cm^{-1})	Isolated species	Frequency	Isolated species
3681	R_1	2720	R_1
3631	R_2	2683	R_2
3375	R_1	2506	R_1
3360	R_2	2495	R_2
		2303(ν_1)	$D^{10}BO$
		2259(ν_1)	$D^{11}BO$
2130	$B_2O_3(^{10}B)$	2130	$B_2O_3(^{10}B)$
2110	$R_1(^{10}B)$	2104	$R_1(^{10}B)$
2090	$R_2(^{10}B)$	–	–
2063	$B_2O_3(^{11}B)$	2063	$B_2O_3(^{11}B)$
2025	$R_1(^{11}B)$	2012	$R_1(^{11}B)$
2002	$R_2(^{11}B)$	–	–
1855(ν_2)	$H^{10}BO$	1663(ν_2)	$D^{10}BO$
1817(ν_2)	$H^{11}BO$	1648(ν_2)	$D^{11}BO$
1441	$R_1(^{10}B)$	1420	$R_1(^{10}B)$
1426	$R_2(^{10}B)$	1405	$R_2(^{10}B)$
1400	$R_1(^{11}B)$	1377	$R_1(^{11}B)$
1383	$R_2(^{11}B)$	1364	$R_2(^{11}B)$
1230	B_2O_3		
764(ν_3)	$H^{10}BO$	617(ν_3)	$D^{10}BO$
754(ν_3)	$H^{11}BO$	606(ν_3)	$D^{11}BO$
490	$B_2O_3(^{10}B)$		
47⁻	$B_2O_3(^{11}B)$		

in Table 6. The decomposition products include B_2O_3, a hydrogen bonded species and HBO which was observed for the first time spectroscopically. The identity of HBO was confirmed by isotopic shifts in the spectrum of $H^{10}BO$ and DBO. These isotope effects support a linear structure for HBO which is isoelectronic with HCN. The formation of molecular B_2O_3 by photodissociation of $H_2B_2O_3$ at low temperatures is interesting since B_2O_3 has been produced previously at high temperatures by evaporation from the liquid phase. No evidence was obtained for an intermediate formed by loss of a single H atom. It appears that B_2O_3 is formed either by consecutive loss of two H atoms or by a concerted mechanism eliminating an H_2 molecule. The H-bonded intermediate is interesting since it involves a rearrangement of B-H to O-H bonds. The infrared spectrum of this species shows two O-H, two B = O and two B-OH stretching frequencies. These observations suggest the formation of two slightly different H-O-H bonded clusters by association of B-OH and O = B-OH molecules. The formation of these clusters in low temperatures matrices probably occurs within the cavity created by the $H_2B_2O_3$ molecule.

Table 7. Frequencies (cm^{-1}) for Σ^+ vibrations of HNBH in Ar matrices

Isotopic species	ν_2		ν_2		ν_2	
	Obsd	Calcd	Obsd	Calcd	Obsd	Calcd
H^{14}N^{11}BH	3700	3700		2800	1785	1785
H^{14}N^{10}BH	3700	3700	2823	2823	1822	1822
D^{14}N^{11}BD	2790	2762		2194	1595	1583
D^{14}N^{10}BD	2790	2767		2237	1610	1596
H^{15}N^{11}BH	3684	3689		2799	1762	1762
H^{15}N^{10}BH	3684	3689		2822	1799	1799
D^{14}N^{11}BH	2840	2836	2730	2713	1734	1731
D^{14}N^{10}BH		2858		2715	1772	1767
H^{14}N^{11}BD	3695	3699		2225	1624	1618
H^{14}N^{10}BD	3695	3700		2275		1629

Amine-Borane

Photolysis[73] of H$_3$NBH$_3$ with 121.5 nm radiation yields imidoborane, HBNH, which has been of theoretical interest[5, 9]. Spectral shifts observed for several isotopic species containing ^{10}B, ^{15}N, and D show clearly that the spectrum is due to HNBH which is isoelectronic with HBO, HCN and HCCH. From the spectrum of the isolated species two of the Σ^+ and one of the π-type vibration frequencies for a linear molecule have been obtained. The location of the missing Σ^+ (B-H stretch) frequency has been calculated. A comparison of observed and calculated frequencies for HBNH is given in Table 7. Another isolated product observed in these experiments is identified as HNB. This radical may be generated by photodissociation of HNBH subsequent to its formation. In this respect the photolysis mechanism would be similar to the formation of C$_2$H from acetylene.

Borazine

Photolysis of borazine with 121.5 nm wavelength radiation leads to an isolated species with multiple BN bonds[73]. The identity of this product (or products) has not been established. However, it is noteworthy that the monomeric imidoborane is not one of the products of photodissociation.

B. Photoionization Studies

Borazine, substituted borazines and some boron hydrides are ionized by absorption of 121.5 nm radiation (H-α line). Types of ion sources used in these studies are illustrated in Fig. 16. The absorption process results in loss of an electron to form a cation without fragmentation:
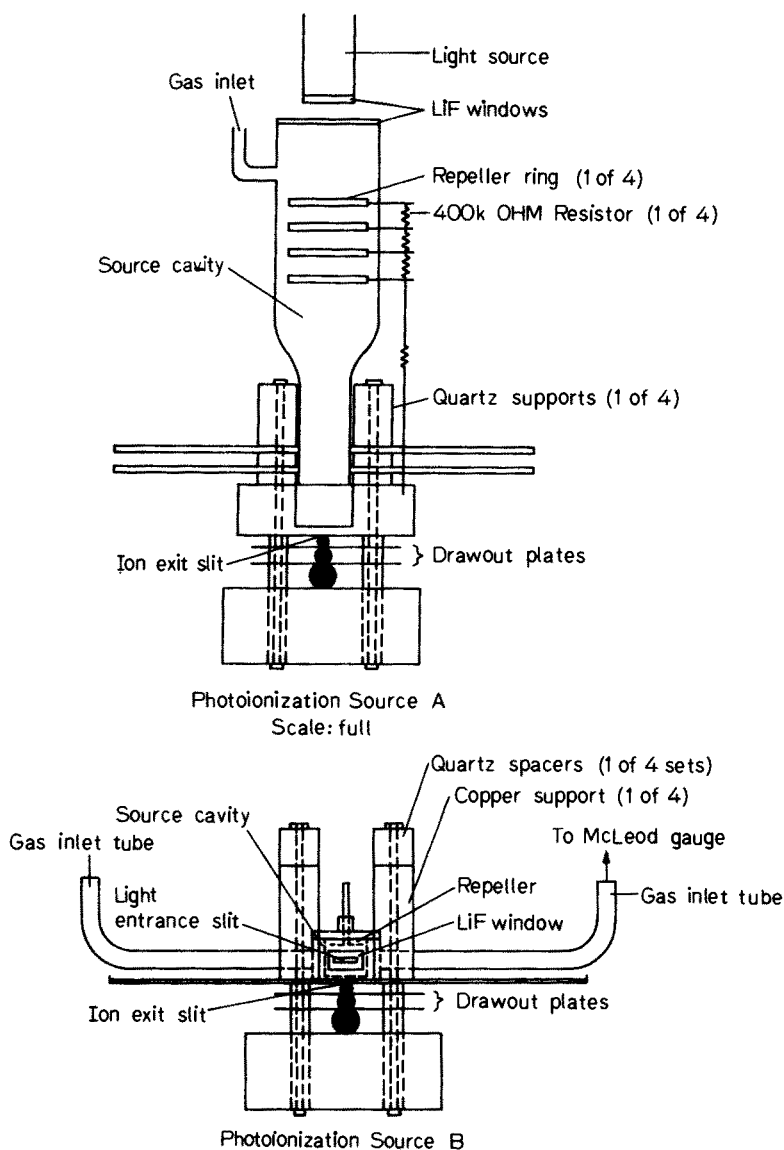
Light source

Gas inlet

LIF windows

Repeller ring (1 of 4)

400k OHM Resistor (1 of 4)

Source cavity

Quartz supports (1 of 4)

Ion exit slit

} Drawout plates

Photoionization Source A
Scale: full

Quartz spacers (1 of 4 sets)

Copper support (1 of 4)

Source cavity

Gas inlet tube

To McLeod gauge

Light entrance slit

Repeller

Gas inlet tube

LiF window

Ion exit slit

} Drawout plates

Photoionization Source B

Fig. 16. Ion sources used to investigate the chemistry of photoionized borazines

$$R + h\nu \xrightarrow{\text{121.5 nm}} R^+ + e^-$$ (70)

From published photoelectron data for these compounds we can infer that cations formed under these conditions will carry some excess internal energy. The photoelectron spectrum of borazine indicates no significant change in the structure of the cation relative to the precursor although a slight Jahn-Teller distortion is possible. The alternate cation structure
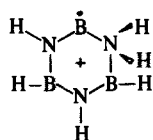
which can not be reached directly by photoionization of borazine, may also be relatively stable. Theoretical calculations for the analogous benzene cation have been reported[38].

The borazine cation formed by irradiation of borazine reacts with a second molecule in a bimolecular proton transfer reaction[28]

$$(58)$$
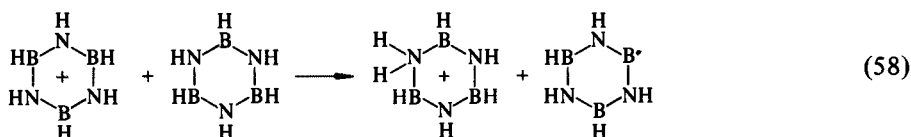
Experiments with B-trideuterioborazine show that the proton leaving the cation was originally bound to a B site and that the proton added to a second borazine molecule is bound at a N site. The effect of pressure on the reaction chemistry is illustrated in Fig. 17. Borazine cation undergoes proton transfer reactions with a number of Bronsted bases. In all cases studied a proton bound to B in the cation is the one transferred. This indicates that the B-borazinyl radical (structure XX) is stable relative to the N-borazinyl isomer (XXI).
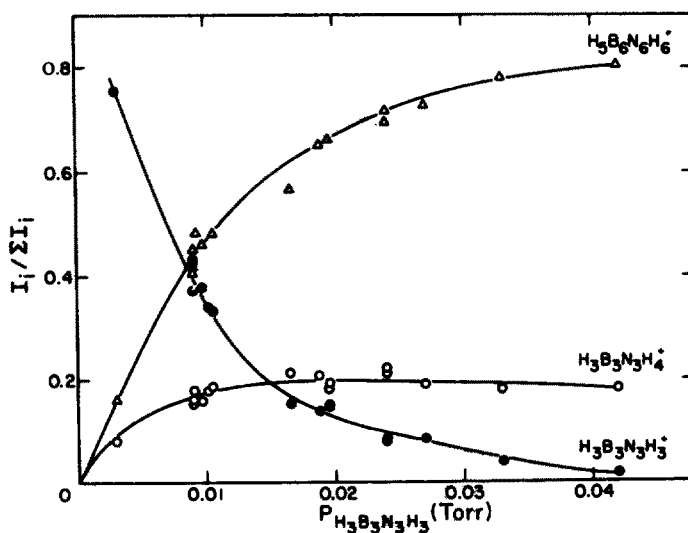
Fig. 17. Effect of source pressure on the relative intensities of ions in the mass spectra of borazine (ionizing radiation = 10.2 e.v.)

33

Borazinium ion undergoes reaction with borazine to form a protonated isomer of diborazinyl.

$$B_3N_3H_7^+ + B_3N_3H_6 \longrightarrow B_6N_6H_{11}^+ + H_2 \tag{59}$$
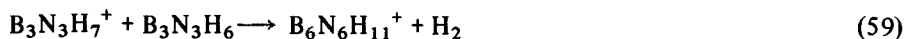
B- and N-Trimethylborazines.

In the gas phase B- and N-trimethlyborazine cations undergo the respective proton transfer reactions[29]

$$H_3N_3B_3(CH_3)_3^+ + H_3N_3B_3(CH_3)_3 \longrightarrow H_4N_3B_3(CH_3)_3^+ + H_3N_3B_3(CH_3)_2(CH_2)^. \tag{60}$$

and

$$H_3B_3N_3(CH_3)_3^+ + H_3B_3N_3(CH_3)_3 \longrightarrow H_4B_3N_3(CH_3)_3^+ + H_3B_3N_3(CH_3)_2(CH_2)^. \tag{61}$$
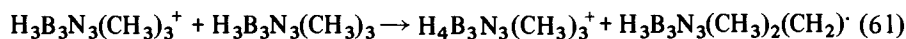
In both systems the proton transferred originates from a methyl group in the cation. These experiments along with other photochemical studies indicate that radical structures XXII and XXIV are preferentially stable relative to their isomers XXIII and XXV respectively.

B-trimethylborazinium ion reacts with B-trimethylborazine to eliminate CH_4 and form a cation $(CH_3)_5B_6N_6H_6^+$.

(XX)

(XXI)

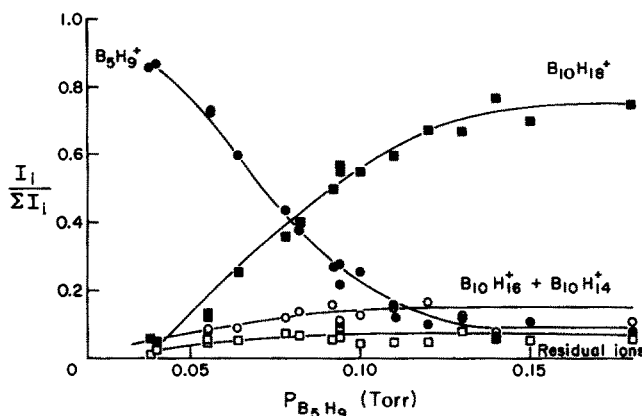(XXII)

(XXIII)

(XIV)

(XXV)
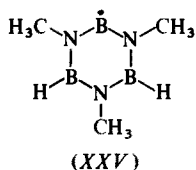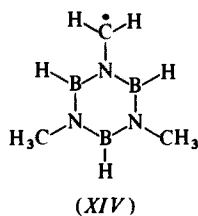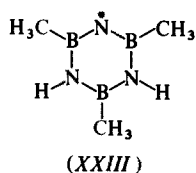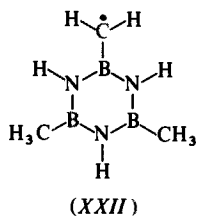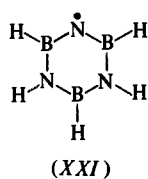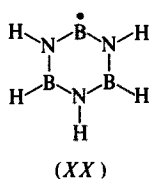
Fig. 18. Reaction profiles of $B_5H_9^+$ ions produced by photoionization of B_5H_9

Pentaborane(9)

The $B_5H_9^+$ cation in its ground electronic state undergoes condensation reactions with B_5H_9 to form $B_{10}H_{14}^+$ and $B_{10}H_{16}^+$. An intensity pressure profile for this system is illustrated in Fig. 18. The addition complex $B_{10}H_{18}^+$ is formed by a three body mechanism at high pressures. Although pentaborane cation does not undergo a proton transfer reaction with B_5H_9 it does react in this manner with a number of Bronsted bases. A mechanistic study[110], using $B_5H_8D^+$ with deuterium in the apical site, has shown that the proton transferred originates preferentially from a basal site in the cation. It is inferred from these measurements that the 2-B_5H_8 boranyl radical is slightly more stable than the 1-B_5H_8 isomer. These results are compatible with photosensitization experiments with B_5H_9 which lead to 2,2-$B_{10}H_{16}$ as one of the stable products. The proton affinity of B_5H_8 was found to be 8.0 eV.

C. Laser-Induced Photochemistry

Laser photolysis techniques have been employed for separating boron isotopes and for promoting chemical reactions of boron compounds. Most of the work in this area has been limited to sources in the infrared region of the optical spectrum. Many boron compounds have electronic transitions in the far UV ($\lambda < 200$ nm) which is not a readily accessible region for one photon absorption studies. Some experimental results using dye lasers and frequency doubling have been reported[91]. Several simple boron compounds including B_2H_6, HBF_2, BCl_3 and F_3PBH_3 have absorption bands that fall within the frequency range of the CO_2 laser near 10 microns. Difluoroborane has a resolved vibration-rotation band that provides selective matching with CO_2 laser lines[23]. To achieve isotope separation, a photochemically activated species must undergo a chemical change before it is collisionally quenched or before it reemits radiation. By multiphoton absorption a molecule receives sufficient internal energy in a succession of fast quantum jumps to reach a dissociative state. Boron

35

isotope separation has been obtained by photolysis of BCl_3 with intense single pulses of CO_2 laser radiation[2, 3, 14]. The multiphoton process

$$BCl_3 + nh\nu \longrightarrow BCl_2^{\cdot} + Cl^{\cdot} \tag{62}$$

is isotopically specified by matching frequencies of CO_2 laser lines with absorption bands of $^{10}BCl_3$ or $^{11}BCl_3$. Isotope separation may also be achieved by chemical reactions that transform an activated species into an isolable reaction product. Laser irradiation of BCl_3 in the presence of H_2S or H_2 yields the reaction products $HSBCl_2$ and $HBCl_2$, respectively[35]. The process

$$BCl_3^* + H_2S \longrightarrow HSBCl_2 + HCl \tag{63}$$

probably accounts for the removal of the activated reagent which can be isotopically selected. The reaction of BCl_3 with H_2 may occur through a multiphoton mechanism that involves initial dissociation of BCl_3 (reaction 62) followed by secondary reactions of the dissociation products with H_2[22]. A bimolecular process involving a three center reaction of H_2 with BCl_3 may also be considered. The mechanism written as follows:

$$\tag{64}$$
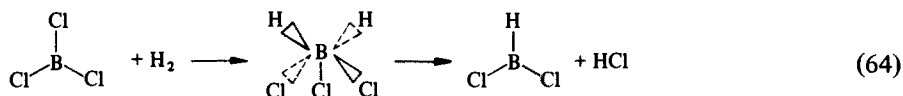
is similar to the proposed for that rapid thermal H-D exchange between HBF_2 and D_2[22]. Diborane(6) and PF_3 are products of the laser-induced photochemical decomposition of F_3PBH_3. Lory, Bauer and Manucci[74] proposed for the rate determining step,

$$BH_3(g) + F_3PBH_3^* \longrightarrow B_2H_6 + PF_3 \tag{65}$$

where $F_3PBH_3^*$ is in an excited vibrational state.

Reactions of diborane(6)[6, 95] and methylboranes[7] under an intense flux of CO_2 laser radiation have been investigated. The nature of the processes is somewhat controversal. The major question concerns the distinction between true photolysis and rapid pyrolysis. At high gas pressures used in these experiments internal energy from excited molecules near the laser beam can be transferred by collisions to cooler molecules resulting in a large temperature gradient within a cell. The technique of laser heating was used by Schaub and Bauer[96] to study reaction kinetics. These investigators used SF_6, a strong absorber of CO_2 radiation, as a heat bath to transfer thermal energy to a reagent gas. Irradiation of B_2H_6 at moderately high pressures with a CO_2 laser yields products of B_5H_9, B_5H_{11}, and $B_{10}H_{14}$[95]. These are also the pyrolyses products of B_2H_6 obtained in hot-cold reactors. The compound $B_{20}H_{16}$ reported in an earlier laser study of B_2H_6 by Bachman and coworkers[6] was not obtained in experiments of Shatos and coworkers[93, 95]. The Doctoral thesis of Rinck[90] reports chemistry of the reaction of laser irradiated B_2H_6 and other boron compounds with a number of reactants. A summary of experimental observations on these systems is presented in Table 8.

Table 8. Reactions of boron compounds irradiated by a CO_2 laser

Irradiated molecule	Reagent molecule(s)	P_I (torr)	P_R (torr)	Power (watts)	Irradiation time (s)	Laser conditions	Products	Observations	Ref.
B_2H_6(neat)		200		1.5	—	c.w. ($\nu = 973\ cm^{-1}$)	B_5H_9, $B_{10}H_{14}$ $B_{20}H_{16}$		6)
B_2H_6(neat)		64–510		7.85	—	c.w. ($\nu = 973\ cm^{-1}$)	B_5H_9, B_5H_{11}, $B_{10}H_{14}\cdot$ $(BH)n$		95)
B_2H_6	O_2	10	10	—	—	Short pulse (free running)	$H_2,B_2O_3(HBO)_3$	Explosion	23)
B_2H_6	O_2	140	30	1.5	10	c.w.	$(HBO)_3$	Fast	90)
B_2H_6	CO	250	250	8	1800	c.w. ($\nu = 970\ cm^{-1}$)	$B_{12}H_{10}(CO)_2$ BH_3CO boron hydrides		90)
B_2H_6	BF_3	150	60	5–7	1800	c.w. ($\nu = 972\ cm^{-1}$)	HBF_2 boron hydrides		23, 90)
B_2H_6	BCl_3	170	60	5	1800	c.w. ($\nu = 940\ cm^{-1}$)	$HBCl_2$ boron hydrides Chlorinated boron hydrides		
B_2H_6	BBr_3	150	10	5–7	1800	c.w. ($\nu = 970\ cm^{-1}$)	$HBBr_2$ boron hydrides Brominated boron hydrides		90)
B_2H_6	H_2S $H_2B_2O_3$	280	40	6.5	1800	c.w. ($\nu = 970\ cm^{-1}$)	$B_2H_6S,HB(SH)_2$ $(HBO)_3$		8)
BCl_3	C_2H_4	200	250	10	900	c.w. ($\nu = 940\ cm^{-1}$)	C_2H_2,CH_4,C_6H_6 $C_4H_6,C_6H_5BCl_2$		90)
$B(CH_3)_3$	O_2	170	10	5–6	3600	c.w. ($\nu = 970\ cm^{-1}$)	$(CH_3BO)_3,C_2H_4$ CH_3OH,C_2H_6		90)

37

Table 8. (continued)

Irradiated molecule	Reagent molecule(s)	P_I (torr)	P_R (torr)	Power (watts)	Irradiation time (s)	Laser conditions	Products	Observations	Ref.
B(CH$_3$)$_3$	CO	200	200	14	7200	c. w. ($\nu = 970$ cm^{-1})	[(CH$_3$)$_3$CBO]$_3$		90)
HBF$_2$	D$_2$	10					DBF$_2$		8)
H$_3$B$_3$N$_3$H$_3$	O$_2$	10	20			Short pulse (free running)	B$_2$O$_3$ + permanent gases	Explosion	8)
SF$_6$	B$_2$H$_6$	200	90	4.5	90	c. w. ($\nu = 940$ cm^{-1})	B$_{20}$H$_{16}$		90)
SF$_6$	B$_2$H$_6$O$_2$	8	8/40	10	< 1	c. w. ($\nu = 936$ cm^{-1})	H$_2$,B$_2$O$_3$		96)

VIII. References

1. Abufhete, M. et al.: J. Organometal Chem. *42*, 19 (1972)
2. Ambartzumian, R. V. et al.: Chem. Phys. Letters *25*, 515 (1974)
3. Ambartzumian, R. V., Letokhov, V. S.: Acc. Chem. Res., *10*, 61 (1977)
4. Armstrong, D. R., Clark, D. T.: Chem. Commun., *99*, (1970)
5. Armstrong, D. R., Clark, D. T.: Theor. Chem. Acta, *24*, 307 (1972)
6. Bachmann, H. R. et al.: Chem. Phys. Lett. *29*, 627 (1974)
7. Bachmann, H. R. et al.: Chem. Phys. Lett. *33*, 261 (1975)
8. Bachmann, H. R. et al.: Chem. Ber. *109*, 3331 (1976)
9. Baird, N. C., Datta, R. K.: Inorg. Chem. *11*, 17 (1972)
10. Beachley, O. T., jr.: Inorg. Chem. *8*, 981 (1969)
11. Beachley, O. T., jr.: J. Am. Chem. Soc. *94*, 4223 (1972)
12. Bernstein, E. R., Reilly, J. P.: J. Chem. Phys. *57*, 3960 (1972)
13. Bock, J., Fuss, W.: Angew. Chem. *83*, 169 (1971)
14. Bourimov, V. N., Letokhov, V. S., Ryabov, E. A.: J. Photochem. *5*, 49 (1976)
15. Brown, H. C., Kabalka, G. W.: J. Am. Chem. Soc. *92*, 612 (1970)
16. Brown, H. C., Midland, M. M.: J. Am. Chem. Soc. *93*, 3291 (1971)
17. Brundle, C. R., Robins, M. B., Kuebler, N. A.: J. Am. Chem. Soc. *94*, 1466 (1972)
18. Bryce-Smith, D.: Pure Appl. Chem. *16*, 47 (1968)
18 a. Burwasser, H., Pease, R. N.: J. Phys. Chem. *60*, 1589 (1956)
19. Chalvet, O., Daudel, R., Kaufman, J.: J. Am. Chem. Soc. *87*, 399 (1965)
20. Charles, S. W., Whittle, E.: Trans. Faraday Soc. *56*, 794 (1960)
21. Charles, S. W., Pearson, J. J., Whittle, E.: ibid. *57*, 1356 (1961)
22. Curtis, P., Porter, R. F.: Chem. Phys. Letters *37*, 153 (1976)
23. Curtis, P. M.: Ph. D. Thesis, Cornell University (1979)
24. Chung, Vo Van et al.: Chemistry Lett. 209 (1976)
25. Davies, D. W.: Trans. Faraday Soc. *56*, 1613 (1960)
26. Davies, D. W.: ibid. *64*, 2881 (1968)
27. Desjardins, C. D. et al.: J. Photochem. *1*, 153 (1972/73)
28. DeStefano, A., Porter, R. F.: Inorg. Chem. *14*, 2882 (1975)
29. DeStefano, A., Porter, R. F.: J. Phys. Chem. *80*, 2818 (1976)
30. Doiron, C. E., Macbeath, M. E., McMahon: Chem. Phys. Lett. *59*, 90 (1978)
31. Doty, J. C. et al.: J. Organometal. Chem. *32*, C35 (1971)
31 a. Doty, J. C. et al.: ibid. *38*, 229 (1972)
32. Eisch, J. J., Tarmao, K., Wilcek, R. J.: J. Am. Chem. Soc. *97*, 895 (1975)
33. Fehlner, T. P.: J. Am. Chem. Soc. *91*, 8355 (1977)
34. Franz, D. A., Mitler, V. R., Grimes, R. N.: ibid. *94*, 412 (1972)
35. Freund, S. M., Ritter, J. J.: Chem. Phys. Lett. *32*, 255 (1975)
36. Frost, D. C. et al.: Chem. Phys. Lett. *5*, 291 (1970)
37. Gaines, D. F., Hildebrandt, S. J.: J. Am. Chem. Soc. *96*, 557 (1974)
38. Gallup, G. A., Steinheider, D., Gross, M. L.: Int. J. Mass Spectrom. Ion Phys. *22*, 185 (1976)
39. Glogowski, M. E. et al.: J. Organometal. Chem. *54*, 51 (1973)
40. Glogowski, M. E. et al.: J. Organometal. Chem. *74*, 175 (1974)
41. Grimm, F. A., Porter, R. F.: Inorg. Chem. *1*, 706 (1968)
42. Grisdale, P. J. et al.: J. Organometal. Chem. *14*, 63 (1968)
43. Grisdale, P. J., Williams, J. K. R.: ibid. *22*, C19 (1970)
44. Grisdale, P. J. et al.: J. Org. Chem. *36*, 544 (1971)
45. Hancock, K. G., Uriarte, A. K.: J. Am. Chem. Soc. *92*, 6374 (1970)
45 a. Hancock, K. G., Dickenson, D. A.: ibid. *94*, 4396 (1972)
46. Hancock, K. G., Dickenson, D. A.: ibid. *95*, 280 (1973)
47. Hancock, K. G., Kramer, J. D.: ibid. *95*, 3425 (1973)
48. Hancock, K. G., Uriarte, A. K., Dickenson, D. A.: ibid. *95*, 6980 (1973)
49. Hancock, K. G. et al.: J. Organometal. Chem. *90*, 23 (1975)

50. Hawthorne, M. F., Pilling, R. L.: J. Am. Chem. Soc. *88*, 3873 (1966)
51. Hellner, L., Vermeil, C.: J. Chimie Phys. *71*, 1269 (1974)
52. Hirata, T., Gunning, J. E.: J. Chem. Phys. *27*, 477 (1957)
53. Hoffmann, R.: J. Chem. Phys. *40*, 2474 (1964)
54. Hoffman, R. W.: Dehydrobenzene and cycloalkynes, Weinheim: Verlag-Chemie 1967
55. Holmes, J. L., Kutschke, K. O.: Trans. Faraday Soc. *58*, 333 (1962)
56. Inatome, M., Kuhn, L. P.: Tetrahedron Lett. *1*, 73 (1965)
57. Ishikawa, H., Noyes, W. A., jr.: J. Chem. Phys. *37*, 583 (1962)
58. Jacobs, L. E., Platt, J., Rand Schaeffer, G. W.: J. Chem. Phys. *16*, 116 (1948)
59. Kaldor, A.: J. Chem. Phys. *55*, 4641 (1971)
60. Kline, G. A., Porter, R. F.: Inorg. Chem. *16*, 11 (1977)
61. Kline, G.: Ph. D. Thesis, Cornell University (1978); Kline, G., Porter, R. F.: Inorg. Chem. *19*, 447 (1980)
62. Kreye, w. C., Marcus, R. A.: J. Chem. Phys. *37*, 419 (1962)
63. Kroner, J. et al.: Tetrahedron *28*, 1585 (1972)
64. Kuznesof, P. M., Shriver, D. F.: J. Am. Chem. Soc. *90*, 1683 (1968)
65. Labarre, J. et al.: Theor. Chem. Acta. *2*, 1219 (1964)
66. Lee, G. H., Porter, R. F.: Inorg. Chem. *6*, 648 (1967)
67. Leyden, R. N. et al.: J. Am. Chem. Soc. *100*, 3758 (1978)
68. Lipscomb, W. N.: Lecture Third Internat. Meet., Boron Chemistry (Munich, July 5–9, 1976). Pure Appl. Chem. *49*, 701 (1977)
69. Lissi, E. A., Larrondo, L.: J. Photochem. *2*, 429 (1973/74)
70. Lloyd, D. R., Lynaugh, N.: Phil. Trans. Roy. Soc. (London) *A268*, 97 (1970)
71. Lloyd, D. R., Lynaugh, N.: J. Chem. Soc., D 125 (1974)
72. Lory, E. R., Porter, R. F.: J. Am. Chem. Soc. *93*, 6301 (1971)
73. Lory, E. R., Porter, R. F.: ibid. *95*, 1766 (1973)
74. Lory, E. R., Bauer, S. H., Manuccia, T.: J. Phys. Chem. *79*, 545 (1975)
75. Miyamoto, N. et al.: Tetrahedron Lett. *48*, 4597 (1971)
76. Mousseron-Canet, M., Mani, J. C.: Photochemistry and molecular reactions, Chap. 5, Paris: Dunod 1969
77. Müller, K. D., Niedenzu, K.: Inorg. Chim. Acta *25*, L53 (1977)
78. Nadler, M., Porter, R. F.: Inorg. Chem. *6*, 1739 (1967)
79. Nadler, M. P., Porter, R. F.: Inorg. Chem. *8*, 599 (1969)
80. Neiss, M. A., Porter, R. F.: J. Am. Chem. Soc. *94*, 1438 (1972)
81. Neiss, M. A., Porter, R. F.: J. Phys. Chem. *76*, 2630 (1972)
82. Oertel, M., Porter, R. F.: Inorg. Chem. *9*, 904 (1970)
83. Oertel, M.: Ph. D. Thesis, Cornell University (1971)
84. Perkins, P. G., Wall, D. H.: J. Chem. Soc. A. 235 (1966)
85. Peyerimhoff, S. D., Buenker, R. J.: Theor., Chem. Acta. *19*, 1 (1970)
86. Platt, J. R., Klevens, H. B., Schaeffer, G. W.: J. Chem. Phys. *15*, 598 (1947)
87. Plotkin, J. S., Sneddon, L. G.: J. C. S. Chem. Comm., *95*, (1976)
88. Porter, R. F., Yeung, E. S.: Inorg. Chem. *1*, 1306 (1968)
89. Porter, R. F., Grimm, F. A.: Adv. Chem. Ser. *72*, 94, (1968)
90. Rinck, R.: Doctoral Dissertation University Munich, Germany (1976)
91. Robin, M. B., Kuebler, N. A.: J. Mol. Spectrosc. *70*, 472 (1978)
92. Rockwood, S. D., Hudson, J. W.: Chem. Phys. Lett. *34*, 542 (1975)
93. Roothan, C. C. J., Mulliken, R. S.: J. Chem. Phys. *16*, 118 (1948)
94. Schultz, R. V., Sato, F., Todd, L. J.: Organometal. Chem. *21*, 115 (1977)
95. Shatas, S. et al.: Inorg. Chem. *17*, 163 (1978)
96. Shaub, W. M., Bauer, S. H.: Int. J. Chem. Kin. *1*, 509 (1975)
97. Silverstein, H. T., Beer, D. C., Todd, L. J.: J. Organometal. Chem. *21*, 139 (1970)
98. Spielman, J. R., Scott, J. E.: J. Am. Chem. Soc. *87*, 3512 (1965)
99. Stock, A., Friederici, K., Press, O.: Ber. dtsch. chem. Ges. *46*, 3353 (1913)
100. Trofimenko, S., Cripps, H. N.: J. Am. Chem. Soc. *87*, 655 (1965)
101. Trofimenko, S.: J. Am. Chem. Soc. *88*, 1899 (1966)
102. Turbini, L. J.: M. S. Thesis, Cornell University (1972)

103. Turbini, L. J.: Ph. D. Thesis, Cornell University (1974)
104. Turbini, L. J., Porter, R. F.: Org. Mag. Resonance *6*, 456 (1974)
105. Turbini, L. J., Porter, R. F.: Inorg. Chem. *14*, 1252 (1975)
106. Turbini, L. J., Golenwsky, G. M., Porter, R. F.: Inorg. Chem. *14*, 691 (1975)
107. Turbini, L. J., Mazanec, T. J., Porter, R. F.: J. Inorg. Nucl. Chem. *37*, 1124 (1975)
108. Uriarte, A. K., Hancock, K. G.: Inorg. Chem. *12*, 1428 (1973)
109. Utimoto, K., Tanaka, T., Nozaki, H.: Tetrahedron Lett. *12*, 1167 (1972)
110. Wang, Jia-Shan, Destefano, A. J., Porter, R. F.: Inorg. Chem. *17*, 1374 (1978)
111. Ward, H. R., Wishnok, J. S.: J. Am. Chem. Soc. *90*, 5353 (1968)
112. Wegner, P. A., Guggenberg, L. J., Muetterties, E. L.: ibid. *92*, 3473 (1970)
113. Williams, J. L. R. et al.: Chem. Commun. (3), 109 (1967)
114. Williams, J. L. R., Grisdale, P. J., Doty, J. C.: J. Am. Chem. Soc. *89*, 4538 (1967)
115. Williams, J. L. R. et al.: ibid. *89*, 5153 (1967)
116. Williams, J. L. R. et al.: ibid. *90*, 53 (1968)
117. Williams, J. L. R. et al.: J. Organometal. Chem. *14*, 53 (1968)
118. Yanase, M., Koyanagi, M., Kanda, Y.: Memoirs Faculty of Science, Kyushu University, Ser. C. *8*, 35 (1972)
119. Young, W. F. et al.: Can. J. Chem. *49*, 233 (1961)

Gas Electron Diffraction
A Tool of Structural Chemistry in Perspectives

István Hargittai

Department of Structural Studies, Research Laboratory for Inorganic Chemistry, Hungarian Academy of Sciences, Budapest Pf. 117, H-1431, Hungary

Table of Contents

1 Introduction

Gas electron diffraction is one of the two principal techniques used to determine molecular geometry in the vapor phase (the other is microwave spectroscopy). It provides fundamental information for structural chemistry: bond lengths, bond angles, and angles of internal rotation. It is also used for conformational analysis. Furthermore, characteristics of the intramolecular motion, such as mean amplitudes of vibration are determined by this technique. As the gas electron diffraction method is based on the phenomenon that a beam of fast electrons is scattered by the potential resulting from the charge distribution in the molecule, it is obvious that the resulting interference pattern contains a wealth of structural information extending over the area enumerated above (e.g., electron density distribution). Thus further development of the experimental technique may open or widen new possibilities of application.

It is now fifty years from the date when Mark and Wierl reported the first gas electron diffraction investigation of molecular structure[1]. This historic paper is reproduced in Fig. 1. Up to now the number of gas electron diffraction papers is exceeding 2000. Although the annual production may not be rapidly increasing, selected powerful groups around the world are working in this field and are providing unique information on chemical structure. The experimental centers concentrate in the United States, the Soviet Union, Norway, Japan, Great Britain, Hungary, the Netherlands, the Federal Republic of Germany, and France. A few other countries are expected to join their number. Data produced in the experimental centers are analyzed in many more laboratories.

The aim of the present work is to review a series of current studies and in doing so to demonstrate the present status of gas electron diffraction molecular structure determinations. This review is not intended to be comprehensive but it is hoped to be characteristic. For convenience a relatively large number of examples will be discussed from the author's own laboratory. The discussion of the various topics of current research is preceded by a historical review. This is only in part to pay tribute to those who have advanced the technique during its 50 years to the present level. More significantly, I consider the history of gas electron diffraction to be very instructive with its ups and downs and turning points and the interrelationship of its development with that of other fields. A detailed account of the history has yet to be written, and this is by far not the purpose of the present review. I shall restrict myself to enumerate some events. Even this may suffer from bias and ignorance. I would dare to say, however, that some reevaluation of the history may be needed from time to time. This is not to say that e. g., some events or discoveries may become nonevents or nondiscoveries but that their relative importance may change in perspective. An example of this I consider to be the discovery of the Bastiansen-Morino shrinkage effect whose relative importance has not yet ceased to increase as it signifies the contribution of the intramolecular motion to the determination of molecular geometry in a broader sense.

Several selected topics are considered in the present review to illustrate rather than to cover exhaustively the present development of gas electron diffraction struc-

Über Elektronenbeugung am einzelnen Molekül.

Die experimentelle Erfahrung über die Beugung schneller Elektronen an Metallfolien[1] hat wesentliche Unterschiede gegenüber der Streuung von Röntgenstrahlen in zwei Punkten ergeben: 1. Bei Röntgenstrahlen ist die Wechselwirkung zwischen Lichtwelle und Ladung, bei Elektronen die erheblich stärkere zwischen Ladung und Gitterpotential verantwortlich. Dies und die stärkere photographische Wirkung der Elektronen führt bei Streuung am gleichen Objekt zu Belichtungszeiten, die sich für Elektronen und Röntgenstrahlen wie 1:10000 verhalten. 2. Abgesehen von ganz kleinen Winkeln wirken auf die Elektronen im wesentlichen die Atomkerne, während bei den Röntgenstrahlen nur die Elektronenhülle der Atome zur Geltung kommt.

Beide Umstände lassen es als möglich erscheinen, durch Streuung von schnellen Elektronen an einem Dampfstrahl innermolekulare Interferenzen in kurzen Zeiten zu erhalten. Bekanntlich haben DEBYE, BEWILOGUA und EHRHARDT[2] erfolgreiche Versuche zur Beugung von Röntgenstrahlen an Tetrachlorkohlenstoff angestellt. Sie erhielten bei 20stündiger Belichtungszeit einen vermeßbaren Interferenzring, aus dem sich nach der DEBYEschen Theorie unter Zugrundelegung einer tetraedrischen Anordnung der Chloratome ein Abstand a von 3,3 Å zwischen den Cl-Atomen berechnet.
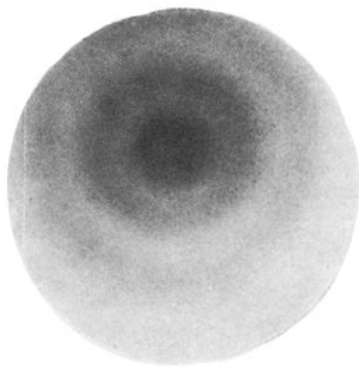
Fig. 1. Elektroneninterferenzen an Tetrachlorkohlenstoff. 36 kV Elektronen

Unsere Versuche, einen Elektronenstrahl an Tetrachlorkohlenstoff zu beugen, ergaben bei einer Belichtungszeit von 1–3 Sekunden zwei deutliche Ringe (Fig. 1), ein dritter ist angedeutet. Bei der abgebildeten Aufnahme war die Röhrenspannung 36 kV (λ = 0,065 Å) der Abstand: Dampfstrahl (0,2 mm Düsenöffnung) bis Film 350 mm und d_1 = 18 mm und d_2 = 32,5 mm ergeben nach den für das erste und zweite Maximum gültigen Winkelbeziehungen

$$\sin \vartheta_1/2 = \frac{5}{8} \frac{\lambda}{a} \text{ und } \sin \vartheta_2/2 = \frac{9}{8} \frac{\lambda}{a} \text{ für den Abstand der Cl-Atome im } CCl_4 \text{ den Wert } a = 3,14 \text{ Å.}$$

Es wurde noch die Spannungsabhängigkeit untersucht. Der Ringdurchmesser d_1 bei 31 kV (λ = 0,085 Å) ist 23,6 bei 49 kV (λ = 0,055 Å) d_1 = 15,5 mm. Ein Versuch an Chloroformdampf ergab zwei etwas diffusere Maxima, während sich am Wasserdampfstrahl nur diffuse Streuung ohne Maximum ergab

---

[1] Eine ausführliche Arbeit über die Beugung schneller Elektronen an Al-, Ag- und Au-Folien und die quantitative Auswertung der Interferenzintensitäten erscheint demnächst in der Z. Physik

[2] Physik. Z. 30, 84 (1929). Wir möchten bemerken, daß Herr W. BOTHE nach einem Vortrag von DEBYE auf der Röntgentagung in Zürich ebenfalls die Möglichkeit von Elektronenbeugungsversuchen an Gasen zur Diskussion stellte

Fig. 1. The reproduction of the first report by Mark and Wierl on a gas electron diffraction experiment[1]

tural studies. While many areas may have been left out inadvertently, two extremely important ones are purposely omitted:

investigation of non-rigid structures, large-amplitude motion, conformational equilibria as some recent reviews give excellent coverage of these topics by Bastiansen et al.[2], by Spiridonov et al.[3] and by Lowrey[4],

combined utilization of electron diffraction and spectroscopic data (see e. g.[5, 6]).

Furthermore, the structural results cited here for illustration will be overwhelmingly from inorganic chemistry. A review of recent electron diffraction results on extensive classes of organic molecules has been written recently by Vilkov[7]. Finally I mention another recent review by Kuchitsu[8] in which the basic ideas of the electron diffraction determination of the geometry of free molecules as well as the physical meaning of the geometrical parameters are succinctly discussed.

2 Fifty Years in Retrospect

Two important theoretical discoveries preceded the first experimental realization of gas electron diffraction. One of them was by Debye (1915) who examined the X-ray diffraction by rigid, randomly oriented systems of electrons[9]. He found that the interference effects do not cancel, on the contrary, strongly influence the average intensity distribution as a function of the scattering angle. This distribution depends on the distances between the electrons. Instead of the systems of electrons, molecules may also be considered. The collection of randomly oriented molecules shows strong interference effect in which the intensity distribution depends on the geometry of the molecule. The other theoretical achievement was de Broglie's discovery (1924) concerning the wave nature of moving electrons[10]. The first electron diffraction experiments on crystals were reported in 1927 simultaneously by two groups[11, 12]. Then followed the report in 1930 by Mark and Wierl[1] on the first gas electron diffraction experiment and structural data appeared for a series of simple molecules[13].

At the beginning the interatomic distances were determined by measuring the positions of the maxima and minima on the interference pattern. Soon, however, a more direct method was proposed by Pauling and Brockway[14] for determining the interatomic distances. They obtained a so-called radial distribution by Fourier-transforming the estimated intensity data. The radial distribution is related to the probability distribution of interatomic distances. The position of maximum on the radial distribution gives the interatomic distance, while its halfwidth provides information on the associated vibrational amplitude.

The influence of molecular vibrations on the interference pattern was first studied by James in 1932[15]. He discussed the intensity distribution (of X-ray scattering) by vibrating molecules, and determined the dependence of the intensity distribution on the vibrational amplitudes.

However, at that time it was not possible to carry out a quantitative evaluation of the electron scattering intensity distribution. The positions of maxima and minima of the molecular interference pattern could be determined surprisingly well against the steeply falling background of atomic scattering intensity, due to the exaggerating

ability of the human eye ("visual" electron diffraction technique). The relative intensities, however, could only be roughly estimated.

A breakthrough was due to the introduction of the rotating sector proposed independently by Finbak[16] and P. P. Debye[17]. This rotating sector is a metallic disc of special shape and is placed into the path of the scattered electrons in order to compensate for the steeply falling background. Using the rotating sector it was then possible to quantitatively elucidate the intensity distribution for a wide scattering angle range. Suitable photometers have been developed for the determination of the optical density distribution of the photographic plate that recorded the interference pattern.

By the early fifties a technique was developed mainly by J. and I. L. Karle[18—20] to quantitatively treat the experimental data in order to obtain accurate geometrical and vibrational parameters. The new technique was called the "sector-microphotometer" method. As the name has been used ever since, today it has a wider meaning than just a reference to the experimental technique, and it usually signifies all the experimental, computational, and theoretical developments of the electron diffraction technique.

From the middle of the fifties new experimental equipments have been built with high precision (e. g.[21, 22]) and the use of fast electronic computers made their strong impact as well. With increasing accuracy of structure determination, the failures of some of the theoretical approximations have become apparent. Thus, e. g., attention turned to the failure of the first Born approximation, especially for molecules containing atoms with very different atomic numbers[23].

The more detailed interpretation of the results and their critical comparison with those obtained by other physical techniques necessitated a closer look at the physical meaning of the geometrical parameters determined[24].

The scope of structure determinations has also expanded. One of the most important, early chemical applications of electron diffraction was the determination of conformational mixtures by Hassel and Bastiansen and their coworkers[25]. The Nobel-prize of Hassel in 1969 signifies this research.

In addition to stable free molecules, stable free radicals[26, 27], unstable free radicals[28, 29], and ions[30] have also been studied.

After some earlier attempts[31], extensive high-temperature electron diffraction studies have begun at the Moscow State University[32] and eventually in other laboratories.

A major step in the data analysis was the application of the least-squares technique[33].

Although successful attempts have been reported on electron density distribution measurements by electron diffraction[34] and other extensions of the technique[35], its principal application has remained the determination of molecular geometry and intramolecular motion. To increase accuracy and to extend structural information for more complicated molecules, the most promising recent development is the combined analysis of diffraction and spectroscopic data. The studies of Kuchitsu, cf.[36] have to be mentioned here, followed by an increasing number of investigations by others.

In conclusion I mention the detailed and interesting account of the history of gas electron diffraction by J. Karle[37].

3 The Challenge of Inorganic Structures

Inorganic molecules have a great variety of structures which often seem to be "unusual" from the point of view of the classical theories of valency. Experimental data have stimulated the development of modern theories of bonding. It may be especially important in these structural studies to consider concurring evidences from various techniques. High-temperature vapors are particularly rich in interesting molecular species. Electron diffraction is a unique tool for the determination of the structure of the high-temperature species apart from some simple molecules for which microwave spectroscopy may be applicable. Direct information on the vapor composition or the experimental conditions necessary to optimize it, comes from mass spectrometry. The electron diffraction analysis is also facilitated to a great extent by the knowledge of molecular symmetry and calculated vibrational amplitudes. In addition to the complementary role of these techniques in collecting experimental information, strong and useful interplay is possible in the interpretation of results obtained by these methods. The interrelationship of electron diffraction with mass spectrometry and vibrational spectroscopy is sketched in Fig. 2. This scheme was compiled from the viewpoint of the electron diffraction analysis. Some examples of application will be discussed below.
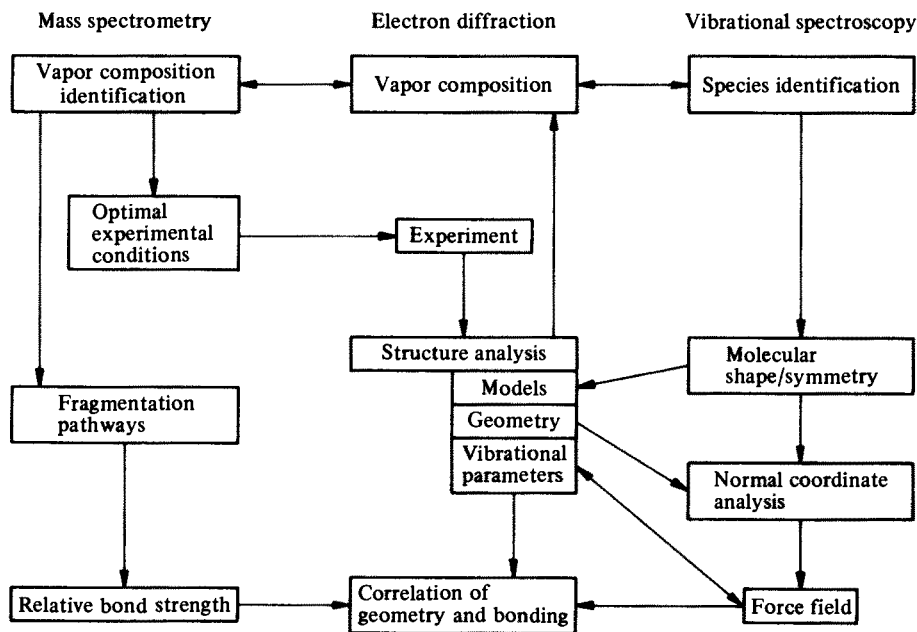
Fig. 2. Interrelationship of electron diffraction with mass spectrometry and vibrational spectroscopy

3.1 High-Temperature Electron Diffraction

Of course, there is no unique definition for the temperature range called high-temperatures. In structural studies, however, temperatures above, say, 300 °C are called high-temperatures. High-temperature vapors may also be defined as vapors of compounds that are solids at ordinary temperatures and pressures.

Although the electron scattering theory, basic principles of experimentation and interpretation are the same at any temperature, high-temperature conditions pose specific problems in the experiments and interpretation of the data[38].

The main experimental difficulty in the high-temperature electron diffraction technique is to introduce the high-temperature vapor into the way of the electron beam without disturbing the electron beam by an electromagnetic field from the heating system. An additional difficulty arises when light radiation reaches the photographic plate from the glowing nozzle system. The most commonly used protection is a thin layer of Indian ink on the photographic plate which is then washed away before developing the plate[39]. Another protection may be a thin metallic foil[40].

For many years electron bombardment has been most commonly used for heating the nozzle[38]. During the last five years a very convenient, so-called "radiation" nozzle system has been developed[41, 42]. This system is illustrated in Fig. 3.

The radiation nozzle system has been used for studying a series of transition metal dihalide molecules. Typical molecular intensity distributions are shown in Fig. 4 for manganese(II) chloride. The quickly damping character of the intensity distribution relates to the large-amplitude motion in the molecule due to the high temperature (~ 750 °C) conditions of the experiment. Fig. 5 shows the radial distribution from the same experiment which also well demonstrates the straightforward manner of structure determination of such simple molecules.

The interatomic distance determined for transition metal dihalides are collected in Table 1. These results give us also a good example of interpretational difficulties in high-temperature electron diffraction. Because of the large-amplitude bending vibrations, the distances between the halogen atoms appear to be shorter than they would be expected in a motionless molecule. This effect is called shrinkage effect and is illustrated by Fig. 6. The shrinkage (δ) is the difference between the actual halogen-halogen interatomic distance and twice the bond distance:

$$\delta = 2r(\text{M-X}) - r(\text{X} \cdots \text{X})$$
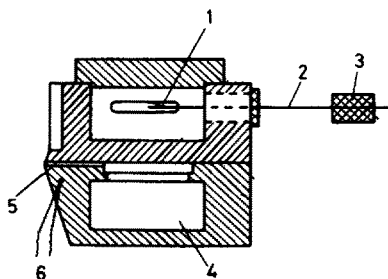
Fig. 3. "Radiation" nozzle system for high-temperature electron diffraction experiment for compounds with low volatility (1 — filament, 2 — supporting rod, 3 — ceramic supporter, 4 — sample container, 5 — nozzle capillary, 6 — thermocouple)
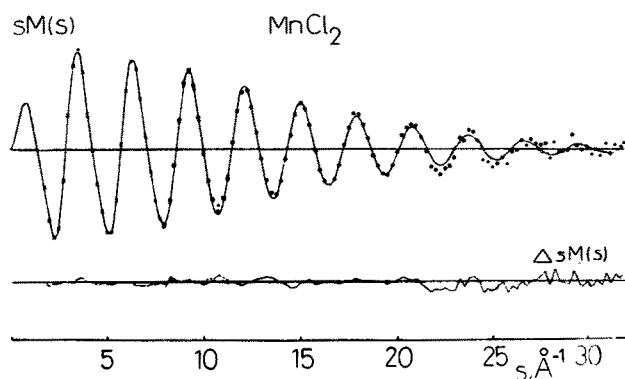
Fig. 4. Experimental (dots) and theoretical (full line) molecular intensities of manganese (II) chloride[42]
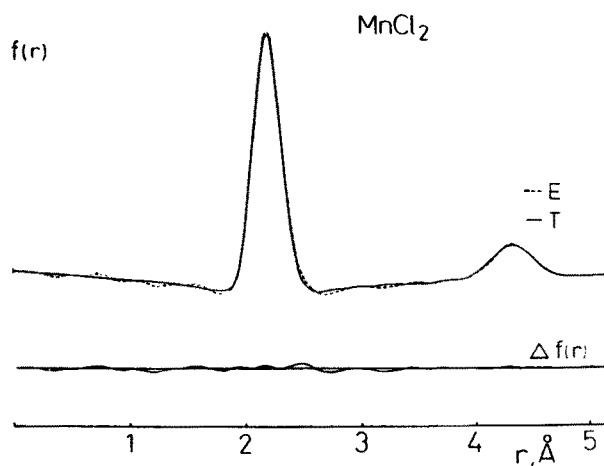
Fig. 5. Experimental (E) and theoretical (T) radial distributions of manganese(II) chloride[42]

Table 1. Interatomic distances, shrinkages, and bending vibrational frequencies of first row transition metal dihalides

MX_2	r_g (M-X), A	r_g (X...X), A	δ, A	T (°C)	$\nu_2 (cm^{-1})^a$		Ref.
					ED	SP[49]	
$MnCl_2$	2.205(5)	4.324(15)	0.085	800	93	83	42)
$FeCl_2$	2.162(5)	4.205(12)	0.119	625	72	88	43)
$CoCl_2$	2.120(5)	4.125(21)	0.115	750	78	94	44)
$NiCl_2$	2.056(4)	4.018(76)	0.094	800	90	85	45, 46)
$FeBr_2$	2.310(5)	4.464(9)	0.156	625	50	–	43)
$NiBr_2$	2.212(5)	4.326(13)	0.098	670	69	69	47)

a ED – estimated from shrinkage effect
  SP – matrix isolation infrared spectroscopy

Fig. 6. Illustration for the origin of the shrinkage effect in MX_2 molecules; r_e is the equilibrium $X \cdots X$ distance, r is the instantaneous $X \cdots X$ distance during vibration. Because of the perpendicular (bending) vibrations, the average internuclear distance, $r_g = \int r(\gamma)P(\gamma) \, d\gamma$ is less than the equilibrium distance; here $P(\gamma) \, d\gamma$ expresses the probability that the angle X-M-X lies between γ and $\gamma + d\gamma$
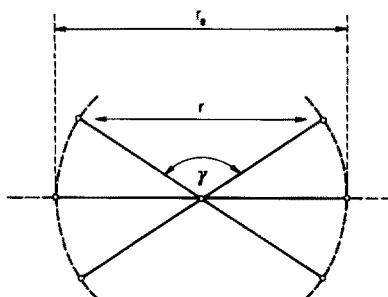
Of course here we supposed that the MX_2 molecules would be strictly linear in their motionless state[48]. There is experimental evidence from spectroscopic and dipole moment measurements to support this assumption[49, 50]. The interpretational difficulties caused by the shrinkage effect were by far outweighed by the additional information which was possible to gain on the bending vibrational motion. It was possible to estimate the bending frequencies from the shrinkage effect for the transition metal dihalides[48]. They are also given in Table 1. These low-frequency data are difficult to get from spectroscopic measurements. This method can be used for other classes of compounds as well. However, the accuracy requirements for such estimates are favorable for high-temperature data only. This can be well seen on the plots of Fig. 7 showing the shrinkage *versus* bending frequency curves for a wide

Fig. 7. Shrinkage (δ) *versus* bending frequency (ν_2) curves calculated for a series of temperatures[48]

51

temperature range. The limitations and possible error sources of such estimates have been discussed[48].

As for the possible correlation between geometry and electronic structure, consider the variation of ionic radii with atomic number in the first row transition metal series[51]. If the points for Ca, Mn, and Zn are connected, i. e., for atoms with a spherically symmetrical distribution of d electrons, the ionic radii of the other atoms are smaller than interpolation would yield from the Ca-Mn-Zn line. The nonuniform distribution of d electrons around the nuclei is assumed to be the reason for this contraction of the ionic radii. The data available so far on the bond lengths for the vapor-phase dichlorides are seen in Fig. 8.

Krasnov et al.[53] have determined the structures of $LuCl_3$, $LaBr_3$, $GdBr_3$, and $LuBr_3$ and found experimental verification of the lanthanoide contraction[51] as calculated by Waber and Cromer[54]. On the basis of experimental and calculated data they estimated the metal-halogen bond distances for the whole series of lanthanides. Their estimates are reproduced in Table 2. Two more recent experimental data are also cited[55, 56] showing fairly good agreement with the predictions.

3.2 Combined Electron Diffraction — Quadrupole Mass Spectrometric Experiment

In up-to-date structure investigation the need often arises to determine the structure of "exotic species" like high-temperature vapors, free radicals or reaction products.
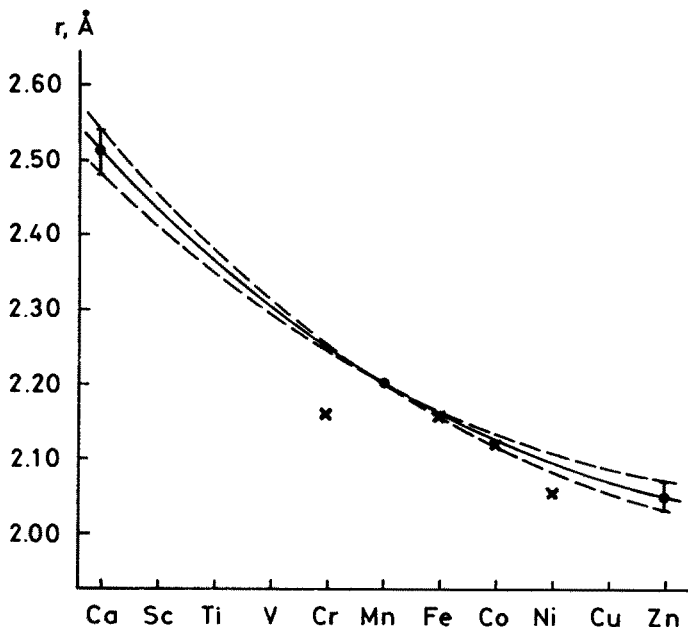
Fig. 8. The average bond lengths determined for some transition metal dichlorides by electron diffraction; the length of the vertical bar indicates experimental uncertainty; the line connect the data points for $CaCl_2$, $MnCl_2$ and $ZnCl_2$

Table 2. Estimated and experimental (underlined) bond lengths (A) of lanthanoide trihalides[53]

Ln	r(Ln-F)	r(Ln-Cl)	r(Ln-Br)	r(Ln-I)
La	2.20	2.597	2.741	2.946
Ce	2.18	2.578	2.722	2.927
Pr	2.17	2.561	2.705	2.910
Nd	2.15	2.545	2.689	2.894
Pm	2.13	2.529	2.673	2.878
Sm	2.12	2.515	2.659	2.864
Eu	2.11	2.501	2.645	2.850
Gd	2.10	2.489[55]	2.640	2.845
Tb	2.09	2.478[56]	2.628	2.833
Dy	2.08	2.472	2.616	2.821
Ho	2.06	2.460	2.604	2.809
Er	2.05	2.450	2.594	2.799
Tm	2.04	2.438	2.582	2.787
Yb	2.03	2.428	2.572	2.777
Lu	2.02	2.417	2.561	2.766

The application of electron diffraction may be hindered, however, by the lack of knowledge of the vapor composition or by the insufficient concentration of the species to be investigated. The solution to this problem is the simultaneous mass spectrometric and electron diffraction measurements. In this combined experiment the vapor composition and the optimal experimental conditions are determined prior to and during the diffraction experiment. We have employed this combined technique in the Budapest laboratory and are aware of similar attempts at the University of Oslo and The University of Texas at Austin.

The main requirements to the quadrupole mass spectrometer in the combined experiment are the following:

(i) The mass spectrometric experiment should have no influence on the electron scattering experiment; the electron beam should not be deformed by any electromagnetic field.

(ii) The mass spectrometer should have high sensitivity, fast scanning and large enough mass range.

A good coupling is characterized by the following criteria:

(a) The mass spectrometer detects the primary molecular beam only.

(b) This primary molecular beam reaches the ion source in sufficient quantity.

(c) The mass spectrometer is contaminated by the sample as little as possible.

(d) No radiation from the mass spectrometer (e. g., light radiation from the ion source) reaches the photographic plate of the diffraction experiment.

All the above considerations were taken into account in the coupling[57] of the Soviet-made type EG-100A electron diffraction apparatus and type NZ-850 quadrupole mass spectrometer developed and built in the Institute of Nuclear Research (ATOMKI), Hungarian Academy of Sciences, Debrecen[58] Fig. 9 illustrates the combined experimental setup.

The determination of the structure of the unstable germanium dichloride molecule serves here as an example of the application of the combined experiment. The

Quadrupole mass spectrometer   Electron diffraction unit   High-temperature nozzle system
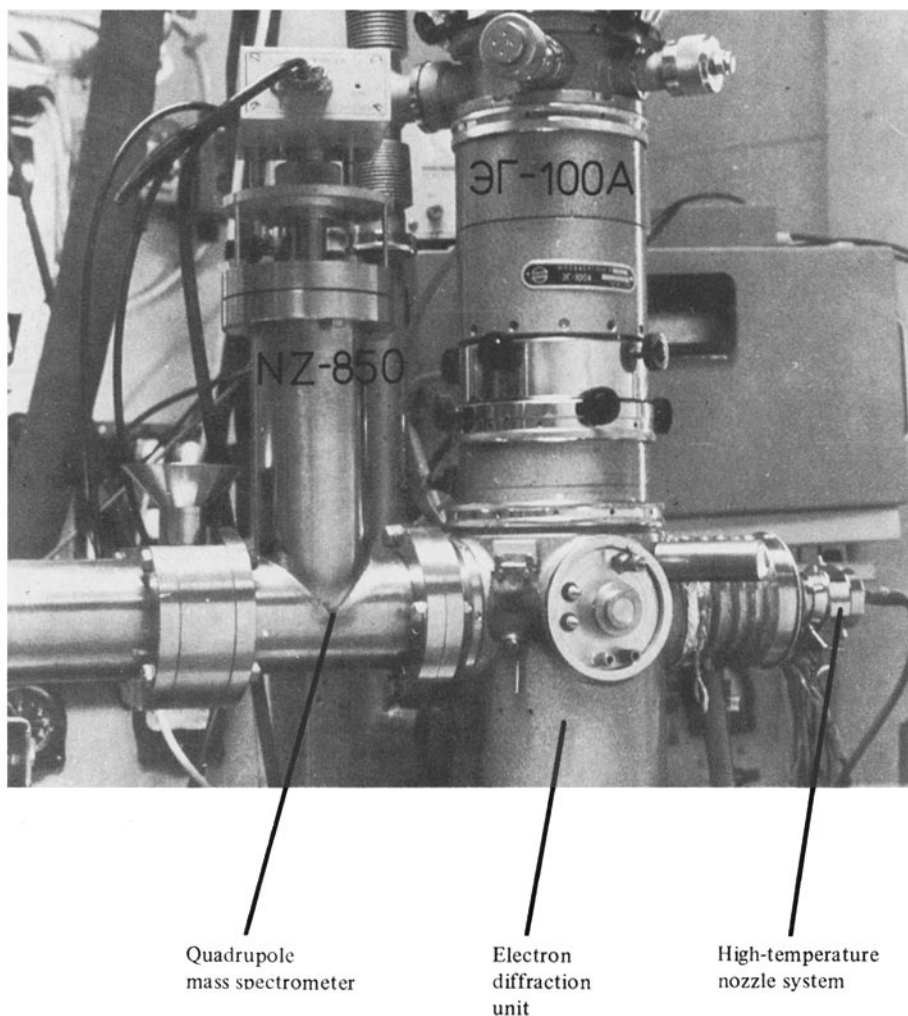
Fig. 9. The setup of the combined electron diffraction – quadrupole mass spectrometric experiment in the Budapest laboratory incorporating an EG-100A electron diffraction unit and an NZ-850 quadrupole mass spectrometer

dichloride species were prepared directly near the electron beam in a reactor-nozzle-system shown in Fig. 10. The reaction

$$Ge(metal) + GeCl_4(gas) \longrightarrow GeCl_2(gas)$$
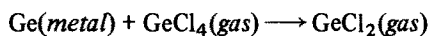
was applied. The dichloride species by far predominated and were present in a sufficient amount at the nozzle (and container) temperature of 660 °C. A portion of the mass spectrum recorded at 660 °C is shown in Fig. 11a. In order to show that this mass spectrum originates mainly from dichloride species indeed, another spec-

Nozzle tip   Solid sample   Gas inlet
                            (reactor)
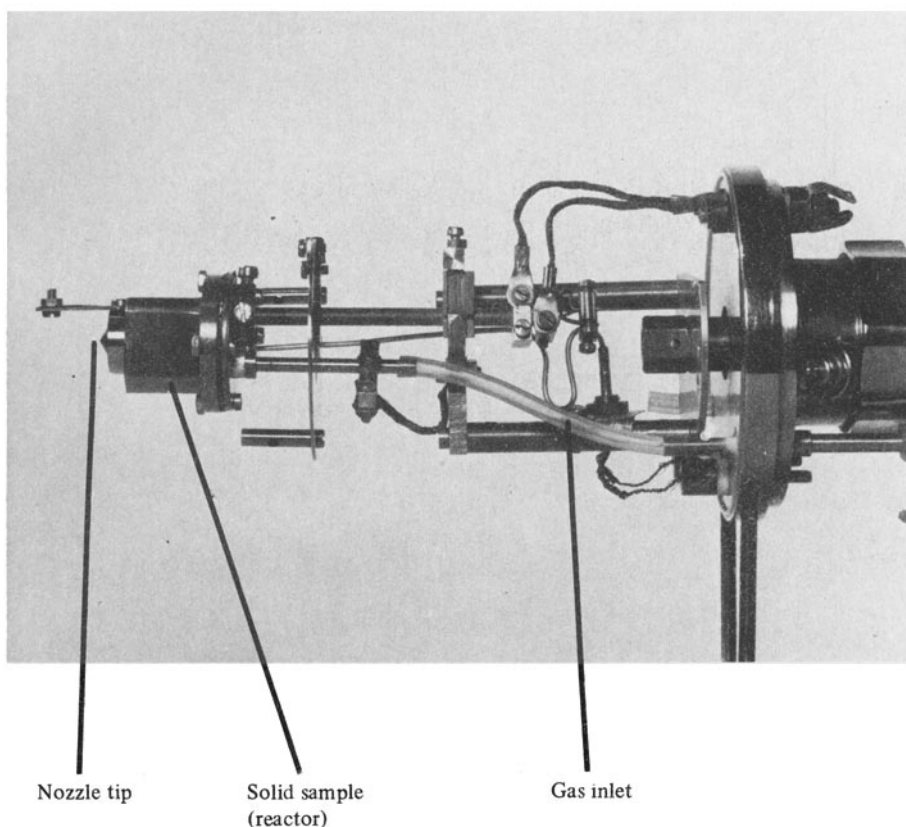
Fig. 10. The reactor-nozzle-system as applied for the electron diffraction investigation of germanium dichloride[59]

trum recorded at 120 °C is also shown (Fig. 11b.). Note the changes in the ratios of ion intensities, e. g., $GeCl_2^+/GeCl_4^+$ or $GeCl_2^+/GeCl_3^+$. Additional evidence for the vapor composition was obtained later in the structure analysis when the presence of any appreciable amount of the tetrachloride species could be ruled out in the least-squares refinement.

The structure of germanium dichloride is characterized by the following parameters

	r_a	l
Ge-Cl (Å)	2.183(4)	0.0805(18)
Cl $\cdots$ Cl(Å)	3.352(14)	0.166(4)

the bond angle Cl-Ge-Cl is 100.3(4)°. It is interesting to compare the structure of $GeCl_2$ with that of carbenes and other analogs and discuss the structural variations in terms of electron pair repulsions and nonbonded interactions[59].
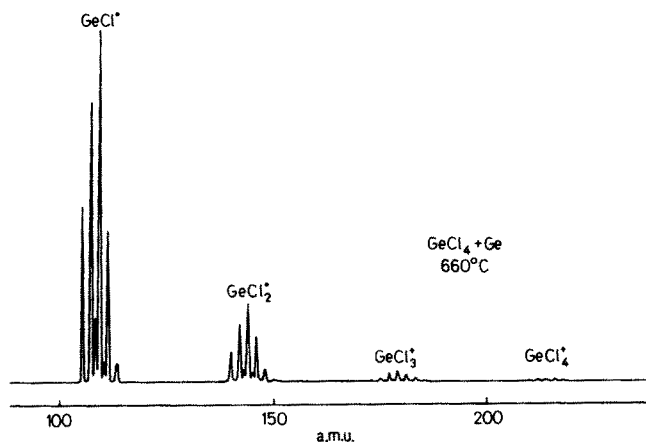
Fig. 11a. Mass spectrum from the Ge + GeCl$_4$ system at 660 °C[59]
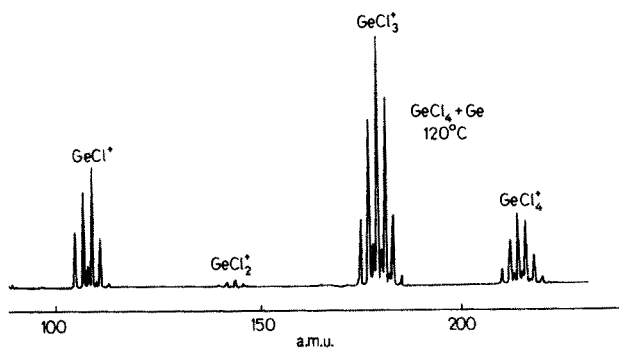
Fig. 11b. Mass spectrum from the Ge + GeCl$_4$ system at 120 °C[59]

3.3 Monomers and Dimers

Mass spectrometric studies on iron(II) chloride[60] and iron(II) bromide[61] showed that monomers are the major species in the vapor phase, while concentration of the dimer, Fe$_2$X$_4$, increases with temperature in its certain interval. The electron diffraction data[43] on iron(II) chloride could be well approximated by monomers only, while the data on the bromide indicated the presence of a detectable amount of dimeric species. This can be seen on the radial distribution of Fig. 12. It was found that there was about 10% dimeric species present under the experimental conditions (nozzle temperature around 625 °C). As regards the relative scattering power, this constituted about 20%, and allowed only the determination of a limited amount of structural information. The electron diffraction date were consistent with a bridge structure characterized by the same Fe-Br$_t$ bond length as that of the monomeric

56

$$Br_t\!\!-\!\!Fe\!\!\overset{\displaystyle Br_b}{\underset{\displaystyle Br_b}{\diagup\!\!\diagdown}}\!\!Fe\!\!-\!\!Br_t$$
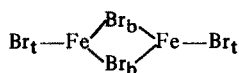
species (cf. Table 1) and by a considerably longer bridge bond, r (Fe-Br_b) = 2.534(13)Å. The four-membered ring was found to be puckered. The orientation of the terminal bonds could not be determined unambiguously. The experimental data could be better approximated with at least one of the terminal bonds being equatorial than with both of them being axial. The curve shown in Fig. 12 was calculated for a model with two equatorial terminal bonds.

Many inorganic molecules are present as dimers (or higher associates) in the vapor phase at the pressure necessary for the electron diffraction experiment. The reaction

$$M_2(vapor) \rightleftharpoons 2M(vapor)$$
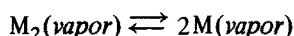
can be shifted towards the dissociation of the dimeric species by a considerable increase in temperature. However, with increasing temperature the vapor pressure may become too large for the electron diffraction experiment. The solution is overheating the unsaturated vapor using a double effusion chamber nozzle system.

The first electron diffraction experiment using a double effusion chamber for overheating the unsaturated vapor was carried out on aluminium(III) chloride[62]. A common heating system was used for the two chambers in this experiment. Electron bombardment was utilized. Presently used double effusion chambers are based on the radiation nozzle system[41, 63].
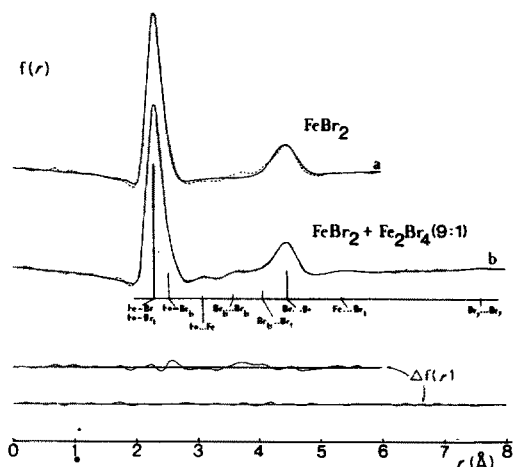
Fig. 12. Experimental (– – –) and theoretical (——) radial distributions for the $FeBr_2$ + Fe_2Br_4 system[43]; (a) The theoretical curve was computed for the monomer only; (b) The theoretical curve was computed for a monomer/dimer ratio of 9:1
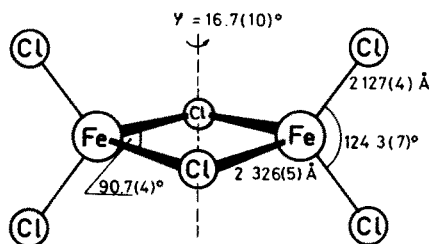
Fig. 13. The molecular model and geometrical parameters of dimeric iron(III) chloride[65]

In the course of our studies of iron-chloride systems, the structure determination of both monomeric and dimeric iron(III) chlorides are scheduled. Prior to the electron diffraction experiments, a mass spectrometric investigation of the vapor composition of iron(III) chloride was carried out as a function of the temperature under the electron diffraction experimental conditions[64]. It was established that a nozzle temperature of 190 °C provides sufficient vapor pressure and the vapor consists of only dimeric molecules. In order to produce monomeric molecules whose relative abundance is an order of magnitude greater as regards the dimers, the chamber containing the nozzle had to be heated to 450 °C while the other chamber, containing the sample was kept at about 200 °C. The analysis of the dimeric structure has been completed[65] while that of the monomer is in progress.

The experimental data for the Fe_2Cl_6 molecules could be best approximated by a model with a puckered four-membered ring (C_{2v} symmetry). However, the deviation from the D_{2h} symmetry may be a consequence of large-amplitude vibrations around the imaginary axis connecting the two bridging chlorine atoms (cf. Fig. 13). Similar large-amplitude torsional motion has been observed in dimeric aluminium(III) chloride molecules and analogous systems by Hedberg et al.[66]. The geometrical parameters of Fe_2Cl_6 are shown in Fig. 13. The difference between the terminal and bridging Fe-Cl bond lengths is about 0.2 Å thus very similar to that observed in the Fe_2Br_4 molecule (see above). These data suggest a considerable difference in the strength of the terminal and bridging bonds, the former being much stronger than the latter.

3.4 Donor-Acceptor Complexes

It is especially important to investigate the molecular structure of coordination compounds in the vapor phase because the relatively weak coordination interactions may be considerably influenced by intermolecular interactions in solutions and especially in crystals. It has been shown that the geometrical variations can be correlated with other properties of the molecular complexes[67]. In particular the structural changes in the $F_3B \cdot N(CH_3)_3$ and $Cl_3B \cdot N(CH_3)_3$ molecules[68] relative to the respective monomeric species unambiguously indicated boron trichloride to be a stronger acceptor than boron trifluoride. Data on the geometry and force field have also been correlated[68, 69].

Special mention is made here of the correlation of the electron diffraction and mass spectrometric results on the compounds

$Cl_3Al \cdot NH_3$, $Cl_3Ga \cdot NH_3$

$Br_3Al \cdot NH_3$, $Br_3Ga \cdot NH_3$
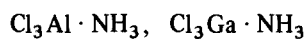
from the point of view of complex stability and relative bond strength[70].

The mass spectrometric behavior (the types and abundance ratios of the fragments) shows variations from compound to compound depending on the changes of both the metal and halogen atoms. Substitution of aluminium by gallium or that of chlorine by bromine considerably decreases the stability of the molecular ion.

The primary processes of fragmentation is either the splitting off a halogen atom or an ammonia molecule. The former is dominating for the aluminium compounds (in fact, for $Cl_3Al \cdot NH_3$ no loss of ammonia occurs) while the latter also becomes important for the gallium compounds. The relative occurrence of the two kinds of processes is about the same for $Cl_3Ga \cdot NH_3$. For illustration, the mass spectra of $Cl_3Al \cdot NH_3$ and $Cl_3Ga \cdot NH_3$ are shown in Fig. 14.
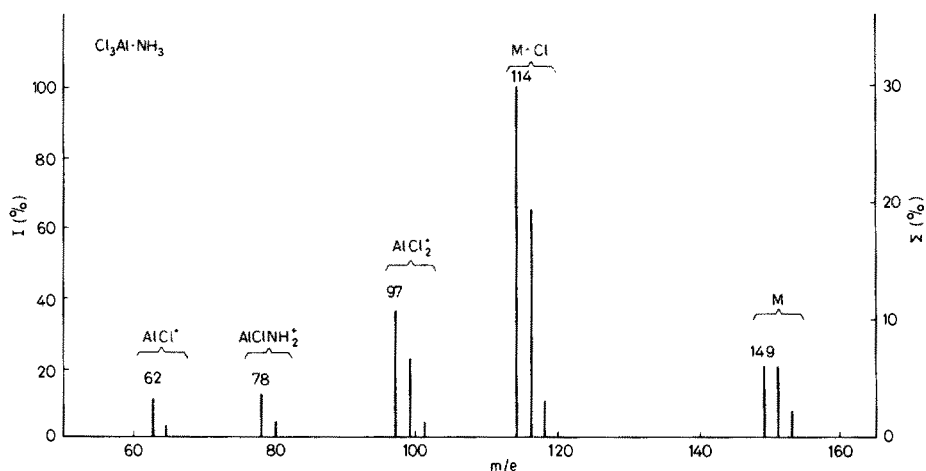
Fig. 14a. The mass spectrum of $Cl_3Al \cdot NH_3$[70]
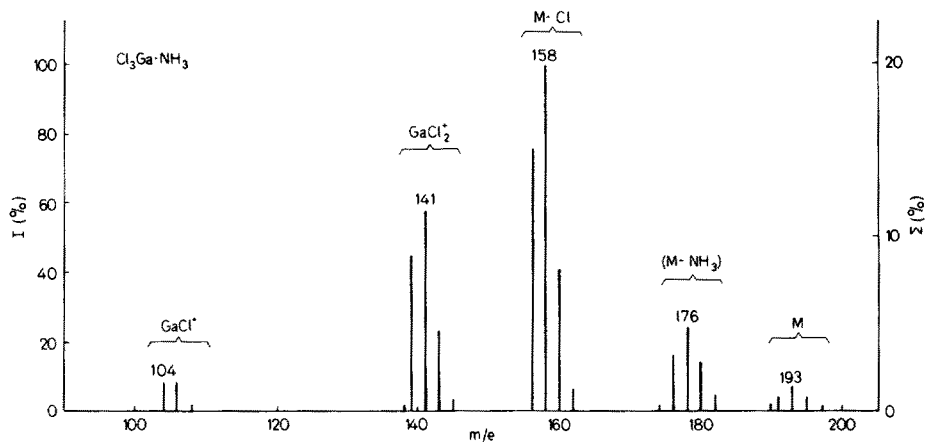
Fig. 14b. The mass spectrum of $Cl_3Ga \cdot NH_3$[70]

Table 3. Parameters characterizing the metal bond configuration in some donor-acceptor complexes

	$Cl_3Al \cdot NH_3$[71)]	$Br_3Al \cdot NH_3$[73)]
r_g(Al-X), Å	2.101(5)	2.266(5)
⩣ X-Al-X (°)	116.9(4)	116.1(3)
r_g(Al-N), Å	1.998(19)	1.999(19)
	$Cl_3Ga \cdot NH_3$[72)]	$Br_3Ga \cdot NH_3$[73)]
r_g(Ga-X), Å	2.144(5)	2.290(5)
⩣ X-Ga-X (°)	117.1(3)	116.6(3)
r_g(Ga-N), Å	2.058(11)	2.082(33)

The geometrical parameters determined by electron diffraction are summarized in Table 3. Consider the difference between the Al-N and Ga-N coordination bond lengths relative to the difference between the metal-chlorine bond lengths,

r(Ga-N) − r(Al-N)   0.061 Å

r(Ga-Cl) − r(Al-Cl)   0.042 Å

Although the coordination bond lengths are determined with large uncertainty, their *difference* can be viewed with more confidence. The bond length variations suggest a weaker Ga-N coordination iinkage relative to the Ga-Cl bond with respect to the relative strengths Al-N/Al-Cl. This observation is strikingly consistent with the notion on the relative bond strength deduced from the comparison of the respective mass spectra.

4 A Variety of Structural Problems

4.1 Metallocenes

Table 4 collects the metallocene molecules whose electron diffraction structure determination was not yet or was only preliminarily covered by Hargittai and Hargittai's book[67)]. For discussion of stereochemical implications the reader is referred to the cited book and the original papers. Only a few comments are given here. The reanalysis of the original experimental data on $Ti(C_5H_5)_2Cl_2$ and $Zr(C_5H_5)_2Cl_2$ have resulted in drastic changes for some of the parameters. Most notably the new metal-chlorine bond lengths are r(Ti-Cl) = 2.318(8) Å and r(Zr-Cl) = 2.459(15) Å. In the vapor phase the cyclopentadienyl rings of the $Ti(C_5H_5)_2BH_4$ molecules seem to take an orientation of relatively high symmetry (Fig. 15) with regard to each other and the Ti ⋯ B axis. The crystal structure analysis resulted in a structure with lower

Table 4. Metal-carbon and carbon-carbon bond lengths in some metallocenes

Compound	r(M-C), Å	r(C-C), Å	Ref.
$Be(C_5H_5)_2$	see text	1.423(2)	74)
$Mg(C_5H_5)_2$	2.339(4)	1.423(2)	75)
$Ti(C_5H_5)_2BH_4$	2.382(6)	1.423(3)	76)
$Ti(C_5H_5)_2Cl_2$	2.372(6)	1.397(3)	77)
$Zr(C_5H_5)_2Cl_2$	2.492(9)	1.391(7)	77)
$V(C_5H_5)_2$	2.280(5)	1.434(3)	78)
$Cr(C_5H_5)_2$	2.169(4)	1.431(2)	78)
$Mn(C_5H_5)_2$ | high-spin	2.433(8)	1.427(2)	79)
| low-spin	2.144(12)		79)
$Fe[C_5(CH_3)_5]_2$	2.064(3)	1.439(2)	80)
$Co(C_5H_5)_2$	2.119(3)	1.429(2)	81)
	2.113(3)	1.430(3)	82)

symmetry[83]. The results of two independent studies of cobaltocene are in good agreement.

The story of the beryllocene structure determination has been told in Hargittai and Hargittai's book[67] up to the early 70s. There seemed to be then two models. One is Haaland et al.'s[84] in which the two cyclopentadienyl rings are parallel and staggered and the beryllium atom is situated on the coinciding five-fold symmetry axes of the two rings and may occupy two alternative positions. This C_{5v} symmetry model came from electron diffraction and was thought to represent the vapor-phase structure. The other model was Wong et al.'s[85] resulting from an X-ray diffraction analysis of crystals at $-120\,°C$. One of the two parallel rings is slipped by 1.2 Å in this model representing essentially a σ-bonded and π-bonded ring system. The X-ray diffraction data on a room temperature crystal pointed to an even more complex model[86]. Wong et al.'s slip model originally was not found to be compatible with
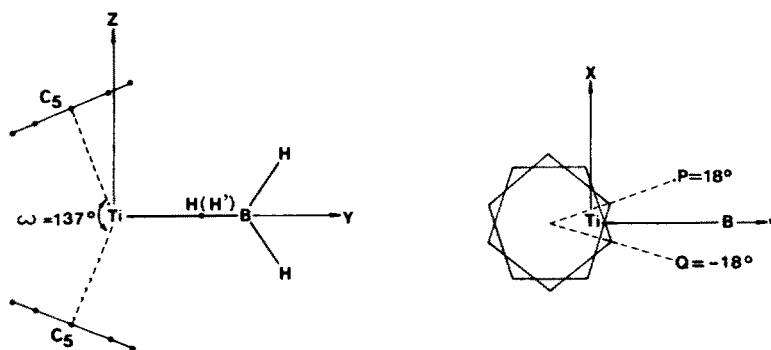
Fig. 15. The molecular model of bis(cyclopentadienyl)-titanium borohydride from an electron diffraction analysis[76] as projected in two planes; The angles ω, P, and Q are indicated; P = 0° and Q = 0° when the apexes of the rings are projected onto the Ti-B bond

the gas electron diffraction data[87]. Thus, for a time at least, beryllocene was thought to be an interesting example of drastically differing structures in the vapor and crystalline phases[67].

It was due to quantum chemical calculations with increasing degree of sophistication that the beryllocene story was continued. From the point of view of electron diffraction it has both structural and methodological interest. The general features of the results of calculations[88–93] are the following: A rather low symmetry structure having one pentahapto (π-bonded) and one monohapto (σ-bonded) ring appears to be the most likely. Even the ferrocen-like D_{5h} (or D_{5d}) model appears to be considerably more stable than the C_{5v} model. The "dynamic" or "fluxional" character of the beryllocene structure has also been repeatedly emphasized.

It was on this background that Haaland et al.[74] reinvestigated the beryllocene structure by electron diffraction. They again confirmed the compatibility of the C_{5v} model with the experimental data. However, they also found a slip model by moving the ring at the longest distance from the metal atom sideways to about 0.8 Å. The notion of large-amplitude motion is also consistent with the experimental data.

Further details of the beryllocene structure may be expected from more rigorous calculations. However, the stimulating effect of the theoretical calculations on extending the experimental work has already been well demonstrated.

A remark seems here to be appropriate also concerning the comparison of electron diffraction, X-ray diffraction and theoretical results. There are inherent differences between the two diffraction experiments due to the difference in the nature of the physical phenomena involved and also the structures may be different indeed due to the difference in molecular environment especially when weak intramolecular interactions are of interest. The theoretical calculations yielding the equilibrium structure are, on the other hand, closer to the unperturbed vapor-phase structure, but the relevant experimental data carry the consequences of averaging over the intramolecular motion. This may conceal important structural features especially in the case of large-amplitude motion as compared with the equilibrium structure.

4.2 Finer Structural Details in Benzene Derivatives

Detecting, reliably determining and interpreting small structural differences may be of great importance in our understanding of the nature of forces governing molecular structure. Electron diffraction is generally not easily suited to detecting these small differences because of the increasingly strong correlation among (geometrical and vibrational) parameters characterizing the contributions of similar interatomic distances. Nevertheless it is possible in some fortunate cases although it is always favorable to utilize additional information.

The deformation of the benzene ring in substituted benzenes is a sensitive indicator of substituent effects. Extensive experimental evidence accumulated over the past two decades, mainly from X-ray diffraction studies of solid state samples[94]. However, the first report of a ring distortion in a benzene derivative was done by Keidel and Bauer in their pioneering (1956) gas-phase electron diffraction study of the molecular structure of phenylsilane[95]. Recently a

study[96, 97)] of the toluene structure demonstrated[1] the enhanced possibilities as well as the difficulties of electron diffraction in solving similar problems. The structure analysis of p-xylene[97)] has demonstrated that gas-phase electron diffraction is an especially suitable tool for accurately measuring ring distorsions in symmetrically substituted benzene derivatives. It should be pointed out that such molecules lack a permanent dipole moment and are, accordingly, unaccessible for microwave spectroscopy. Some structural results obtained for p-xylene are shown in Fig. 16 together with those on toluene for comparison. In addition to the ring deformation, the results clearly indicate the methyl C-H bond to be somewhat longer than the phenyl C-H bond. Although these differences have large standard deviations and they seem to be sensitive to the conditions of the analysis, in no case were they found to vanish or to become negative. Thus it is puzzling that the opposite trend was observed by a parallel independent study of the toluene molecule[98)].

Small structural differences should, of course, always be treated cautiously in electron diffraction work. It is also to be realized, however, that the reliability of the determination of these small differences depends not only on the determination of the parameters directly involved in describing them but contributions from other, usually nonbond distances may play important role. This was clearly seen in the determination of the ring deformatin of p-xylene where the long $C \cdots C$ distances were particularly instrumental[97)].

It is worth mentioning that the electron diffraction results obtained for toluene under the assumption of a D_{6h} symmetry ring were consistent with the later results of less constrained refinement, when combined with the available limited amount of microwave spectroscopic structural information[99)], viz. the substitution coordinates of the hydrogen atoms adjacent to the ring. Thus the following angles were obtained[96)] α 118.6°, β 120.9°, γ 120.0°, and δ 119.5°. It is also comforting that there is complete agreement between the electron diffraction results (Fig. 16) and those from ab initio MO calculations[100)].
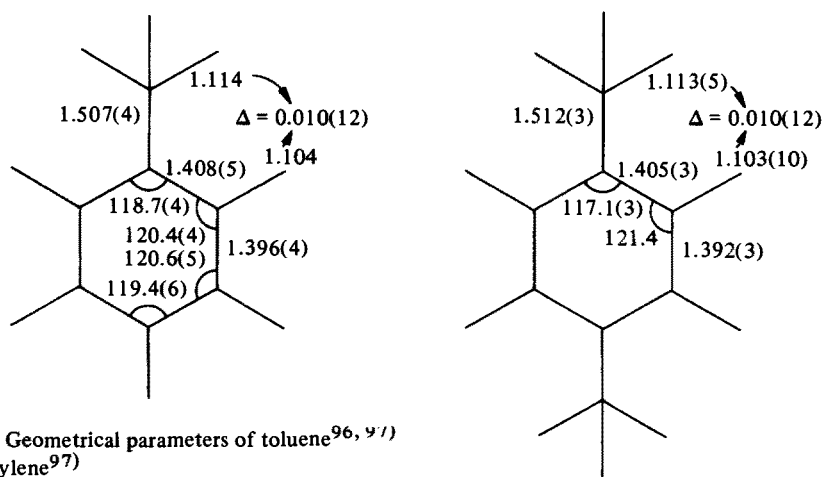
Fig. 16. Geometrical parameters of toluene[96, 97)] and p-xylene[97)]

1 Originally the electron diffraction data on toluene have been analysed assuming D_{6h} symmetry for the benzene ring[96)]. Later this constraint was removed and the carbon ring was allowed to assume C_{2v} symmetry[97)]. The results of this later work are cited here

The deformation of the benzene ring has also been determined in the electron diffraction study of *o*-phenylene-sulfite by Schultz et al.[101]. This seemingly com-

plicated molecule proved to be a good subject for the electron diffraction determination of the five-membered ring structure as well since the presence of the adjacent benzene ring apparently reduces the intramolecular mobility of the five-membered ring. Its envelope conformation and the axial orientation of the S=O bond have been unambiguously determined.
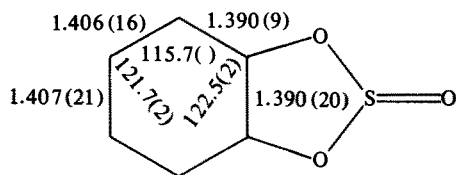
4.3 Metal Borohydrides

The elucidation of their structure has proved to be an intricate task and considering their very interesting bonding peculiarities, very few have been studied so far[67]. In spite of repeated investigations, many structural details of even the examined compounds have yet to be cleared up. The history of the structural studies of beryllium borohydride is especially fascinating. It has been described in detail[67], and of the electron diffraction work, three major instances may be singled out. First Bauer[102] proposed a chain model in which the H-B · · · Be · · · B-H skeleton was linear. Later Almenningen et al.[103] established that the three metal atoms were at the corners of a roughly equilateral triangle. More recently Gundersen et al.[104] confirmed essentially the original Bauer model. Beryllium borohydride is mentioned here for two reasons. One is that Haaland et al.[105] found the electron diffraction scattering to strongly depend on the circumstances in which the beryllium borohydride sample was prepared for the scattering experiment. This indicates at least that some weak interactions may be extremely important in forming this structure. Although it is a difficult experiment, it is hoped that further extensive work is forthcoming. The other factor is that nonempirical MO calculations on beryllium borohydride are expected to appear in the near future. What makes one hope for this is the appearance of such calculations on similar systems with gradually growing complexity[106].

4.4 Revival of Interest in Main Group Elements

The noticeable renaissance of main group chemistry is well reflected by the relatively large number of structures with main group elements determined by electron diffraction. Consider as examples the molecules with boron, silicon, phosphorus, or sulfur.

The numbers of such molecules whose structure has been elucidated since the beginning of 1977 up to the beginning of 1979 are at least

boron	~10
silicon	~15
phosphorus	~16
sulfur	~26

These figures are based on published and submitted papers. Among others, carboranes, donor-acceptor complexes of boron, ring molecules with silicon, phosphoranes, sulfones have received much attention. The lack of gas-phase structural studied of other classes of compounds, e. g., sulfuranes, is also noteworthy. The above elements were selected as most typical. Much interest is concentrated however on other elements as well, which may have been somewhat neglected in the past. The increase of the amount of structural data is also facilitating demand for further extension of the circle of compounds studied.

4.5 Some General Remarks

One of the dangers in an electron diffraction analysis is the so-called multiple solutions which are gradually becoming more and more numerous. I am afraid that the reason for their increasing number is that they may have been overlooked on occassions in the past. Some recent examples include $Cl_3Al \cdot NH_3$[71], $SeOCl_2$[107], $(CH_3)_2GeCl_2$[108]. However, this problem is widely considered now and has been repeatedly discussed. The solution is usually found by involving independent structural information. Very often these multiple solutions comprise basicly similar models with somewhat, or more considerably, differing geometrical parameters.

Another dilemma may be posed when some, usually more symmetrical form with large-amplitude motion on one hand, and a mixture of two or more less flexible models equally well reproduce the experimental data. This problem is dealt with by papers on large-amplitude motion.

Another kind of problem may be when some types of models are entirely left out of consideration. Examples for this may be found, e. g., among organometallic structures including those discussed in this review. It seems to me that more benefit of the doubt should be given to more models especially in areas which are new to structural elucidation.

Finally, in a vast number of structure analyses we tend to ignore small structural differences. They may often be indeed unaccessible to electron diffraction. It is not always obvious, however, how such assumptions will influence the determination of principal parameters for which generally great accuracy may be claimed. Carefulness dictates the testing the influence of such assumptions and the incorporation of the results of the tests into the error estimates. It is hoped, however, that other sources, e. g., quantum chemical calculations will aid electron diffraction by providing reliable information on the small structural differences. They may often be calculated reliably even when the actual parameters themselves may be much less reliable.

5 The Importance of Qualitative Models, Experimental Data and Nonempirical Calculations

The electron diffraction molecular structure research is in a fruitful and mutually beneficiary relationship with nonempirical quantum chemical investigations as well as with the development of qualitative models on bonding and molecular geometry. Of the latter the valence shell electron pair repulsion (VSEPR) model[109] and the considerations on nonbonded atom-atom interactions[110] are especially promising in accounting for a large body of data on molecular geometry of inorganic compounds. The qualitative models serve well the systematization of experimental data and provide models to be investigated. On the other hand, new experimental data constantly provide tests for the models and facilitate the recognition of limitations of these models. It is the knowledge of limitations that makes the application of a qualitative model more reliable. Finally, the non-empirical calculations are expected to play the role of yet another physical tool for structure determination, to open up new possibilities for complementary utilization of experiment and theory, and to interpret accumulated data and established structural variations. Some recent results will serve here for illustration of the interrelationship of electron diffraction work with qualitative models and nonempirical calculations.

One of the basic rules of the VSEPR model states that multiple bonds have larger space requirement and exercise stronger repulsion than single bonds ("the multiple bond rule"). The relationship of the bond angles in XSO_2Y sulphones
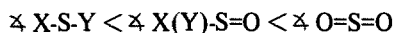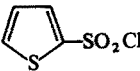
$$\angle \, X\text{-}S\text{-}Y < \angle \, X(Y)\text{-}S\text{=}O < \angle \, O\text{=}S\text{=}O$$

Table 5. Bond angles around the sulphur in XSO_2Y sulphones

Compound	$\angle \, (°)$			Ref.
	X-S-Y	X(Y)-S=O	O=S=O	
FSO_2F	96	108	124	[111]
CH_3OSO_2F	97	107, 109	124	[112]
CF_3SO_2Cl	99	108, 108	122	[113]
CCl_3SO_2Cl	98	108, 109	122	[114]
CH_3SO_2F	98	106, 110	123	[115]
$ClSO_2Cl$	100	108	123	[116]
CH_3OSO_2Cl	103	106, 109	122	[117]
CH_3SO_2Cl	101	107, 109	121	[118]
$CH_3SO_2CH_3$	103	108	120	[119]
$CH_2=CHSO_2Cl$	100	106, 110	122	[120]
$C_6H_5SO_2Cl$	101	106, 110	122	[121]
$OCNSO_2Cl$	98	108, 108	123	[122]
$(CH_3)_2NSO_2Cl$	103	106, 109	123	[123]
⬡–SO_2Cl	101	109	122	[124]

is invariant to the ligand X and Y and convincingly demonstrates the validity of the above rule in a large series of molecules. The relevant electron diffraction results are collected in Table 5.

Another one of the VSEPR rules referred to as "the electronegativity rule" states that with increasing ligand electronegativity more electron density is drawn away from the valence shell of the central atom and the repulsion from the bonding pair decreases. A consequence of this is the shortening of the S=O bonds in XSO_2Y sulphones as the electronegativity of the X or/and Y ligands increases. At the same time the shortening of the S=O bonds is accompanied by a slight opening of the O=S=O bond angle (cf. "the electronegativity rule" *and* "the multiple bond rule"). The changes in the geometry of the SO_2 group are shown in Fig. 17. Other structural variations in the sulfone series may be more difficult to predict as they occur as a result of competing effects[115, 125].
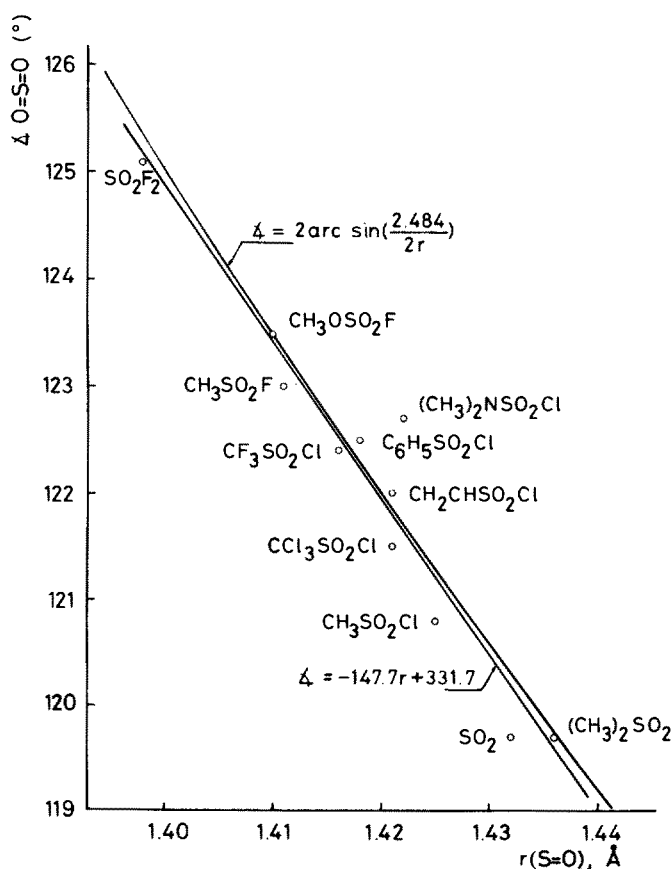
Fig. 17. O=S=O bond angles (α) and S=O bond lengths (r) in XSO_2Y sulfones; Circles: experimental values (for sources see Table 5 and Ref.[125]); The empirical relationship $\alpha = -147.7r + 331.7$ was found by a least squares procedure; the trigonometrical expression utilizes the remarkable phenomenon of the O $\cdots$ O distance being constant (2.484 Å) in a large series of sulfone molecules

As the variations of the S=O bond lengths and the O=S=O bond angles are considered, a striking constancy of the O $\cdots$ O distance can be observed. Indeed, the empirical relationship

$$\measuredangle \, O{=}S{=}O = -147.7 \, r \, (S{=}O) + 331.7 \quad (\sigma = 0.6°)$$

and the sine rule

$$\measuredangle \, O{=}S{=}O = 2 \, \text{arc} \, \sin \left[\frac{r(O \cdots O)}{2r(S{=}O)} \right]$$

using $r(O \cdots O) = 2.484$ Å give hardly different results.

The constancy of the O $\cdots$ O distance in the sulfone molecules calls attention to the importance of nonbonded interactions in addition to the electron pair repulsions in forming the sulfone geometry. It also points to the usefulness and even necessity of considering the nonbond distances in addition to bond lengths and bond angles when discussing structural variations. Finally, it proved to have methodological significance in the electron diffraction structure analyses of sulfones. As the tetrahedral sulfur bond configuration results in strong correlation among the respective nonbond distances and amplitudes, it has been advantageous to use $r(O \cdots O)$ as independent parameter and to assume it to be 2.484 Å or take it from microwave measurements if available and refine it in the last stage of the analysis only

It appears that the electron pair repulsions and atom-atom interactions both are important in establishing the molecular geometry. The actual structure depends on the relative magnitude of the various interactions.

The nonbond atom-atom interactions are apparently increasingly important as the ligand size *versus* the central atom size increases. It is almost two decades ago that Bartell[110] introduced a set of intramolecular van der Waals radii which correspond to the minimum distance of the atoms X and Y in the triatomic fragment XAY (these radii are also called nonbond 1,3 radii). Later Glidewell[126] has extended such radii for heavier elements as well. It is astonishing how Bartell's original radii are still applicable. Thus, for instance his 1,3 radius for fluorine is 1.08 Å, and the mean value of F $\cdots$ F distances in 40 molecules containing CF_3 group was found[127] to be 2.162 Å with a standard deviation of only 0.008 Å. Such consideration on the F $\cdots$ F nonbond distances served as basis to prefer one[128] over another[129] electron diffraction result on tetrafluoro-1,3-dithiethane when two sets of results showed a 2% systematic difference.
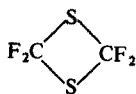
Experimental geometries on analogous sulphides, sulpoxides, and sulphones called attention[130] to an apparent failure of the VSEPR model to account for the bond angle variations in AX_4, BX_3E, CX_2E_2 series, where X is ligand and E is a lone electron pair. The experimental results are illustrated by Figs. 18a and b. The

X-S-X (°)
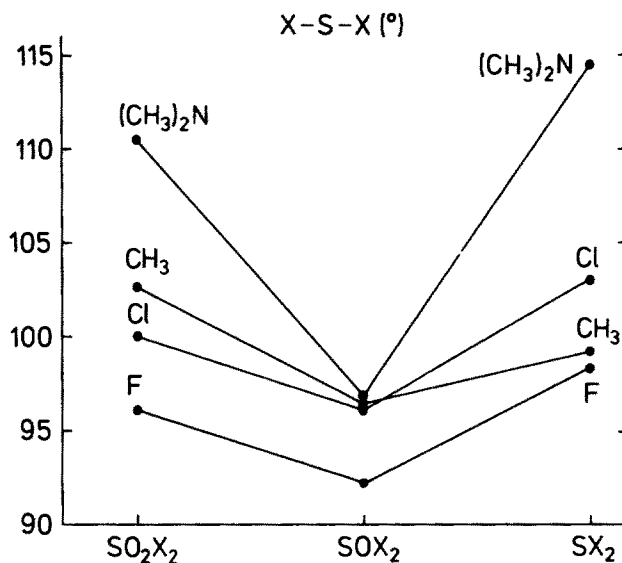
Fig. 18a. The bond angles X-S-X in a series of sulfones, sulfoxides, and sulfides[125]
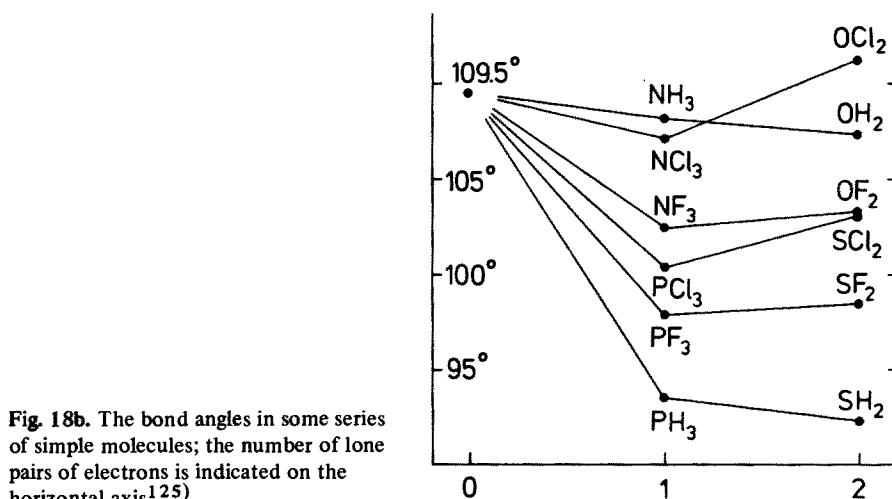
Fig. 18b. The bond angles in some series of simple molecules; the number of lone pairs of electrons is indicated on the horizontal axis[125]

experimental results have been closely reproduced by *ab initio* MO calculations, a detailed account of which have been recently communicated[131]. In addition to reproducing the experimentally observed structural variations, the theoretical results expressed in terms of localized orbitals have resolved the apparent discrepancy between the geometries and the original VSEPR predictions. Of the results of the theoretical calculations, only one aspect is mentioned here. Cruickshank[131] suggested to consider the triple angle averages, i. e., the averages of the angles to the other

three ligands around the central atom (a lone pair of electrons (lp) is also looked at as a ligand). Some typical triple angle averages are given below

S-F	$102°$	O-F	$104°$
S-H	$104°$	O-H	$107°$
S=O	$113-114°$		
S-lp	$114-115°$	O-lp	$112-114°$
P-F	$105°$	N-F	$104°$
P-H	$104°$	N-H	$106°$
P-lp	$122°$	N-lp	$114°$

A remarkable constancy of the triple angle averages was observed for a given bonding or lone pair orbital. The average angular space required by a lone pair or the S=O double bond is considerably greater than that required by a single bond in complete agreement with the VSEPR predictions. If considering the triple angle averages, the apparent contradiction between the experimental bond angles of Fig. 18a and b and the VSEPR model can be resolved. Thus, for example, while the bond angle in SF_2 is greater than the bond angle in PF_3, the angular requirement of the S-F bond is less than that of the P-F bond. Also, the phosphorus lone pair is larger than the sulfur lone pair. Similar considerations may be applied to the OF_2, NF_3 molecule-pair. The apparent contradictions could be resolved for the SX_2, SOX_2, SO_2X_2 series as well. Thus revealing the lone pair positions by the calculations, the overall competition for angular space around the central atom could be understood. Conversely, the experimental data facilitated the search for a better understanding of the VSEPR model.

6 Empirical Relationships

In the world of increasingly important nonempirical calculations we may tend to underestimate the usefulness of empirical relationships. They have been useful, however, and the range of their application may well extend as the wealth of new geometrical data is being incorporated in the existing empirical relationships or is used for establishing new ones. Some examples of empirical relationships follow here, in which geometrical parameters, primarily bond distances are utilized (they come both from electron diffraction and microwave spectroscopy). More details and examples of application can be found, of course, in the respective sources.

(*i*) Bond length *vs.* bond stretching frequency[132, 133]. A good linear relationship has been established between the S=O bond length (r) and S=O bond stretching frequency ($\tilde{\nu}$)[1] in the XSO_2Y sulphone series:

$$\tilde{\nu} = -3695.0r + 6549.4 \qquad (\sigma = 9 \text{ cm}^{-1})$$

---

[1] $\tilde{\nu} = \left[\frac{1}{2}(\nu_{as}^2 + \nu_s^2)\right]^{1/2}$
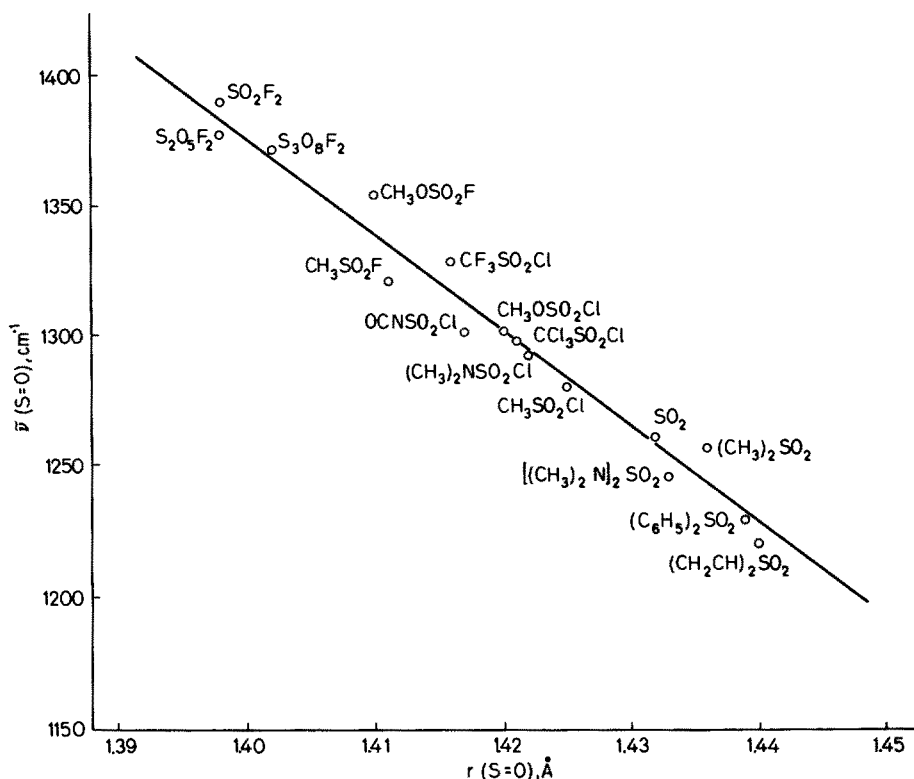
Fig. 19. Correlation between the average stretching S=O frequency and the S=O bond length in a series of XSO_2Y sulfones[125]

The bond lengths refer to vapor-phase structures while the frequencies come from spectra recorded on liquid-phase samples. The incorporated data are illustrated by Fig. 19.

(ii) Bond length vs. bond stretching force constant[132]. A second degree relationships is cited here, again for the XSO_2Y sulphone series·

$$f = 1369.14r^2 - 1854.11r + 631,889 \qquad (\sigma = 0.13 \text{ mdyn/Å})$$

(iii) Bond length vs. ligand electronegativity[133]. Both linear and second degree relationships are given here between the S=O bond length and the sum of ligand electronegativities $\chi_X + \chi_Y$ in the XSO_2Y sulphone series

$$\Sigma \chi = -91.28r + 135.54 \qquad (\sigma = 0.10)$$

$$\Sigma \chi = 436.69r^2 - 1328.65r + 1012.00 \qquad (\sigma = 0.07)$$

The corresponding curves with the data used to obtain them are shown in Fig. 20.

71
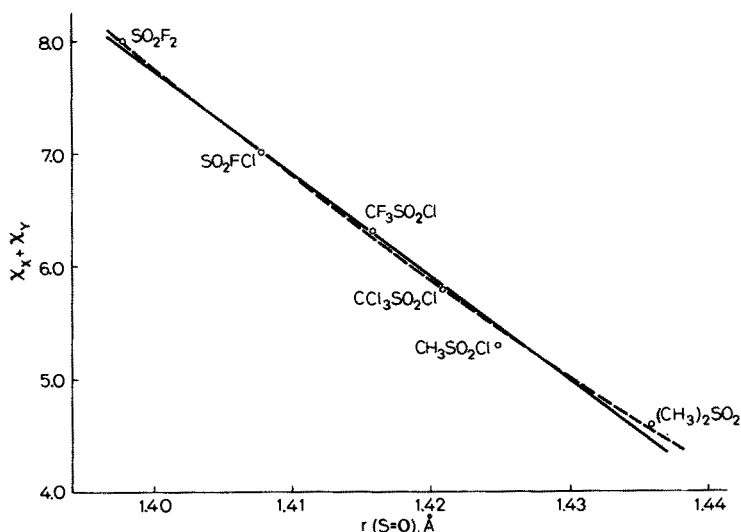
Fig. 20. Correlation between the sum of the X and Y ligand electronegativities and the S=O bond length in XSO_2Y sulfones[133]

The results can be used to predict unknown structural parameters and to establish a group electronegativity scale that will include

$$XF > XOF > XCF_3 > XNCO > XCl > XOCH_3 > XCH_3$$

etc.

(*iv*) Internuclear distance (*r*) vs. mean vibrational amplitude (ℓ). Mastryukov and Cyvin[134] established the following relationship for C-C bonds from a statistical treatment of 57 electron diffraction measurements covering the distance range $1.208b \leqslant r \leqslant 1.549$ Å,

$$\ell(C\text{-}C) = -0.028974r^2 + 0.124162r - 0.071856 \quad (\sigma \ell = 0.0034 \text{ Å})$$

They also treated[135] 71 electron diffraction measurements involving both bonds and nonbonded interactions in the distance range $1.217 \leqslant r \leqslant 5.618$ Å and established the following relationship:

$$\ell(CC) = -0.000147r^2 + 0.023398r + 0.013837 \quad (\sigma \ell = 0.0123 \text{ Å})$$

For further ℓ vs. *r* relationships see Refs.[136−139].

(*v*) Bond distance vs. bond strength (bond dissociation energy). Szabó and Konkoly Thege[140] communicated the following relationship

$$r(C\text{-}C) = 1.740 - 0.0025D(C\text{-}C)$$

72

where D is the bond dissociation energy in kcal/mol (1 kcal/mol = 4.18 kJ/mol). They also found that the same amount of dissociation energy change corresponded to about a ten times larger change in inorganic bond lengths than in the length of the C-C bonds.

(*vi*) Relationships between various geometrical parameters. The relationship between the S=O bond length and O=S=O bond angle in XSO_2Y sulfones has already been mentioned in the previous section. Here the interesting correlation between bond angles of $C-CH_2-C$ fragments is cited after Mastryukov and Osina[141]:

$$\angle\ H\text{-}C\text{-}H = -0.175 \angle\ C\text{-}C\text{-}C + 126.1 \qquad (\sigma_{HCH} = 1.89°)$$

Experimental data from 17 electron diffraction and 13 microwave spectroscopic measurements have been used in establishing this relationship, and the C-C-C bond angles ranged from 50.8° to 116.6°. One of its applications is in the structure analysis of molecules with nonequivalent methylene groups.

7 Compilation and Dissemination of Structural Information

A majority of the electron diffraction structural papers appear in a handful of journals including Acta Chem. Scand. (A), Acta Chim. (Budapest), Bull. Chem. Soc. Japan, Dokl. Akad. Nauk S.S.S.R., Inorg. Chem., J. Am. Chem. Soc., J. Chem. Phys., J.C.S. Dalton Trans., J. Mol. Struct., Trans. Faraday Soc., Vestn. Mosk. Univ. Khim., Z. Naturforsch. (a), Zh. Strukt. Khim. Reviews on structural studies comprising a certain period of time (Spec. Periodic Reports) or a class of compounds or the activity of a laboratory (e. g., Kém. Közlem.) and others appear. A systematic collection of the electron diffraction literature along with all other gas-phase molecular structure information is carried out in the Sektion für Strukturdokumentation of the University of Ulm. A hopefully complete bibliography of gas electron diffraction literature (from the very beginning through 1979)[142] is expected to appear in the near future as a result of the activity of the Ulm center. A computerized storage and retreavel system of annotated bibliography is under way. This system will be capable to answer a great variety of questions that may occur in molecular structure literature search.

The compilations of the Ulm center served basis for the Landolt-Börnstein, New Series Vol. II/7[143] containing the geometrical parameters of free polyatomic molecules determined by experimental techniques. This volume covers the period between 1960 and the middle of 1974. The critical and selective approach makes this volume even more valuable, and ways to make further steps in this direction have been suggested[144].

8 Expectations of the Future

Gas electron diffraction is a unique tool of structural chemistry capable of solving important and interesting problems very often unsolvable by other techniques. It has not developed into a mass-producing technology and hardly ever will. It is not to say that it has achieved the possible sophistication and there are still steps in the analysis that may further be automated. However, I envision its mainstream direc-

tion in a different route. It is a unique tool for solving unique problems. Even though attempts may be made to develop gas electron diffraction into routine technique of certain aspects of chemical analysis, I see its main application where its main capability is, and that is solving molecular structures. Although the primary purpose of gas electron diffraction is to increase our factual knowledge on molecular structure and to facilitate our understanding the nature of forces that build molecules and govern their structural variations, I would not like to avoid the question of where is gas electron diffraction in today's world of ever growing importance of mission oriented research. It is probably true that gas electron diffraction is some steps away from immediate industrial application. However, it is not unrelated to currently used industrial processes. There is need for thermodynamic functions which utilize molecular parameters. Moreover, with increasing importance of vapor-phase processes especially at high temperatures, the formation and behavior including the structure of the species present is to be understood to get these processes under control. The potential of applicability and fundamental scientific interest coincide in this area as also in the case of the study of unstable species, reaction intermediates, etc. As a general influence of the emphasis on mission oriented research, I see the shift of the materials themselves into the center of attention. In this way gas electron diffraction may be viewed as an important tool of materials science. This is increasingly true as gas electron diffraction is being combined with other techniques, primarily with mass spectrometry and matrix isolation vibrational spectroscopy. Being a materials science will eventually stimulate methodological development primarily in experimentation but eventually in computational techniques and finally in theory as well. Much emphasis will always be given to interpreting the physical meaning of the information collected as under the often unusual experimental conditions these species may be far from what their structure in the minimum of the potential energy would be.

Extrapolating from its history and considering its unique capabilities, furthermore, seeing the increasing potential of combined utilizations with other physical techniques and theoretical calculations, and finally, recognizing the needs of fundamental chemical research and materials science in a broader sense, I envision a firm and growingly important place for gas electron diffraction in the future.

9 References

1. Mark, H., Wierl, R.: Naturwiss. *18*, 205 (1930)
2. Bastiansen, O., Kveseth, K., Møllendal, H.: Topics in Curr. Chem. *81*, 99–172 (1979)
3. Spiridonov, V. P., Ishchenko, A. A., Zasorin, E. Z.: Usp. Khim. *47*, 101 (1978)
4. Lowrey, A. H.: Diffraction studies on noncrystalline substances. Hargittai, I., Orville-Thomas, W. J. (eds.). Budapest: Akadémiai Kiadó; Amsterdam: Elsevier in press (1980)
5. Kuchitsu, K., Oyanagi, K.: Faraday Discuss. Chem. Soc. *62*, 20 (1977)
6. Spiridonov, V. P., Gershikov, A. G., Zasorin, E. Z., Butayev, B. D., Prikhodko, A. Ya.: Diffraction studies on noncrystalline substances. Hargittai, I., Orville-Thomas, W. J. (eds.). Budapest: Akadémiai Kiadó; Amsterdam: Elsevier in press (1980)
7. Vilkov, L. V.: Diffraction studies on noncrystalline substances. Hargittai, I., Orville-Thomas, W. J. (eds.). Budapest: Akadémiai Kiadó; Amsterdam: Elsevier in press (1980)

8. Kuchitsu, K.: Diffraction studies on noncrystalline substances. Hargittai, I., Orville-Thomas, W. J. (eds.). Budapest: Akadémiai Kiadó; Amsterdam: Elsevier in press (1980)
9. Debye, P.: Ann. Phys. *46*, 809 (1915)
10. De Broglie, L.: Philos. Mag. *47*, 446 (1924)
11. Davisson, C. H., Germer, L. H.: Nature *119*, 558 (1927)
12. Thompson, G. P., Reid, A.: Nature *119*, 890 (1927)
13. See e. g., Wierl, R.: Ann. Phys. [5] *13*, 453 (1932)
14. Pauling, L., Brockway, L. O.: J. Amer. Chem. Soc. *57*, 2684 (1935)
15. James, R. W.: Phys. Z. *33*, 737 (1932)
16. Finbak, Chr.: Avh. Nor. Vidensk.-Akad. Oslo 13 (1937)
17. Debye, P. P.: Phys. Z. *80*, 404 (1939)
18. Karle, I. L., Karle, J.: J. Chem. Phys. *17*, 1052 (1949)
19. Karle, J., Karle, I. L.: J. Chem. Phys. *18*, 957 (1950)
20. Karle, I. L., Karle, J.: J. Chem. Phys. *18*, 963 (1950)
21. Brockway, L. O., Bartell, L. S.: Rev. Sci. Instrum. *25*, 569 (1954)
22. Bastiansen, O., Hassel, O., Risberg, E.: Acta Chem. Scand. *9*, 232 (1955)
23. Glauber, R., Schomaker, V.: Phys. Rev. *89*, 667 (1953)
24. Bartell, L. S.: J. Chem. Phys. *23*, 1219 (1955)
25. Hassel, O.: Tidsskr. Kjemi, Bergves. Metall. *3*, 32 (1943); English translation: *30*, 25 (1970); Bastiansen, O., Hassel, O.: Tidsskr. Kjemi, Bergves. Metall. *8*, 96 (1946); Bastiansen, O.: Om noen av de forhold som hindrer den fri dreibarhet om en enkeltbilding, Dissertation. A. Garnaes' boktrykkeri, Bergen, 1948; Brunvoll, J.: Elektrondiffraksjonmetoden brukt til konformasjonanalyse, Dissertation. Trondheim 1962
26. Andersen, P.: Structure investigation of organic free radicals, carbanions and carbonium ions. Selected Topics in Structure Chemistry. Andersen, P., Bastiansen, O., Furberg, S. (eds.). Oslo: Universitetsforlaget 1967: Andersen, P.: Kém. Közl. *43*, 523 (1975)
27. Bohn, R. K., Bauer, S. H.: Inorg. Chem. *6*, 304 (1968)
28. Schäfer, L.: J. Am. Chem. Soc. *90*, 3919 (1968)
29. Leggett, T. L. Kennerly, R. E., Kohl, D. A.: J. Chem. Phys. *60*, 3264 (1974); Ivey, R. C., Schultze, P. D., Leggett, T. L., Kohl, D. A.: J. Chem. Phys. *60*, 3174 (1974); Andersen, P., Astrup, E. E.: 5th Hungarian Conference on X-ray, Electron and Neutron Diffraction (1970)
30. Turman, B., Ingrams, J., Hanson, H. P.: Bull. Am. Phys. Soc. *13*, 834 (1968); Hanson, H. P.: Kém. Közl. *37*, 361 (1972)
31. E. g.: Maxvell, R. L., Hendricks, S. B., Mosley, V. M.: Phys. Rev. *52*, 968 (1937); Maxvell, L. R., Mosley, V. M.: Phys. Rev. *55*, 238 (1939)
32. Frost, A. V., Akishin, P. A., Gurvich, L. V., Kurkchi, G. A., Konstantinov, A. A.: Vestn. Mosk. Univ. Ser. Khim. No. *12*, 85 (1953); Akishin, P. A., Vinogradov, M. I., Danilov, K. D., Levkin, N. P., Martinson, E. N., Rambidi, N. G., Spiridonov, V. P.: Prib. Tekh. Eksp. No. *2*, 70 (1958)
33. E. g.: Bastiansen, O., Hedberg, L., Hedberg, K.: J. Chem. Phys. *27*, 1311 (1957); Hedberg, K., Iwasaki, M.: Acta Crystallogr. *17*, 529 (1964); Seip, H. M.: Program KCED 21, Least-Squares Refinement. University of Oslo 1968; Andersen, B., Seip, H. M., Strand, T. G., Stølevik, R.: Acta Chem. Scand. *23*, 3224 (1969)
34. See e. g. Bonham, R. A.: Rec. Chem. Prog. *30*, 185 (1969)
35. See e. g. Bartell, L. S.: Trans. Am. Crystallogr. Ass. *2*, 134 (1966)
36. Kuchitsu, K.: MTP International Review of Science. Physical Chemistry Series One, Vol. 2. Allen, G. (ed.). Molecular Structure and Properties. London: Butterworths 1972
37. Karle, J.: Diffraction studies on noncrystalline substances. Hargittai, I., Orville-Thomas, W. J. (eds.). Budapest: Akadémiai Kiadó: Amsterdam: Elsevier in press (1980)
38. See e. g. Akishin, P. A., Rambidi, N. G., Spiridonov, V. P.: The characterization of high-temperature vapors. Margrave, J. L. (ed.). New York: Wiley 1967
39. Akishin, P. A., Rambidi, N. G.: Zh. Fiz. Khim. *213*, 111 (1960)
40. Kakumoto, K., Ino, T., Kodera, S., Kakinoki, J.: J. Appl. Cryst. *10*, 100 (1977)
41. Ivanov, A. A.: Prib. Tekh. Eksp. No. *2*, 237 (1974)

42. Hargittai, I., Tremmel, J., Schultz, Gy.: J. Mol. Struct. *26*, 116 (1975)
43. Vajda, E., Tremmel, J., Hargittai, I.: J. Mol. Struct. *44*, 101 (1978)
44. Tremmel, J., Ivanov, A. A., Schultz, Gy., Hargittai, I., Cyvin, S. J., Eriksson, A.: Chem. Phys. Lett. *23*, 533 (1973)
45. Hedberg, K.: private communication. 1973
46. Hargittai, I., Cyvin, S. J.: unpublished calculation 1975
47. Molnár, Zs., Schultz, Gy., Tremmel, J., Hargittai, I.: Acta Chim. (Budapest). *86*, 223 (1975)
48. Hargittai, I., Tremmel, J.: Coord. Chem. Rev. *18*, 257 (1976)
49. Thompson, K. R., Carlson, K. D.: J. Chem. Phys. *49*, 4379 (1968)
50. Büchler, A., Stauffer, J. L., Klemperer, W.: J. Chem. Phys. *40*, 3471 (1964)
51. Cotton, F. A., Wilkinson, G.: Advanced inorganic chemistry. New York: Interscience 1972
52. Schultz, Gy., Tremmel, J., Hargittai, I.: preliminary unpublished
53. Krasnov, K. S., Giricheva, N. I., Girichev, G. V.: Zh. Strukt. Khim. *17*, 667 (1976)
54. Waber, J. T., Cromer, D. T.: J. Chem. Phys. *42*, 12 (1965)
55. Danilova, T. G., Girichev, G. V., Giricheva, N. I., Krasnov, K. S., Zasorin, E. Z.: Izv. Vyssh. Uchebn. Zaved. Khim. Khim. Tekhnol. *20*, 1069 (1977)
56. Girichev, G. V., Danilova, T. G., Giricheva, N. I., Krasnov, K. S., Zasorin, E. Z.: Izv. Vyssh. Uchebn. Zaved. Khim. Khim. Tekhnol. *30*, 1233 (1977)
57. Bohátka, S., Berecz, I., Tremmel, J., Hargittai, I.: Proc. 7th Intern. Vac. Congr. and 3rd Intern. Conf. Solid Surfaces, p. 193. Vienna 1977
58. Berecz, I., Bohátka, S., Gál, J., Paál, A.: ATOMKI Közl. *19*, 123 (1977)
59. Schultz, Gy., Tremmel, J., Hargittai, I., Berecz, I., Bohátka, S., Kagramanov, N. D., Maltsev, A. K., Nefedov, O. M.: J. Mol. Struct. *55*, 207 (1979)
60. Schoonmaker, R. C., Porter, R. F.: J. Chem. Phys. *29*, 116 (1958)
61. Porter, R. F., Schoonmaker, R. C.: J. Phys. Chem. *63*, 626 (1959)
62. Rambidi, N. G., Zasorin, E. Z.: Teplofiz. Vys. Temp. *2*, 705 (1964)
63. Tremmel, J., Hargittai, I.: Hung. Sci. Instrum. in press
64. Tremmel, J., Hargittai, I.: unpublished
65. Hargittai, M., Tremmel, J., Hargittai, I.: J. Chem. Soc. Dalton Trans. 87 (1980)
66. Hedberg, K.: private communication; Shen, Q.: Dissertation, Oregon State University, 1973
67. Hargittai, M., Hargittai, I.: The molecular geometries of coordination compounds in the vapor phase. Budapest: Akadémiai Kiadó; Amsterdam: Elsevier 1977
68. Hargittai, M., Hargittai, I.: J. Mol. Struct. *39*, 79 (1977)
69. Cyvin, B. N., Cyvin, S. J., Hargittai, M., Hargittai, I.: Z. Anorg. Allg. Chem. *440*, 111 (1978)
70. Hargittai, M., Tamás, J., Bihari, M., Hargittai, I.: Acta Chim. (Budapest) *99*, 127 (1979)
71. Hargittai, M., Hargittai, I., Spiridonov, V. P., Pelissier, M., Labarre, J.-F.: J. Mol. Struct. *24*, 27 (1975)
72. Hargittai, M., Hargittai, I., Spiridonov, V. P.: J. Mol. Struct. *30*, 31 (1976)
73. Hargittai, M., Hargittai, I., Spiridonov, V. P., Ivanov, A. A.: J. Mol. Struct. *39*, 225 (1977)
74. Almenningen, A., Haaland, A., Lusztyk, J.: J. Organomet. Chem. *170*, 271 (1979)
75. Haaland, A., Lusztyk, J., Brunvoll, J., Starowieyski, K. B.: J. Organomet. Chem. *85*, 279 (1975)
76. Mamaeva, G. I., Hargittai, I., Spiridonov, V. P.: Inorg. Chim. Acta *25*, L123 (1977)
77. Ronova, I. A., Alekseev, N. V.: Zh. Strukt. Khim. *18*, 212 (1977)
78. Gard, E., Haaland, A., Novak, D. P., Seip, R.: J. Organomet. Chem. *88*, 181 (1975)
79. Almenningen. A.. Haaland, A., Samdal, S.: J. Organomet. Chem. *149*, 219 (1978)
80. Almenningen, A., Haaland, A., Samdal, S., Brunvoll, J., Robbins, J. L., Smart, J. C.: J. Organomet. Chem. *173*, 293 (1979)
81. Almenningen, A., Gard, E., Haaland, A., Brunvoll, J.: J. Organomet. Chem. *107*, 273 (1976)
82. Hedberg, A. K., Hedberg, L., Hedberg, K.: J. Chem. Phys. *63*, 1262 (1975)
83. Melmed, K. M., Coucouvanis, D., Lippard, S. J.: Inorg. Chem. *12*, 232 (1973)
84. Haaland, A.: Acta Chem. Scand. *22*, 3030 (1968); Almenningen, A., Bastiansen, O., Haaland, A.: J. Chem. Phys. *40*, 3434 (1964)
85. Wong, C.-H., Lee, T.-Y., Chao, K.-J., Lee, S.: Acta Cryst. *B28*, 1662 (1972)

86. Wong, C.-H., Lee, T.-Y., Lee, T.-J., Chang, T. W., Liu, C. S.: Inorg. Nucl. Chem. Lett. *9*, 667 (1973)
87. Drew, D. A., Haaland, A.: Acta Cryst. *B28*, 3671 (1972)
88. Marynick, D. S.: J. Am. Chem. Soc. *99*, 1436 (1977)
89. Chiu, N. S., Schäfer, L.: J. Am. Chem. Soc. *100*, 2604 (1978)
90. Jemmis, E. D., Alexandratos, S., Schleyer, P. v. R., Streitwieser, A., Schaefer, H. F.: J. Am. Chem. Soc. *100*, 5695 (1978)
91. Demuynck, J., Rohmer, M. M.: Chem. Phys. Lett. *54*, 567 (1978)
92. Gleiter, R., Böhm, M. C., Haaland, A., Johansen, R., Lusztyk, J.: J. Organomet. Chem. *170*, 285 (1979)
93. See addendum in the paper Boldyrev, A. I., Charkin, O. P.: Zh. Strukt. Khim. *18*, 783 (1977)
94. Domenicano, A., Vaciago, A., Coulson, C. A.: Acta Cryst. *B31*, 221 (1975); *B31*, 1630 (1975); Domenicano, A., Mazzeo, P., Vaciago, A.: Tetrahedron Lett. 1029 (1976)
95. Keidel, F. A., Bauer, S. H.: J. Chem. Phys. *25*, 1218 (1956)
96. Seip, R., Schultz, Gy., Hargittai, I., and Szabó, Z. G.: Z. Naturforsch. *32a*, 1178 (1977)
97. Domenicano, A., Schultz, Gy., Kolonits, M., Hargittai, I.: J. Mol. Struct. *53*, 197 (1979)
98. Iijima, T.: Z. Naturforsch. *32a*, 1063 (1977)
99. Kreiner, W. A., Rudolph, H. D., Tan, B. T.: J. Mol. Spectrosc. *48*, 86 (1973)
100. Pang, F., Pulay, P., Fogarasi, G., Boggs, J. E.: Seventh Austin Symposium on Gas Phase Molecular Structure, p. 94, Austin, Texas 1978
101. Schultz, Gy., Serke, I., Kapovits, I.: J. Chem. Soc. Faraday Trans. II *75*, 1612 (1979)
102. Silbiger, G., Bauer, S. H.: J. Am. Chem. Soc. *68*, 312 (1946); Bauer, S. H.: J. Am. Chem. Soc. *72*, 622 (1950)
103. Almenningen, A., Gundersen, G., Haaland, A.: Acta Chem. Scand. *22*, 859 (1968)
104. Gundersen, G., Hedberg, L., Hedberg, K.: J. Chem. Phys. *59*, 3777 (1973)
105. Brendhaugen, K., Haaland, A., Novak, D. P.: Acta Chem. Scand. A *29*, 801 (1975)
106. Boldyrev, A. I., Charkin, O. P., Rambidi, N. G., Avdeev, V. I.: Chem. Phys. Lett. *44*, 20 (1976); *50*, 239 (1977)
107. Gregory, D., Hargittai, I., Kolonits, M.: J. Mol. Struct. *31*, 261 (1976)
108. Vajda, E., Hargittai, I.: Acta Chim. (Budapest) *91*, 185 (1976)
109. See e. g. Gillespie, R. J.: Molecular geometry. London: Van Nostrand Reinhold Co. 1972
110. Bartell, L. S.: J. Chem. Phys. *32*, 827 (1960)
111. Lide, D. R., Mann, D. E., Frisrom, R. M.: J. Chem. Phys. *26*, 734 (1957); Hagen, K., Cross, V. R., Hedberg, K.: J. Mol. Struct. *44*, 187 (1978)
112. Hargittai, I., Seip, R., Nair, K. P. R., Britt, Ch. O., Boggs, J. E., Cyvin, B. N.: J. Mol. Struct. *39*, 1 (1977)
113. Brunvoll, J., Hargittai, I., Kolonits, M.: J. Chem. Soc. Dalton Trans. 1299 (1977)
114. Brunvoll, J., Hargittai, I., Seip, R.: Z. Naturforsch. *33a*, 222 (1978)
115. Hargittai, I., Hargittai, M.: J. Mol. Struct. *15*, 399 (1973)
116. Hargittai, I.: Acta Chim. (Budapest) *60*, 321 (1969)
117. Hargittai, I., Schultz, Gy., Kolonits, M.: J. Chem. Soc. Dalton Trans. 1299 (1977)
118. Hargittai, M., Hargittai, I.: J. Chem. Phys. *59*, 2513 (1973)
119. Hargittai, M., Hargittai, I.: J. Mol. Struct. *20*, 283 (1974)
120. Brunvoll, J., Hargittai, I.: Acta Chim. (Budapest) *94*, 333 (1977)
121. Brunvoll, J., Hargittai, I.: J. Mol. Struct. *30*, 361 (1976)
122. Brunvoll, J., Hargittai, I., Seip, R.: J. Chem. Soc. Dalton Trans. 299 (1978)
123. Hargittai, I., Brunvoll, J.: Acta Chem. Scand. A *30*, 634 (1976)
124. Brunvoll, J., Hargittai, I., Székely, T., Pappalardo, G. C.: J. Mol. Struct. in press (1980)
125. Hargittai, I.: Sulphone molecular structures. Lecture Notes in Chemistry. Vol. 6. Springer: Berlin, Heidelberg, New York 1978
126. Glidewell, C.: Inorg. Chim. Acta *20*, 113 (1976)
127. Hargittai, I.: J. Mol. Struct. *54*, 287 (1979)
128. Smith, Z., Seip, R.: Acta Chem. Scand. A *30*, 759 (1976)
129. Chiang, J. F., Lu, K. C.: J. Phys. Chem. *81*, 1682 (1977)

130. Hargittai, I.: Second European Crystallographic Meeting, Collected Abstracts, Keszthely, 1974; Hargittai, I., Baranyi, A.: Acta Chim. (Budapest) *93*, 279 (1977)
131. Schmiedekamp, A., Cruickshank, D. W. J., Skaarup, S., Pulay, P., Hargittai, I., Boggs, J. E.: J. Am. Chem. Soc. *101*, 2002 (1979)
132. Brunvoll, J., Hargittai, I.: Acta Chim. (Budapest) *96*, 337 (1978)
133. Hargittai, I.: Z. Naturforsch. *34a*, 755 (1979)
134. Mastryukov, V. S., Cyvin, S. J.: J. Mol. Struct. *29*, 15 (1975)
135. Cyvin, S. J., Mastryukov, V. S.: J. Mol. Struct. *30*, 333 (1976)
136. Osina, E. L., Mastryukov, V. S., Vilkov, L. V., Cyvin, S. J.: Zh. Strukt. Khim. *16*, 1065 (1975)
137. Mastryukov, V. S., Osina, E. L.: Zh. Strukt. Khim. *17*, 173 (1976)
138. Mastryukov, V. S., Osina, E. L., Vilkov, L. V., Cyvin, S. J.: Zh. Strukt. Khim. *17*, 80 (1976)
139. Mastryukov, V. S.: Zh. Strukt. Khim. *17*, 86 (1976)
140. Szabó, Z. G., Konkoly Thege, I.: Acta Chim. (Budapest) *86*, 127 (1975)
141. Mastryukov, V. S., Osina, E. L.: J. Mol. Struct. *36*, 127 (1977)
142. ZAED Physics Data. Bibliography of Electron Diffraction 1930–1979 to be published
143. Landolt-Börnstein, New Series, Group II, Vol. 7. Structure data of free polyatomic molecules. Callomon, J. H., Hirota, E., Kuchitsu, K., Lafferty, W. J., Maki, A. G., Pote, C. S., Buck, I., Starck, B., Hellwege, K. H., Hellwege, A. M. (eds.). Springer: Berlin, Heidelberg, New York 1976
144. Hargittai, I.: Acta Chim. (Budapest) *96*, 406 (1978)

Chemical and Stereochemical Properties of Compounds with Silicon or Germanium-Transition Metal Bonds

Ernesto Colomer and Robert J. P. Corriu

Laboratoire des Organomètalliques, Equipe de Recherche Associèe au C.N.R.S. No. 554, Université des Sciences et Techniques du Languedoc, Place Eugène Bataillon, 34060 Montpellier-cédex (France).

Table of Contents

E. Colomer, R. J. P. Corriu

1 Introduction

Since the first complex having a covalent bond between silicon and iron, $(CH_3)_3SiFe(CO)_2(\eta^5\text{-}C_5H_5)$, was prepared in 1956[1], the chemistry of compounds of group IV_B metals bonded to transition metals has expanded very rapidly. Up to now, a few hundred compounds of this type are known, and some excellent reviews have been published dealing with their synthesis and properties[2-6].

In this article we will review:

a) The synthesis of compounds with transition metal-silicon or germanium bonds in which the group IV_B element is chiral (tin will be excluded because, at present, stereochemistry at tin is at the beginning);

b) the chemical and especially stereochemical properties of complexes of this type.

2 Preparative Methods

Many reactions may be successfully utilized in the synthesis of compounds with sigma bonds between group IV_B metals and transition metals, but none is of general applicability. Moreover, the problem is complicated in the case of optically active compounds since:

a) not all functions are easily available, in particular SiBr, and GeBr,

b) some compounds are racemized in solution,

c) racemization may occur in the course of the reaction.

We can classify the methods of synthesis into two main types, namely nucleophilic substitutions and metal IV_B hydride reactions.

2.1 Nucleophilic Substitutions

The transition metal-group IV_B metal bond can be formed both by attack of a transition metal anion at a group IV_B halide and by attack of an alkali metal derivative of the group IV_B element at a suitable transition metal complex.

2.1.1 Transition Metal Anions

Transition metal anions have widely been used in the synthesis of the first row transition metal derivatives of group IV_B metals; however only in one case does the reaction take place with chlorosilanes

$$(\eta^5\text{---}C_5H_5)Fe(CO)_2^{\ominus} + Cl\text{---}Si \underset{Me}{\overset{Ph}{\cdots}} 1\text{-}Np \longrightarrow (\eta^5\text{---}C_5H_5)Fe(CO)_2\text{---}Si \underset{1\text{-}Np}{\overset{Ph}{\cdots}} Me$$

$$R(+) \qquad\qquad S(-)$$
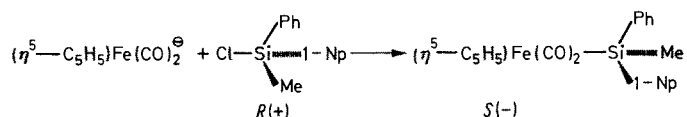
$Np =$ naphthyl

This reaction proceeds with inversion of configuration at silicon and with a stereoselectivity of about 62 %[7-9].

Other transition metal anions fail in giving the expected compounds[10].

Germanium halides react more easily but are useless for the preparation of optically active compounds. Indeed, optically active bromo-germanes are not known, and chlorogermanes rapidly racemize in ether or tetrahydrofuran[11].

2.1.2 Alkali Metal Derivatives of Group IV$_B$ Elements

These derivatives are useful because of the ability of group IV$_B$ metals to give anions and especially of germanium which yields optically active germyllithiums from the corresponding hydrides with complete retention of configuration[12].

R = Me, n - Bu , M = Li
R = H , M = Na, K
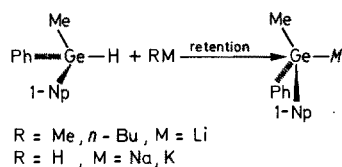
This process may be regarded as the reverse and the complement of the preceding reaction. It has mainly been utilized where transition metal anions are not available (e.g. in Ti, Ni and Cu group).
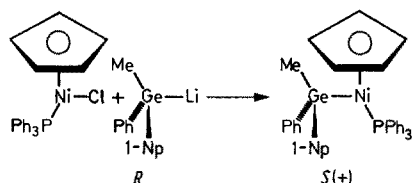
This reaction was first studied in the case of a achiral compound[13] and then applied to the optically active model[14].

Lithium derivatives of triphenylsilanes have also been used to replace halogens in halogenopentacarbonylmetallates of the chromium group[15].

$$[(CO)_5MoCl] \, Et_4N + Ph_3SiLi \rightarrow [(CO)_5MoSiPh_3] \, Et_4N \, .$$

However, the substitution of the halogen is not general and halogen-metal exchange takes place[14, 16-18].

$$Ph_3GeLi + M\text{-}X \rightarrow Ph_3GeX + MLi$$
X = halogen, M = $(CO)_5Mn$, $(\eta^5\text{-}C_5H_5)Fe(CO)_2$
$$Ph_3GeLi + Ph_3GeX \rightarrow Ph_6Ge_2$$
$$M\text{-}X + MLi \rightarrow M_2 \, .$$
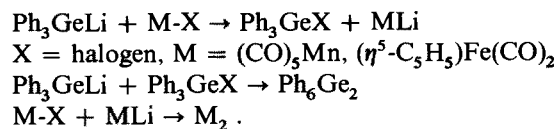
More interestingly, replacement of neutral ligands such as CO by group IV_B anions is also possible

$$GeCl_3^- + Mo(CO)_6 \rightarrow [Cl_3GeMo(CO)_5]^- \quad {}^{19-22)}.$$
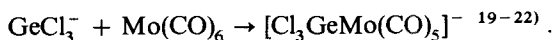
Optically active germyllithium reacts in this way with a number of metal carbonyls[14, 23]:

$M = Cr(CO)_5$, $Mo(CO)_5$, $W(CO)_5$, $Fe(CO)_4$,

$(\eta^5-C_5H_5)Mn(CO)_2$
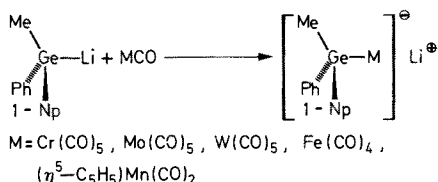
These anions are usually isolated as tetraethylammonium and sometimes tetraphenylarsonium salts.

This reaction allows the preparation of a new type of complexes with nitrosyl ligands[23].

$M = Mo, W$; $R_3 = Ph_3$ or $MePh\,1-Np$, $M' = Ge, Sn$
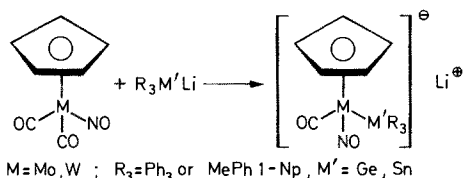
We assume that all these reactions take place with retention of configuration at germanium because germyllithium always reacts with this stereochemistry[24]. The convenience of this method is related to the ease of formation of the lithium derivative. At present, only optically active germyllithiums are available. However, this reaction is suitable method of introduction of a chiral ligand without loss of optical activity, and the ligand is strongly bonded to the transition metal as revealed by the reactivity of these complexes.

2.2 Metal IV_B Hydride Reactions

These reactions are important because they play a prominent role in hydrosilylation and hydrogermylation processes.

They proceed by insertion of the transition metal between the group IV_B element-hydrogen bond. We can distinguish two types of reactions, those associated with the elimination of a neutral ligand and those involving the elimination of a neutral molecule.

2.2.1 Insertion Reactions with Elimination of a Neutral Ligand

These reactions have been extensively studied for optically inactive compounds of silicon and first row transition-metal carbonyls[25].

In the case of the optically active silane, only cymantrene undergoes oxidative addition[26, 27]:

$$R(+) + Si-H \xrightarrow{h\nu} S(-)$$
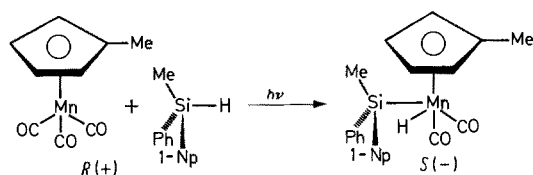
This same reaction has been applied to the synthesis of chiral functional complexes[28].

$$+ R'-Si-H \xrightarrow{h\nu}$$

R = Ph; R' = 1-Np; X = H, F, Cl, OMe
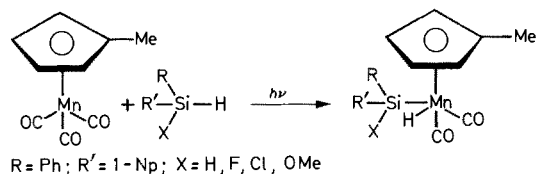
The stereochemistry is assumed to involve retention of configuration. This assumption is very plausible, since retention has already been observed[29-31] for Pt insertion in a Si-H bond, as well as for homogeneous and heterogeneous hydrosilylation[32-34] and hydrogermylation[35]. Moreover, the Si-H bond is known to react generally with retention of configuration[36]. Finally, in a parent reaction of SiH with $CO_2(CO)_8$, X-ray structural analysis reveals that the reaction proceeds with retention of configuration (see Sect. 2.2.2).

This method is not suitable for germanium since metal carbonyls fail in reacting with Ge-H bonds[37] or give very low yields of insertion complexes, e.g.:

$$+ Ph_3GeH \xrightarrow{h\nu} \quad 38)$$

5%
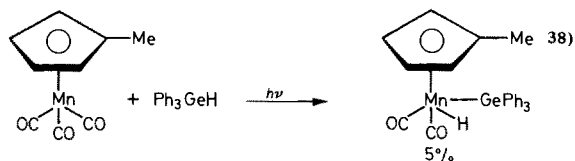
Such compounds can, however, be obtained through a side reaction:

$$Ph_3GeLi + [HFe_3(CO)_{11}] Et_4N \rightarrow [Ph_3GeFe(CO)_4] Et_4N$$

$$\downarrow HCl$$

$$Ph_3GeFe(H)(CO)_4 . \quad 37)$$

83

23)

R$_3$=Ph$_3$ or MePh 1 - Np
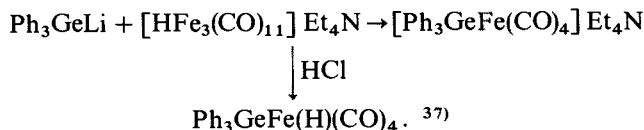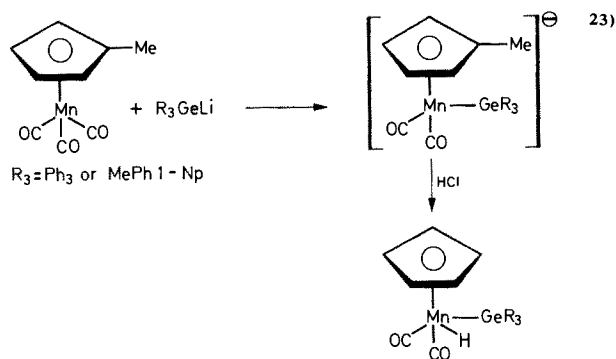
For the silicon-manganese and iron complexes structural determinations show that silicon and hydrogen are in *cis* positions[39, 40].

The platinum complex $Pt(PPh_3)_2C_2H_4$ is inserted into Si-H and Ge-H bonds with the elimination of ethylene ligands[31, 41]:

$$Pt(PPh_3)_2C_2H_4 + R_3MH \rightarrow cis-[Pt(PPh_3)_2(H)(MR_3)]$$

$$R(+) \qquad\qquad\qquad S(-)$$

M = Si R_3 = MePh 1-Np
M = Ge R_3 = EtPh 1-Np
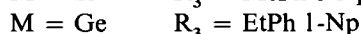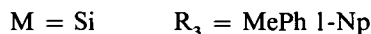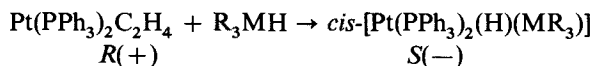
The main difference between Pt and Mn is that the platinum complex has 16 electrons and undergoes addition of silane before eliminating ethylene, following path 1

Path 1: $Pt(PPh_3)_2C_2H_4 \longrightarrow R_3M-Pt(PPh_3)_2C_2H_4 \longrightarrow R_3M-Pt(PPh_3)_2$

(R$_3$MH)   (H)   (C$_2$H$_4$)   (H)
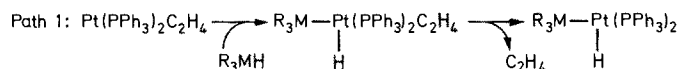
The reverse process is valid for the manganese complex (path 2)

Path 2: $C_5H_5Mn(CO)_3 \longrightarrow C_5H_5Mn(CO)_2 \longrightarrow C_5H_5Mn(CO)_2$

(CO)   (R$_3$MH R$_3$M   H)
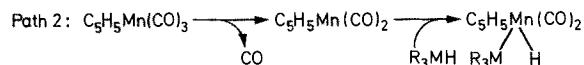
2.2.2 Insertion Reactions with Elimination of Hydrogen in a Neutral Molecule

These reactions resemble those described in section 2.2.1 because both types involve insertion of the transition metal into the Si-H or Ge-H bond. However, here the molecule eliminated is not a neutral ligand but is formed by deinsertion of two ligands which are sigma bonded to the transition metal after the addition of R_3MH.

$L_2PtCl_2 \longrightarrow L_2 Pt Cl_2 \longrightarrow L_2PtCl$

(R$_3$MH)   (R$_3$M   H)   (HCl   R$_3$M)
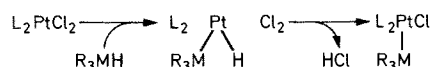
Thus, several complexes with platinum-silicon or germanium bonds have been obtained[29, 31].

$$cis\text{-}[PtCl_2(PMe_2Ph)_2] + R_3SiH \rightarrow trans\text{-}[PtCl(R_3Si)(PMe_2Ph)_2]$$
$$R(+) \qquad\qquad\qquad\qquad S(+)$$

$R_3 = MePh \ 1\text{-}Np$

$$trans\text{-}[PtHCl(PMe_2Ph)_2] + R_3GeH \rightarrow trans\text{-}[PtCl(R_3Ge)(PMe_2Ph)_2]$$
$$R(+) \qquad\qquad S(+)$$
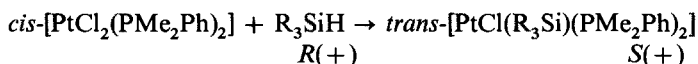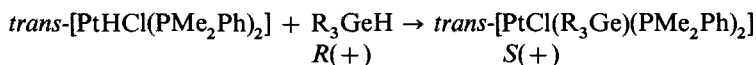
$R_3 = EtPh \ 1\text{-}Np$.

The absolute configuration of the silicon complex has been established by an X-ray study and shown to be (S) starting from the (R) silane, involving retention of configuration[42].

Another type of compound is probably obtained by the following reaction:

$$cis\text{-}[PtMe_2(PMe_2Ph)_2] + R_3SiH \rightarrow [PtH(SiR_3)(PMe_2Ph)_2] + R_3SiMe \quad ^{31)}$$
$R_3 = MePh \ 1\text{-}Np$
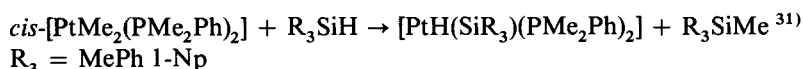
unfortunately the complex could not be crystallized and the structure is elucidated by experiments with other silicon hydrides[43].

Silicon and germanium hydrides react with cobalt, manganese and rhenium carbonyls affording complexes having a silicon (or germanium)-metal bond. These reactions, described previously for inactive compounds[44-46] have been used in the synthesis of optically active silyl and germyl-transition metals:

$$(CO)_8Co_2 + R_3MH \rightarrow (CO)_4CoMR_3 + H_2$$
$$R(+) \qquad S(+)$$
$R_3 = MePh \ 1\text{-}Np, \ M = Si^{32)}, \ M = Ge^{47)}.$
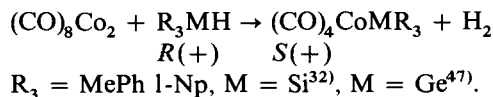
This reaction proceeds with retention of configuration since the absolute configuration of the $(+)$-complex has been shown to be S [48] by X-ray analysis.

Analogously, phosphorus substituted carbonyls react with germanes
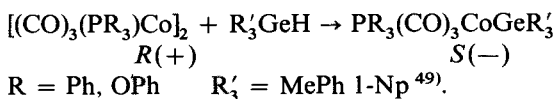
$$[(CO)_3(PR_3)Co]_2 + R_3'GeH \rightarrow PR_3(CO)_3CoGeR_3'$$
$$R(+) \qquad\qquad\qquad S(-)$$
$R = Ph, OPh \qquad R_3' = MePh \ 1\text{-}Np \ ^{49)}.$

The stereochemistry is assumed to involve retention of configuration by analogy with the above reaction. The obtained complex appears to be *trans* by IR spectroscopy.

Dimanganese decacarbonyl reacts with optically active silanes, but the complex cannot be crystallized[23]

$$Mn_2(CO)_{10} + R_3SiH \xrightarrow{\Delta} (CO)_5MnSiR_3 + H_2$$
$$R(+) \qquad\qquad S(-)$$
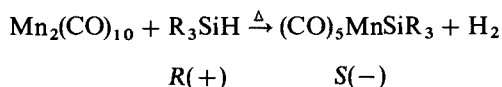
$R_3 = MePh \ 1\text{-}Np$

Phosphine-containing compounds are prepared by reaction of $[PPh_3(CO)_4Mn]_2$ with silanes[50] and this reaction allows the synthesis of an optically active complex[23]

$$[PPh_3(CO)_4Mn]_2 + R_3SiH \rightarrow PPh_3(CO)_4MnSiR_3 + H_2$$
$$R(+) \qquad\qquad S(-)$$
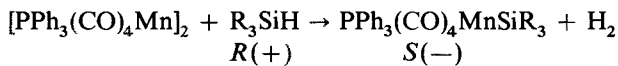
R_3 = MePh 1-Np .

This reaction could probably be performed with reagents containing Ge-H bonds. In the latter two cases, the stereochemistry is assumed to involve retention of configuration by analogy with the former complexes.

Table 1. Optically active complexes

Complex	$[\alpha]_D^{25}$ (°)	Melting point[h] (°C)	Ref.
R-$[(CO)_5CrGeR_3]$ Et_4N	+149[c]	124–125 (120–122)	23)
S-$[(CO)_5MoGeR_3]$ Et_4N	−135[c]	114–115 (96–97)	14)
S-$[(CO)_5WGeR_3]$ Et_4N	−103[c]	116–117 (94–95)	14)
S-$PPh_3(CO)_4MnSiR_3$	−150[d]	201–203	23)
S-$(\eta^5$-$CH_3C_5H_4)Mn(CO)_2(H)SiR_3$	−78[d]	80–81 (77–78)	26, 27)
R-$[(\eta^5$-$CH_3C_5H_4)Mn(CO)_2GeR_3]$ Et_4N	+3.4[c]	59–60 (53–55)	38)
S-$(\eta^5$-$C_5H_5)Fe(CO)_2SiR_3$	−41.5[e]	117 (133)	7, 9)
S-$(CO)_4CoSiR_3$	+2[f]	93 (100)	47)
S-$[PhC(O)(CO)_3CoSiR_3]$ $(PPh_3)_2N$	+1.3[c]	172–175	58)
S-$(CO)_4CoGeR_3$	+2.7[g]	92.5–93 (96.5–97.5)	47)
S-$P(OPh)_3(CO)_3CoGeR_3$	−3.5[d]	123–124 (74–76)	65)
S-$PPh_3(CO)_3CoGeR_3$	−5.4[d]	198–199 (210–211.5)	65)
S-$(\eta^5$-$C_5H_5)(PPh_3)NiGeR_3^b$	+89[d]	51–55 (102–104)	14)
S-$trans$-$PtCl(SiR_3)(PMe_2Ph)_2$	+72[d]	158–160	31)
S-$trans$-$PtBr(SiR_3)(PMePh)_2$	+70[d]	164.5–166	31)
S-$trans$-$PtI(SiR_3)(PMe_2Ph)_2$	+55[d]	183–184	31)
S-cis-$PtH(SiR_3)(PPh_3)_2$	+18[d]	106–107	31)
S-$trans$-$PtCl(GeR_3')(PMe_2Ph)_2$	+13.5[d]	145–146	31)
S-$trans$-$PtH(GeR_3')(PPh_3)_2$	−6.0[d]	84–88	31)

R_3 = MePh l-Np, R_3' = EtPh l-Np

[a] crystallizes with one molecule of benzene or toluene
[b] crystallizes with one molecule CH_2Cl_2
[c] in CH_2Cl_2
[d] in benzene
[e] in cyclohexane
[f] in pentane
[g] in pentane, this compound shows a rotation strongly dependent on solvent: +7.8° in cyclohexane. −3.2° in benzene
[h] in brackets melting point of the racemic compound

3 Chemical Properties

Instead of studying the chemical behaviour of these complexes classifying them into different groups, we shall distinguish a few types of reactions that a large number of compounds, even with quite different structure, may undergo.

3.1 Cleavage of Silicon (or Germanium)-Transition Metal Bonds by Deinsertion

The oxidative addition at a transition metal is utilized in the synthesis of these complexes. The opposite reaction, i.e. reductive elimination, is a general route to the cleavage of the metal-metal bond, especially in complexes also containing a hydrogen-transition metal bond.

Structural investigations on $(\eta^5\text{-}C_5H_5)Mn(CO)_2(H)SiPh_3$ [39] reveal that, the hydrogen atom is located 1.55 Å from the manganese atom and 1.76 Å from the silicon atom. The complex has a square pyramidal geometry with the·cyclopentadienyl on the top
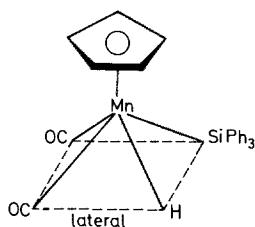
and no diagonal isomer was observed.

The hydrogen-silicon distance is surprisingly short as the sum of the van der Waals radii is 3.1 Å for these elements.

This structure may be related to the ease of deinsertion of these compounds in the presence of phosphines. The reaction takes place at room temperature without irradiation:

$$(\eta^5\text{-}C_5H_5)Mn(CO)_2HSiR_3 \xrightarrow{PR'_3} (\eta^5\text{-}C_5H_5)Mn(CO)_2PR'_3 + HSiR_3$$
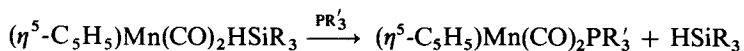
This behavior is interpreted by Graham and Hart-Davis[51] as a resonance hybrid of two canonical forms:
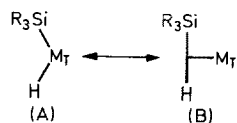
Form A is a transition metal hydride while in form B the silicon hydride behaves as a two electron ligand. The electrons donated by the ligand to the transition metal happen to be a bonding pair in $H-SiR_3$ instead of a non-bonding pair in $:PPh_3$.

This is consistent with the impossibility of replacing a carbonyl by another ligand[38]; the silane is always expulsed before.

NMR studies of these compounds show that the chemical shifts in

$(\eta^5\text{-}CH_3C_5H_4)Mn(CO)_2(H_a)SiPh\,1\text{-}Np$
$\quad\quad\quad\quad\quad\quad\quad\quad\quad\quad\quad |$
$\quad\quad\quad\quad\quad\quad\quad\quad\quad\quad\quad H_b$
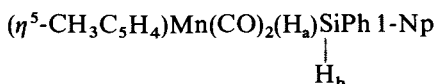
for H_a and H_b are distinct ($\delta H_a = -11.46$ ppm, $\delta H_b = 6.73$ ppm relative to TMS in CD_2Cl_2, $JH_aH_b = 4.5$ hz)[38].

Electron rich reagents can displace the metal IV_B hydride and in the case of optically active complexes this reaction proceeds with retention of configuration.

$$(-)\,cis\text{-}[PtH(SiR_3)(PPh_3)_2] \xrightarrow[\text{retention } 92.5\%]{PhC\equiv CH} (+)\,R_3SiH + [Pt(PPh_3)_2\,PhC\equiv CH], \quad {}^{31)}$$

$$(-)\,(\eta^5\text{-}CH_3C_5H_4)Mn(CO)_2(H)SiR_3 \xrightarrow[\text{retention } 91\%]{P(OPh)3 \text{ or } PPh3} (+)\,R_3SiH +$$
$$+\,(\eta^5\text{-}CH_3C_5H_4)Mn(CO)_2P(OPh)_3$$
$$\text{or}$$
$$(\eta^5\text{-}CH_3C_5H_4)Mn(CO)_2PPh_3$$
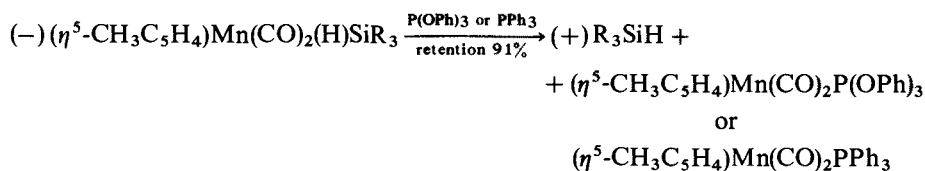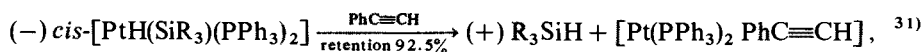
$R = MePh\,1\text{-}Np.^{27)}$

This type of reaction also occurs with germanium derivatives:

$${}^{23)}$$
$$(\eta^5\text{-}CH_3C_5H_4)Mn(CO)_2(H)GePh_3 \xrightarrow{PPh_3} Ph_3GeH + (\eta^5\text{-}CH_3C_5H_4)Mn(CO)_2PPh_3.$$
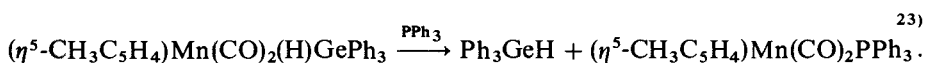
The action of other reagents leading to this cleavage is not clearly understood, since the transition metal moiety decomposes:

$$(-)(\eta^5\text{-}CH_3C_5H_4)Mn(CO)_2(H)SiR_3 \xrightarrow[\text{retention } 61 \text{ to } 72\%]{Cl_2.\ CCl_4 \text{ or } MeLi} (+)\,R_3SiH.\quad {}^{27)}$$
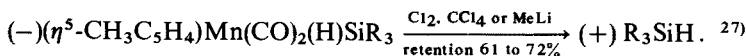
Deinsertion is not limited to hydrido complexes since alkyl and halogeno derivatives undergo the same type of reaction:

$$(+)\,trans\text{-}[PtCl(SiR_3)(PMe_2Ph)_2] \xrightarrow[\text{retention } 51.5\%]{Br_2} (-)\,ClSiR_3.\quad {}^{31)}$$

$${}^{38)}$$
$$(\eta^5\text{-}CH_3C_5H_4)Mn(CO)_2(Me)SiR_3 \xrightarrow{PPh3/h\nu} (\eta^5\text{-}CH_3C_5H_4)Mn(CO)_2PPh_3 + CH_3SiR_3.$$
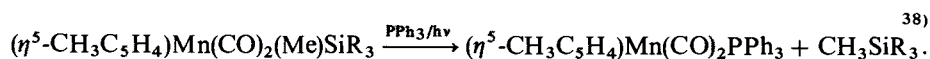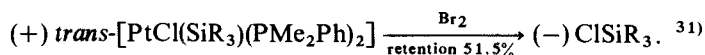
However, deinsertion involving two electron ligands is not a general reaction for all the hydride complexes. Indeed, the iron complex $(CO)_4Fe(H)SiPh_3$ undergoes CO replacement rather than deinsertion[38]:

$$(CO)_4Fe(H)SiPh_3 \xrightarrow{\text{P(OPh)}_3} P(OPh)_3(CO)_3Fe(H)SiPh_3 .$$
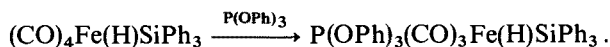
This behavior must be related to the Si-H distance, 2.73 Å[40] which is closer to the sum of the van der Waals radii, 3.1 Å, and corresponds to almost independent ligands.

The structure of complexes having a silicon hydride moiety fixed on the metal is important since such intermediates are involved in hydrosilylation reactions[44]. Manganese and iron hydrides seem to be two limiting cases, the former showing a short silicon-hydrogen distance (a value close to the silicon-hydrogen sigma bond), the latter showing no interaction between silicon and hydrogen. These extreme structures are reflected in their chemical behavior:
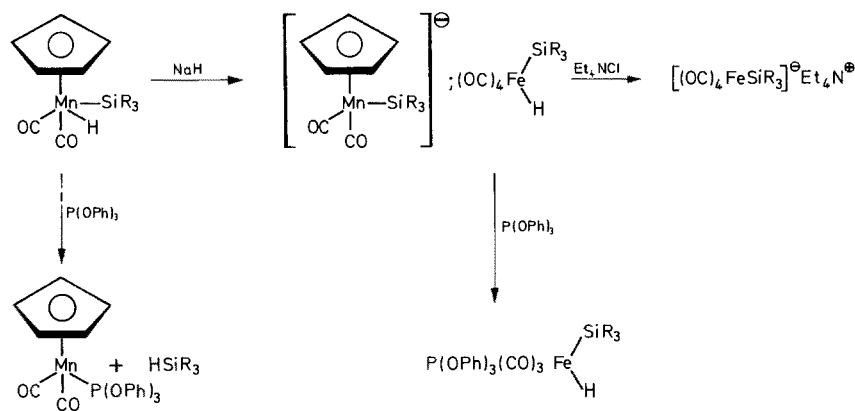
The manganese complex undergoes deinsertion with phosphines, phosphites, halogens and lithium compounds, and the hydrogen is abstracted only by strong bases (sodium hydride). Conversely, the iron complex, instead of SiH deinsertion, undergoes carbon monoxide replacement with phosphites and cleavage of the iron-silicon bond by halogens. The hydrogen abstraction takes place even with weak bases like tetraethylammonium chloride.

Cowie and Bennett explain the short Si-H distance in the manganese complex in terms of steric hindrance[52]; however, the chemical behavior of this complex is not consistent with this interpretation.

These results (bond lenght, deinsertion, NMR) can be explained as an equilibrium which is established slowly between a three-center complex and two independent compounds (cf. Graham Ref.[51]).
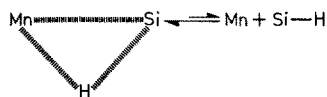
We have confirmed this, showing the H/D exchange in the protonation of the anion $[(\eta^5\text{-}CH_3C_5H_4)Mn(CO)_2Si(D)Ph\ 1\text{-}Np]^-$ (or SiH) with HCl (or DCl) which yields the same mixture of MnH-SiD and MnD-SiH[38]. Since this exchange takes place in spite of the fact that Mn-H and Si-H bonds are distinct and coupled in NMR, one may come to the conclusion that a slow equilibrium develops.

3.2 Ligand Exchange Reactions

Metal-metal bonds are neither formed nor cleaved in these reactions.

Although these reactions are well known in transition metal chemistry, only few have hitherto been applied to complexes in which the transition metal is bonded to a chiral silicon or germanium atom.

UV irradiation of $(\eta^5\text{-}C_5H_5)Fe(CO)_2SiR_3$ with phosphines results in CO substitution (*Scheme 1*).

Scheme 1

$[\alpha]_D^{25} = -112°$

$[\alpha]_D^{25} = +128°$

$[\alpha]_D^{25} = +139°$

$[\alpha]_D^{25} = -163°$
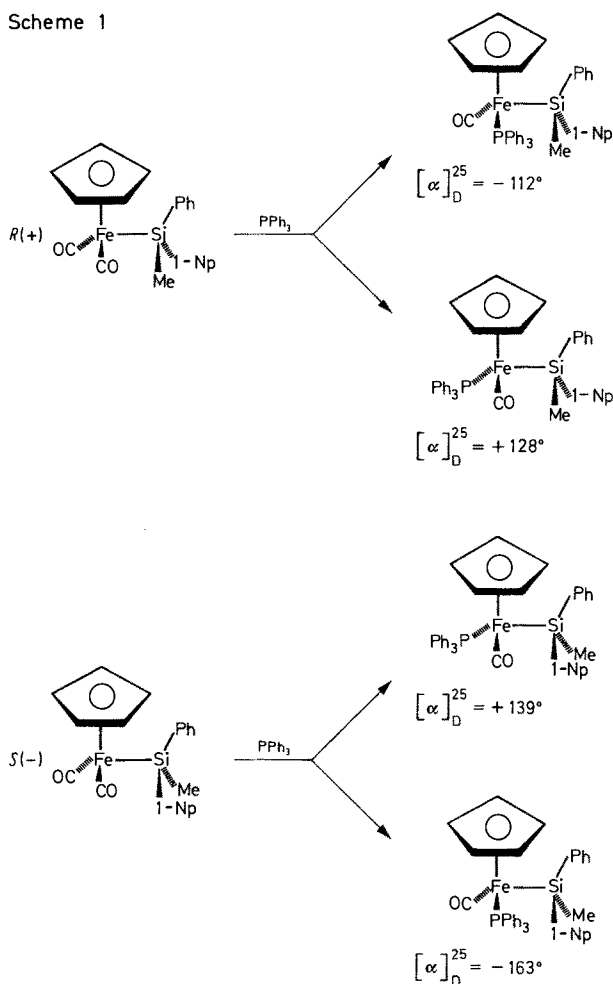
The configurations around the iron atom are unknown while those around silicon are the only known.

The same pattern is applied to the substitution by other phosphorus ligands: $P(C_6H_{11})_3$, $P(n-C_4H_9)_3$ and $P(OEt)_3$ [9] (Table 2).

Table 2. Optical rotations, melting points and ^1H-NMR chemical shifts of $(\eta^5-C_5H_5)(CO)(PR_3)$-FeSiMePhI-Np complexes

R	$[\alpha]_D^{25}$ (°)[a]	m.p. (°C)	$\delta\ CH_3$ (ppm)[b]	$\delta\ C_5H_5$ (ppm)[b]
Ph	-112	217	0.24	4.14
Ph	$+128$	173	0.24	4.28
C_6H_{11}	$+\ 30$	184–185	0.88	4.55
C_6H_{11}	$+122$	163	0.08	4.53
$n-C_4H_9$	$+\ \ 2.9$	oily[c]	0.88	4.50
			0.14	4.45
OEt	$+\ \ 13.6$	oily[c]	1.00	4.34
			0.95	4.34

[a] in cyclohexane   [b] in $CDCl_3$ relative to TMS   [c] mixture of two diastereoisomers

For $(CO)_4CoMR_3$ complexes, substitution of a carbonyl residue requires very drastic conditions[10] and optically active phosphine-substituted complexes could not be obtained in this manner. In Section 2.2.2 we have described an alternative synthesis of $L(CO)_3CoGeMePh$ 1-Np [L = PPh_3, $P(OPh)_3$].

3.3 Cyclometalation Reactions

UV irradiation of optically active $(\eta^5-C_5H_5)Fe(CO)_2SiR_3$ (R_3 = MePh 1-Np) with triphenyl phosphite gives an orthometalated complex with elimination of hydrogenosilane with complete retention of configuration. The hydrogen of the silane is not abstracted from the solvent as is proved by performing the reaction in C_6D_6 [53].

$$R(+)-(\eta^5-C_5H_5)Fe(CO)_2SiR_3 \xrightarrow{P(OC_6H_5)_3\ (2\ mol)} (\eta^5-C_5H_5)Fe-o-C_6H_4OP(OC_6H_5)_2 \cdot$$
$$60\%$$
$$\cdot [P(OC_6H_5)_3] + S(-)-R_3SiH.$$
$$71\%$$
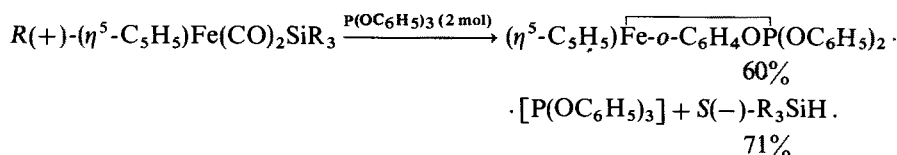
However, when the irradiation is carried out with 1 mol of phosphite under mild conditions (100 W lamp instead of 450 W) only one carbonyl is replaced and R_3SiH is also formed[54].

The following mechanism is suggested in agreement with these observations (*Scheme 2*):

Scheme 2
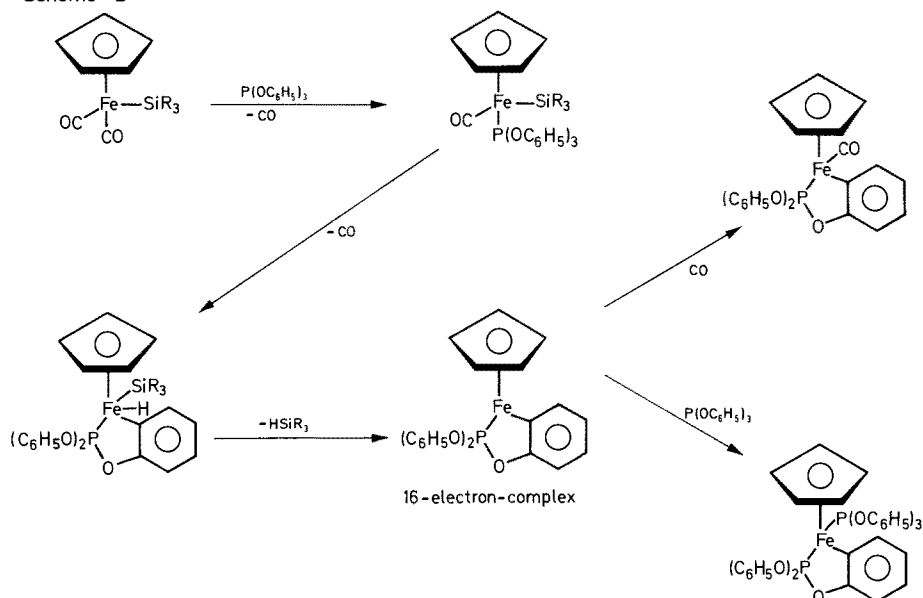
However, an alternative mechanism has been suggested to us by Prof. H. Saku-rai. It involves the homolytic cleavage of the iron-silicon bond (*Scheme 3*).

Scheme 3
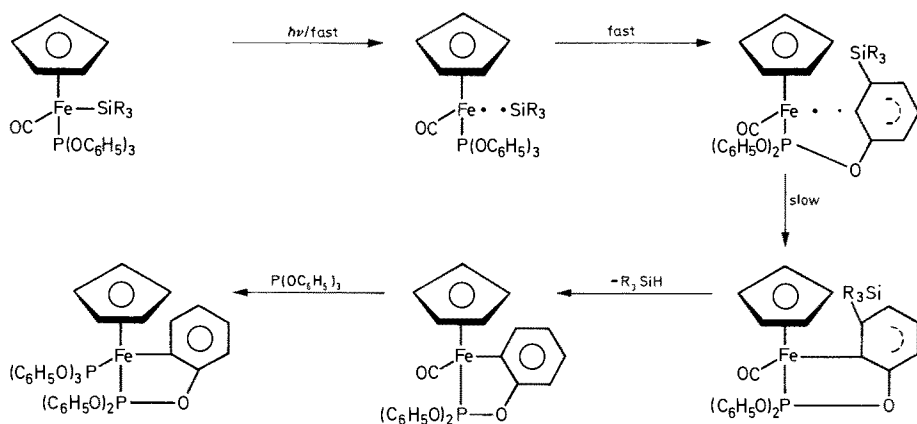
Both mechanisms explain the complete retention of configuration at silicon because free silyl radicals are not involved. The 16-electron complex may add both one phosphite molecule (when it is present in excess) or one carbonyl (formed in the first steps and remaining in solution before being slowly evolved).

This reaction has been shown to be general for other phosphines with sp^2 carbon atoms in the right positions for giving five — membered rings after cyclometalation:

$P(CH_2C_6H_5)_3$, $P(SC_6H_5)_3$, $PPh(allyl)_2$, $P(allyl)_3$, $PPh(1\text{-Np})_2$, PMePh 1-Np. Cyclo-metalation is possible with $PPh(CH_2CH_2Ph)_2$ and $P(O\text{-totyl})_3$, the former compound yielding a six-membered ring and the latter undergoing metalation at an sp^3 carbon atom. However, drastic conditions are necessary (450 w lamp). The results obtained reveal that:

a) Only sp^2 carbon-hydrogen bonds may be metalated except under drastic conditions,

b) five-membered rings are preferred to six-membered rings,

c) only these two ring sizes are formed[54].

Products containing as ligands $PPh(1\text{-Np})_2$ have two centers of chirality and two racemic diastereoisomers have been separated. The reaction of optically active PMePh 1-Np leads to a racemic mixture since the phosphine is racemized under UV irradiation[54]:
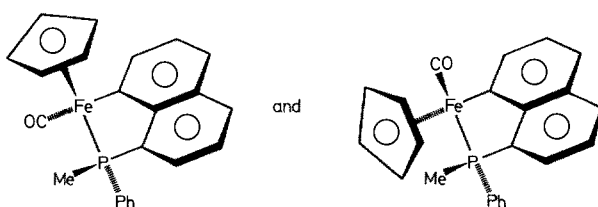
3.4 Direct Cleavage of Transition Metal-Silicon or Germanium Bonds

3.4.1 Nucleophilic Cleavage

Under this term we shall consider only nucleophilic attack at the group IV_B metal, the transition metal behaving as a leaving group. Nucleophiles may cleave the M_T-M_{IVB} bond with both retention and inversion of configuration at the group IV_B metal.

The first cleavage reported is the displacement of platinum in silicon-platinum complexes by $LiAlH_4$ and is believed to proceed by nucleophilic attack at silicon:

$(+) \, trans[PtCl(SiR_3)(PMe_2Ph)_2] \xrightarrow[\text{retention 93\%}]{LiAlH4} (+) R_3SiH$, [31]

$(-) \, cis[PtH(SiR_3)(PPh_3)_2] \xrightarrow[\text{retention 97\%}]{LiAlH4} (+) R_3SiH$. [31]
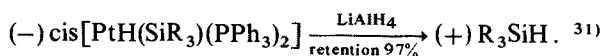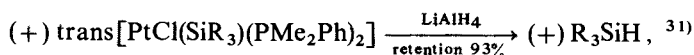
The second type involves cleavage of the silicon-manganese hydride occurring with inversion of configuration:

$S(-)(\eta^5\text{-}CH_3C_5H_4)Mn(CO)_2(H)SiR_3 \xrightarrow[\text{inversion 80\%}]{LiAlH4} S(-) R_3SiH$. [27]

In this case, where cleavage may proceed both by nucleophilic attack and deinsertion, it has been proved that the former possibility occurs:

$$(\eta^5\text{-}CH_3C_5H_4)Mn(CO)_2(H)SiPh_3 \xrightarrow{\text{LiAlD}_4} Ph_3SiD,$$

$$(\eta^5\text{-}CH_3C_5H_4)Mn(CO)_2(D)SiPh_3 \xrightarrow{\text{LiAlH}_4} Ph_3SiH.$$
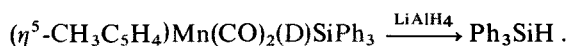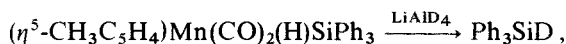
The hydrogen atom comes from the nucleophile and not from the complex[27].

The iron-silicon complexes are cleaved by $LiAlH_4$ with retention of configuration[9]:

$$R(+)\text{-}(\eta^5\text{-}C_5H_5)Fe(CO)_2SiR_3 \xrightarrow[\text{retention 66\%}]{\text{LiAlH}_4} S(-)\text{-}R_3SiH,$$

$$(-112°)(\eta^5\text{-}C_5H_5)Fe(CO)(PPh_3)SiR_3 \xrightarrow[\text{retention 54\%}]{\text{LiAlH}_4} S(-)\text{-}R_3SiH.$$
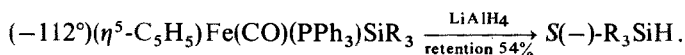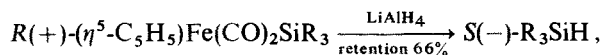
The comparison between iron and manganese complexes, despite their electronic and geometrical resemblances, is difficult because of the highly specific hydrogen-silicon interactions in the case of the manganese complexes. The difference in stereochemistry can certainly be attributed to these interactions in the manganese complex.

The cobalt-silicon complex is cleaved by $LiAlH_4$ with inversion of configuration[47]:

$$S(+)\text{-}(CO)_4CoSiR_3 \xrightarrow[\text{inversion 91\%}]{\text{LiAlH}_4} S(-)\text{-}R_3SiH.$$
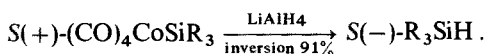
On the other hand, for cobalt-germanium complexes, the stereochemistry strongly depends on ligand L[49] (Table 3).

Table 3. Stereochemistry of cleavage with $LiAlH_4$ of $(CO)_3LCoGeR_3$

Ligand	Stereochemistry
CO	Inversion 87%
P(OPh)$_3$	Inversion 87%
PPh$_3$	Inversion 60%
C(OEt)n-Bu	Retention 55%

Cobalt and manganese complexes are cleaved by other nucleophiles with inversion of configuration (55–74%)[27,47]:

$$M\text{-}SiR_3 \xrightarrow{R'OH} R'SiR_3$$

$M = (CO)_4Co, (\eta^5\text{-}CH_3C_5H_4)Mn(CO)_2H$
$R' = Me, H$
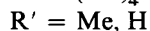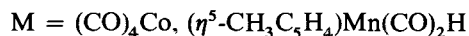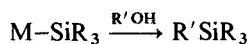
In contrast, iron-silicon bonds are less labile. They are cleaved only by water with retention of configuration (59–66%) affording siloxanes instead of silanols $(L = CO)$[9]:

$$(\eta^5\text{-}C_5H_5)Fe(CO)LSiR_3 \xrightarrow{\ H_2O\ } (R_3Si)_2O$$
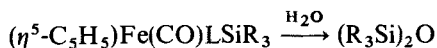
When L = phosphine the complex is stable to water and, in all cases, iron-silicon complexes are inert to methanol.

These observations show that the stereochemistry of cleavage is strongly dependent on the ease of substitution of the transition metal. It has been observed in silicon chemistry that good leaving groups are displaced with inversion of configuration while poor ones are displaced with retention[55]. Indeed, $(CO)_4Co$ is a poor nucleophile[56] and would constitute a good leaving group whereas $(\eta^5\text{-}C_5H_5)Fe(CO)_2$ and $(\eta^5\text{-}C_5H_5)Fe(CO)PPh_3$ representing good nucleophiles would be poor leaving groups.

In cobalt-germanium complexes, substitution of one carbonyl by electron-donating ligands should increase the nucleophilicity of the transition metal moiety[10]. The ability of the transition metal to be substituted should decrease for $L(CO)_4Co$ in the order $CO \geqq P(OPh)_3 > PPh_3 > C(OEt)R$. The same order is found in the stereochemistry of cleavage, going from good inversion of configuration $(L = CO, P(OPh)_3)$ to retention$(L = C(OEt) nBu)$.

Platinum behaves as a poor leaving group although literature does not provide any data on the nucleophilicity of $PtX(PR_3)_2$.

3.4.2 Electrophilic Cleavage

Electrophiles such as halogens may cleave the transition metal-silicon (or germanium) bonds. We have already seen that in the case of the hydrido complexes they induce deinsertion reactions with retention of configuration at silicon (cf. Sect. 3.1).

In the case of complexes with "normal" sigma bonds between both metals, electrophilic attack takes place with retention of configuration:

$$S(+)(CO)_4CoSiR_3 \xrightarrow[\text{retention } 66-80\%]{X_2} S(-) R_3SiX \ \ [47]$$

$X = Cl, Br$

$$(\eta^5\text{-}C_5H_5)Fe(CO)LSiR_3 \xrightarrow[\text{retention } 53-63\%]{X_2} R(+)\text{-}R_3SiX + (\eta^5\text{-}C_5H_5)Fe(CO)LX \ \ [9]$$
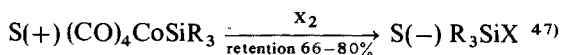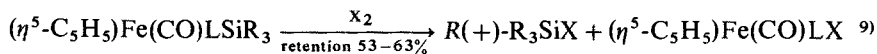
$X = Cl, Br$

$L = CO, PPh_3, P(C_6H_{11})_3$.

However, it is possible to change the stereochemistry of cleavage by varying the nature of the electrophile by the addition of other reagents such as $AlCl_3, PPh_3, P(OEt)_3$.

The cobalt complex is cleaved by Cl_2/PPh_3 with complete racemization, whereas the iron complexes may be cleaved with retention, inversion or racemization, depending on the electrophile and the substrate (Table 4).

Table 4. Cleavage Reactions of $(\eta^5-C_5H_5)Fe(CO)(L)SiR_3$

L	Reagent[a]	stereoselectivity (%)
CO	Cl_2	56 Retention
CO	$Cl_2/AlCl_3$	61 Retention
CO	Cl_2/PPh_3	no reaction
CO	$Cl_2/P(OEt)_3$	64 Inversion
CO	Br_2	53 Retention
PPh_3	Cl_2	63 Retention
PPh_3	$Cl_2/AlCl_3$	53 Retention
PPh_3	Cl_2/PPh_3[b]	Racemisation
PPh_3	Cl_2/PPh_3	58 Inversion
PPh_3	$Cl_2/P(OEt)_3$	no reaction
$P(C_6H_{11})_3$	Cl_2	55 Retention
$P(C_6H_{11})_3$	$Cl_2/P(C_6H_{11})_3$	60 Inversion
$P(OEt)_3$	Cl_2	79 Inversion
$P(OEt)_3$	$Cl_2/AlCl_3$	91 Retention
$P(OEt)_3$	Cl_2/PPh_3	no reaction
$P(OEt)_3$	$Cl_2/P(OEt)_3$	73 Retention

[a] 2 mol of co-reagent $(PR_3, AlCl_3)$/mol complex
[b] 0.3 mol of co-reagent/mol complex

The different stereochemistries of cleavage may be explained by *Scheme 4*:

Scheme 4
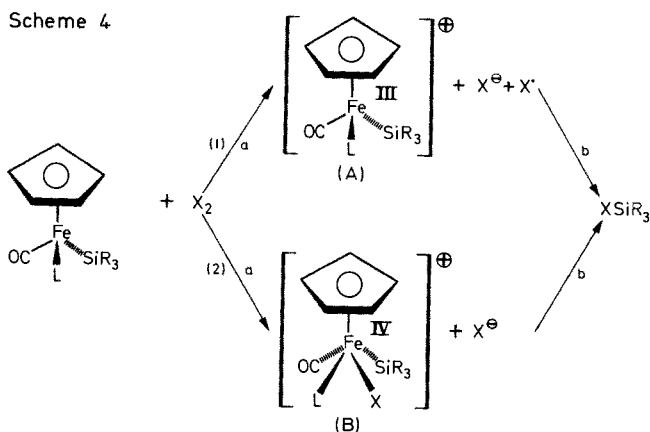
Both processes (1) and (2) are possible. The reagent $Cl_2(AlCl_3$ is likely to produce the electrophile Cl^+ which cleaves directly the Si-Fe bond with retention of con-

figuration in all cases. Step (a) may give intermediate B which may undergo reductive elimination of R_3SiCl with retention of configuration.

The other reagents, which generate a less powerful electrophile would react according to pathway (1) to afford intermediate A. This may be cleaved by nucleophilic attack at silicon. This step may take place either with retention or inversion of configuration, depending on the nature of the reagents and on the ligands around the iron atom[9]. The iron complex obtained, even when X = I, is always racemic. This fact is explained by both routes, (a) and (b), since they involve the planar iron intermediate, $(\eta^5\text{-}C_5H_5)Fe(CO)L$ which loses its stereochemistry.
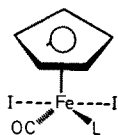
Iodine may attack both sides of the planar intermediate to yield a racemic complex.

3.5 Nucleophilic Attack at Carbonyl Ligands

Organometallics such as Grignard and lithium reagents give rise to deinsertion in hydrido complexes (cf. Sect. 3.1). However, their reactivity is quite different toward "normal" sigma bonded transition metal-group IV_B metal complexes.

Iron complexes are unreactive to these organometallics:

$$(\eta^5\text{-}C_5H_5)Fe(CO)(L)SiR_3 \xrightarrow[\text{CH3MgBr}]{\text{CH3Li or}} \text{no reaction}$$
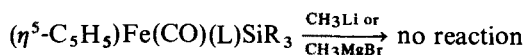
$$L = CO, PR_3 .$$

However, cobalt complexes, treated with a tenfold excess of Grignard or lithium reagents lead to the formation of anionic species[47, 57] (Scheme 5):

Scheme 5

97
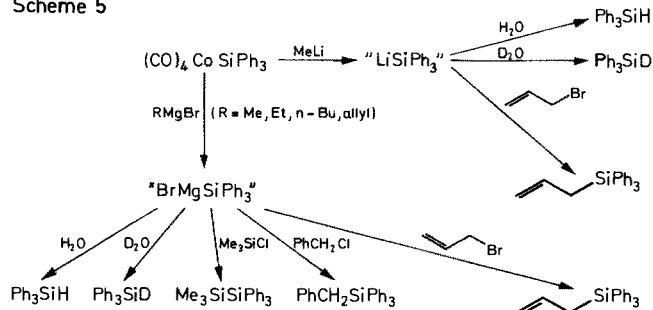
These reactions take place with predominant retention of configuration at silicon (*Scheme 6*)

Scheme 6

$S(+) (CO)_4 Co SiR_3 \xrightarrow{\text{MeLi}} \text{"LiSiR}_3\text{"}$

$\downarrow \text{MeMgBr}$ $H_2O \downarrow \begin{array}{c} \text{retention} \\ 70\% \end{array}$

$\text{"BrMgSiR}_3\text{"} \xrightarrow[\text{retention 55\%}]{H_2O} R(+) - R_3SiH$

$\diagdown\!\diagup\!\diagdown\!\diagup^{Br} \downarrow \text{retention 57\%}$

$S(+) \diagup\!\diagdown\!\diagup\!\diagdown^{SiR_3}$
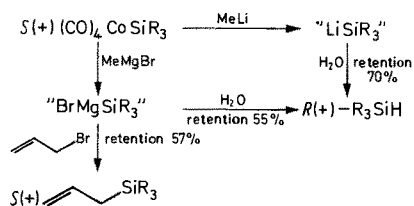
Surprisingly, the germanium complex displays a clearly different behavior. While allylmagnesium bromide leads to the germyl *Grignard* reagent, it undergoes substitution at germanium with MeMgBr[47, 57] (*Scheme 7*):

Scheme 7

$(CO)_4 CoGePh_3 \xrightarrow[(R = Me, Ph)]{RMgBr} RGePh_3$

$\downarrow$

$\diagdown\!\diagup\!\diagdown\!\diagup^{MgBr}$ $\xrightarrow{H_2O} HGePh_3$

$\downarrow$

$\text{"BrMgGePh}_3\text{"} \xrightarrow{D_2O} DGePh_3$

$\diagdown\!\diagup\!\diagdown\!\diagup^{Br}$

$\diagdown\!\diagup\!\diagdown\!\diagup^{GePh_3}$
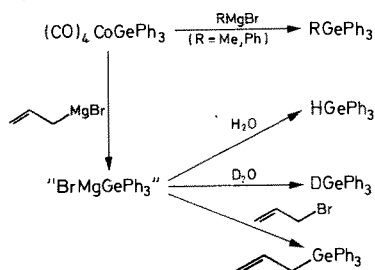
However, these compounds react quite differently with a stoichiometric amount of lithium reagent. Let us consider first the reaction of PhLi[58] (*Scheme 8*):

Scheme 8

$S(+) - (CO)_4CoSiR_3 \xrightarrow{\text{PhLi}} [PhC(O)(CO)_3CoSiR_3] Li$

$\xrightarrow{\text{heat}}$ $\downarrow (PPh_3)_2 NCl$

$S(-) - PhCOSiR_3 \qquad S(+) - [PhC(O)(CO)_3Co SiR_3](PPh_3)_2N$
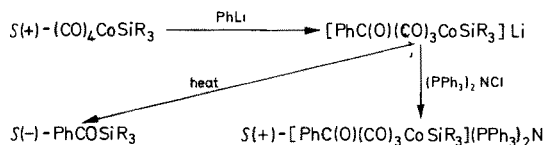
The IR spectrum reveals a *trans* structure for the imminium salt. The formation of benzoylsilane proceeds with complete retention of configuration at silicon and can be explained by both direct formation of a silicon-carbon bond (a) and formation of a silyloxycarbene (b)[49]. However, *cis* elimination (a) does not appear to be favored in a *trans* structure (*Scheme 9*):

Scheme 9
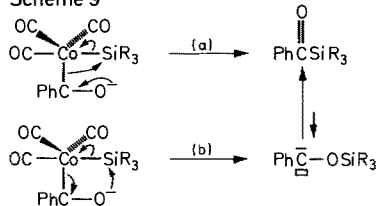
In the case of germanium, salts and neutral carbenes are both easily isolated[59] (*Scheme 10*):

Scheme 10

$R = Me, Et, n\text{-}Pr, n\text{-}Bu, Ph$
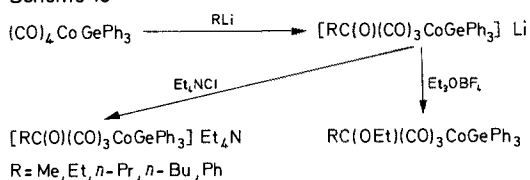
and a crystallographic study has revealed these compounds to be *trans* trigonal bipyramids[59].

The optically active carbene can be synthesized but unfortunately it cannot be crystallized:

$$S(+)\text{-}(CO)_4CoGeR_3 \xrightarrow{n\text{-}BuLi} \xrightarrow{Et_3OBF_4} S(-)\text{-}n\text{-}BuC(OEt)(CO)_3CoGeR_3$$
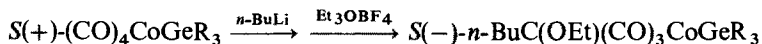
As previously shown[60], transition-metal stabilized carbenes cannot be used as sources of free carbenes, due to their chemical inertness. However, selected reagents can operate specific transformations on these complexes[49] (*Scheme 11*):

The different sites of attack by these reagents are denoted by figures.

It is difficult to explain the differences in reactivity toward similar reagents such as Grignard reagents, alkyl and even germyllithiums. Indeed, alkyllithiums behave as bases whereas methyl Grignard reagents substitute at germanium and germyllithiums at carbon in the ethoxy group.

$AlCl_3$ and $SnCl_4$ cleave the germanium-cobalt bond. In the case of $SnCl_4$, the trichlorostannyl derivative can be isolated.

A peculiar reaction occurs when carbene anions are trapped with chlorosilanes; the tetracarbonyl cobalt complex is recovered in high yield:

$$[RC(O)(CO)_3CoGePh_3]\,Li \xrightarrow{R_3SiCl} (Co)_4CoGePh_3 \quad [59]$$

$R_3 = Me_3, Ph_2H, Me_2H$.

99

Scheme 11

Ph$_3$GeCl
+
Ph$_2$GeCl$_2$

Ph$_3$Ge CH$_3$

$\xrightarrow{1}$ AlCl$_3$

CH$_3$MgBr / 1

Cl$_3$SnCo(CO)$_3$C$\big\langle^{OCH_2CH_3}_{CH_2R}$ $\xleftarrow[2]{SnCl_4}$ Ph$_3$Ge Co(CO)$_3$ C$\big\langle^{OCH_2CH_3}_{CHR}$ $\xrightarrow[3]{Ph_3GeLi}$ Ph$_3$GeCo(CO)$_3$C$\big\langle^{O^{\ominus}Li^{\oplus}}_{CH_2R}$
+
Ph$_3$GeCl

+
Ph$_3$GeEt

$\xleftarrow{Et_3OBF_4}$

LiAlH$_4$ / 1

RLi or NaH / 4

$\overset{H}{\underset{4}{\big|}}$ Ph$_3$GeH

Ph$_3$GeCo(CO)$_3$ C$\big\langle^{OCH_2CH_3}_{\underline{C}HR}$

R'X

Ph$_3$GeCo(CO)$_3$ C$\big\langle^{OCH_2CH_3}_{CHRR'}$
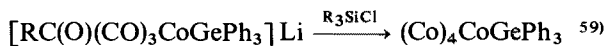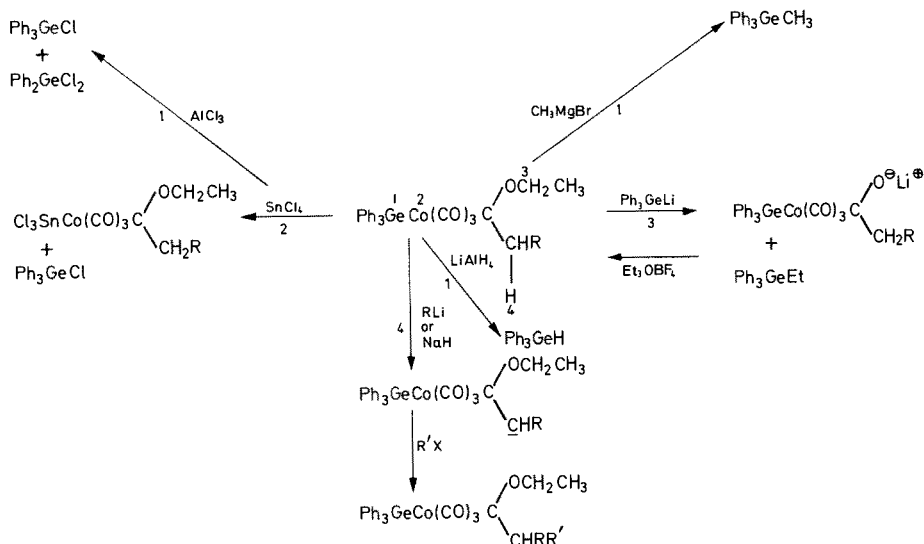
The same anomaly is observed with anions in α position to the carbene. These anions are conveniently trapped with MeI or Et$_3$OBF$_4$; however, trapping with chlorosilanes gives again high yields of tetracarbonyl derivatives (*Scheme 12*):

Scheme 12

Ph$_3$GeCo(CO)$_3$C$\big\langle^{OEt}_{\underline{C}HR}$ $\xrightarrow{MeI}$ Ph$_3$GeCo(CO)$_3$C$\big\langle^{OEt}_{\underset{Me}{\overset{|}{CHR}}}$

R$_3$SiCl

Et$_3$OBF$_4$

(CO)$_4$CoGePh$_3$

Ph$_3$GeCo(CO)$_3$C$\big\langle^{OEt}_{\underset{Et}{\overset{|}{CHR}}}$
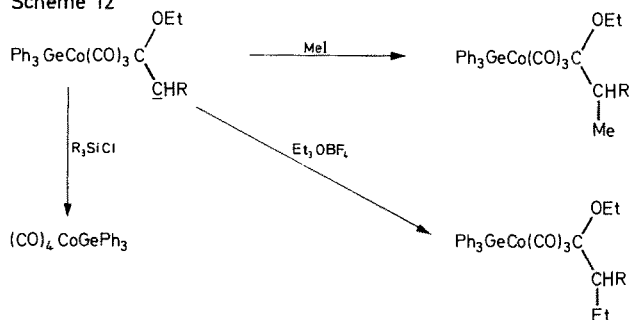
The particular behavior of these anions is difficult to explain. It could be related to the unusually short bond lengths in the carbene moiety[59].

3.6 Substitution Reactions at Silicon without Cleavage of the Silicon-Metal Bond

Although substitutions at germanium and tin bonded to transition metals are well known, only a few reports describe substitutions at silicon[61, 62].

However, manganese hydrides undergo substitution at silicon without cleavage of the silicon-manganese bond[28] (*Scheme 13*):

Scheme 13
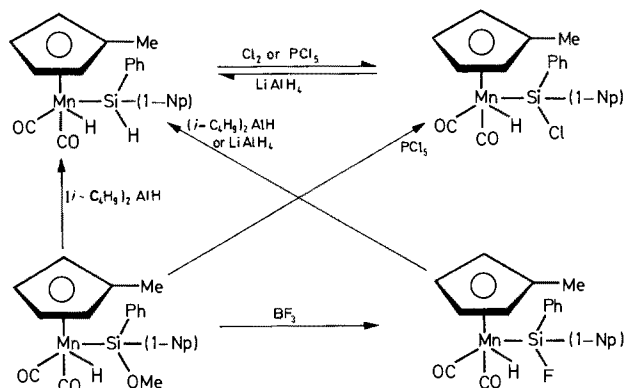
Substitution at silicon in an optically active silicon-manganese hydride has also been observed:
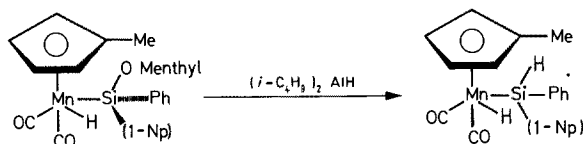
However, the product obtained is racemic (cf. Sect. 3.1).

3.7 Formation and Properties of Anions

3.7.1 Formation of Anions

We have discussed the direct formation of anions by reaction of silyl- or germyl-lithiums with metal carbonyls (cf. Sect. 2.12):

$$M(CO) + R_3GeLi \rightarrow [R_3GeM]\,Li$$

$$M = Cr(CO)_5,\ Mo(CO)_5,\ W(CO)_5,\ Fe(CO)_4,\ (\eta^5\text{-}C_5H_5)Mn(CO)_2\,.$$
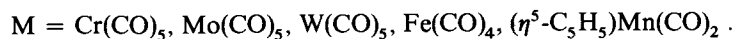
It is known that transition metal hydrides exhibit acidic properties and it has been reported that in some cases complexes containing a group IV_B metal ligand react with weak bases[63]:

$$(\eta^5\text{-}C_5H_5)Mn(CO)_2(H)SiCl_3 \xrightarrow{\text{Et}_3N} [(\eta^5\text{-}C_5H_5)Mn(CO)_2SiCl_3]\,Et_3NH$$

$$\text{or } (CO)_4Fe(H)SiR_3 \xrightarrow{\text{Et}_3N} [(CO)_4FeSiR_3]\,Et_3NH$$

$$R = Ph,\ Cl\,.$$
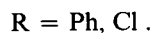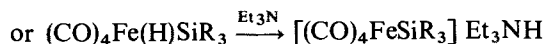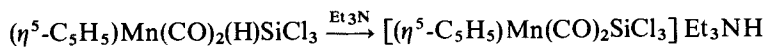
However, this reaction is not a general one. For instance, the triphenylsilyl derivative of manganese is inert to amines.

Strong bases such as NaH or RLi react with all the hydrides[28]:
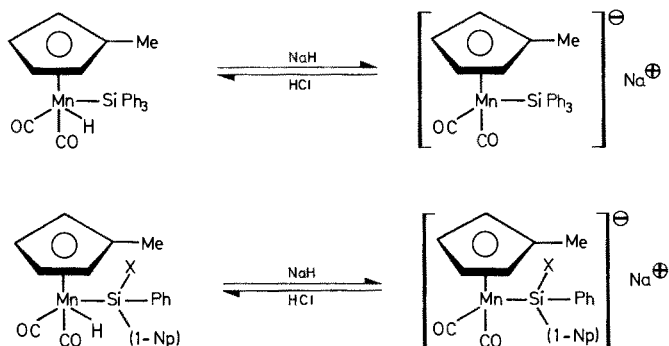
X = H, F, Cl, OMe, alkyl, aryl

All theses anions are isolated as tetraethylammonium or μ-nitrido-bis-(triphenylphosphorus) salts, except those where X = CH$_3$, OMe which cannot be crystallized.

Lithium reagents display a more complicated reactivity as basic agents. Non-functional hydrides undergo deinsertion (cf. Sect. 3.1) while functional ones undergo hydrogen abstraction followed by substitution of the corresponding function.

However, phenyllithium does not substitute fluorine or methoxy and methyllithium affords a mixture of fluorinated and methylated anions (*Scheme 14*):

Scheme 14
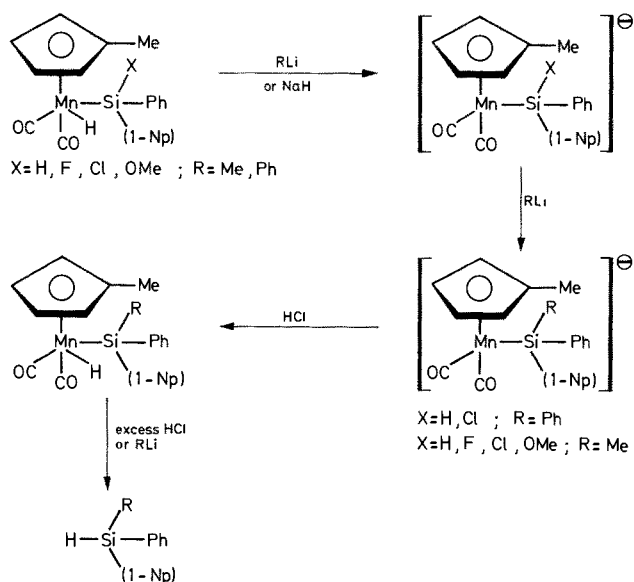
It should be pointed out that substitution at silicon takes place after hydrogen abstraction, since the anion, prepared on reaction with NaH, undergoes substitution when treated with RLi.

Lithium aluminum hydride exhibits the reverse reactivity toward manganese hydrides (cf. Sect. 3.6):
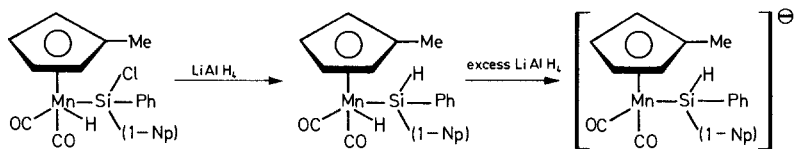
Indeed, this reagent first attacks silicon and then (excess) behaves as a base abstracting the acidic hydrogen.

Anions prepared by direct reaction of germyllithium with metal carbonyls or by hydrogen abstraction are obviously identical and reveal the same reactivity.

3.7.2 Reactivity

3.7.2.1 Reactions with Hydrogen Chloride

Treatment of these anions with an ethereal solution of hydrogen chloride gives the corresponding neutral complexes[28, 38] (*Scheme 15*).

Scheme 15
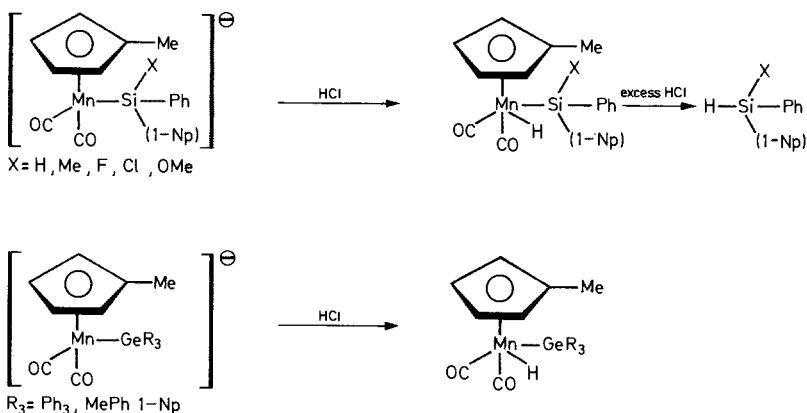
This reaction exclusively leads to hydrides where hydrogen is *cis* to silicon or germanium and which are identical to those obtained by oxidative addition of Si-H or Ge-H complexes to (η^5-methylcyclopentadienyl)tricarbonylmanganese.

However, anions containing Cr, Mo and W undergo deinsertion of germane with retention of configuration at germanium[15, 64]:

$$S(-)\text{-}[(CO)_5MoGeR_3]\,Et_4N \xrightarrow[\text{retention }81\%]{HCl} [(CO)_5MoCl]\,Et_4N + R(+)\text{-}R_3GeH$$

$$\longrightarrow (CO)_5Mo(H)GeR_3 + Et_4NCl$$
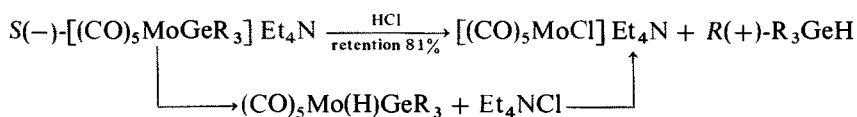
This reaction probably proceeds via the neutral hydride that undergoes reductive elimination of germane. The stereochemistry observed (retention of configuration) is in agreement with a reductive elimination and with the assumption that the formation of the molybdenum-germanium bond proceeds with retention of configuration (cf. Sect. 3.1.2).

3.7.2.2 Alkylation Reactions

Cyclopentadienyl-manganese, -molybdenum and -tungsten anions react with organic halides to give species with five independent ligands[23, 38] (*Scheme 16*):

Scheme 16

M = Si, Ge
R₃= Ph₃,MePh 1 - Np
R' = Me, Et, X = I
R' = CH₂= CH —CH₂ , Ph CH₂, X = Br
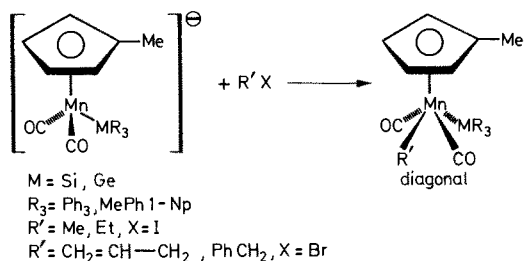
diagonal

Only the diagonal isomer is formed in these reactions. The structures have been elucidated by IR and ^{1}H-NMR spectra of the compounds in which R' = CH$_2$Ph. In the lateral isomer, the manganese atom should be chiral and the benzylic protons should display a different shift (see below). A single signal is actually observed.

It seems interesting to point out here that treatment with hydrogen chloride leads exclusively to the lateral hydride complexes.

The reaction with acetyl chloride affords the diagonal methyl derivative after CO deinsertion, as in the case of MeI (*Scheme 17*):

Scheme 17

+ MeCOCl ⟶

—Me

Mn
OC   SiPh₃
COMe CO
unstable

↓ −CO

—Me

Mn
OC   SiPh₃
Me   CO
diagonal

MeI
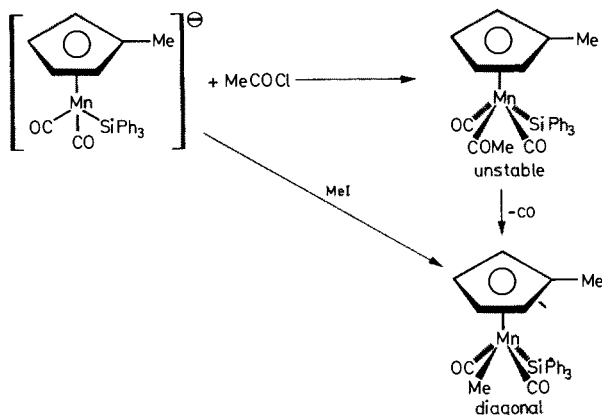
In contrast, evidence for the formation of *cis* and *trans* isomers is provided by H¹NMR studies of crude reaction mixtures in the molybdenum and tungsten series (*Scheme 18*):

Scheme 18

M_T = Mo, W
M   = Ge, Sn
R_3 = Ph₃, MePh 1−Np
R′ = Me, Et   X = I
R′ = CH₂=CH−CH₂, PhCH₂   X = Br

R′X ⟶

OC   MR₃
ON   R′
minor

+

OC   R′
ON   MR₃
minor

+

OC   MR₃
R′   NO
major
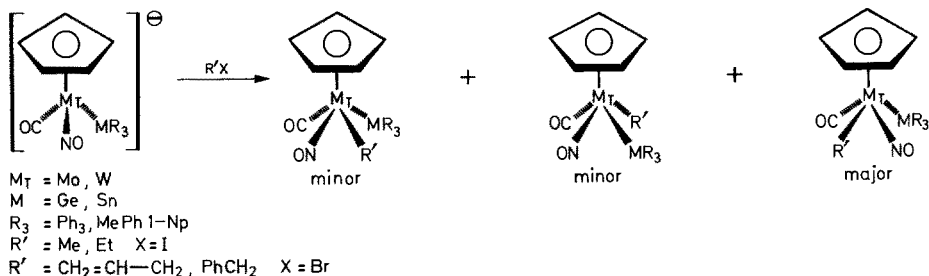
All these complexes are square pyramids, the cyclopentadienyl ligand occupying an apical position[65]. When R = Ph, three pairs of enantiomers are obtained, since the transition metal is asymmetric, and the major enantiomer (i.e. the *trans*) is obtained by cristallization.

The chirality at the transition metal is evidenced by the magnetic non-equivalence of the benzylic protons in the benzyl derivative:

Mo
OC   GePh₃
CH₂Ph NO
trans

Δν = 24 Hz

J 10 Hz   J 10 Hz

3 ppm

$δ_{rel.}$ TMS
(in C₆D₆)
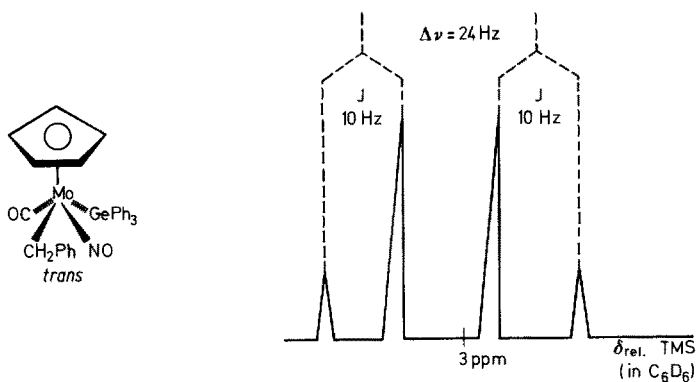
In the case of asymmetric germanium, six racemic diastereoisomers are formed, but until now none of them could be isolated by crystallization.

These complexes are isomerically stable up to 140 °C.

The reactions described above provide a general method of synthesis for a new class of complexes bearing five different and independent ligands and, to our knowledge, only two reports mention this type of compounds without providing a general method of synthesis[66, 67]. Surprisingly, these compounds are isomerically stable[68].

4 Conclusion

Complexes with silicon (or germanium)-transition metal bonds in which silicon or germanium is optically active are very stable both chemically and optically.

The introduction of a group IV_B metal into transition metal complexes modifies the behavior of these complexes and a wide variety of reaction sites may result. Thus, reactions at silicon without cleavage of the transition metal-silicon bond are possible in some cases.

As pointed out in Section 3.1, the particular nature of the Si-H bond in transition metal complexes may explain some features of hydrosilylation.

Anions derived from transition metal-group IV_B metal bonds may be interesting as potential asymmetric catalysts in phase transfer reactions. This field is developing now and, in general, the use of these complexes as catalysts is at the beginning.

5 References

1. Piper, T. S., Lemal, D., Wilkinson, G.: Naturwissenschaften *43*, 129 (1956)
2. Young, J. F.: Adv. Inorg. Chem. Radiochem. *11*, 91 (1968)
3. Aylett, B. J.: ibid. *11*, 249 (1968)
4. Brooks, E. H., Cross, R. J.: Organomet. Chem. Rev. A. *6*, 227 (1971)
5. Ang, H. G., Lau, P. T.: ibid. 8, 235 (1972)
6. Höfler, F.: Topics Current. Chem. *50*, 129 (1974)
7. Corriu, R. J. P., Douglas, W. E.: J. Organomet. Chem. *51*, C 3 (1973)
8. Cerveau, G. et al.: J. Chem. Soc., Chem. Commun. *1975*, 410
9. Cerveau, G. et al.: J. Organomet. Chem. *135*, 373 (1977)
10. Curtis, M. D.: Inorg. Chem. *11*, 802 (1972)
11. Carre, F., Corriu, R., Leard, M.: J. Organomet. Chem. *24*, 101 (1970)
12. Brook, A. G., Peddle, G. J. D.: A. Amer. Chem. Soc. *85*, 2338 (1963)
   Eaborn, C., Hill, R. E. E., Simpson, P.: J. Organomet. Chem. *15*, 1, *37*, 267, 275 (1968)
   Corriu, R. J. P., Guerin, G.: IX Internat. Conf. Organomet. Chem.. Sept. 3–7. 1979 Dijon (France)
13. Colomer, E., Corriu, R. J. P., Meunier, B.: J. Organomet. Chem. *71*, 197 (1974)
14. Colomer, E., Corriu, R. J. P.: J. Chem. Soc. Chem. Commun. *1978*, 435
15. Isaacs, E. E., Graham, W. A. G.: Can. J. Chem. *53*, 467 (1975)

16. Piper, T. S., Wilkinson, G.: J. Inorg. Nucl. Chem. *3*, 104 (1956)
17. Brooks, E. H., Cross, R. J., Glockling, F.: Inorg. Chim. Acta *2*, 17 (1968)
18. Cross, R. J., Glockling, F.: J. Organomet. Chem. *3*, 253 (1965)
19. Ruff, J. K.: Inorg. Chem. *6*, 1502 (1967)
20. Kruck, Th., Breuer, H.: Chem. Ber. *107*, 263 (1974)
21. Kruck. Th., Job, E., Klose, U.: Angew. Chem. Int. Ed. Engl. *7*, 374 (1968)
22. Kruck. Th.. Herber, B.: Angew. Chem. Int. Ed. Engl. *8*, 679 (1969)
23. Colomer, E., Corriu, R. J. P.: Unpublished results
24. Carre, F., Corriu, R.: J. Organomet. Chem. *65*, 349 (1974)
25. Jetz, W., Graham, W. A. G.: Inorg. Chem. *10*. 4 (1971)
26. Colomer, E., Corriu, R., Vioux, A.: J. Chem. Soc. Chem. Commun., 1976, 175
27. Colomer, E., Corriu, R., Vioux, A.: J. Chem. Res. *1977*, 168, *1977*, 1939
28. Colomer, E., Corriu, R. J. P., Vioux, A.: Inorg. Chem., 18, 695 (1979)
29. Eaborn, C. et al.: J. Organomet. Chem. *34*, 153 (1972)
30. Eaborn, C., Tune, D. J., Walton, D. R. M.: J. Chem. Soc. Chem. Commun. *1972*, 1223
31. Eaborn, C., Tune, D. J., Walton, D. R. M.: J. Chem. Soc. Dalton *1973*, 2255
32. Sommer, L. H., Lyons, J. E., Fujimoto, H.: J. Amer. Chem. Soc. *91*, 7051 (1969)
33. Brook, A. G., Pannell, K. H., Anderson, D. J.: J. Amer. Chem. Soc. *90*, 4375 (1968)
34. Corriu, R. J. P., Moreau, J. J. E.: J. Organomet. Chem. *85*, 19 (1975); *120*, 337 (1976)
35. Corriu, R. J. P., Moreau, J. J. E.: J. Organomet. Chem. *40*, 55, 73 (1972)
36. Sommer, L. H.: Stereochemistry, mechanism and silicon, p. 111. New York: McGraw-Hill 1965
37. Isaacs, E. E., Graham, W. A. G.: J. Organomet. Chem. *85*, 237 (1975)
38. Colomer, E., Corriu, R. J. P., Vioux, A.: Unpublished results
39. Hutcheon, W. L.: Ph. D. Thesis. University of Alberta. Edmonton 1971
40. Simpson, K. A.: Ph. D. Thesis. University of Alberta. Edmonton 1973
41. Eaborn, C., Ratcliff, B., Pidcock, A.: J. Organomet. Chem. *43*, 5 (1972); *65*, 181 (1973)
42. Eaborn, C. et al.: J. Organomet. Chem. *54*, 1, 1973
43. Eaborn, C., Pidcock, A., Ratcliff, B.: J. Organomet. Chem. *66*, 23 (1974)
44. Chaik, A. J., Harrod, J. F.: J. Amer. Chem. Soc. *87*, 1133 (1965), *89*, 1640 (1967)
45. Baay, Y. L., MacDiarmid, A. G.: Inorg. Chem. *8*, 986 (1969)
46. Jetz, W. et al.: Inorg. Chem. *5*, 2217 (1966)
47. Colomer, E., Corriu, R. J. P.: J. Organomet. Chem. *133*, 159 (1977)
48. Dahan, F., Jeannin, Y.: J. Organomet. Chem. *136*, 251 (1977)
49. Cerveau, G. et al.: J. Organomet. Chem., 1981, in press
50. Schrieke, R. R., West, B. O.: Aust. J. Chem. *22*, 49 (1969)
51. Hart-Davis, A. J., Graham, W. A. G.: J. Amer. Chem. Soc. *94*, 4388 (1971)
52. Cowie, M., Bennett, M. J.: Inorg. Chem. *16*, 2321 (1977)
53. Cerveau, G., Colomer, E., Corriu, R.: J. Organomet. Chem. *136*, 349 (1977)
54. Cerveau, G. et al.: J. Organometal. Chem. 1981, in press
55. Corriu, R. J. P., Guerin, C.: J. Organomet. Chem. *198*, 231 (1980)
56. King, R. B.: Accounts Chem. Research *3*, 417 (1970)
57. Colomer, E., Corriu, R. J. P.: J. Chem. Soc. Chem. Commun. *1976*, 176
58. Colomer, E., Corriu, R. J. P., Young, J. C.: J. Chem. Soc. Chem. Commun. *1977*, 73
59. Carre, F. et al.: J. Organomet. Chem. *179*, 215 (1979)
60. Casey, C. P.: Transition metal organometallics in organic synthesis, p. 189. New York: Academic Press 1976
61. Chatt, J., Eaborn, C., Kapoor, P. N.: J. Organomet. Chem. *13*, 21 (1968)
62. Malisch, W.: Chem. Ber. *107*, 3835 (1974)
63. Jetz, W., Graham, W. A. G.: Inorg. Chem. *10*, 1647 (1971)
64. Cerveau, G., Colomer, E., Corriu, R. J. P.: Unpublished results
65. Barnett, K. W., Slocum, B. W.: J. Organomet. Chem. *44*, 1 (1972)
66. King, R. B., Reimann, R. H.: Inorg. Chem. *15*, 179 (1976)
67. Ginzburg, A. G., Setkina, V. N., Kursanov, D. N.: IX Internat. Conf. on Organomet. Chem. September 3–7, 1979, Dijon (France)
68. Wolf, R.: La Recherche *6*, 818 (1975)

The Analytical Chemistry of Technetium

Klaus Schwochau

Institute of Chemistry, Nuclear Research Center (KFA)
D-5170 Jülich, Federal Republic of Germany

Table of Contents

1 Introduction

1.1 Discovery and Occurrence

In 1937 the element of the atomic number 43 was discovered by Perrier and Segrè[1] who showed that radioactivity obtained by irradiation of molybdenum with deuterons was due to isotopes of the missing element ekamanganese. The metastable isomers ^{95m}Tc and ^{97m}Tc had been produced by the nuclear reactions

^{94}Mo (d, n) ^{95m}Tc

and

^{96}Mo (d, n) ^{97m}Tc .
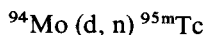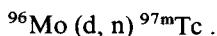
Perrier and Segrè suggested the name technetium[2], since it was the first element to be prepared artificially. 20 isotopes and numerous isomers with half-lives between about one second and several million years have hitherto been known (Table 1).

Table 1. Isotopes and isomers of technetium[3]

Nuclide	Half-life	Decay	Nuclide	Half-life	Decay
^{91}Tc	3.2 m	β^+, γ	^{99}Tc	2.1×10^5 a	β^-
^{92}Tc	4.4 m	β^+, γ	^{100}Tc	15.8 s	β^-, γ
^{93m}Tc	43.5 m	ε, γ	^{101}Tc	14 m	β^-, γ
^{93}Tc	2.7 h	$\varepsilon, \beta^+, \gamma$	^{102m}Tc	4.3 m	β^-, γ
^{94}Tc	53 m	β^+, γ	^{102}Tc	6.3 m	β^-, γ
^{94}Tc	4.9 h	$\varepsilon, \beta^+, \gamma$	^{103}Tc	50 s	β^-, γ
^{95m}Tc	60 d	$\varepsilon, \beta^+, \gamma$	^{104}Tc	18.0 m	β^-, γ
^{95}Tc	20 h	ε, γ	^{105}Tc	7.6 m	β^-, γ
^{96m}Tc	52 m	ε, γ	^{106}Tc	36 s	β^-, γ
^{96}Tc	4.3 d	ε, γ	^{107}Tc	21 s	β^-, γ
^{97m}Tc	91 d	γ	^{108}Tc	5.0 s	β^-, γ
^{97}Tc	2.6×10^6 a	ε	^{109}Tc	1 s	β^-
^{98}Tc	4.2×10^6 a	β^-, γ	^{110}Tc	0.83 s	β^-, γ
^{99m}Tc	6.0 h	γ, β^-			

The isotopes with the longest half-lives are ^{97}Tc (2.6×10^6a), ^{98}Tc (4.2×10^6a) and ^{99}Tc (2.1×10^5a). In the range of the mass numbers of long living isotopes, stable isobars of the neighboring elements molybdenum and ruthenium are known. Thus, according to Mattauch's rule, no stable technetium nuclides should exist. The primordial occurrence of any long-lived isotope in the earth's crust can be excluded with regard to the earth's age of about 4.6×10^9 years.

Until technetium was produced by nuclear reactions there had been numerous efforts to demonstrate the occurrence of the lacking element in the nature. In this context, the works of Noddack and Tacke[4] as well as Berg and Tacke[5] should be

mentioned. It was not unexpected that when Noddack et al. announced the discovery of rhenium in 1925 they also claimed to have found element 43 by X-ray spectroscopy in concentrates of the minerals sperrylite, gadolinite and columbite. They called the new element masurium. However, their observations were not confirmed by other investigators[6-8]. Noddack et al. did not succed in concentrating and isolating the element 43, thus their claim to discovery was not generally accepted.

Until it was known that the half-life of ^{98}Tc is much shorter than 10^8 years[9, 10], Herr[11] looked for technetium-98 in a number of minerals from Norway and South Africa by neutron activation analysis. This most sensitive method was also used by Alperovitch et al.[12] and Anders et al.[13] to detect this isotope in nature. According to the nuclear reaction

$$^{98}\text{Tc (n, } \gamma) \ ^{99m}\text{Tc} \xrightarrow{6.0\,\text{h}} \ ^{99}\text{Tc} + \gamma$$
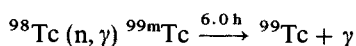
the formation of ^{99m}Tc could be established in some samples. However, the results did not prove the primordial occurrence of ^{98}Tc, since neutron reactions of the nuclides ^{98}Mo, ^{99}Ru as well as of U and Th may also lead to the formation of ^{99m}Tc.

In 1956 Boyd and Larson[14] thoroughly sought for technetium in various samples using analytical methods of high sensitivity such as neutron activation, mass spectrometry, emission spectroscopy, spectrophotometry, and polarography. Not one of their numerous concentrates revealed traces of natural technetium. It now seems clear that primordial technetium does not exist in nature.

Nevertheless, the earth's crust contains technetium. ^{99}Tc is formed by spontaneous fission of ^{238}U as well as by slow neutron-induced fission of ^{235}U. The first isolation of naturally occurring technetium was reported by Kenna and Kuroda[15], who isolated about 10^{-3} μg ^{99}Tc from 5.3 kg of pitchblende.

Soon after the optical emission spectrum of technetium was known, Moore[16] looked for technetium lines in the spectrum of the sun and suggested that the absorption lines at 3195 Å could arise from Tc-II. Later on, the suggestion was shown to be erroneous[17, 19]. However, in 1952 Merrill[20] identified lines due to Tc-I in S-type stars such as R Andromeda, R Geminorum, and others. Some years later, he also observed Tc-I-lines in the N-type stars[21]. N- and S-type stars belong to the relatively cold stars. The discovery of technetium in a number of stars has been of great significance. Considering the half-life of 4.2×10^6 a of the longest-living nuclide ^{98}Tc, the synthesis of a heavy element in the stars was detected for the first time and has led to new theories of the production of heavy elements by neutron capture in the stellar interior.

Among the long-lived isotopes of technetium, only ^{99}Tc can be obtained in weighable amounts. It may be produced by either neutron irradiation of highly purified molybdenum or neutron-induced fission of uranium-235. The nuclides ^{97}Tc and ^{98}Tc are exclusively produced in traces by nuclear reations. Because of the high fission yield of more than 6%, appreciable quantities of technetium-99 are isolated from uranium fission product mixtures. Nuclear reactors with a power of 100 MW produce about 2.5 g of ^{99}Tc per day[22].

1.2 Nuclear Properties and Laboratory Handling

^{99}Tc is a week β^- emitter (E_{max} = 0.29 MeV); β^- emission is not accompanied by γ iradiation, but secondary X-rays (Bremsstrahlung) may become important with larger amounts of the isotope. With a half-life of 2.1×10^5 a ^{99}Tc decays into the stable ^{99}Ru. The specific activity of ^{99}Tc comes to 3.78×10^{10} transmutions per minute and gram, corresponding to 17 μ Ci/mg. The nuclear spin is 9/2 $\hbar$ and the nuclear magnetic moment $+5.657$ nuclear magnetons.

The handling of ^{99}Tc on a small scale (<20 mg) does not present a danger to health provided some elementary precautions are taken. Technetium can be handled in a well ventilated fume cupboard. Nothing unnessary is placed into the cupboard. Normal microchemical practice is observed. The walls of ordinary laboratory glassware give adequate protection against the weak β^- emission[23]. Care must be taken to avoid contamination of the laboratory by fumes or dusts; precaution is necessary in handling technetium compounds of higher vapor pressure. For example, the vapor pressure of technetium heptoxide amounts to 10^{-1} mm Hg at 100 °C [24]. Injected technetium is rapidly eliminated[25] from most organs, but is selectively filtered from the blood, retained by the stomach and, in particular, by the thyroid gland[26] where it is concentrated up to 24% of the activity introduced. Chemical forms of ^{99m}Tc are presently the most widely used radiopharmaceuticals for radionuclide imaging of the brain, liver, lung, and skeleton, and, to a lesser extent, in thyroid scintigraphy[26 a].

1.3 General Properties

As expected there is a close resemblance in the chemical behaviour of technetium and rhenium whereas the properties of both elements differ considerably from those of manganese. The electronic configuration of technetium in the ground state is $4d^6 5s$. Technetium is a silver-grey metal which tarnishes slowly in moist air. Like rhenium and ruthenium it crystallizes in a closest packed hexagonal lattice with the metal atoms having the coordination number 12. In Table 2 some properties of technetium are compared with those of manganese and rhenium.

The atomic radius of technetium is by 0.02 Å smaller than that of rhenium, whereas the difference of the atomic radii of technetium and manganese is almost 0.1 Å. The density of the technetium metal is slightly higher than that of lead. The melting point of 2250 °C is remarkably high, but nearly 1000 °C lower than that of rhenium. Because of the extraordinarily high critical temperature of superconductivity[27], alloys and intermetallic compounds of technetium have been suggested to be a promising material for superconducting magnets[28]. The MeO_4^-/MeO_2 potential decreases from permanganate via pertechnetate to perrhenate such that the oxidation state $+7$ is the most stable for technetium as for rhenium.

Metallic technetium dissolves in oxidizing acids such as dilute or concentrated nitric acid, in aqua regia and in concentrated sulfuric acid. It is insoluble in hydrochlorid acid of any strength. The oxidizing dissoluion leads to colorless TcO_4^-. In oxygen at 500 °C technetium burns to Tc_2O_7 [29], and in fluorine at

Table 2. Properties of manganese. technetium. and rhenium

Parameter	Mn	Tc	Re
Atomic radius [Å]	1.261	1.358	1.373
Density [g × cm^{-3}]	7.47	11.50	21.04
Melting point [°C]	1247	2250	3180
Critical temperature [K]	<0.15	7.7	2.4
MeO$_4^-$/MeO$_2$ Potential [V]	+1.695	+0.738	+0.510

400 °C to the corresponding hexafluoride[30]. Above 300 °C it reacts with chlorine to form $TcCl_4$ as the major product[31]. At elevated temperatures technetium combines with sulfur to give the disulfide TcS_2, and with carbon to form the carbide TcC[32].

Technetium compounds of the oxidation states 0 to +7 have hitherto been isolated, pertechnetates being the most stable. Also, compounds of quadrivalent technetium are fairly stable. Oxidation states lower than +4 can easily be oxidized to the quadrivalent or heptavalent state, whereas penta- and hexavalent technetium readily disproportionate into the hepta- and quadrivalent states.

Many compounds of technetium and rhenium are of analogous composition and of corresponding physical and chemical properties. Because of the very similar ionic radii, isotypic crystal structure formation of analogous compounds could often be observed. Technetium remarkably differs from manganese by the high stability of pertechnetate compared with permanganate. Moreover, divalent technetium does not exist as a hydrated ion but only as a stabilized complex.

2 Separation

2.1 Separation of Technetium from Uranium Fission Products

As already mentioned the fission yield of technetium-99 is very high and amounts to more than 6%. With the development of atomic power engineering the production of technetium will increase steadily. However, the isolation of technetium does not fit into most schemes of processing nuclear fuels. Technetium is mainly obtained at plants processing waste solutions remaining after the separation of uranium and plutonium. The technetium content in solutions to be processed amounts to 5–100 mg/l [33]. The composition of the metal recovery waste solution after purification of the nuclear fuel in the redoxprocess (extraction process involving the use of methyl isobutyl ketone as the solvent and aluminum nitrate as the salting out agent) and in the purex-process (extracting agent tri-n-butyl phosphate, salting out agent nitric acid) is shown in Table 3.

During recycling of the fuel technetium follows the majority of the other fission products into the waste solutions. After storage for several years, the level of the radioactivity in the waste solutions has fallen sufficiently to allow the extraction

Table 3. Compositions of typical metal recovery waste solutions[23]

	Redox process	Purex process
$Al(NO_3)_3$	1.4 M	—
NH_4NO_3	1.9 M	—
$Hg(NO_3)_2$	0.0125 M	—
HNO_3	—	3.9 M
^{137}Cs	0.87 Ci/l	4.4 Ci/l
^{90}Sr	0.94 Ci/l	4.6 Ci/l
^{106}Ru	0.10 Ci/l	9.0 Ci/l
^{144}Ce	0.87 Ci/l	88.7 Ci/l
^{147}Pm	1.06 Ci/l	17.0 Ci/l[a]
^{99}Tc	6.5 mg/l	41 mg/l[a]
Fe, Ni, Cr	small, variable	—

[a] estimated

of the longer-living fission products including technetium. Such operations must be conducted using remote handling techniques and extensive γ ray shielding as afforded by hot cells. The first gram of technetium was isolated in 1952 from the redox-process waste according to the flow diagram shown in Fig. 1.

Tetraphenylarsonium pertechnetate is precipitated in the presence of perchlorate as the carrier. The mixed salts are disolved in concentrated sulfuric acid and the solution is electrolyzed at platinum electrodes. The black deposit (TcO_2) obtained is dissolved in perchloric acid, technetium heptoxide is distilled out of the solution
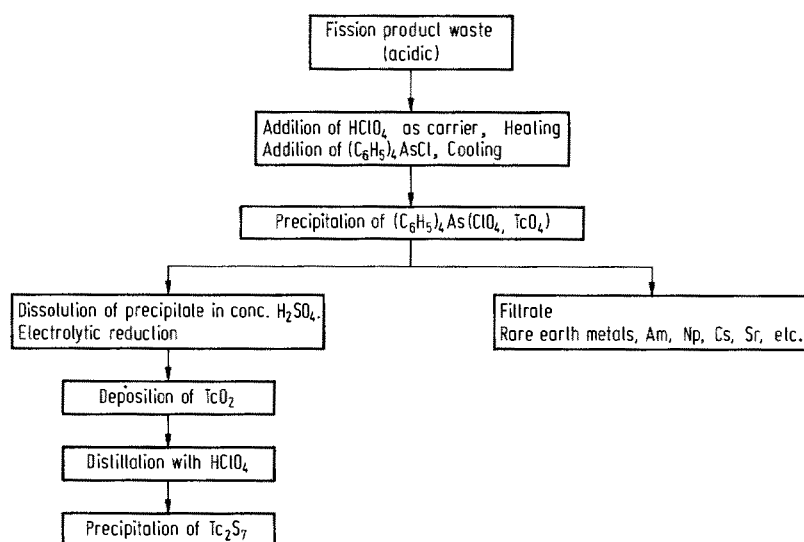
Fig. 1. Extraction of technetium from redox process waste[34]

115

and the element is finally isolated by precipitation of the heptasulfide, which can be reduced by hydrogen to the metal.

Disadvantages of using tetraphenylarsonium chloride are the high cost of the reagent and its necessary high consumption, since the electrolysis procedure decomposes the tetraphenylarsonium ions. In order to recover tetraphenylarsonium chloride the tetraphenylarsonium pertechnetate (perchlorate) precipitate is dissolved in ethanol and the solution passed through the bed of a strongly basic anion exchanger in the chloride form. TcO_4^- and ClO_4^- are strongly adsorbed and finally eluted with 2 M $HClO_4$. Tetraphenylarsonium chloride being in the effluent may be isolated and purified by recrystallization[23].

Subsequently, solvent extraction was applied to recover the fission product technetium from the residue remaining after the fluorination of irradiated uranium fuel elements[35]. The residue was leached with concentrated aluminum nitrate solution, which was extracted by 0.3 M trilaurylamine in a hydrocarbon diluent. After separation of uranium, neptunium, and aluminum nitrate, technetium was back extracted into a 4 N sodium hydroxide solution.

Campbell[36] has studied the separation of technetium by extraction with tributyl phosphate from a mixture of fission products cooled for 200 days. Nearly complete separation of pertechnetate is achieved by extraction from 2 N sulfuric acid using a 45 % solution of tributyl phosphate in kerosene. Ruthenium interferes with the separation and is difficult to remove without loss of technetium; other radioisotopes can be removed by a cation-exchange process. However, this separation procedure has not been widely applied because of the adverse influence of nitrate.

Goishi and Libby[37] have investigated the extraction of pertechnetate from alkali solutions with pyridine. Later work[38] showed that a better extraction is obtained using a mixture of sodium hydroxide and sodium carbonate as the aqueous phase. Since the uranyl carbonate complex is not extracted into pyridine, this system may be used for the separation of technetium from uranium. Distribution coefficients of fission products in pyridine are given in Table 4. Substituted pyridine such as 2,4-dimethylpyridine or 4-(5-nonyl)pyridine[39]) are useful for separating technetium from solutions containing appreciable amounts of aluminum nitrate.

The extraction with pyridine may be one of the most suitable processes of recovering technetium. The scheme described in Fig. 2 was used at the Oak Ridge National Laboratory[33].

Table 4. Distribution coefficients of uranium fission products in pyridine. Extraction from 0.25 M NaOH + 2.0 M Na_2CO_3[38]

Isotope	Distribution coefficient
^{99}Tc	7.4×10^2
^{137}Cs	2.87×10^{-3}
^{106}Ru	1.27×10^{-1}
^{95}Zr, ^{95}Nb	6×10^{-4}
$^{152-155}$Eu	6×10^{-3}
^{90}Sr	3.48×10^{-3}

Waste from Purex process

Evaporation → Precipitate ^{95}Zr, ^{95}Nb

Precipitation of Fe^{3+} with NH_3 at pH 2.5 → Precipitate $Fe(OH)_3$ + Ru

Precipitation of rare earth metals with NH_3 at pH 8 → Precipitate to be used for separating ^{144}Ce and ^{147}Pm

Precipitation of alkaline earth metals with Na_2CO_3 → Precipitate ^{90}Sr, Ca, Ba carbonates to be used for separating ^{90}Sr

Reduction of TcO_4^- with N_2H_4. Co-precipitation of $Fe(OH)_3$ and Tc with NH_3 → Solution to be used for separating ^{137}Cs

Dissolution of $Fe(OH)_3$ + Tc in HNO_3. Precipitation of Fe^{3+} with NH_3 → $Fe(OH)_3$ precipitate with admixtures of fission products

Adjustment of solution to 0.25 M NaOH and 2.0 M Na_2CO_3. Extraction of TcO_4^- with pyridine → Aqueous phase to waste

Organic phase for steam distillation → Recovery of pyridine

Saturation of aqueous phase with $(NH_4)_2CO_3$ → Crystallization of NH_4TcO_4

Recrystallization of NH_4TcO_4 → NH_4TcO_4 chemical purity 99.99 %

Fig. 2. Scheme of the extraction of technetium from a waste solution using pyridine[33]

A method of obtaining technetium in the processing of consumed nuclear fuels in gaseous diffusion plants has been reported[40]. TcF_6 is formed along with UF_6 during fluorination of uranium and escapes together with this compound. Adsorbing technetium hexafluoride on a bed of magnesium fluoride, one can concentrate technetium and separate it from uranium. Pertechnetate is extracted with 2.4-dimethylpyridine. The use of this method has clearly reduced the cost of the isolation of technetium and increased its production.

The solvent extraction of pertechnetate with cyclohexanone has proved to be an efficient and selective method which can be applied to the separation of ^{99}Tc from long-lived fission products in the burn-up analysis[41]. The recovery of technetium from the fission products is about 93%.

The known process of distillation of technetium heptoxide from sulfuric acid has been successfully applied to the separation of microgram amounts of technetium from fission elements[42].

Chromatographic methods for the separation of technetium from fission products are based on the strong sorption of pertechnetate from weakly acidic, neutral, and

alkaline media by basic anion-exchange resins, whereas most of the other fission products are not adsorbed under the same conditions. Appreciable sorption of TcO_4^- takes place even from solutions with high concentrations of nitrate (Table 5) which are usually in the waste solutions.

Table 5. Distribution of pertechnetate between Dowex-1 anion exchange resin and alkaline (0.25 N NaOH) solutions of increasing $NaNO_3$ concentration[38]

$NaNO_3$ Concentration (mol/l)	Distribution Coefficient of TcO_4^-
0	4,500
0.5	575
1.0	340
2.0	190
3.0	142
4.0	125
5.0	121
6.0	122

Roberts et al.[43] have developed an effective and economic chromatographic method for isolating technetium from neutral industrial solutions of the purex process. The solution with a high nitrate concentration is passed through a column containing the anion exchanger De-Acidite FF in the OH^--form. After desorption of pertechnetate by nitric acid technetium is separated from traces of ruthenium by oxidizing the latter to RuO_4 and sorbing ruthenium ions remaining in solution by a cation exchanger. Technetium is precipitated as Tc_2S_7. In one step a high yield (80%) of technetium with a purity of about 99% can be achieved.

A radiochemical procedure is proposed[44] for the determination of technetium activities from mixed fission products of uranium and thorium. The chief decontamination step is the extraction of TcO_4^- into a tetrapropylammonium hydroxide-bromoform mixture from 4.0 M NaOH solutions. Decontamination factors of 10^7 with chemical yields of 50–70% have been obtained.

A selective separation of fission technetium induced by fission of ^{235}U can be performed by stopping the speed of the Tc nuclides in solid KCl and $SrCl_2$ catchers[45]. At temperatures of 300 to 750 °C, 30% to 85% of Tc is selectively released. Purified nitrogen is used for the transportation of the nuclides from the target to the detector. The release is accelerated by increasing the temperature and adding $ZrCl_4$ as a carrier.

2.2 Volatilization Methods

Owing to the volatility of technetium heptoxide, Tc (VII) may be co-distilled with strong acids[46] (Fig. 3).
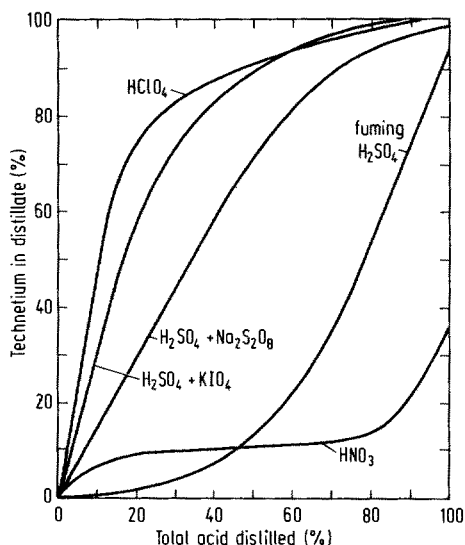
Fig. 3. Co-distillation of technetium with acids[47]

The use of perchloric acid gives good yields; up to 75% of technetium is distilled with the first 20% of the distillate. With nitric acid, aqua regia, sulfuric acid and fuming sulfuric acid the distillation of technetium is incomplete; a considerable amount begins to distill only when more than 50% of the acid has passed into the distillate. The addition of oxidants ($KBrO_3$, $K_2Cr_2O_7$, $Na_2S_2O_8$, $KMnO_4$) to acids such as H_2SO_4 or H_3PO_4 considerably increases the extent of co-distillation. HCl, HBr and HI do not volatilize technetium, since these acids reduce Tc (VII) to form non-volatile hexahalide complexes of Tc (IV).

However, a more detailed study[42] of the co-distillation with sulfuric acid has revealed that technetium can be distilled quantitatively with H_2SO_4 provided the acid and the distillation apparatus are free from contaminations. Reducing agents only inhibit distillation but display no effect on the complete separation of technetium. If, for example, bromide ions are present, distillation begins at 155 °C instead of 110 °C thus resulting in a rapid and quantitative distillation of technetium.

2.2.1 Separation of Technetium from Rhenium

The property of pertechnetate to be easily reduced by hydrochloric acid is utilized in its separation from rhenium by distillation. Perrier and Segrè[48, 49] separated both elements by distillation from a mixture of sulfuric and hydrochloric acid at 180–200 °C. Under these conditions about 90% of rhenium is said to pass into the distillate, but almost all the technetium which is reduced to Tc (IV) remains in solution. The separation factor was found to be 50.

Another distillation method involves reduction of pertechnetate by hydroxylamine[50]. Rhenium is distilled from sulfuric acid. This method can be used for the separation of about 10 mg of rhenium from microamounts of technetium.

Partial separation of technetium and rhenium is possible by distillation from perchloric acid[46, 50], since the first fraction is enriched by technetium. However, ruthenium is oxidized by perchloric acid to RuO_4 and volatilized together with technetium.

In consequences of the great differences in vapor pressures of the heptoxides and acids at low temperatures, technetium may be partially separated from rhenium by repeated alternating evaporation with nitric acid and hydrochloric acid[51]]

2.2.2 Separation of Technetium from Molybdenum

Distillation methods using sulfuric acid are the most efficient for isolating technetium produced by neutron irradiation of kilogram amounts of molybdenum. Boyd et al.[47] have used this method to separate technetium from pure molybdenum which had been irradiated for one year. In this case for each gram of molybdenum 6 ml of concentrated surfuric acid are added and about 75 % of technetium is passed into the distillate. When double the amount of acid is added, nearly 90 % of technetium are found in the distillate. More than 98 % of technetium are extracted after two distillations.

Procedure: The irradiated molybdenum is dissolved in conc. sulfuric acid and technetium is distilled with the acid. The distillate obtained is diluted to 4 M H_2SO_4, heated to boiling and treated with bromic water. A platinum salt (1 mg of Pt/200 ml solution) is added to the solution as collector, and technetium is co-precipitated with the platinum sulfide. The precipitate is dissolved in NH_4OH/H_2O_2 mixture and the solution evaporated to dryness. The residue is dissolved in conc. H_2SO_4 or $HClO_4$ and technetium separated from platinum by distillation. The solution is diluted and the sulfide precipitated.

The concentrate obtained usually contains considerable amounts of molybdenum. In order to reduce the molybdenum content, technetium can be distilled from a mixture of $HClO_4/H_3PO_4$ [52, 53]. In this mixture molybdenum is bound as the non-volatile molybdatophosphate complex.

2.3 Solvent Extraction

The extraction of technetium by different organic solvents is used in numerous separation and concentration procedures. Technetium is extracted as pertechnetate or, in lower oxidation states, as a complex compound. TcO_4^- can be extracted by the following main types of reactions[54]:

$$TcO_4^- \text{ (aq)} + H^+ \text{ (aq)} \leftrightarrows HTcO_4 \text{ (org)} \tag{1}$$

$$TcO_4^- \text{ (aq)} + M^+ \text{ (aq)} \rightleftarrows MTcO_4 \text{ (org)} \tag{2}$$

$$TcO_4^- \text{ (aq)} + MX \text{ (org)} \leftrightarrows MTcO_4 \text{ (org)} + X^- \text{ (aq)} . \tag{3}$$
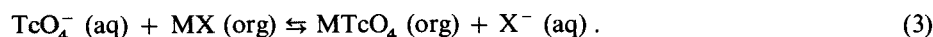
In process (1) solvents containing a donor group have been used. In process (2) large cations such as $(C_4H_9)_4N^+$, $(C_6H_5)_4P^+$, or $(C_6H_5)_4As^+$ with hydrophobic

groups can be applied together with organic solvents like chloroform. In process (3) the cation M^+ is insoluble in the aqueous phase. The extraction will then take place through an ion exchange reaction[54].

The general conclusions deduced by Boyd and Larson[55] who have studied the extraction of technetium from acid, alkaline, and neutral media are as follows:

a) The extraction of pertechnetate by aliphatic and aromatic hydrocarbons and chlorohydrocarbons is negligible even when the latter possess relatively large dielectric constants. A prerequisite of efficient extraction by a pure liquid appears to be the presence of an electron donor atom in its molecule, e.g. a basic oxygen or nitrogen atom.

b) A appreciable dielectric constant of the medium favors the extraction by a liquid, even when the latter contains only weak donor atoms.

c) The extraction of pertechnetate decreases within a homologous series on increasing the hydrocarbon character of the molecules of the extracting agent.

As a rule, extraction is much more efficient from acid than from neutral salt or alkaline aqueous solutions (Fig. 4).
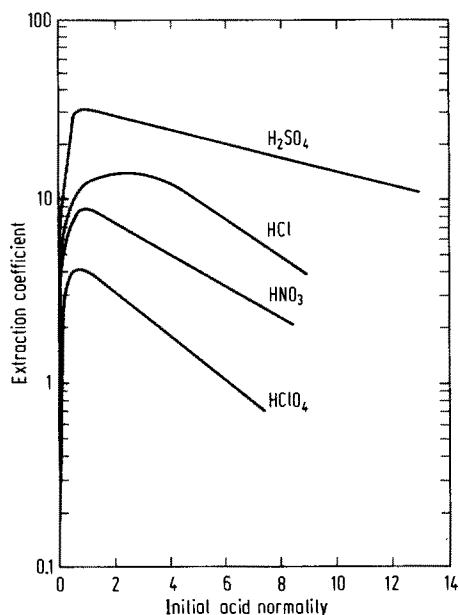
Fig. 4. Extraction of pertechnetate from aqueous solutions with cyclohexanol as a function of acid concentration[55]

Curves similar to those in Fig. 4 have also been observed with cyclohexanone, tri-n-butyl phosphate and with solutions of TBP in a liquid hydrocarbon. The extraction increases rapidly upon the addition of small amounts of acid and, after a maximum value is reached, an exponential decrease is observed. Some of the higher extraction coefficients of organic liquids or solutions are given in Table 6. The values have been selected from data found by Boyd and Larson[55].

Table 6. Extraction of pertechnetate from various aqueous solutions at 25 °C[55]

Extractant	Dielectric constant	Extraction coefficient		
		1 N H_2SO_4	1 N Na_2SO_4	1 N NaOH
3-Pentanol	13.6	9.5	3.1	0.24
2-Methyl-2-butanol	5.8	10.4	4.0	0.73
Cyclohexanol	15.0	32	3.6	0.77
2-Pentanone	15.4	38	32	15
3-Pentanone	17.0	35	6.2	2.5
Cyclohexanone	18.3	93	14	6.7
Dibutoxytetraethylene glycol	5.9	6.5	0.50	0.32
β,β'-Dichlorodiethyl ether	21.1	1.5	0.073	0.05
Tributyl phosphate	7.9	44	8.3	7.5
Trioctylphosphine oxide[a]	—	41	0.017	0.013
Tridecylphosphine oxide[a]	—	49	—	0.023
Trihexylphosphine oxide[a]	—	46	0.051	0.017
Di-n-decylamine[a]	—	47	0.036	0.003
Tri-n-octylamine[a]	—	110	0.004	0.002
Tri-isooctylamine[a]	—	72	0.003	0.002
Pyridine[a]	12.3	—	—	180
Cetyl-dimethyl-benzylammonium chloride[b]	—	105	18	—
Dimethyl-didodecenylammonium chloride[b]	—	100	65	99
Toluene	2.4	0.057	<0.01	<0.01
Benzene	2.3	0.017	<0.01	<0.01

[a] 0.1 M in cyclohexane
[b] 0.1 M in toluene

In general tertiary alcohols are more powerful extractants than secondary or primary alcohols of the same oxygen-to-carbon ratio. Aromatic or alicyclic alcohols reveal higher extraction coefficients than straight-chain alcohols of the same oxygen-to-carbon ratio. Among the ketones methyl ketones have the largest and symmetric ketones the smallest extraction efficiency. Aromatic or alicyclic ketones show higher extraction coefficients than n-aliphatic ketones of the same oxygen-to-carbon ratio. Polyethers are more effective extractants than normal ethers of the same O:C atom ratio. Compared with tri-n-butyl phosphate at equal concentrations in an inactive solvent the more strongly basic tri-n-alkylphosphine oxides are substantially more effective. Changes in the size of the phosphine oxide molecule seem to be unimportant. In going from primary to secondary and tertiary amine solutions in cyclohexane the extraction from acid solutions increases. Among the tertiary amines extraction coefficients decrease with decreasing basicity. Quaternary ammonium salts dissolved in inert solvents ensure efficient extraction not only from acid but also from neutral and alkaline solutions.

The dependence of the extraction coefficient of pertechnetate on the salt concentration and kind of anions being an aqueous solutions is shown in Fig. 5.
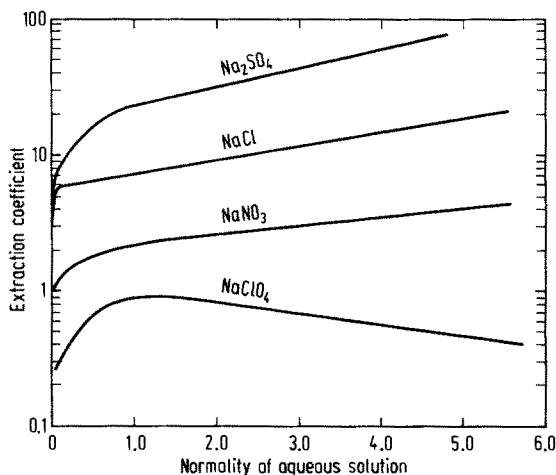
Fig. 5. Extraction of pertechnetate from aqueous salt solutions with tri-n-butyl phosphate[55]

With all solvents studied including cyclohexanol, methyl ethyl ketone and cyclohexanone, heptavalent technetium is extracted most effectively from sodium sulfate and weakest from sodium nitrate or sodium perchlorate solutions. The data in Fig. 5 appear to be consistent with those on the solubilities of various sodium salts in pure tri-n-butyl phosphate. For example, the solubility of Na_2SO_4 in TBP is extremely small compared with $NaClO_4$.

The slight extractability of TcO_4^- from perchlorate solutions and the almost non-extractability by non-polar solvents in used for the re-extraction of technetium into the aqueous phase by either shaking the organic phase with perchlorate solution or by diluting the extractant with a non-polar solvent. As shown in[56], after 3–4 fold dilution of methyl ethyl ketone by hexane, the distribution coefficient in the system organic solvent/water is only about 6×10^{-5}.

As already mentioned in section 2.1 pertechnetate may be efficiently extracted by pyridine from alkaline solutions[37, 38]. Since pyridine derivates are less soluble in the aqueous phase than pyridine, they extract technetium more efficiently even from nitrate solutions. For example, the distribution coefficients of technetium in the extraction from a 2 M $(NH_4)_2CO_3$ solution with a high nitrate concentration by pyridine and 2-methylpyridine are 7.5 and 242, respectively[38]. Higher distribution coefficients can be achieved by using 3-methyl- or 4-methyl-pyridines. The pyridine derivates are the most promising reagents for the extraction of technetium from nitrate solutions.

Extraction with a solution of methyltricaprylammonium chloride in chloroform results in nearly quantitative isolation of pertechnetate from aqueous media, ranging from 4 M sulfuric acid or 9 M hydrochlorid acid to pH 13[57]. A 1:1 pertechnetate-organic cation adduct seems to be formed at any pH; an excess of the organic reagent is only necessary if extraneous anions can compete with pertechnetate.

123

Pertechnetate in neutral and alkaline media can be extracted into solutions of tetra-alkylammonium iodides in benzene or chloroform. With tetra-n-heptylammonium iodide (7.5×10^{-4} M) in benzene distribution coefficients up to 18 can be obtained[58]. A solution of N-benzoyl-N-phenylhydroxylamine[59] (10^{-3} M) in chloroform can be used to extract pertechnetate from perchloric acid solution with a distribution coefficient of more than 200, if the concentration of $HClO_4$ is higher than 6 M [60]. The distribution of TcO_4^- between solutions of trilauryl-ammonium nitrate in o-xylene and aqueous solutions of nitrate has been measured. In 1 M (H, Li) NO_3 and 0.015 M trilaurylammonium nitrate the overall equilibrium constant has been found to be log K = 2.20 at 25 °C. The experiments support an ion exchange reaction[54]. Pertechnetate can also be extracted with rhodamine-B hydrochloride into organic solvents. The extraction coefficient of Tc (VII) between nitrobenzene containing 0.005 %of rhodamine-B hydrochloride and aqueous alcoholic ^{99m}Tc solution containing 0.0025 % of the hydrochloride, amounts to more than 5×10^3 at pH 4.7[61].

The extraction of Tc (VII) and Tc (IV) from nitric acid has been investigated as function of tetraphenylarsonium chloride concentration in chloroform[61 a]. The ratio K_d/c_0 (distribution coefficient divided by the concentration of tetraphenyl-arsonium chloride in the organic phase) is found to be approximately constant. Tc (VII) can be separated from 3 M HNO_3 by extraction with 0.1 M tetraphenyl-arsonium chloride in chloroform while Tc (IV) is not extracted under the same conditions.

The principal disadvantage of all extraction methods is the inevitable introduction of organic compounds which may reduce TcO_4^- and cause difficulties in subsequent steps. Therefore, it is advisable to have some small amounts of an oxidizing agent, such as hydrogen peroxide, present during the extraction.

In addition to pertechnetate various complex compounds of lower valent technetium can be extracted (Table 7).

Table 7. Extractability of complex compounds of technetium[62]

Agent forming the complex	Extractant	Ref.
Thiocyanate	Ethers, alcohols, ketones	[63]
p-Thiocresol	Chloroform, tetrachloromethane, ether, benzene	[64]
1,5-Diphenylcarbohydrazide	Tetrachloromethane	[65]
Potassium xanthate	Chloroform, tetrachloromethane	[66]
α-Picolinic acid	Chloroform	[67]
Cupferron	Ether, chloroform	[68]
Toluene-3,4-dithiol	Tetrachloromethane	[69]
Sulfosalicylic acid	Isoamyl alcohol, toluene, ether	[67]

2.3.1 Separation of Technetium from Rhenium

Since the extraction behavior of pertechnetate is nearly equal to that of perrhenate, the separation of both elements is difficult and often involves reduction of Tc (VII) to lower oxidation states.

Salaria et al.[70] suggest the separation of technetium and rhenium as cupfer-ronates of pertechnetate and perrhenate which have different solubilities in chloro-form. Pertechnetate can partially be extracted from 4 M H_2SO_4 by shaking the solution with chloroform, which is pre-equilibrated with a solution of 1 % cupfer-ron in 4 M H_2SO_4. The main part of perrhenate remains unextracted.

An efficient method has been developed by Pozdnyakov and Spivakov[71]. In alkaline solution pertechnetate, in contrast to perrhenate, is reduced by hydrazine sulfate. After reduction technetium is no more extracted by methyl ethyl ketone. The distribution coefficient of technetium is by a factor up to 2500 smaller than that of rhenium.

Procedure: Hydrazin sulfate is added to a mixture of pertechnetate and per-rhenate in 3–6 N NaON or KOH until its concentration is about 3×10^{-2} M. The solution is stirred and, after 10 min, rhenium is extracted by an equal volume of methyl ethyl ketone. For complete separation of rhenium from technetium the extraction must be repeated 2–3 times. After a twofold extraction 99 % of techne-tium and only 0.8 % of rhenium remain in the aqueous phase.

Pertechnetate can also be reduced by p-thiocresol in acetic acid solution. With an excess of the reducing agent technetium forms a complex compound which readily dissolves in non-polar solvents such as chloroform, toluene or benzene. Only up to 1 % of rhenium passes into the organic phase[64].

Kiba et al.[72] propose the separation of technetium from rhenium by carbon tetrachloride extraction using potassium ethyl xanthate as reducing agent.

Procedure: A solution of NH_4TcO_4 (2 ml) in 0.1 M aqueous ammonia con-taining ^{99}Tc (~ 10 ppm) is acidified by the addition of 1.5 N HCl (2 ml). To this mixture a 0.5 M freshly prepared aqueous solution of potassium xanthate (1 ml) is added. The mixture is placed in a separatory funnel and mixed by rotating the funnel. Then CCl_4 is added (5 ml) and the mixture is shaken for 20 min. More than 99 % of technetium can be extracted into CCl_4 while rhenium entirely remains in the aqueous phase.

The different behavior of technetium and rhenium may arise because Re (VII) is not reduced by xanthic acid to the same oxidation state as Tc (VII). Other suitable extracting solvents are chloroform, 1.1.1-trichloroethane and isopropyl ether.

2.3.2 Separation of Technetium from Molybdenum

A very efficient extraction method for separating technetium from molybdenum is based on the extraction of tetraphenylarsonium pertechnetate with chloro-form[73, 74]. The molybdate ion is not extracted. It is advisable to have small amounts of an oxidizing agent[46] such a hydrogen peroxide present during the extraction so that TcO_4^- will not be reduced by impurities of $(C_6H_5)_4AsCl$. The concentration of tetraphenylarsoniumchloride should be 3–5 times that of per-technetate. The extraction by the former in chloroform from ammonia or hydro-chloric acid solutions (up, to 5 % HCl) yields a distribution coefficient of about 10^3; molybdenum and ruthenium are almost completely separated. Re-extraction of pertechnetate is achieved by shaking the organic phase with 0.2 N $HClO_4$.

The following procedure can be used for the separation of ^{99m}Tc from molybdate irradiated by neutrons:

Ammonium molybdate is dissolved in a 0.5 % solution of NH$_4$OH and ^{99m}Tc is extracted by 0.05 M tetraphenylarsonium chloride in chloroform. The phases are separated and chloroform is distilled off. The residue is dissolved in water, and the solution is twice passed through a column of Dowex-50. $(C_6H_5)_4As^+$ is adsorbed by the cation exchanger, while ^{99m}TcO$_4$ can be eluted.

The separation of ^{99m}Tc from irradiated MoO$_3$ samples can be performed by solvent extraction with triisooctylamine[75]. A 10^{-3} M solution of triisooctylamine in 1,2-dichloroethane is a suitable extractant for separating ^{99m}TcO$_4$ from Mo (VI) dissolved in 1 M HCl. Less than 0.5 % of Mo (VI) is extracted into the organic phase.

After Baishya et al.[76] isobutyl methyl ketone extracts ^{99m}Tc from the decay products of ^{99m}Mo-labelled molybdate in the pH range 0.5–13.0. The use of complexing agents is unnecessary.

Appreciable separation of pertechnetate from molybdate is achieved by pyridine as extracting agent[37,77]. However, the high boiling point of pyridine complicates the recovery of technetium by steam distillation of pyridine. Therefore, this method is rarely used.

Technetium and molybdenum can also be separated by extracting molybdate with ethyl ether from a medium 1.2 M in both NH$_4$SCN and HCl[78]. Mo (VI) and Tc (VII) undergo reduction and complex formation in this medium. After extraction pure technetium is left in the aqueous phase in 80 % yield.

Pertechnetate and molybdate are reduced in acetic acid media by p-thiocresol and form complex compounds. As mentioned above the technetium compound can be extracted by chloroform. Since the blue molybdenum complex is insoluble in this solvent separation of technetium from molybdenum can be achieved[64].

Tetra-n-heptylammonium iodide in benzene extracts TcO$_4^-$ and MoO$_4^{2-}$ from an aqueous phase of pH 10.5. However, TcO$_4^-$ is extracted much better. A separation factor of about 14 has been found. Thus, only a few cycles of solvent extraction are required to separate efficiently technetium from molybdenum[58].

2.3.3 Separation of Technetium from Ruthenium

The separation of technetium from ruthenium involves major difficulties due to the presence of a large number of oxidation states and ionic forms of ruthenium, some of which are capable of being extrated with technetium. However, the separation is accomplished by the extraction of pertechnetate with pyridine in 4 N NaOH[79]. In alkaline media ruthenium is reduced by the organic solvent to lower valences and is not extracted. The extraction of ruthenium from the aqueous phase can be achieved only in the presence of an oxidant in the solution (e.g. a hypochlorite oxidizing to RuO$_4^{2-}$ which is extracted with pyridine).

The extraction of TcO$_4^-$ with methyl ethyl ketone, acetone, and pyridine results in a ruthenium decontamination factor of about 10^5. Another effective separation method is based on the extraction of technetium as triphenylguanidinium pertechnetate from sulfuric acid by means of chlorex (β-chloroethyl ether). Pertechnetate can be re-extracted with 3 N NH$_4$OH solution[80].

2.4 Chromatographic Methods

2.4.1 Ion Exchange Chromatography

Pertechnetate is strongly adsorbed by highly basic anion exchangers and can be eluted only by ions with a very high affinity for the resin, such as perchlorate. The ratio of the distribution coefficients of pertechnetate and perrhenate is about 1.6 to 2, comparable to adjacent rare earth metals. Technetium and rhenium may be separated by ion-exchange chromatography. However, efficient separations require some care and tend to be slow. On the other hand, cation exchange resins adsorb technetium only to a negligible extent so that pertechnetate can be rapidly separated from cationic elements[46].

TcO_4^- is sorbed much more efficiently from neutral salt solutions than from solutions of acids having the corresponding anions. The absorption from different acids increases in the sequence $HClO_4 < HNO_3 < H_2SO_4 < HCl$.

2.4.1.1 Separation of Technetium from Rhenium

Atteberry and Boyd[81] have separated TcO_4^- and ReO_4^- on Dowex-2 resin using a mixture of 0.1 M $(NH_4)_2SO_4$ and 0.1 M $(NH_4)_2SCN$ as eluent. The two elution peaks are partially resolved, but the cross contamination is rather high. Much better results are obtained if perchlorate is used as the elutriant[82-84]. Because of some peculiarities of commercial resins, the highest practically attainable separation factors of TcO_4^- and ReO_4^- are 10^4–10^5 [46]. It has been found that the volumes of the eluents consumed in the elution of pertechnetate and perrhenate are inversely proportional to the perchlorate concentration. The separation on Dowex 1-X4 is described in Fig. 6. Partial reduction of TcO_4^- or ReO_4^- reduces the efficiency of the chromatographic separation since the elution peaks frequently become blurred[82].

Pirs and Magee[85] have used the resin Amberlite IRA-400 in the chloride form to separate manganese, technetium, and rhenium. Manganese is easily separated by
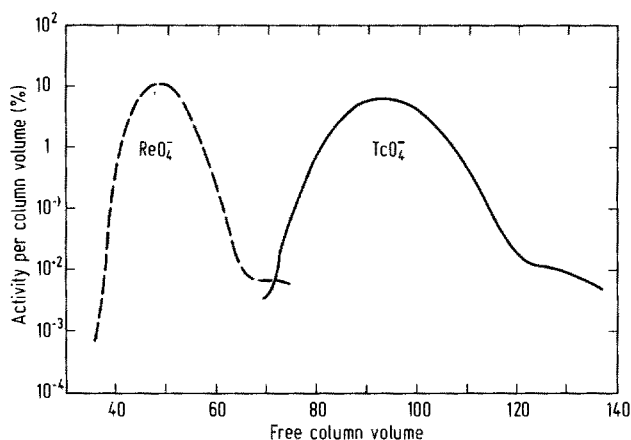
Fig. 6. Anion exchange separation of pertechnetate and perrhenate. Dowex 1-X4, ClO_4^- form, column eluted with 0.1 M NH_4ClO_4[82]

reducing permanganate with hydrogen peroxide to the Mn^{2+} ion which is not adsorbed on the anion exchange resin. Mixtures of TcO_4^- and ReO_4^- in 0.1–0.3 M hydrochlorid acid are passed through the column and both anions are adsorbed. Rhenium is eluted with a 5% solution of NH_4SCN in 0.1–0.2 M hydrochloric acid. After washing the column with water technetium is eluted with 0.1 N nitric acid. Since the separation is highly efficient it is fairly easy to separate 10 μg technetium from 15 mg of manganese and 0.8 mg of rhenium.

2.4.1.2 Separation of Technetium from Molybdenum

The chromatographic separation of technetium from molybdenum is based on the different extent to which molybdate and pertechnetate are adsorbed from alkaline and acid solutions. The distribution coefficient of molybdate between the anion exchanger Dowex 1-X8 and 3 M NaOH is 12, while it is 10^3 for pertechnetate under the same conditions. Molybdate is also adsorbed to a much lesser extent from hydrochloric acid solutions than pertechnetate. Thus, molybdenum can be eluted by hydroxide or HCl solutions while nitric acid, perchlorate or thiocyanate are used for the elution of technetium[62].

Hall and Hohns[86] have found that 10 μg of technetium can be separated quantitatively from as much as 50 g of molybdenum using the Amberlite IRA-400 anion exchange resin in the perchlorate form. The irradiated metal is dissolved in a $NaOH/H_2O_2$ mixture and the solution passed through the column. Molybdate is removed by elution with 10% NaOH solution; pertechnetate is eluted with 0.5 M NH_4SCN.

Technetium can also be isolated quantitatively from molybdate using Dowex-1 resin in the chloride form[87]. Molybdate can be eluted with 0.1 M hydrochloride acid; pertechnetate, however, is firmly adsorbed under these conditions. It can be readily eluted with 4.0 M nitric acid. The only drawback of this separation is the need to recover technetium from nitric acid solution. If the acid is evaporated with great care, losses may be kept quite low.

2.4.2 Adsorption Chromatography

2.4.2.1 Separation of Technetium from Rhenium

Šebesta et al.[88] describe a method for the separation of ^{99m}Tc and $^{186+188}Re$ by adsorption chromatography using a solution of N-benzoyl-N-phenylhydroxylamine in chloroform sorbed on Chromosorb W DMCS. The mixture of the radionuclides of technetium and rhenium in 5 M $HClO_4$ is passed through the column. While ^{99m}Tc is sorbed rhenium is washed out with 5 M $HClO_4$.

^{99m}Tc can be eluted with 0.05 M $HClO_4$. The fraction of ^{99m}Tc is radiochemically pure; the decontamination has been estimated to be higher than 10^3.

Carvalho[89] has studied the separation of technetium from rhenium by electrophoresis and paper chromatography. Good separations can be obtained by electrophoresis using either alkaline hydrazine sulfate or a solution of $SnCl_2$ in hydrochloric acid as electrolytes. Both elements can sufficiently be separated by paper

chromatography under reducing conditions, e.g. by using a paper impregnated with hydrazine sulfate; the paper is eluted with ethanol.

A more efficient method of paper chromatography was developed by Beckman and Lederer[90] making use of the formation of a technetium complex with thiourea in nitric acid. TcO_4^- is reduced by this reagent, in contrast to ReO_4^-. The paper is eluted with 2 N HCl. The R_f values of technetium and rhenium have been found to be very different, namely 0.2 and 0.7, respectively.

A fairly effective paper chromatographic separation of technetium and rhenium can be achieved by using 1:1 butanol-conc. HCl as the mobile phase[91]. Hydrochloric acid causes selective reduction of TcO_4^- with the formation of a chloride complex which is less mobile in this system. Under this condition the R_f values of technetium and rhenium, on Whatmann No. 1 paper, are 0.70 and 0.77, respectively.

2.4.2.2 Separation of Technetium from Molybdenum

For the extraction of ^{99m}Tc from molybdenum irradiated by neutrons or separated from uranium fission products, inorganic sorbents, especially aluminum oxide have widely been applied. In preparing a ^{99m}Tc generator from irradiated molybdenum[92], MoO_3 is dissolved in conc. nitric acid, the solution is diluted and passed through an aluminum oxide column. The column is then eluted by 0.2 N H_2SO_4 to extract ^{99m}Tc. If molybdenum is adsorbed by Al_2O_3 as molybdatophosphate instead of molybdate, the exchange capacity of molybdenum increases from 1.2 g to 8 g per 100 g of Al_2O_3 [93].

Tucker et al.[97] have separated ^{99m}Tc from the fission product ^{99}Mo using chromatographic aluminum oxide washed by dilute nitric acid at pH 1.5. ^{99}Mo dissolved in the same dilute HNO_3 of pH 1.5 is passed through the column which is then eluted with 0.1 M HNO_3. ^{99m}Tc is only slightly adsorbed and can easily be eluted while molybdenum is retained on the column. The purity of technetium is 99.99%.

Instead of aluminum oxide hydrated ZrO_2 can be used to adsorb irradiated molybdate. ^{99m}Tc is eluted with 2 M HNO_3 [95].

D'Olieslager et al.[96] made use of a kieselguhr column supported with 30% of bis-(2-ethylhexyl) hydrogen phosphate. Molybdenum dissolved in 0.1 to 1 M of HNO_3, $HClO_4$, HCl or H_2SO_4 is strongly adsorbed, but much less from > 4 M HCl or H_2SO_4. Accordingly, it is possible to separate technetium and molybdenum after adsorption on to a column from 0.1 M HCl. Technetium is eluted with 5% NaCl solution and molybdenum with 8 M HCl.

Also thin-layer chromatography is applied to the separation of both elements[96 a]. Pertechnetate and molybdate can be separated on silica gel or alumina with mixtures of 1 M HCl methanol or 1 M HCl ethanol (1:5) as solvent[97] and also on cellulose MN 300 with butanol saturated with 1 M HCl[98].

Bailey and Yaffee[99] separated TcO_4^- and MoO_4^{2-} by paper electrophoresis with acetic acid or ammonium acetate solutions. The most efficient separation is achieved with a 0.5% solution of CH_3COONH_4 and a voltage of 60 V/cm.

2.5 Electrodeposition Methods

Technetium metal can be electrodeposited from an acidic solution of pertechnetate using a platinum, nickel or copper cathode. Electrolysis of neutral, unbuffered solutions, alkaline solutions, and sulfuric acid solutions lower than 2 N yield a black deposit of hydrated TcO_2 [100]. The current efficiencies are generally poor but the deposition is reasonably quantitative. The deposition requires the application of relatively negative cathode potentials and is therefore non-selective. Polarography indicates that the overpotentials for the evolution of hydrogen on technetium are rather low; hence, electrolysis from acidic media will always include concurrent discharge of hydrogen [101].

Boyd et al.[47] have electroplated technetium under a variety of conditions. Optimum results are obtained at pH 5.5 in the presence of about 10^{-3} M fluoride concentration. Yields are higher when copper instead of platinum cathodes are used. At a current density of 100 mA/cm^2 98.5% of technetium is deposited in 2 h. However, yields of 98–99% are obtained at similar current densities even with platinum cathodes, at pH 2 to 5 and fluoride concentrations of 5×10^{-3} M with plating times of up to 20 h [46].

Voltz and Holt[102] determined the optimum conditions necessary for the electrodeposition of macroamounts of technetium from an aqueous bath of NH_4TcO_4. The results reveal that technetium can be deposited in macro-amounts as a bright metal from aqueous solutions. A bath containing 1 M $(NH_4)_2SO_4$ and 0.006–0.024 M NH_4TcO_4 with H_2SO_4 added to give a pH of about 1.0 can be electrolyzed at 1–2 A/dm^2. Thus, a metallic cathodic deposit of technetium with a current efficiency range of 18–30% is obtained.

Box[103] recommends the addition of oxalic acid, tartaric acid or another dicarboxylic acid, to sulfuric acid for plating technetium either as a metal or oxide. On copper electrodes in 0.7 M oxalate and 0.45 M sulfuric acid, more than 99% of technetium metal is plated at 1.0–1.3 A/cm^2 from a pertechnetate solution. However, from 0.4 M oxalate and 1.9 M sulfuric acid it is the oxide that is deposited.

Flagg and Bleidner[104] electrolyzed carrier-free $^{95}Tc + ^{96}Tc$ on a platinum cathode in dilute sulfuric acid and obtained a 99.5% yield at -0.8 V vs. the saturated calomel electrode (SCE.).

A partial separation of technetium from molybdenum and rhenium may be obtained at a controlled cathode potential of -1.1 V vs. SCE. However, deposition only takes place at technetium concentrations of 10^{-4} M or greater[46].

In order to deposit ^{99m}Tc from irradiated molybdenum, methods have been proposed that are based on deposition in non-aqueous solutions, particularly from ethereal $MoCl_2$ solutions or molybdenum hydroxyquinolate[105, 106].

2.6 Precipitation Methods

Pertechnetate forms sparingly soluble salts with several large cations, e.g. $(C_6H_5)_4As^+$, nitrogen $C_{20}H_{17}N_4^+$, Tl^+, Ag^+, and Cs^+. The solubility of the per-

technetates has been found to be slightly higher that of the corresponding per-rhenates.

From neutral or alkaline solutions pertechnetate is precipitated by tetraphenyl-arsonium chloride; at 0 °C the precipitation is feasible at concentrations as low as 5 mg Tc/l [34, 46]. At lower concentrations ReO_4^-, ClO_4^-, IO_4^- or BF_4^- may be used as carriers. Decontamination from other fission products is excellent; a single-step β^- decontamination factor of 10^5 has been reported [46]. The principal remaining contaminations are Zr, Nb, and Ru. Co-precipitation with $(C_6H_5)_4AsReO_4$ is one of the fastest separation methods for technetium. Removal of technetium from the organic cation can be accomplished by wet combustion, by electrolysis in conc. sulfuric acid, or by passing an alcohol solution of the precipitate through a strongly basic anion exchanger in the chloride form. The organic cation passes through the column, while pertechnetate is adsorbed and may be eluted with perchloric acid [23].

Nitron-, thallium, cesium-, and silver pertechnetate are appreciably soluble in water and therefore less suitable for precipitation and separation of technetium. From aqueous ammonia solution, pertechnetate can be co-precipitated with $MgMH_4PO_4$ [107].

Technetium heptasulfide is precipitated from pertechnetate solutions 2–4 N in HCl or H_2SO_4 by means of hydrogen sulfide [108, 109]. Thioacetamide [46] or sodium thiosulfate can be used to advantage instead of H_2S [110]. As little as 3 mg/l of technetium may be separated from 4 M H_2SO_4. Precipitation is sluggish and in-complete, if not all of the technetium is in the oxidation state $+7$. At trace levels the sulfides of Pt, Re, Cu, or Mn can be used as carriers. The process of co-precipitation has been studied in detail [47, 111]. The collection of Tc_2S_7 by copper sulfide at acid concentrations of 0.2–3 N is very effective and offers the advantage that copper is easily separable from TcO_4^-. The sulfide is dissolved in ammoniacal hydrogen peroxide, the peroxide destroyed by boiling and the copper removed by passing the solution through a cation exchanger [111].

2.6.1 Separation of Technetium from Rhenium

Co-precipitation of Re_2S_7 with platinum sulfide from conc. hydrochloric acid solutions of microamounts of technetium and rhenium is suitable for the separation of technetium from rhenium [47], since technetium is only slightly co-precipitated under these conditions (Fig. 7). At concentrations of 9 M HCl and above, virtually no technetium is co-precipitated with platinum sulfide at 90 °C, whereas rhenium is removed quantitatively even up to 10 M HCl. The reduction of per-technetate at high chloride concentration may be the reason for this different behavior, because complete co-precipitation of technetium from sulfuric acid solutions up to 12 M has been observed. However, the separation of weighable amounts of technetium from rhenium by precipitation with hydrogen sulfide in a medium of 9–10 M HCl is not quantitative, since several percent of technetium coprecipitate with rhenium and measurable amounts of rhenium remain in solu-tion [46]. Multiple reprecipitation of Re_2S_7 is therefore necessary.

Microgram quantities of technetium and weighable quantities of rhenium may be separated by the fractional crystallization of $KTcO_4$ and $KReO_4$; the latter is
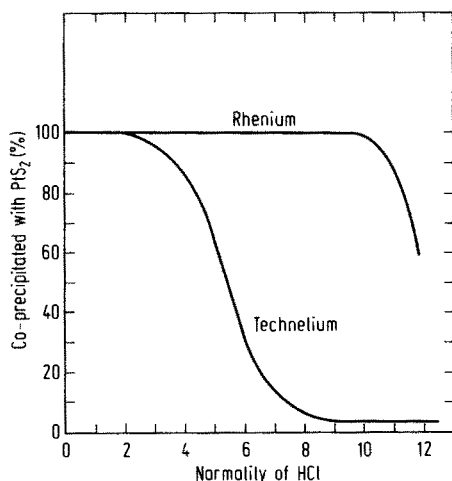
Fig. 7. Co-precipitation of microamounts of technetium and rhenium with platinum sulfide at 90 °C as a function of hydrochloric acid concentration[47]

considerably less soluble[47] (Fig. 8). Evidently, a Nernst distribution holds for the partition of pertechnetate between saturated potassium perrhenate solution and crystalline $KReO_4$.

Satisfactory separation of pertechnetate from perrhenate can be achieved by reducing Tc (VII) with hydrochloric acid and co-precipitating technetium with $Fe(OH)_3$ [112]. Technetium can then be oxidized to the heptavalent state by oxidizing the precipitate in conc. nitric acid and precipitating $Fe(OH)_3$ with ammonia.

The fact that $K_2[TcCl_6]$ significantly differs from $K_2[ReCl_6]$ in its instability toward hydrolysis in aqueous solutions[23], may also be utilized for a separation of technetium from rhenium.
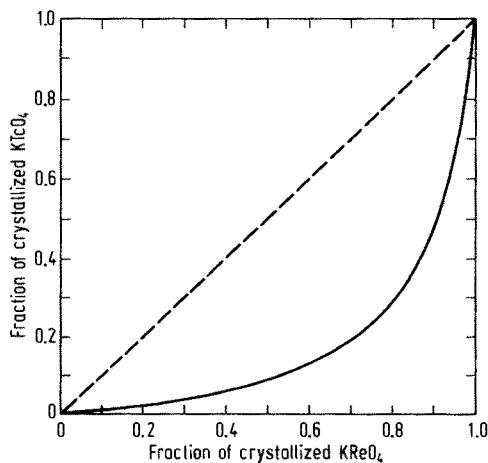
Fig. 8. Separation of $KTcO_4$ from $KReO_4$ by fractional crystallization[47]

2.6.2 Separation of Technetium from Molybdenum

Some precipitation methods have been applied to the separation of technetium from molybdenum when the former occurs as a radio-active daughter-product of the latter. The separation of technetium is performed by co-precipitation with tetraphenylarsonium perrhenate from an alkaline molybdate solution[113]. In this way, also ruthenium remains in solution. Molybdate may be precipitated away from pertechnetate using 8-hydroxyquinoline[111] or α-benzoinoxim; Pb^{2+} or Ag^+ ions can also be used[104]. Kuzina and Spitsyn[114] have developed a method for concentrating technetium from ammoniacal molybdate solutions by co-precipitating pertechnetate with the slightly soluble crystalline $MgNH_4PO_4$.

3 Methods of Determination

3.1 Radiometric Methods

The earliest method for the determination of technetium was based on the measurement of the β^- activity of ^{99}Tc whose specific activity amounts to 37.8×10^3 disintegrations per minute and microgram. The low energy of the β^- particles ($E_{max} = 0.29$ MeV) introduces a number of difficulties into measurements involving self-absorption in the specimen, back scattering of β particles and geometry of counting. In order to avoid these errors the sample should be thoroughly prepared for counting. In practice, an ordinary end-window counter with a mica window can determine about 0.1 μg of ^{99}Tc. The use of special low-background apparatus permits to raise the sensitivity by another two or three orders of magnitude.

The most sensitive method for determining trace amounts of technetium is the neutron activation[14]. The ^{99}Tc sample is irradiated by slow neutrons. The radioactive isotope ^{100}Tc with a half-life of 15.8 s is formed by the reaction $^{99}Tc(n, \gamma) \, ^{100}Tc$, the neutron capture cross section of which is comparatively large (20 barns), so that it is possible to determine amounts $< 2 \times 10^{-11}$ g of ^{99}Tc. However, the method is not widely used since the half-life of ^{100}Tc is very short. Moreover, this method is only convenient when a reactor or a neutron source is available.

The radiometric method is used to determine ^{99}Tc in environmental water samples[115]. The work provides a carrier-free procedure for the determination of ^{99}Tc in aqueous solutions as low as 0.5 dpm/l. The chemical separation is followed by electrodeposition on a stainless-steel cathode involving determination of ^{99}Tc by counting.

The increased use of ^{99}Tc in weighable amounts has necessitated the development of a procedure for the determination of this isotope in excreted samples. A rapid separation of ^{99}Tc can be effected by co-precipitation of ^{99}Tc from urine with copper sulfide[116] and counting it in a proportional β counter. For samples possibly containing other activities, the procedure applied involves measurement

by liquid scintillation counting in order to increase the counting efficiency for this low-energy β^- emitter. Before scintillation counting ^{99}Tc is purified by solvent extraction and anion exchange.

A technique for the determination of ^{99}Tc amounts as little as 4×10^{-12} g by neutron activation analysis has been described by Foti et al.[117]. ^{99}Tc in triply distilled water is irradiated in a thermal neutron flux of 5×10^{13} neutrons per cm^2 and per second to produce ^{100}Tc. Other radionuclides are removed by co-precipitation with Fe(OH)$_3$. Then, ^{100}Tc is co-precipitated twice with tetraphenylarsonium perrhenate which can be removed by sublimation. The chemical purification of ^{100}Tc requires 40–45 s and the technetium yield is about 53%.

Trace amounts of ^{99}Tc are also determined in filter paper and vegetable samples by neutron activation analysis[118]. The procedure consists of the following major steps: separation of technetium from the sample, thermal neutron irradiation of the ^{99}Tc fraction to produce ^{100}Tc, post-irradiation separation and purification of ^{100}Tc from other activated nuclides, and counting of the 16 s ^{100}Tc in a low-background β counter. The estimated detection limits for ^{99}Tc in this procedure are 5×10^{-12} g in filter paper and 9×10^{-12} g in vegetable samples.

A method has been developed for the determination of technetium-99 in mixed fission products by neutron activation analysis[118 a]. ^{99}Tc is separated from most fission products by a cyclohexanone extraction from carbonate solution, the stripping into water by addition of CCl$_4$ to the cylohexanone phase, and the adsorption on an anion exchange column. Induced ^{100}Tc radioactivity is determined using X-ray spectrometry to measure the 540 and 591 keV lines. The sensitivity of the analysis under these conditions is approximately 5 ng. The method has been successfully applied to reactor fuel solutions.

3.2 Spectroscopic Methods

The optical emission spectrum of technetium is uniquely characteristic of the element[119–121] with a few strong lines relatively widely spaced as in the spectra of manganese, molybdenum and rhenium. Twenty-five lines are observed in the arc and spark spectra between 2200 and 9000 Å. Many of these lines are free from ruthenium or rhenium interferences and are therefore useful analytically[23]. Using the resonance lines of Tc-I at 4297.06, 4262.26, 4238.19, and 4031.63 Å as little as 0.1 μg of technetium can be reliably determined.

The atomic absorption characteristics of technetium have been investigated with a technetium hollow-cathode lamp as a spectral line source[122]. The sensitivity for technetium in aqueous solution is 3.0 μg/ml in a fuel-rich acetylene-air flame for the unresolved 2614.23–2615.87 Å doublet under the optimum operating conditions. Only calcium, strontium, and barium cause severe technetium absorption suppression. Cationic interferences are eliminated by adding aluminum to the test solutions. The atomic absorption spectroscopy can be applied to the determination of technetium in uranium and its alloys and also successfully to the analysis of multicomponent samples.

Several measurements of the X-ray emission spectrum of technetium have been reported[123, 124]. The lines $K_{\alpha_2} = 677.90$ X, $K_{\alpha_1} = 673.57$ X, $K_{\beta_1} = 600.20$ X and

$K_{\beta_2} = 588.99$ X can be used for the detection and determination of technetium. An X-ray fluorescence method has been developed for the determination of technetium in solution[125]. At concentrations of less than 1.0 mg Tc per ml there are not interelement effects. Therefore, it is possible to ascertain technetium in its compounds without previous decomposition, provided that the compounds are soluble in water or dioxane. The detection limit is about 4 μg Tc.

Technetium isotopes formed upon irradiation of a molybdenum target by protons with an energy of 22 MeV[126] have been ascertained by mass spectrometry. After separation of technetium by ion exchange, the isotopes ^{95}Tc (0.5%), ^{97}Tc (56.0%), ^{98}Tc (17.3%) and ^{99}Tc (26.7%) are detected. The sensitivity of this method is very high; 5×10^{-9} g of technetium can be detected. Mass spectrometric determination of technetium is also described by Kukavadze et al.[127]. Pertechnetate is reduced to technetium metal and Tc^+ ions are produced at 1600 to 1800 °C.

An isotope dilution mass spectrometric method involves the addition of a known quantity of ^{97}Tc followed by chemical separation, purification, and measurement of the ^{97}Tc/^{99}Tc isotopic ratio[127 a]. An improved technique has been developed for the analysis of ^{99}Tc in environmental samples. After spiking with ^{97}Tc the isolated technetium is concentrated onto anion exchange beads. Determination of as little as 1 pg has been achieved through the enhanced ionization efficiency afforded by the resin bead source[127 b].

3.3 Spectrophotometric Methods

3.3.1 Visible and Ultra-Violet Absorptions

Several spectrophotometric methods for the determination of small amounts of technetium are available.
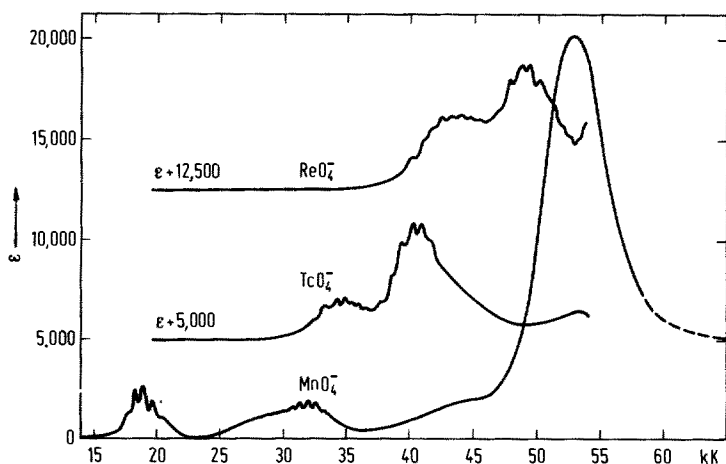
Fig. 9. Electronic spectra of aqueous solutions of permanganate, pertechnetate, and perrhenate[128]

135

Aqueous solutions of pertechnetate absorb fairly strong[128] in the ultraviolet range (Fig. 9). A simple method of ascertaining technetium involves measurement of the optical density of aqueous TcO_4^- solutions at the absorption maxima of 244 and 287 nm with the molar extinction coefficients of 5690 and 2170 mol^{-1} $\times l \times cm^{-1}$, respectively[128]. Beer's law is obeyed up to a concentration of about 10^{-3} $mol \times l^{-1}$; less than 1 μg of technetium can be determined spectrophotometrically. This method is particularly advantageous in the simultaneous determination of technetium and rhenium.

The strong absorptions of the complex technetium (IV) hexahalides[129] (Fig. 10) can also be utilized for spectrophotometric determinations. A sensitive method has been developed using hexachlorotechnetate (IV) [130]. When pertechnetate is heated for 50–60 min in conc. hydrochloric acid, it is reduced to the complex $[TcCl_6]^{2-}$. The absorption curve of $[TcCl_6]^{2-}$ in conc. HCl has a maximum at 338 nm where technetium can be determined in the presence of microgram amounts of rhenium or molybdenum. The molar extinction coefficient is said to be 32.000 (after Jørgensen and Schwochau[129] it amounts to 10.600). About 0.1 μg Tc/ml can be determined. Rhenium present in quantities up to 30 μg/ml has almost no influence on the determination of technetium. The error in the determination of the latter in the presence of molybdenum at a weight ratio of 1:1 is 1–2%.

Pertechnetate reduced in the presence of thiocyanate in an acid medium forms a red-violet thiocyanate complex with a maximum extinction at 513 nm. A yellow thiocyanate complex with a lower valence state of technetium is formed simultaneously[63]. The red-violet complex $[Tc(NCS)_6]^-$ and the yellow complex
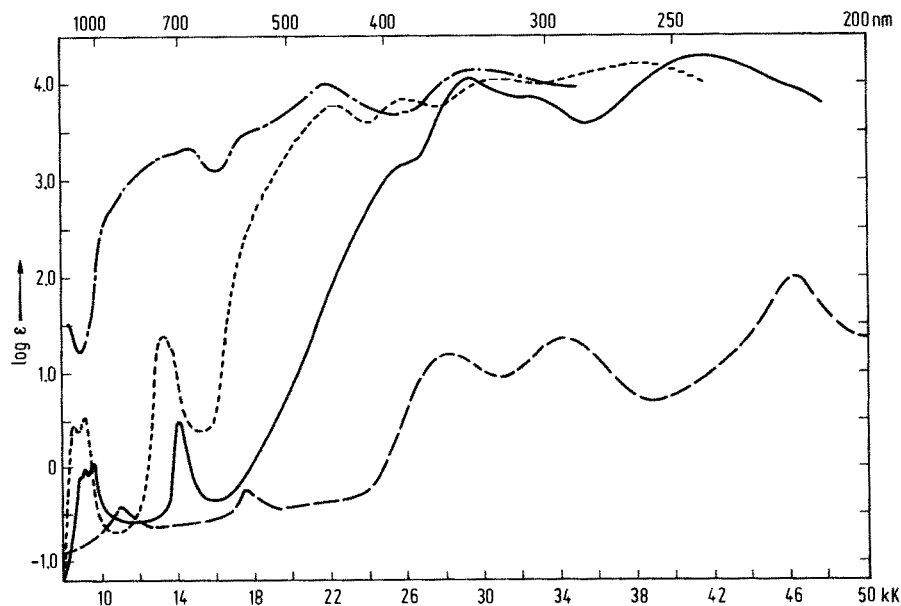
Fig. 10. Absorption spectra of hexahalogeno-complexes of technetium(IV)[129] —·—·— $K_2[TcI_6]$; ·········· $K_2[TcBr_6]$; ———— $K_2[TcCl_6]$; – – – – $K_2[TcF_6]$

$Tc(NCS)_6]^{2-}$ are coupled in a redox system (Fig. 11), the potential of which is found to be $E^0_{25\,°C} = +0.53$ V in 1 M H_2SO_4 [131]. The following procedure given by Crouthamel[63] is based on a final volume of 10 ml:
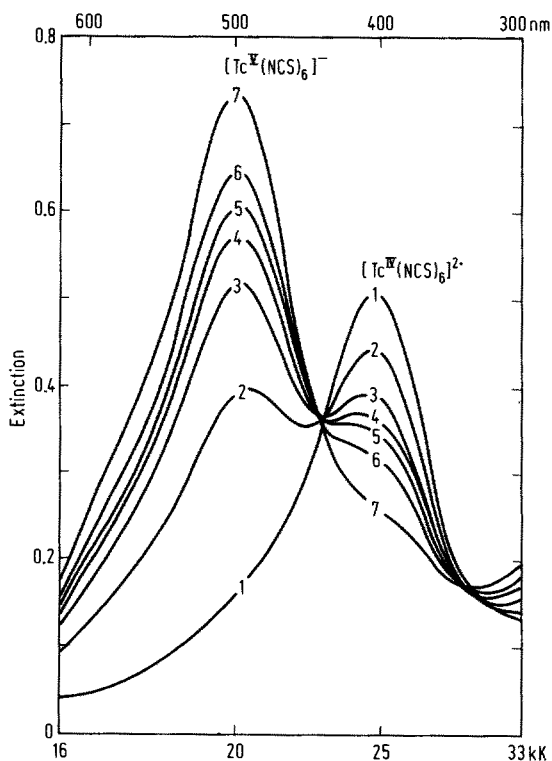
Fig. 11. Redox system of the complex anions $[Tc(NCS)_6]^{2-}$ and $[Tc(NCS)_6]^-$ [131] $[Tc^{IV}(NCS)_6]^{2-}$ $\leftrightarrows [Tc^V(NCS)_6]^- + e^-$; $E^0_{25\,°C} = +0.53$ V

Technetium (VII) is adjusted to 3.5 to 4.0 M sulfuric acid solution. Hydrochloric, nitric and other volatile acids may be volatilized below 100 °C without loss of technetium (VII). The volume of the reduction medium is limited to 4.0 ml and that of conc. sulfuric acid to less than 1 ml to prevent possible phase separation of the final acetone solution. Then 4.0 M aqueous ammonium thiocyanate (0.5 ml) is added to the 3.5 to 4.0 M sulfuric acid solution of technetium (VII).

This amount of thiocyanate is sufficient for both complete reduction and complex formation. Reduction is allowed to proceed for 30 to 45 s after the addition of the thiocyanate. A bright red color can readily be observed at a technetium (VII) concentration of 0.1 µg per ml. Acetone (6 ml) is then added and the volume of the solution mixed and adjusted to 10 ml with distilled water. At this point, the color has generally developed to less than 50% of its final intensity. Quartz 1-cm glass-stoppered cells are filled with the technetium solution and placed in a 20 °C water-cooled spectrophotometer. The extinction will approach a maximum intensity in 1 to 3 h. The maximum extinction occurs at 510 nm with a molar extinction coefficient and standard deviation of 47,500 ± 500 in 60 vol.% of the acetone-aqueous medium. An additional examination of the analysis may be carried out by extract-

137

ing the thiocyanate complex with 5 ml of ether. The resulting medium is a mixed acetone-ether medium in which the molar extinction coefficient and standard deviation is 52,200 ± 500 at the 513 nm maximum.

The non-aqueous medium favors the formation of the red-violet complex. The yellow complex is poorly soluble in a wide variety of organic solvents. Molybdenum, uranium, and iron interfere with the determination since these elements form colored thiocyanate complexes. Disadvantages of this method are the long time required and the formation of the yellow thiocyanate complex which cannot be excluded.

This technique of Crouthamel has been improved by Howard and Weber[132] and used for the determination of technetium in uranium materials. Technetium, 0.3 to 30 μg in a 3 N acid solution, is determined in the presence of uranium (up to 5 g) within 15 min and with standard deviations of ±0.03 μg at 0.50 μg of technetium and ±0.1 μg at 30.0 μg of technetium. Pertechnetate is reduced to Tc (IV) with ascorbid acid in the presence of iron (III) which prevents reduction below Tc (V). The red technetium (V) thiocyanate complex is extracted into butyl acetate; coextracted iron (III) thiocyanate is removed with a phosphate wash. The extinction of the technetium extract is measured at 585 nm (molar extinction coefficient 15,500) in the presence of molybdenum, or at 510 nm (molar extinction coefficient 50,000) in the absence of molybdenum. Molybdenum is the only known direct interference, 100 μg appearing as 0.4 μg of technetium when the extinction is measured at 585 nm.

Foster et al.[133] have developed a method for determining technetium in dissolved nuclear fuel solutions. Tetrapropylammonium pertechnetate is doubly extracted from a basic medium into chloroform and the colored technetium (V) thiocyanate complex is formed in the chloroform phase by the addition of sulfuric acid, potassium thiocyanate and tetrapropylammonium hydroxide. The colored complex absorbs at 513 nm, has a molar extinction coefficient of 46,000 and is stable for several hours. Of more than 50 metals studied, none impairs measurements at ratios less than 100 to 1 mol with respect to technetium. Most anions do not disturb the determination of technetium. The standard deviation for a single determination is ±0.09 μg over the range of 1 to 20 μg of technetium.

Microgram amounts of pertechnetate can be determined by measuring the extinction of its colored complex with toluene-3,4-dithiol in 2.5 N hydrochloric acid after extraction into carbon tetrachloride[69]. One hour must be allowed for the development of the color. The molar extinction coefficient at 450 nm is 15,000. Beer's law is followed over the range of 1.5 to 16.5 μg Tc per ml. The overall error does not exceed a standard deviation of ±5%. Because many cations interfere, an initial separation of technetium is necessary.

Meyer et al.[134] have used this colored complex of technetium with toluene-3,4-dithiol to determine technetium in fissium. The procedure is applicable to the determination of 0.005 to 0.2% of technetium in 1 g in fissium alloy after dissolution of the latter in a mixture of hydrochloric and nitric acid. Technetium is first separated from uranium, ruthenium and other constituents by distillation from 18 N sulfuric acid. The extinction of the complex of technetium with toluene-3,4-dithiol, formed in 9 N sulfuric acid and extracted into isoamyl acetate, is measured at 455 nm.

The complex formation of technetium, rhenium, and molybdenum with toluene-3,4-dithiol and its analytical application have been studied by Koyama et al.[135].

Thioglycolic acid forms a green complex at pH 8.0 with pertechnetate which is determined by measuring the extinction at 655 nm [136]. Beer's law is obeyed over the range of 2 to 40 μg Tc/ml. The molar extinction coefficient at 655 nm is estimated to be of the order of 1800. The reproducibility is within $\pm 2\%$. A tenfold excess of Cl^-, F^-, Br^-, J^-, PO_4^{3-}, SO_4^{2-}, WO_4^{2-}, and ReO_4^- does not disturb. Significant interferences have only been observed in the case of molybdate, dichromate, and ruthenate.

Procedure: To the $KTcO_4$ solution (5 ml) containing technetium (10 to 200 μg), are added 1 M sodium acetate (1 ml) and then 10% v./v. Thioglycolic acid solution (1 ml) of pH 8.0 $\pm$ 0.2. The flask is heated for 15 min on a boiling water bath. The solution is cooled and diluted to 5 ml volume with water. The pH of the solution is measured to ensure that it is 8.0 $\pm$ 0.2.

p-Thiocresol reduces TcO_4^- to Tc (V) in acetic acid solution and forms a yellow-brown complex which is readily extracted by chloroform, carbon tetrachloride, benzene and ether[64]. Unless the concentration of p-thiocresol is $> 0.1\%$ and the concentration of the acid is high, ReO_4^- is not reduced. The extinction of the technetium complex is measured at 410 nm, where the molar extinction coefficient is 7350. Since the elements of the platinum group, Ru, Pd, Pt, and Rh interfere they must be removed.

Procedure: To the test solution (2 ml) in a separating-funnel are added anhydrous acetic acid (10 ml) and a 5% solution of p-thiocresol in anhydrous acetic acid (0.2 ml). The phases are mixed and allowed to stand for 30 min. The complex is extracted into $CHCl_3$ and the extinction measured.

Miller and Zittel[137] have used 1,5-diphenylcarbazide (0.25% solution in acetone) for the spectrophotometric determination of technetium. 1 to 15 μg of technetium in 10 ml solution can be ascertained by measuring the extinction at 520 nm of the Tc (IV) complex in 1.5 M sulfuric acid. The development of the most intense color takes about 35 min; the reduction of pertechnetate to Tc (IV) is effected by the reagent itself before complexation occurs. The molar extinction coefficient of the complex at 520 nm is 48,600. The relative standard deviation is 2%. Fe^{3+}, Ce^{4+}, and CrO_4^{2-} clearly disturb measurements, VO_4^{3-}, MoO_4^{2-}, ReO_4^-, and Hg^{2+}, however, only slightly. CrO_4^{2-} forms a similar complex, but the technetium complex can be separated from the chromium complex by extracting the former into carbon tetrachloride. According to Fujinaga et al.[138] the method can be improved by the use of 1 M hydrochloric acid instead of sulfuric acid.

Pertechnetate forms a blue complex and perrhenate a brownish-yellow complex with $K_4[Fe(CN)_6]$ in presence of bismuth amalgam. This permits the spectrophotometric determination of both elements in the same solution[67]. The adsorption maxima of the technetium and rhenium complexes are at 680 and 420 nm, respectively. The molar extinction coefficients are 10,800 for technetium and 4,000 for rhenium. Metals forming color or precipitates with $K_4[Fe(CN)_6]$ must first be removed.

Procedure: To 5.7 M hydrochloric acid (2 ml) are added the test solution containing TcO_4^-, bismuth amalgam and a 5% aqueous solution of $K_4[Fe(CN)_6]$.

The mixture is shaken for 15 min, allowed to stand in the dark for 20 min and the extinction is measured at 680 nm.

3.3.2 Infrared Absorption

A method for determining technetium as tetraphenylarsonium pertechnetate by infrared spectroscopy has been proposed by Magee and Al-Kayssi[68]. Tetraphenylarsonium pertechnetate and perrhenate reveal sharp bands at 11.09 μ and 10.94 μ, respectively, which belong to the stretching vibrations $v_3(F_2)$ of the anions. Perrhenate and pertechnetate cannot be ascertained together; permanganate which also interferes with the determination can be removed from acidified test solutions by adding hydrogen peroxide which reduces the permanganate to manganese (II).

Procedure: To the sample which contains 20–300 μg of pertechnetate in 5–20 ml of solution, are added potassium perchlorate solution (2 ml, 1 mg $KClO_4$ per ml) and enough NaCl to make the solution approximately 1 M. The solution is heated and neutralized with ammonia. Pertechnetate is precipitated with aqueous 5% tetraphenylarsonium chloride reagent. The precipitate is filtered, washed and dried, and a 2-mg portion is mixed with potassium bromide (300 mg). The mixture is pressed to form a clear disc by the usual technique. The infrared spectrum is recorded between 10 and 12 μ. The peak absorption is measured at 11.09 μ by the base-line technique.

3.4 Gravimetric Methods

Weighable quantities of technetium are readily and conveniently determined gravimetrically.

The most popular method involves weighing of the precipitate in the form of tetraphenylarsonium pertechnetate[34]. Precipitation is carried out from neutral or alkaline solution at pH 8–9 by adding an excess of tetraphenylarsonium chloride $(C_6H_5)_4AsCl$. Since the precipitated salt is slightly soluble the total volume of the solution is kept to a minimum.

The use of a special microtechnique has permitted the precipitation, weighing, and determination of about 2 μg of technetium with a standard deviation of ± 0.08 μg[139]. The precipitate is filtered, washed with ice-cold water, dried at 110 °C and weighed as $(C_6H_5)_4AsTcO_4$. Permanganate, perchlorate, periodate, iodide, fluoride, bromide, thiocyanate anions and mercury, bismuth, lead, silver, tin and vanadyl cations as well as nitrate concentrations above 0.5 M interfere with the determination.

Technetium can also be precipitated and weighed as nitron pertechnetate $C_{20}H_{17}N_4TcO_4$ [49], which is precipitated at 80 °C from a weak sulfuric acid or acetic acid solution with an excess of a solution of 5% nitron in 3% acetic acid. The precipitate is washed with cold water, dried at 100 °C and weighed. Nitrate, perchlorate, permanganate, periodate, chloride, bromide, and iodide ions disturb the determination.

It should be mentioned that tetraphenylarsonium salts are soluble in alcohol and that the nitron salts dissolve in ethyl acetate. Thus, technetium as well as the organic reagents can be recovered.

The solution of $(C_6H_5)_4AsTcO_4$ is passed through an ion exchange resin in the chloride form. Pertechnetate ions are strongly adsorbed while tetraphenylarsonium chloride is recovered in the runnings. Pertechnetate is then eluted from the resin by 2 N NaOH. Nitron pertechnetate is dissolved in ethyl acetate and the solution is shaken with dilute ammonia. TcO_4^- passes into the aqueous layer while the nitron remains in the ester[140].

In certain cases, a precipitate of technetium heptasulfide, Tc_2S_7, is utilized for the determination of technetium[109]. The precipitation is carried out from 2–4 N hydrochloric or sulfuric acid solutions by passing hydrogen sulfide through a pertechnetate solution. To achieve a better coagulation of the precipitate, the solution is heated to the temperature of a boiling water bath. Tc_2S_7 is usually contaminated with elemental sulfur, which is removed before weighing by multiple washings of the precipitate with carbon disulfide. The lower limit of the concentration at which technetium can be precipitated without introducing carriers is 3 mg/l.

3.5 Electrochemical Methods

3.5.1 Polarography

The existence of various oxidation states of technetium indicates the possibility of using polarography for its quantitative determination. Polarographic reduction of the pertechnetate ion at a dropping mercury electrode has been studied in different supporting electrolytes[141–149].

Pertechnetate in 4 M hydrochloric acid has been found to undergo reduction to the oxidation state +4 [142]; a double wave was obtained corresponding to a one- and a two-electron transfer. The waves are rather poorly defined by half-wave potentials of —0.52 V and —0.68 V vs. SCE. Both waves are irreversible. No reduction occurs in 4 M perchloric acid.

In a 0.5 M KCl solution to which is added hydrochloric acid until pH 2, TcO_4^- gives three diffusion-controlled waves with half-wave potentials of —0.14, —0.91, and —1.12 V vs. SCE[146]. For the first wave the value of the diffusion current constant in the range of 0.01 to 0.2 m M of pertechnetate is fairly constant, suggesting that technetium in concentrations as low as 0.01 m M can be estimated with an accuracy of $\pm 0.8\%$, whereas the second and third wave did not show any constancy in diffusion current constant.

Neutral (1 M LiCl) and alkaline (1 M NaOH) solutions of TcO_4^- in the concentration range of 10^3 to 10^{-4} M have been investigated polarographically with direct and alternating current[141]. Four irreversible waves are observed (Fig. 12). The first two waves with the half-wave potentials of —0.85 V and —1.15 V vs. SCE are clearly recognizable in alkaline solution. They correspond to the electron transition n = 2 and n = 3 and can be used for the analytical determination of technetium. The third and fourth wave are not diffusion controlled and influenced

141
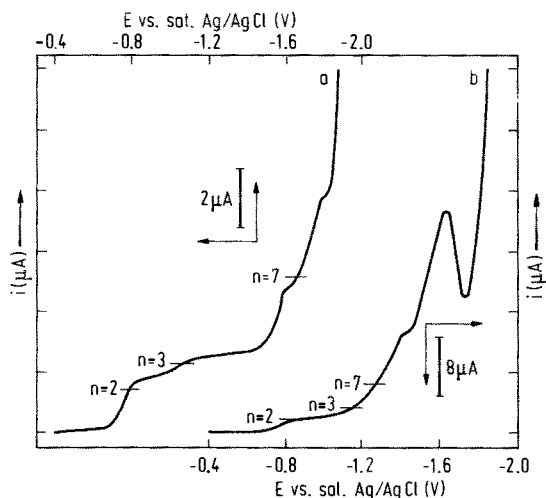
Fig. 12. Polarograms of TcO_4^- in alkaline and neutral solution. a 0.206 mM $KTcO_4$ in 1.0 M NaOH, b 0.206 mM $KTcO_4$ in 1.0 M LiCl[141]

by catalytic effects. For the wave at $E_{1/2} = -0.85$ V, alternating current efficiencies of 70–90% are obtained as a function of the type and concentration of the supporting electrolyte. Thus, technetium can also be determined by alternating current polarography which is advantageous on account of its higher separation capacity compared with the direct current polarographic methods.

The diffusion coefficient of TcO_4^- ascertained conductometrically has been found to be 1.48×10^{-5} cm$^2 \times$ s^{-1} [150] whereas the self-diffusion coefficient measured with the capillary method in the presence of the supporting electrolytes 1 M NaOH and 1 M LiCl amounts to 1.27×10^{-5} and 1.24×10^{-5} cm^2. s^{-1}, respectively[151].
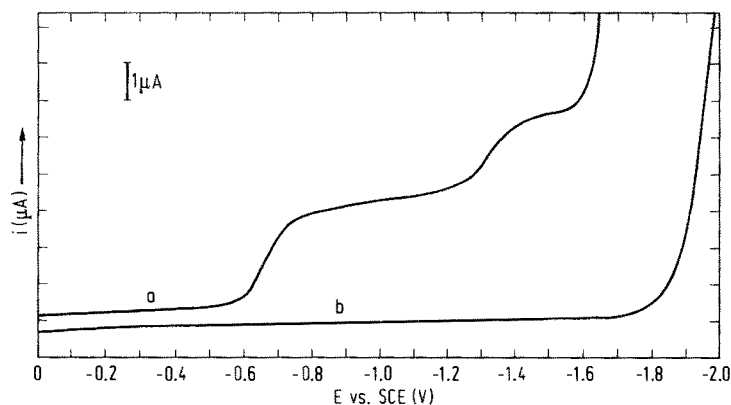
Fig. 13. Polarogram of pertechnetate in pH 7 phosphate buffer. a 1.38×10^{-4} M $KTcO_4$, b residual current curve of buffer[144]

Suitable conditions for the quantitative polarographic determination of technetium as pertechnetate are given by Miller et al.[144] who propose a 0.1 M KCl solution of pH 10 or a phosphate buffer solution of pH 7. Since in pH 7 buffer the current is directly proportional to the concentration of technetium over the range of 0.1 to 1.1 ppm, this medium has been used for the determination of low concentrations of technetium in solutions of fission products by the standard addition technique. The half-wave potential of the used wave is −0.68 V vs. SCE. The reaction appears to be irreversible (Fig. 13). It has been found that neither rhenium, ruthenium nor other fission products interfere. However, tetraphenylarsonium chloride is reduced at a more positive potential than is pertechnetate; therefore, $(C_6H_5)_4AsCl$, if present, must be separated.

Kuzina et al.[148] suggest that technetium can be determined polarographically in neutral solutions using 1 M $NaClO_4$ as supporting electrolyte. A distinct diffusion wave corresponding to a three-electron reduction has been observed with a half-wave potential of −0.8 V vs. SCE. In the range of 5×10^{-3} to 8×10^{-2} M the limiting current has been found to be proportional to the pertechnetate concentration.

For the rapid determination of ^{99m}Tc in a mixture of uranium fission products, Love and Greendale[149] have used the method of amalgam polarography. It consists in a selective reduction of technetium at a dropping mercury electrode at a potential of −1.55 V vs. SCE in a medium of 1 M sodium citrate and 0.1 M NaOH. Under these conditions, technetium is reduced to an oxidation state which is soluble in mercury. The amalgam is removed from the solution of fission fragments and the amount of ^{99m}Tc determined in nitric acid solution of the amalgam by a γ count. For ^{99m}Tc the measurement accuracy is within 1 %, and the decontamination factor from other fission products 10^5.

Astheimer and Schwochau[152] have applied the voltametry method to the determination of low technetium concentrations in the presence of molybdate and perrhenate ions. Using a Kemula electrode technetium is concentrated on a mercury drop from alkaline solution of 6.0×10^{-5} M $KTcO_4$ by electrolysis at a potential of −1.0 V vs. SCE. Anodic stripping in 1 M NaOH yields a characteristic stripping curve (Fig. 14). The height of the peak at −0.33 V is proportional to the concentration of technetium in the range of 10^{-4} to 3×10^{-7} M. Technetium can be detected with an accuracy of $\pm 4\%$. The determination of 0.5 μg of technetium in a 10^4 fold molar excess of ReO_4^- or MoO_4^{2-} is possible.
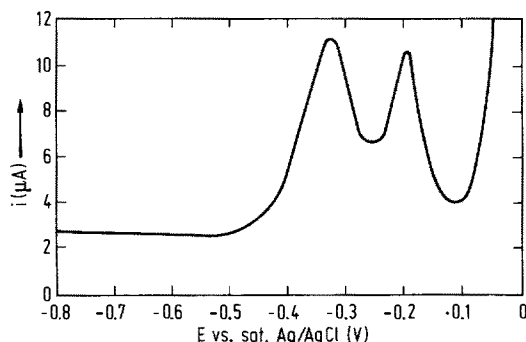
Fig. 14. Anodic stripping curve of a technetium deposit obtained by electrolysis of 6.0×10^{-5} M $KTcO_4$[152]

3.5.2 Coulometry

A controlled potential coulometric method for the determination of technetium has been developed by Terry and Zittel[147]. Pertechnetate is titrated in an acetate buffered (pH 4.7) solution of sodium tripolyphosphate at a potential of -0.70 V vs. SCE. Tc (VII) is said to be quantitatively reduced to Tc (III). In the range of 0.5 to 5 mg of pertechnetate the relative error of the method is $\pm 1\%$ and the relative standard deviation 0.5%. Technetium can be quantitatively removed from the interfering ions Fe (III), Mo (VI), Ru (IV), U (VI), V (IV), F^-, and NO_3^- by distillation from sulfuric acid solution.

Procedure: To the titration cell are added mercury (4–5 ml), a 6% (wt./vol.) $Na_5P_3O_{10}$ solution (10 ml) and a 3.0 M CH_3COONH_4 : 5.5 M CH_3COOH buffer solution (2 ml). The supporting medium is deaerated with an inert gas which is allowed to flow throughout the complete titration. The supporting medium is then reduced at -0.70 V to a background current of 100 μA. The test solution is prereduced at -0.20 V to a background current of 100 μA and subsequently reduced at -0.70 V to a background current of 100 μA.

Recently, Mazzocchin et al.[153] have studied several titration methods for determining relatively large amounts of technetium. The most precise results have been obtained by coulometric titration of TcO_4^- ions with electrogenerated tin (II) according to the procedure suggested by Bard and Lingane[154, 155]. The supporting electrolyte consists of 2.5 M sodium bromide, 0.15 M stannic chloride and 0.2 M hydrochloric acid. The titration reaction is very fast and currents up to 40 mA can readily be employed in the detection of the equivalence point.

4 References

1. Perrier, C., Segrè, E.: Nature (London) *140*, 193 (1937)
2. Perrier, C., Segrè, E.: Nature (London) *159*, 24 (1947)
3. Seelmann-Eggebert, W., Pfennig, G., Münzel, H.: Chart of the nuclides. Gersbach Verlag München 1974
4. Noddack, W., Tacke, I.: Naturwissenschaften *13*, 567 (1925)
5. Berg, O., Tacke, I.: Naturwissenschaften *13*, 571 (1925)
6. Prandtl, W., Franke, G., Grimm, H.: Angew. Chem. *39*, 1049 (1926)
7. Avjaginstew, O.: Nature (London) *118*, 263 (1927)
8. Herszfinkiel, C. R.: Acad. Sci. *184*, 968 (1927)
9. Katcoff, S.: Phys. Rev. *99*, 1618 (1955)
10. Boyd, G. E. et al.: Phys. Rev. *99*, 1030 (1955)
11. Herr, W.: Z. Naturforsch. *9a*, 907 (1954)
12. Alperovitch, E. A., Miller, J. M.: Nature (London) *176*, 299 (1955)
13. Anders, A., Sen Sarma, R. N., Kato, P. H.: J. Chem. Phys. *24*, 622 (1956)
14. Boyd, G. E., Larson, Q. V.: J. Physic. Chem. *60*, 707 (1956)
15. Kenna, B. T., Kuroda, P. K.: J. Inorg. Nucl. Chem. Lett. *23*, 142 (1961)
16. Moore, C. E.: Science *114*, 59 (1951)
17. Greestein, J. L., DeJager, C.: Bull. Astron. Inst. Netherlands *13*, 13 (1956)
18. Greestein, J. L.: Mem. Soc. Roy Sci. *14*, 307 (1953)
19. Nikitin, A. A.: Astron. Zhur *35*, 18 (1958)
20. Merrill, P.: Astrophys. J. *116*, 21 (1952)

21. Merrill, P.: Publ. Astron. Soc. Pacific 68, 70 (1956)
22. Schwochau, K.: Angew. Chem. 76, 9 (1964)
23. Boyd, G. E.: J. Chem. Educ. 36, 3 (1959)
24. Smith, W. T., Cobble, J. W., Boyd, G. E.: J. Amer. Chem. Soc. 75, 5773, 5777 (1953)
25. Hamilton, J. G.: University of California, Radiation Laboratory Declassified Report, UCRL-98, p. 5, 1948
26. Baumann, E. J. et al.: Am. J. Physiol, 185, 71 (1956)
26a. Eckelman, W. C., Levenson, S. M.: Int. J. Appl. Radiat. Isotope 28, 67 (1977)
27. Koch, C. C., Love, G. R.: J. Less-Common Metals 12, 79 (1967)
28. Compton, V. B. et al.: Phys. Rev. 123, 1567 (1961)
29. Boyd, G. E. et al.: J. Amer. Chem. Soc. 74, 556 (1952)
30. Selig, H., Chernick, C. L., Malm, J. G.: J. Inorg. Nucl. Chem. 19, 377 (1961)
31. Guest, A., Lock, C. J. L.: Canad. J. Chem. 50, 1807 (1972)
32. Kemmitt, R. D. W., Peacock, R. D.: The chemistry of manganese, technetium and rhenium. Oxford, New York: Pergamon Press (1973)
33. Kotegov, K. V., Pavlov, O. N., Shvedov, V. P.: Advan. Inorg. Chem. Radiochem. 2, 1 (1968)
34. Parker, G. W., Martin, W. J.: Oak Ridge National Laboratory, Declassified Report ORNL-1116, p. 26, 1952
35. Coleman, C. F., Kappelman, F. A., Weaver, B.: Nucl. Sci. Eng. 8, 507 (1960)
36. Campbell, M. H.: Anal. Chem. 35, 2052 (1963)
37. Goishi, W., Libby, W. F.: J. Amer. Chem. Soc. 74, 6109 (1952)
38. Rimshaw, S. J., Malling, G. F.: Anal. Chem. 33, 751 (1961)
39. Iqbal, M., Ejaz, M.: J. Radioanalyt. Chem. 23, 51 (1974)
40. Sci. News Lett. 83, 264 (1963)
41. Goldstein, G., Dean, J. A.: Radiochim. Acta 5, 18 (1966)
42. Meyer, R. J., Oldham, R. D., Larsen, R. P.: Analyt. Chem. 36, 1975 (1964)
43. Roberts, F. P., Smith, F. M., Wheelwright, E. J.: General Electric Co., Hanford Atomic Products Operation. Richmond, Washington 1962
44. Swindle, D. L., Kuroda, P. K.: Radioanal. Lett. 7, 229 (1971)
45. Neidhart, B. et al.: Radioanal. Lett. 12, 59 (1972)
46. Anders, E.: The Radiochemistry of Technetium. Natural Academy of Sciences, National Research Council, 1960
47. Boyd, G. E., Larson, Q. V., Motta, E. E.: J. Amer. Chem. Soc. 82, 809 (1960)
48. Perrier, C., Segrè, E.: J. Chem. Phys. 5, 712 (1937)
49. Perrier, C., Segrè, E.: J. Chem. Phys. 7, 155 (1939)
50. Koyama, M.: Bull. Chem. Soc. Japan 34, 1766 (1961)
51. Sugarman, N., Richter, H.: Phys. Rev. 73, 1411 (1948)
52. Bainbridge, K. T., Goldhaber, M., Wilson, E.: Phys. Rev. 90, 430 (1953)
53. Michelich, J. W., Goldhaber, M.: Phys. Rev. 82, 672 (1951)
54. Beck, A., Dyrssen, D., Ekberg, S.: Acta Chem. Scand. 18, 1695 (1964)
55. Boyd, G. E., Larson, Q. V.: J. Phys. Chem. 64, 988 (1960)
56. Pinajian, J. J.: Contract W-7405 eng-26 (1965)
57. Salaria, G. B. S., Rulfs, C. L., Elving, P. J.: Anal. Chem. 35, 983 (1963)
58. Shanker, R., Venkateswarlu, K. S., Shanker, J.: J. Less-Common Metals 15, 311 (1968)
59. Vita, O. A., Levier, W. A., Litteral, E.: Anal. Chim. Acta 42, 87 (1968)
60. Fouché, K. F.: J. Inorg. Nucl. Chem. 33, 857 (1971)
61. Turel, Z. R., Shanbhag, P. M., Haldar, B. C.: J. Ind. Chem. Soc. 52, 413 (1975)
61a. Singh, R. N., Krüger, A., Lieser, K. H.: Radiochim. Acta 26, 197 (1979)
62. Lavrukhina, A. K., Pozdnyakov, A. A.: Analytical Chemistry of Technetium, Promethium, Astatine, and Francium. Ann Arbor Humphrey Science Publishers 1970
63. Crouthamel, C. E.: Anal. Chem. 29, 1756 (1957)
64. Al-Kayssi, M., Magee, R. J.: Talanta 10, 1047 (1963)
65. Miller, F. J., Zittel, H. E.: Anal. Chem. 34, 1349 (1962)
66. Jasim, F., Magee, R. J., Wilson, C. L.: Talenta 2, 93 (1959)
67. Al-Kayssi, M., Magee, R. J., Wilson, C. L.: Talanta 9, 125 (1962)
68. Magee, R. J., Al-Kayssi, M.: Anal. Chim. Acta 27, 469 (1962)

69. Miller, F. J.. Thomason, P. F.: Anal. Chem. *33*, 404 (1961)
70. Salaria, G. B. S., Rulfs, C. L., Elving, P. J.: Anal. Chem. *36*, 146 (1964)
71. Poznyakov, A. A., Spivakov, B. Y.: Khimicheskie osnovy estraktsionnogo metoda razdeleniya elementov, p. 133, Moscow: Izdatelstvo Nauka 1966
72. Kiba, T. et al.: Talanta *13*, 1385 (1966)
73. Tribalat, S., Beydon, J.: Anal. Chim. Acta *8*. 22 (1953)
74. Kaotu, U., Chauting, Ch.: Nippon Genshiryoku Kenyusho, Kenkyu Hokoku, Japan Atomic Energy Res. Inst. Res. Repts No. 1036, 3 (1962)
75. Klofutar, C., Štular, V., Krašovec, F.: Z. Analyt. Chem. *214*, 27 (1965)
76. Baishya, N. K., Heslop, R. B., Ramsey, A. C.: Radiochem. Radioanal. Lett. *4*, 15 (1970)
77. Gerlit, J. B.: International Conference on Peaseful Uses of Atomic Energy, Geneva 1955, Vol. 7, p. 145 (United Nations, New York 1956
78. Yoshinaga, O., Toyoaku, K.: J. Chem. Soc. Japan *85*, 128 (1964)
79. Kiba, T., Miura, A., Sugioka, Y.: Bull. Chem. Soc. Japan *36*, 663 (1963)
80. Pozdnyakov, A. A., Basargin, N. N., Gerlit, Y. B.: Dokl. Akad. Nauk. SSSR *144*. 861 (1962)
81. Atteberry, R. W., Boyd, G. E.: J. Amer. Chem. Soc. *75*, 5787 (1953)
82. Sen Sarma, R. N., Anders, E.. Miller, J. M.: J. Phys. Chem. *63*, 559 (1959)
83. Alperovitch, E., Miller, J. M.: Nature *176*, 299 (1955)
84. Boyd, G. E., Larson, Q. V.: J. Phys. Chem. *60*, 707 (1956)
85. Pirs, M., Magee, R. J.: Talanta *8*, 395 (1961)
86. Hall, N. F., Johns, D. H.: J. Amer. Chem. Soc. *75*, 5787 (1953)
87. Huffman, E. H., Oswalt, R. L., Williams, L. A.: J. Inorg. Nucl. Chem. *3*, 49 (1956)
88. Sebesta, F., Posta, S., Řanda, Z.: Radiochem. Radioanal. Lett. *11*, 359 (1972)
89. De Carvalho, R. A. G.: Thesis, Oporto University 1958, 164 pp.
90. Beckman. T. J., Lederer, M.: J. Chromatogr. *5*, 341 (1961)
91. Levi. M., Lederer, M.: J. Inorg. Nucl. Chem. *4*, 381 (1957)
92. Scheer, K. E., Mair-Borst, W.: Nucl. Med. *3*, 214 (1962)
93. Mixheev, N. B., Garhy, M., Moustafa, Z.: Atompraxis *10*, 264 (1964)
94. Tucker. W. D., Green, M. W., Murrenhoff, A. P.: Atompraxis *8*, 163 (1962)
95. Nelson, F., Kraus, K. A.: Seminar on the Practical Application of Short-lived Radioisotopes, IAEA, Vienna 1962
96. D'Olieslager, W., Indesteege, J., D'Hont, M.: Talanta *22*, 395 (1975)
96a. Benes, J.: Collect. Czech. Chem. Commun. *44*, 1406 (1979)
97. Oniciu, L., Cook, G. B.: J. Radioanalyt. Chem. *13*, 247 (1973)
98. Seiler, H.: Helv. Chim. Acta *52*, 319 (1969)
99. Bailey, R. A., Yaffee, L.: Canad. J. Chem. *38*, 1871 (1960)
100. Eakins, J. D., Humphries, D. G.: J. Inorg. Nucl. Chem. *25*, 737 (1963)
101. Rulfs, C. L.: Crit. Rev. Anal. Chem. *1*. 335 (1970)
102. Voltz, R. E., Holt, M. L.: J. Electrochem. Soc. *114*, 128 (1967)
103. Box, W. D.: U.S. Patent 3, 374, 157 (March 19, 1968)
104. Flagg, J. F., Bleidner, W. E.: J. Chem. Phys. *13*, 269 (1945)
105. Barrett, P. T.: Proc. Roy. Soc. *A 218*, 104, 1132 (1953)
106. Rudenko, N. P., Pastukhova, Z. V.: Radiokhimiya *1*, 277 (1959)
107. Spitsyn, V. J., Kuzina, A. F.: Atomnaya Energiya *5*, 141 (1958)
108. Fried, S.: J. Amer. Chem. Soc. *70*, 442 (1948)
109. Rulfs, C. L., Meinke, W. W.: J. Amer. Chem. Soc. *74*, 235 (1952)
110. Geilmann, W., Bode, H.: Z. Anal. Chem. *130*, 222 (1950)
111. Jacobi, E.: Helv. Chim. Acta *31*, 2118 (1948)
112. Jasim, F., Magee, R. J., Wilson, C. L.: Talanta *4*, 17 (1960)
113. Parker, G. W., Kuroda, P. K.: J. Inorg. Nucl. Chem. *5*, 153 (1958)
114. Kuzina, A. F., Spitsyn, V. J.: Zh. Neorg. Khim. *5*, 1006 (1960)
115. Golchert, N. W., Sedlet, J.: Analyt. Chem. *41*, 669 (1969)
116. Fairman, W., Sedlet, J.: U.S. Atomic Energy Comm. Rep. TID-7696 p. 10, 1963
117. Foti, S. C., Delucchi, E., Akamian, V.: Anal. Chim. Acta *60*, 261 (1972)
118. Foti, S. C., Delucchi, E., Akamian, V.: Anal. Chim. Acta *60*, 269 (1972)
118a. Bate, L. C.: Radioelem. Anal.: Prog. Probl. Proc. Conf. Anal. Chem. Energy Technol., 23rd *1979*, 175

119. Meggers, W. F.: Spectrochim. Acta *4*, 317 (1951)
120. Timma, D.: J. Optical Soc. Amer. *39*, 898 (1949)
121. Meggers, W. F., Scribner, B. F.: J. Res. Nat. Bur. Stand. *45*, 476 (1950)
122. Hareland, W. A., Ebersole, F. R., Ramachandran, T. P.: Anal. Chem. *44*, 520 (1972)
123. Burkhart, L. E., Peed, W. F., Saunders, B. G.: Phys. Rev. *73*, 347 (1948)
124. Rogosa, G. L., Peed, W. F.: Phys. Rev. *100*, 1763 (1955)
125. Lux, F., Ammentorp-Schmidt, F., Opavsky, W.: Z. Anorg. Allgem. Chem. *341*, 172 (1965)
126. Boyd, G. E.: Phys. Rev. *99*, 430 (1955)
127. Kukavadze, G. M. et al.: Atomnaya Energ. *8*, 365 (1960)
127a. Kaye, J. H., Rapids, M. S., Ballou, N. E.: Proc. Int. Conf. Nucl. Methods Environ Energy Res., 3rd *1977*, 210
127b. Anderson, T. J., Walker, R. L.: Anal. Chem. *1980*, 52, 709
128. Mullen, P., Schwochau, K., Jørgensen, C. K.: Chem. Phys. Lett. *3*, 49 (1969)
129. Jørgensen, C. K., Schwochau, K.: Z. Naturforschg. *20a*, 65 (1965)
130. Pozdnyakov, A. A.: Zh. Analit. Khim. *20*, 473 (1965)
131. Schwochau, K., Astheimer, L., Schenk, H. J.: J. Inorg. Nucl. Chem. *35*, 2249 (1973)
132. Howard, O. H., Weber, C. W.: Analyt. Chem. *34*, 530 (1962)
133. Foster, R. E., Maeck, W. J., Rein, J. E.: Analyt. Chem. *39*, 563 (1967)
134. Meyer, R. J., Oldham, R. D., Larson, R. P.: Analyt. Chem. *36*, 1975 (1964)
135. Koyama, M. et al.: Chemia Analit. *17*, 679 (1972)
136. Miller, F. J., Thomason, P. F.: Analyt. Chem. *32*, 1492 (1960)
137. Miller, F. J., Zittel, H. E.: Analyt. Chem. *35*, 299 (1963)
138. Fujinaga, T., Koyama, M., Kanchiku, Y.: J. Chem. Soc. Japan *87*, 1243 (1966)
139. Jasim, F., Magee, R. J., Wilson, C. L.: Mikrochim. Acta *5-6*, 721 (1960)
140. Peacock, R. D.: The Chemistry of technetium and rhenium. Amsterdam, London, New York: Elsevier Publ. Co. 1966
141. Astheimer, L., Schwochau, K.: J. Electroanal. Chem. *8*, 382 (1964)
142. Colton, R. et al.: J. Chem. Soc. *1960*, 71
143. Magee, R. J., Scott, J. A. P., Wilson, C. L.: Talanta *2*, 376 (1959)
144. Miller, H. H., Kelley, M. T., Thomason, P. F.: Advances in Polarography. (Cambridge 1959) Vol. II, p. 716. London: Pergamon Press 1960
145. Salaria, G. B. S., Rulfs, C. L., Elving, P. J.: J. Chem. Soc. *1963*, 2479
146. Salaria, G. B. S., Rulfs, C. L., Elving, P. J.: Analyt. Chem. *35*, 979 (1963)
147. Terry, A. A., Zittel, H. E.: Analyt. Chem. *35*, 614 (1963)
148. Kuzina, A. F., Zhdanov, S. J., Spitsyn, V. J.: Dokl. Akad. Nauk. SSSR *144*, 836 (1962)
149. Love, D. L., Greendale, A. F.: Analyt. Chem. *32*, 780 (1960)
150. Schwochau, K., Astheimer, L.: Z. Naturforschg. *17a*, 820 (1962)
151. Astheimer, L., Schwochau, K., Herr, W.: J. Electroanal. Chem. *14*, 161 (1967)
152. Astheimer, L., Schwochau, K.: J. Electroanal. Chem. *14*, 240 (1967)
153. Mazzocchin, G. A. et al.: J. Inorg. Nucl. Chem. *36*, 3783 (1974)
154. Bard, A. J., Lingane, J. J.: Analyt. Chim. Acta *20*, 463 (1959)
155. Bard, A. J.: Analyt. Chem. *32*, 623 (1960)

Author Index Volumes 50–96

The volume numbers are printed in italics

149